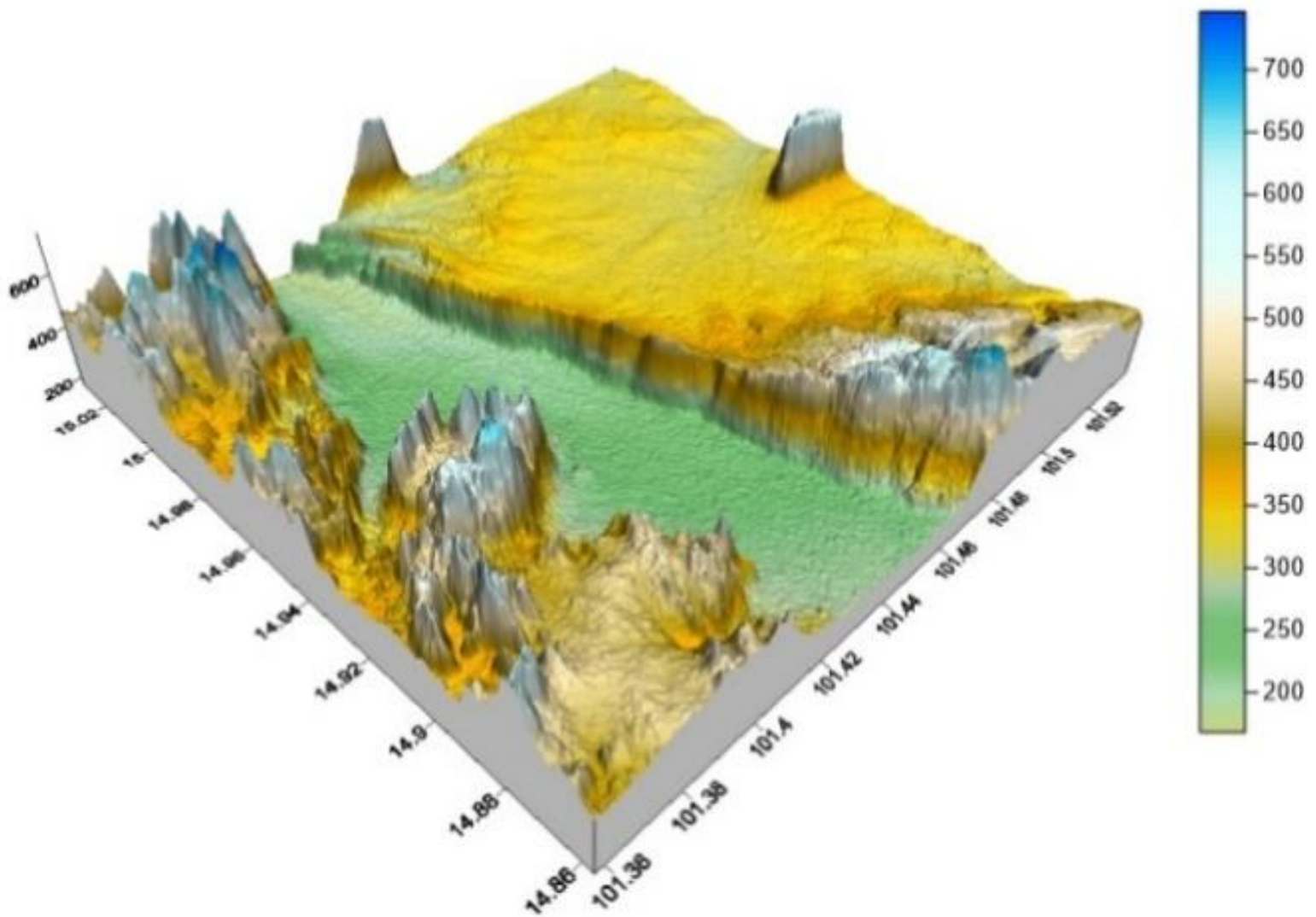




ASEAN

Journal of Scientific and Technological Reports
Online ISSN:2773-8752

Vol. 27 No. 2, March-April 2024



ISSN 2773-8752 (online)

<https://ph02.tci-thaijo.org/index.php/tsujournal/issue/view/17077>





ASEAN

Journal of Scientific and Technological Reports

Online ISSN:2773-8752

ASEAN Journal of Scientific and Technological Reports (AJSTR)

Name	ASEAN Journal of Scientific and Technological Reports (AJSTR)
Owner	Thaksin University
Advisory Board	Assoc. Prof. Dr. Nathapong Chitniratna (President of Thaksin University, Thailand) Assoc. Prof. Dr. Samak Kaewsuksaeng (Vice President for Reserach and Innovation, Thaksin University, Thailand) Assoc. Prof. Dr. Suttiporn Bunmak (Vice President for Academic Affairs and Learning, Thaksin University, Thailand) Assoc. Prof. Dr. Samak Kaewsuksaeng (Acting Director of Reserach and Innovation, Thaksin University, Thailand) Asst. Prof. Dr. Prasong Kessaratikoon (Dean of the Graduate School, Thaksin University, Thailand)
Editor-in-Chief	Assoc. Prof. Dr. Sompong O-Thong, Mahidol University, Thailand
Session Editors	

1. Assoc. Prof. Dr. Jatuporn Kaew-On, Thaksin University, Thailand
2. Assoc. Prof. Dr. Samak Kaewsuksaeng, Thaksin University, Thailand
3. Assoc. Prof. Dr. Rattana Jariyaboon, Prince of Songkla University, Thailand
4. Asst. Prof. Dr. Noppamas Pukkhem, Thaksin University, Thailand
5. Asst. Prof. Dr. Komkrich Chokprasombat, Thaksin University, Thailand

Editorial Board Members

1. Prof. Dr. Hidenari Yasui, University of Kitakyushu, Japan
2. Prof. Dr. Jose Antonio Alvarez Bermejo, University of Almeria, Spain
3. Prof. Dr. Tjokorda Gde Tirta Nindhia, Udayana University in Bali, Indonesia
4. Prof. Dr. Tsuyoshi Imai, Yamaguchi University, Japan
5. Prof. Dr. Ullah Mazhar, The University of Agriculture, Peshawar, Pakistan
6. Prof. Dr. Win Win Myo, University of Information Technology, Myanmar
7. Prof. Dr. Yves Gagnon, University of Moncton, Canada
8. Assoc. Prof. Dr. Chen-Yeon Chu, Feng Chia University, Taiwan
9. Assoc. Prof. Dr. Gulam Murtaza, Government College University Lahore, Lahore, Pakistan
10. Assoc. Prof. Dr. Jompob Waewsak, Thaksin University, Thailand
11. Assoc. Prof. Dr. Khan Amir Sada, American University of Sharjah, Sarjah, United Arab Emirates.
12. Assoc. Prof. Dr. Sappasith Klomkiao, Thaksin University, Thailand
13. Asst. Prof. Dr. Dariusz Jakobczak, National University, Pakistan
14. Asst. Prof. Dr. Prawit Kongjan, Prince of Songkla University, Thailand
15. Asst. Prof. Dr. Shahrul Ismail, Universiti Malaysia Terengganu, Malaysia
16. Asst. Prof. Dr. Sureewan Sittijunda, Mahidol University, Thailand
17. Dr. Nasser Ahmed, Kyushu University, Fukuoka, Japan
18. Dr. Peer Mohamed Abdul, Universiti Kebangsaan Malaysia, Malaysia
19. Dr. Sriv Tharith, Royal University of Phnom Penh, Cambodia
20. Dr. Zairi Ismael Rizman, Universiti Teknologi MARA, Malaysia
21. Dr. Khwanchit Suwannoppharat, Thaksin University, Thailand

Staff: Journal Management Division

1. Miss Kanyanat Liadrak, Thaksin University, Thailand
2. Miss Ornkamon Kraiwong, Thaksin University, Thailand

Contact Us
Institute of Research and Innovation, Thaksin University
222 M. 2 Ban-Prao sub-district, Pa-Pra-Yom district, Phatthalung province, Thailand
Tel. 0 7460 9600 # 7242 , E-mail: aseanjr@tsu.ac.th

List of Contents

Contents	Page
Biogas and Biohythane Production from Anaerobic Co-digestion of Canned Sardine Wastewater with Glycerol Waste Tussanee Srimachai, Tsuyoshi Imai and Kiattisak Rattanadilok Na Phuket	1
Characterization and Development of Venipuncture Practice Rubber Model Based for BCG Economy Framework Keerakarn Somsuan, Siripat Aluksanasuwan, Atthapan Morchang, Arunothai Wanta, Sittiporn Punyanitya	14
Pyrolysis of Latex Sediment from Concentrated Latex Industry and Properties of Pyrolytic Products Fareeda Wongdaeng, Saowapa Chotisuwan, Rattana Jariyaboon, and Prawit Kongjan	21
Income and Expenditure Analysis of Selected Lowland Rainfed Rice Farmers in Tubog, Cawayan, Masbate Roger Y. Ibañez Jr., Jacob Frederick P. Velza, Restiel V. Gaylan, Jonna Mae B. Catimpuhan	29
Environmental Impact Assessment of Onshore Wind Power Plants: A Case Study of a 50 MW Wind Power Plant in Northeastern Thailand Sunisa Kongprasit, Somphol Chiwamongkhonkarn, Fida Ali, Pongsak Makhampom, Yves Gagnon and Jompob Waewsak	39
Prevalence, Virulence Profiles, and Genetic Relatedness of <i>Escherichia coli</i> O45 from Raw meats, Southern Thailand Pharanai Sukhumungoon, Aphisara Sae-lim, Fadeeya Hayeebilan and Pattamarat Rattanachuaay	58
Induction of Gynogenetic Diploids the Tropical Oyster, <i>Crassostrea belcheri</i> 1873 (Ostreids: Ostreoidea) from Southern Thailand. Supatcha Chooseangjaew, Nuntaporn Getlekha, Worawut Koedprang, Chanika Saenge Chooklin, Kattinat Sakulsawasdipan, and Suwat Tanyaros	72
Smartphone-Based Spectrophotometer for Facile and Fast Determination of Lipid Peroxidation in Local Fried Food Trin khawsung, Tanyarath Utaipan, Weeraya Treewanjutha	79
Gid Crypto: Application for End-to-End Encrypt and Decrypt E-mail and Data Alain Jean, and Tossaporn Alherbe	90
Effect of Chlorine Dioxide on Micropropagation of <i>Gymnocalycium mihanovichii</i> LB2178 Agua Dulce (Cactaceae) Phakarat Rotduang, Supawadee Ramasoot and Tassanee Khawniam	103



ASEAN

Journal of Scientific and Technological Reports

Online ISSN:2773-8752



Biogas and Biohythane Production from Anaerobic Co-digestion of Canned Sardine Wastewater with Glycerol Waste

Tussanee Srimachai^{1, 4, 5}, Tsuyoshi Imai² and Kiattisak Rattanadilok Na Phuket^{3, 4, 5*}

¹ College of Innovation and Management, Songkhla Rajabhat University, Songkhla, 90000, Thailand; Tussnee.sr@skru.ac.th

² Division of Environmental Science, Graduate School of Science and Engineering, Yamaguchi University, Yamaguchi, 755-8611, Japan

³ College of Innovation and Management, Songkhla Rajabhat University, Songkhla, 90000, Thailand; panpong1@hotmail.com

⁴ Community Innovation Learning and Transfer Center "Thung Yai Sarapee Model" Songkhla Rajabhat University, Satun campus, Satun 91100, Thailand; Kiattisak.pa@skru.ac.th

⁵ Microbial Resources and Utilization Center SKRU, Songkhla Rajabhat University, Songkhla, 90000, Thailand; panpong1@hotmail.com

* Correspondence: panpong1@hotmail.com (Rattanadilok Na Phuket, K.)

Citation:

Srimachai, T.; Imai, T.; Rattanadilok Na Phuket, K. Biogas and biohythane production from anaerobic co-digestion of canned sardine wastewater with glycerol waste. Title. *ASEAN J. Sci. Tech. Report.* 2024, 27(2), 1-13. <https://doi.org/10.55164/ajstr.v27i2.249551>

Article history:

Received: May 20, 2023

Revised: November 18, 2023

Accepted: January 11, 2024

Available online: February 1, 2024

Publisher's Note:

This article is published and distributed under the terms of the Thaksin University.

Abstract: A biochemical methane potential (BMP) test investigated the effect of glycerol waste (GW) concentration on anaerobic co-digestion with canned sardine wastewater (CSW). They were studied using the single-stage process at mesophilic (P1) and thermophilic (P2) conditions and two-stage mesophilic (P3) processes. The P3 process has provided the most significant potential for improving biogas production in the sardine canning industry. Using 4% GW (v/v), the optimal hydrogen and methane concentrations at P3 are 43.00 ml H₂/g CODr and 303.69 ml CH₄/g CODr, respectively. The P3 process was 11.33 m³ biohythane/m³ mixed substrate, and the biohythane composition contained 43.11% CH₄, 21.45% H₂, and 35.43% CO₂. The modified Gompertz model could simulate satisfactory hydrogen and methane yields, corresponding to high regression coefficients (R²>0.90). Hydrogen-producing bacteria in the H₂ batch reactor were dominated by *Micrococcus sp.* and *Desulfovibrio sp.*, while *Methanosaeta sp.*, *Methanoculleus sp.*, and *Methanosarcina sp.* are the major methanogens in the CH₄ batch reactor. A two-stage process of co-fermenting CSW and GW could be a potential option for simultaneous biofuel recovery and waste treatment.

Keywords: Anaerobic co-digestion; Biochemical methane potential (BMP); Canned Sardine wastewater; Glycerol waste; Biohytan

1. Introduction

Anaerobic digestion (AD) is a biological degradation process that converts organic compounds (carbohydrates, proteins, and fats) to produce methane and carbon dioxide without oxygen. The AD can be divided into four consecutive stages. Firstly, complex organic compounds are hydrolyzed by hydrolytic bacteria to form water-soluble simple organic compounds. In the second stage, soluble simple organic compounds are converted into organic acids, carbon dioxide, hydrogen, and alcohol by acidogenic bacteria (acidogens), which is called acidogenesis. The third stage is acetogenesis, in which the organic acids produced are broken down into acetic acid, carbon dioxide, and hydrogen. Finally, hydrogen and acetic acid are converted into methane by methanogenic bacteria (methanogens), which is methanogenesis [1]. Biogas is the fermentation into AD from organic waste fermentation [2]. Most biogas compositions contain 60-65% of methane, 34-39% of carbon dioxide, and



about 1% of other gas, such as nitrogen and hydrogen sulfide [3]. Additionally, the advantage of AD is highly removed organic, using less energy and excess sediment than aerobic digestion [4]. Likewise, the quantity and quality of biogas depend on the substrate used in the production. If the substrate contains highly toxic (ammonia, hydrogen sulfide, sodium, etc.) that affect methane production, the co-digestion strategy can solve this problem. The co-digestion process is an option to increase the efficiency of AD; one waste stream is mixed with other waste for sharing costs with the treatment advantages of this process can be to dilute the inhibitor, improve the balance of nutrients and synergistic effect of microorganisms resulting in a higher yield of methane [5]. The biochemical methane potential test (BMP) is the most commonly used method by academic and technical professionals to determine the maximal methane production of a given substrate. The BMP test can also be used to estimate rate constants of rate-limiting steps (e.g., the hydrolysis rate of high-particulate substrates) required for optimal design and operation of anaerobic digesters [6].

The canned sardine industry is one of the main industries in Thailand. Most factories are located in the coastal areas in southern and eastern Thailand. Canned sardine wastewater (CSW) contained 100-3,000 mg/l BOD, 1,000-18,000 mg/l COD, and 80-1,000 mg/l nitrogen [4]. CSW is protein-rich wastewater rapidly decomposed into ammonia nitrogen during anaerobic digestion. High concentrations of ammonia could seriously inhibit the activity of methanogens, resulting in less efficiency in the production of biogas and treatment [8]. Generally, total ammonia nitrogen (TAN), i.e., ammonium ion (NH_4^+); Al^+ free ammonia nitrogen (NH_3); FAN, which is generated from the breakdown of protein-based substrates, is generally known as an inhibitor in the AD process [9]. Adjusting the C/N ratio of the substrate by using a co-digestion strategy could potentially reduce the concentration of TAN in an anaerobic system. Yenigum and Demirel [9] reported that a C: N ratio between 25 – 35 is optimal for the AD process due to low and stable TAN and FAN. However, a C: N ratio lower than 15 could lead to a high TAN and FAN level in the AD process. Thus, optimization of the C: N ratio resulted in a stable co-digestion process. Due to these limitations, only a small amount of biogas is produced from CSW and is not worth investing in an anaerobic treatment system. Thus, the AD system for treating the canned sardine industry is unattractive.

Glycerol waste (GW), a by-product of transesterification for biodiesel production, is generated approx. 10 kg-GW for every 100 kg of biodiesel produced. GW contains 50-60% of glycerol, 12-16% of alkalis, 15-18% of methyl esters, 8-12% of methanol, and 2-3% of water [10]. Pure glycerol is used in many industries, such as cosmetics, food, pharmaceuticals, etc. However, the purification process of GW is too expensive. Therefore, AD is currently an alternative method to utilize GW, as GW is a cheap and easy-to-implement high-carbon source for anaerobic biogas production [11]. Rivero et al. [10] reported that the high C of GW could increase the C/N ratio in the mixed substrate, dilute inhibitors of the process through an excess of N, and enhance methane production by about 50-200% in the AD process. Thus, GW is an interesting substrate to be used as a co-substrate in the co-digestion process to solve the high nitrogen content in the AD system and to increase biogas production. Anaerobic co-digestion between animal manure and 3-6% glycerin could produce 570-680 l $\text{CH}_4/\text{g VS}$, a threefold enhancement over feeding only waste [12].

Presently, there are various modes of AD operation, such as one-stage mesophilic AD, one-stage thermophilic AD, two-stage mesophilic AD, and two-stage thermophilic AD. Each operating mode has different advantages and disadvantages. Mesophilic and thermophilic AD are operated at temperatures ranging from 30-40 °C and 45-65 °C, respectively [9]. Yenigum and Demirel [9] suggested that the advantages of thermophilic processes compared to mesophilic processes are higher digestion rates, higher methanogenesis rates, faster solid-liquid separation, and minimized accumulation of bacterial and viral pathogens. The disadvantage of the thermophilic process is that it is operated at high temperatures, causing a higher heating cost [13]. For two-stage AD, the first acidogenic stage produces volatile fatty acids (VFAs), hydrogen, and carbon dioxide. After that, solubilized effluent from the acidogenic stage is fed into the second (methanogenic stage) for methane and carbon dioxide production [14]. The advantages of two-stage AD compared with one-stage AD are increasing net energy balance, higher organic loading rates, enhancing the specific activity of methanogens, increasing methane production rate, and increasing overall COD and VS reduction efficiencies [15]. Researchers have generally found that AD systems operating in a two-stage configuration outperform conventional single-stage systems regarding methanogenesis and digestion stability [14].

The aim of this study is to evaluate the potential of hydrogen and methane production from batch anaerobic co-digestion of CSW and GW by using different operating modes (one-stage mesophilic, one-stage thermophilic, and two-stage mesophilic process) and using mixed anaerobic microflora at differences of GW

concentration. Experimental results are expected to be used for further development of biogas production by using the co-digestion strategy for wastewater generated from the canned sardine industry.

2. Materials and Methods

2.1 Inoculum, GW, and CSW

A mixed anaerobic microbiota was collected from a palm oil biogas plant in southern Thailand (Southern Palm (1978) Co., Ltd.) and used as an inoculum in this study. The inoculum was adapted with CSW to enhance mesophilic and thermophilic inoculum. CSW was mixed with the mixed anaerobic microflora in a 1:1 ratio, after which the pH of the broth was adjusted to the range of 6.8-7.2 by adding 1N NaOH and 1N HCl. The inoculum was then incubated at 37°C and 50°C in mesophilic and thermophilic inoculum incubators. If the inoculum exhibits a constant biogas production rate and composition, the acclimated inoculum can be further used in the experiment. GW was received from the biodiesel plant at Prince of Songkla University (Hat-Yai campus) in southern Thailand. The CSW was collected from Saim International Food Public Co., Ltd in southern Thailand. After collection, CSW was stored at 4 °C before use.

2.2 Biochemical methane potential (BMP)

Experiments were performed in a one-step mesophilic process (P1), a one-step mesophilic process (P2), and a two-step mesophilic process (P3) under anaerobic batch co-digestion (Figure 1). All experiments were performed under batch conditions using 120 mL glass serum bottles (60 mL working volume). P1, P2, and P3 were operated at 37°C, 50°C, and 37°C, respectively. For methanogenesis, 24 ml of inoculum and 36 ml of mixed substrate were placed in each glass serum bottle. Mixed substrates (CSW+GW) were tested at different GW concentrations ranging from 1% to 5% (v/v) and then adjusted to neutral pH. Nitrogen gas (1.5 MPa, 1 minute) was passed through the mixed substrate to replace oxygen, and the mixture was sealed with a silicone rubber and aluminum cap to create an anaerobic state. For the P3 process, the first stage was hydrogen production from the mixed substrate (CSW+GW), and the second stage was methane production from wastewater produced in the first stage. For the first hydrogen production, the inoculum was boiled at 105 °C for 60 min before being used to adjust the pH of the mixed substrate to approximately 5.5. The inoculum was not boiled for the second methanogenesis and was used under the same conditions as the P1 process. Hydrogen and methane production was measured by water displacement. Gas samples in the headspace of all experiments were then analyzed by gas chromatography. All Experiments used distilled water, sucrose, and 100%CSW as control experiments for comparison.

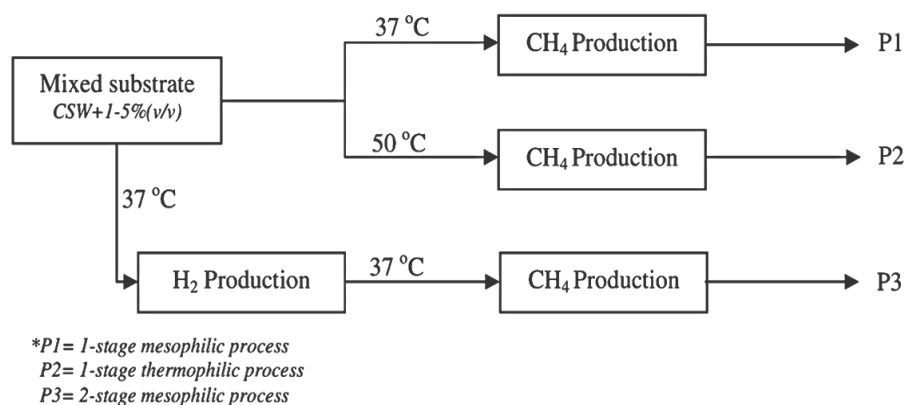


Figure 1. Research procedure

2.3 Kinetic of biogas analysis

In experiments, a modified Gompertz model was used to explain the biogas production from batch anaerobic co-digestion between CSW and GW as shown in Eq.(1) [16].

$$G(t) = G_0 \cdot \exp \left\{ -\exp \left[\frac{R_{\max} \cdot e}{G_0} (\lambda - t) + 1 \right] \right\} \quad (1)$$

Where $G(t)$ is the cumulative hydrogen or methane yield (ml CH₄/g CODr or ml H₂/g CODr) G_0 is the maximum hydrogen or methane yield (ml CH₄/g CODr or ml H₂/g CODr), R_{\max} is the maximum hydrogen or methane production rate (ml CH₄/g CODr-day or ml H₂/g CODr-day), e is the $\exp(1) = 2.7183$, λ is the lag phase time (day) and t is the cultivation time (day).

2.4 Microorganism community analysis by DGGE

Sludge from the optimal condition was collected for community analysis using the DGGE technique. Polymerase chain reactor gradient gel electrophoresis (PCR-DGGE) was used to study microbial community structure in this experiment, the procedure of which was explained by Kongjan et al. [17]. The PCR products from the experiment were purified and sequenced by Macrogen Inc. (Seoul, Korea). The closest matches for partial 16S rRNA gene sequences were identified by database searches in Gene Bank using BLAST [18].

2.5 Analytical methods

pH was measured by using a pH meter (Horiba, Japan). Chemical oxygen demand (COD), total solid (TS), volatile solid (VS), total nitrogen (TN), protein, carbohydrate, and fat were analyzed following the procedures explained in the Standard Method [19]. The volume of biogas was measured by water replacement and biogas composition was monitored by gas chromatograph GC-8APT with thermal conductivity detector (TCD), Shimadzu, Japan [13]. Gas chromatograph GC-8APF analyzed the VFA with a flame ionization detector (FID), Shimadzu, Japan [13].

3. Results and Discussion

3.1 GW and CSW property

The main composition of the CSW was: pH 6.8, total chemical oxygen demand (COD) 12.00 g/l, total solids 8.5 g/l, volatile solids 6.4 g/l, total nitrogen 1.50 g/l, 3.90 g/l protein, 1.91 g/l carbohydrate, 0.13 g/l fat, and C: N ratio 11. The main composition of GW was: pH 8.8, total chemical oxygen demand (COD) 1760 g/l, total solids 969 g/l, volatile solids 910 g/l, total nitrogen 1.7 g/l, protein 1.28 g/l, carbohydrate 845 g/l, fat 63.76 g/l, C: N ratio 949. Table 1 shows the chemical composition of the mixed substrates after co-digestion with GW (1–5% (v/v)). After co-digestion, the concentrations of COD and TN increased from 28 to 82 g/l and from 0.887 to 1.047 g/l. In addition, pH and C: N ratios were improved in the range of 7.28–8.17 and 27–73.

Table 1. The chemical property of the mixed substrate after co-digested with GW

Samples	pH	COD (g/L)	TN (g/L)	C/N ratio
CSW+1%GW	7.28	28.00	0.887	27
CSW+2%GW	7.52	48.00	0.993	43
CSW+3%GW	7.76	56.00	1.004	51
CSW+4%GW	8.01	70.00	1.027	63
CSW+5%GW	8.17	82.00	1.047	73

3.2 Biochemical Methane Potential

For P1, the maximum cumulative methane production was 293.82 ml, with 73.15% methane in biogas during digestion at 1% GW, corresponding to a 244.85 ml CH₄/g CODr methane yield. Methane production was increased by approximately 8.27 times compared to a single digestion of CSW, producing 35.52 mL of methane, corresponding to 62.15% of the methane in biogas. As shown in Figure 2A, adding 2–5% GW to CSW increased methane production by 1.94–3.83 fold, increasing GW concentration and potentially significantly reducing methane production. Moreover, the COD removal efficiency with co-fermentation at 1% GW for 25 25-day fermentation period is about 97.29%, which is consistent with the increased methane production. The P2 process was carried out under thermophilic conditions (°C). The results showed that adding 2% of GW into

CSW could result in the maximum methane production with a methane yield of 255.21 ml CH₄/g CODr (68.48% of methane in biogas) for 14 days of fermentation, as shown in Figure 2B. The methane production increased by about 40.76 fold compared to a single-digestion of CSW, which gave methane 16.29 ml CH₄/g CODr (37.28% of methane in biogas). In addition, P2 introduced higher COD concentrations (28-48 g/l) into the system than P1, allowing methanogens to adapt to optimal conditions in P2 and resulting in higher levels of methane production. So, the efficiency of COD removal was high, about 97.50%, which was similar to P1. Furthermore, increasing the concentration of GW higher than 3% (v/v) could lower methane production but still higher than a single-digestion of CSW (3.06-7.81 fold). Finally, the P3 process was separated into 2 reactors consisting of the reactor for hydrogen production (1-stage) and methane production (2-stage) and operated at mesophilic conditions. P3 could get a high COD compared with P1 and P2 processes. The system can take a high organic loading rate (OLR). The optimum condition for P3 was using 4% GW as a co-substrate, leading to an initial concentration of 70 g-COD/l. The production of maximum hydrogen and methane was 45.40 ml (39.04% of H₂) and 634.11 ml (78.48% of CH₄), corresponding to hydrogen and methane yields of 43.00 ml H₂/g CODr and 303.69 ml CH₄/g CODr, respectively. (Figure 2C). Rivero et al. [10] reported that hydrogen and methane yields of 26 mL H₂/g CODr and 290 mL CH₄/g CODr can be achieved by anaerobic mesophilic co-digestion of sewage sludge at 1% (v/v) GW. Hydrogen and methane production was 648.57 and 7.75 fold of those from the single-digestion of CSW, which could barely generate hydrogen and methane of 0.07 and 81.87 ml, respectively. After 45 days of fermentation, the COD removal efficiencies in 1-stage- and 2-stage fermentation were 31.43% and 93.33%, respectively. The result showed that using GW as a co-substrate in co-digesting with CSW could significantly increase the potential of hydrogen and methane production. As a result, the maximum hydrogen and methane production was obtained in the P3 process. GW can improve the carbon source of CSW and reduce the production of toxic ammoniacal nitrogen, leading to an increase in the C: N ratio, as shown in Table 1. Thus, the proper C/N ratio could enhance microorganism adaptation and increase hydrogen and methane production. Additionally, adjusting the C/N ratio could effectively reduce the inhibition of organic acids [20].

3.3 Effect of volatile fatty acid (VFA)

In all experiments, VFAs detected in the P1 process on 7 days of fermentation were acetic acid, propionic acid, I-butyric acid, and N-butyric acid. Under P1 optimum conditions, adding 1%GW generated total VFAs 801.17 mg/l, containing 91.48 mg/l acetic acid, 619.04 mg/l propionic acid, and 90.65 mg/l N-butyric acids (Figure 3A). Adding GW into CSW in a 2-5% range resulted in higher total VFA accumulation in the AD system. Although VFAs were the main substrate for producing methane by methanogens, their accumulation in the AD system with high concentration could directly inhibit methanogens, consequently causing the final pH to decrease (Figure 4). Decreasing pH in the AD system could majorly reduce methanogen activity. GW as a co-substrate at the concentration of more than 1% (v/v) in P1 resulted in a significant decrease in final pH. (Figure 4A). Using 1%GW as co-substrate, the final pH was 7.78, but the concentration of GW was more than 1% (v/v), and the pH was decreased to a range of 5.6-6.4. Generally, at lower pH, VFA is turned into an undissociated form. This undissociated VFA becomes more toxic to methanogens due to its ability to free cross-membrane cells, leading to dissociated and consequently lower internal pH and, finally, the cause of disruption of homeostasis [21]. Normally, the optimal pH range in the AD system for methane generation is between 6.00 and 8.00 [3]. Franke-Whittle et al. [22] reported that the accumulation of most situations reflected an imbalance between acid producers and consumers, resulting in a pH drop in the system, which could inhibit the growth of methanogens.

For the P2 process, methanogens under thermophilic conditions could take GW up to 2% (v/v) concentration for the highest methane production. The total VFAs detected on 5 days was 2,031.14 mg/l, consisting of 495.35 mg/l acetic acid, 257.80 mg/l propionic acid, 43.11mg/l I-butyric acid, and 1,234 mg/l N-butyric acids (Figure 3B). Adding GW higher than 3% (v/v) resulted in higher VFAs accumulation and pH decrease (Figure. 4B). The final pH of 7.46 was detected under the AD system with 2% (v/v) GW), while Anaerobic co-digesting CSW with GW higher than 2% (v/v) in P2 resulting in pH lower than 6.10. The high performance of P2 thermophilic AD compared to P1 mesophilic AD is definitely due to the advantages of operating under thermophilic conditions.

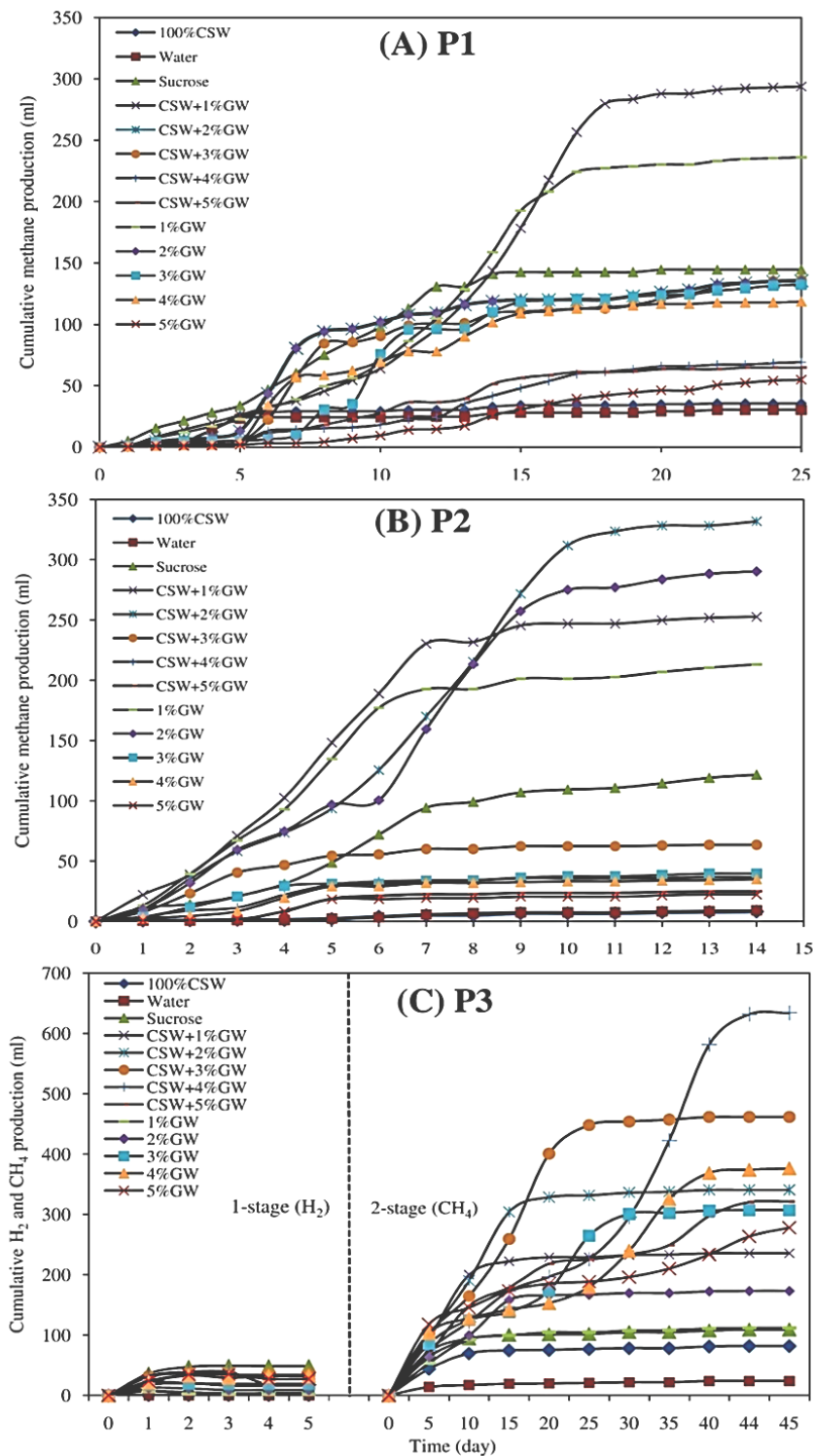


Figure 2. Hydrogen and methane production profile; (A) P1 process, (B) P2 process and (C) P3 process

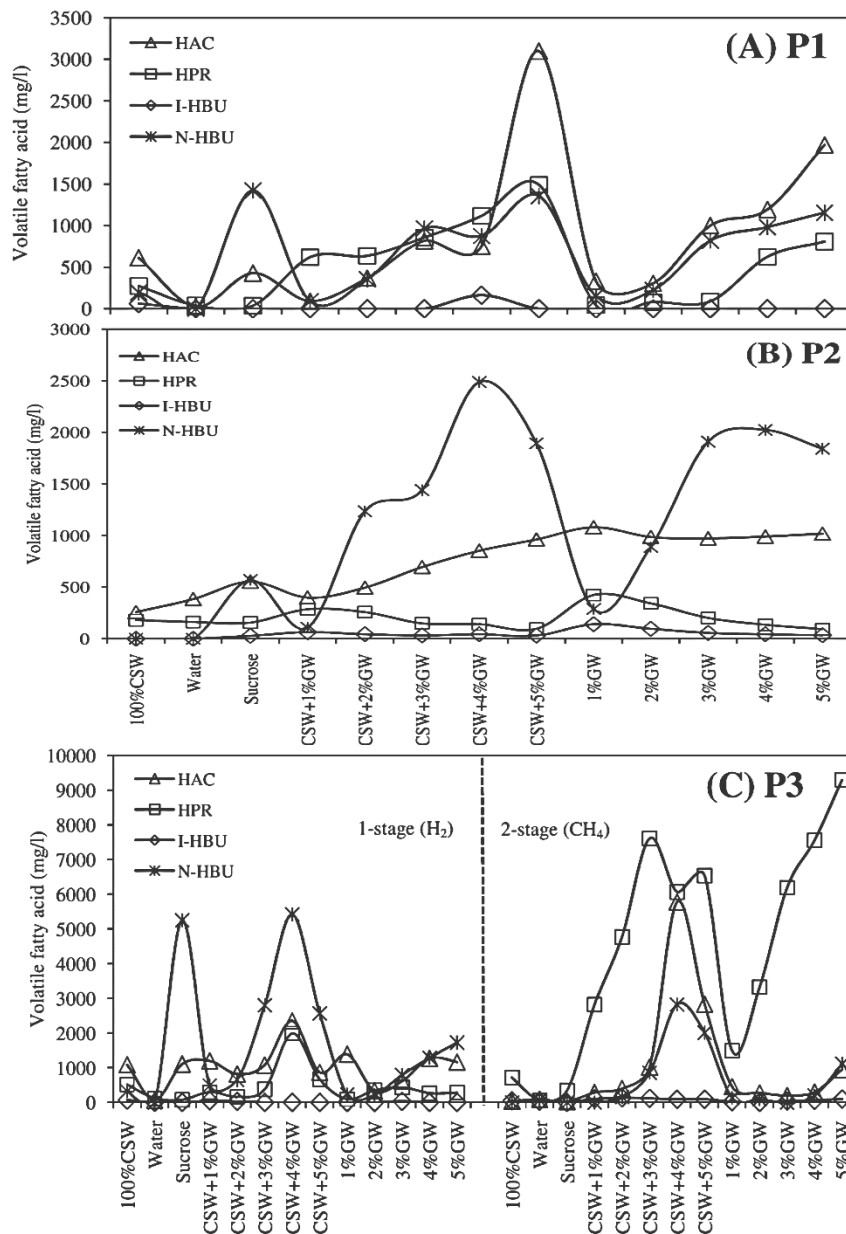


Figure 3. Volatile fatty acid profile; (A) P1 process, (B) P2 process and (C) P3 process

For the P3 two-stage AD process, the increase in the concentration of VFAs followed the increase in the concentration of COD by adding the GW ranging from 1-5% (v/v). In the first fermentation stage with 4% of GW co-digested with CSW having the maximum hydrogen production yield of 43.00 ml-H₂/g-COD_r, the main composition of VFA at 3 days was contained 5,420.53 mg/l N-butyric acid, 2,360.54 mg/l acetic acid and 1,990.05 mg/l propionic acid (Figure 3C). Using the GW as a co-substrate in anaerobic co-digestion for hydrogen production was suitable since hydrogen was generated along with only the formation of N-butyric acid and acetic acid. Other metabolites generated could reduce hydrogen production. Furthermore, the formation of propionic acid could cause a severe reduction in biohydrogen production because propionic acid formation consumes hydrogen previously produced [1]. Sreethawong et al. [23] reported that propionic acid formation should be avoided to improve biohydrogen production. Additionally, the final pH in all co-digestions had pH values ranging from 5.20-5.90 (Figure 4(C)), which corresponded to the experiment of Lue et al. [24] reporting hydrogen production decreased with an increase in pH of more than 6. The effluent from the 1-stage was subsequently digested in the second stage process for methane production. The total VFA at

5 days of fermentation with 4% of GW was 14,756.93 mg/l, which contained 5,779.65 mg/l acetic acid, 6,061.11 mg/l propionic acids, 92.39 mg/l I-butyric acid and 2,823.85 mg/l N-butyric acid (Figure 3C, 5C). The VFA in P3 was generated in a higher concentration than in the P1 and P2 processes; however, the VFA accumulation in the P3 process was lower, corresponding to the final neutral pH (7.60-7.80) in all experiments. This is due to the system having good buffering capacity indicating a balance between acid producers and consumers (Figure 4C). Thus, methanogens in the second stage of P3 could adapt well to hydrogen effluent mainly containing VFA to produce methane higher than P1 and P2. Therefore, high VFA concentration (acetic, propionic, and butyric acid) is not problematic for producing methane for the P3 process.

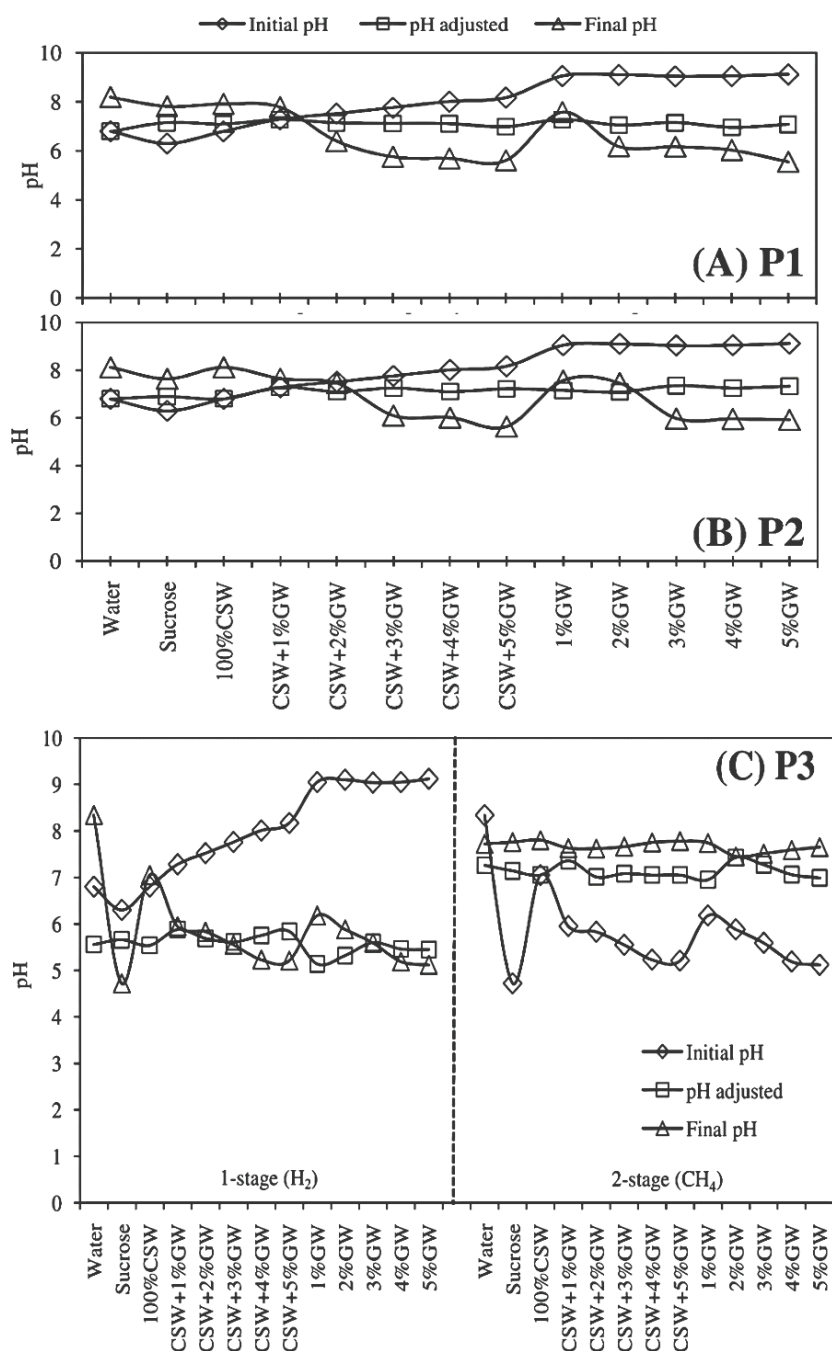


Figure 4. pH profile; (A) P1 process, (B) P2 process and (C) P3 process

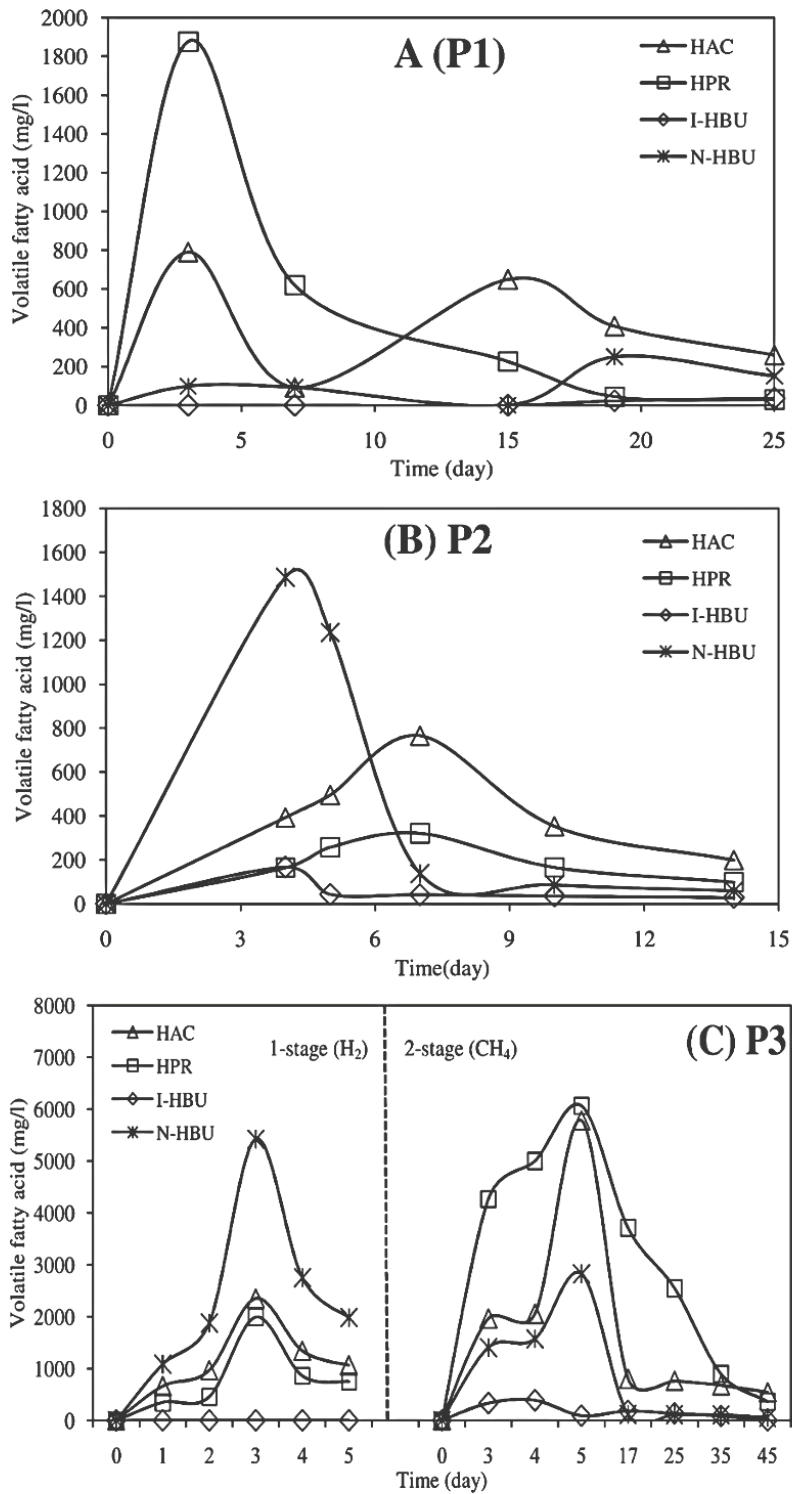


Figure 5. Comparison of the volatile profile under the optimal condition by co-digestion of CSW and GW at different operating processes; (A) P1 process (CSW+1%GW), (B) P2 process (CSW+2%GW), and (C) P3 process (CSW+4%GW)

3.4 Kinetic analysis under the optimal condition

Among three different process configurations, P3 is the best, having the maximum concentration of COD (70 g/l), resulting in maximum methane production. In the optimal condition of 3 processes, the methane

yield of P3 (CSW+4%GW) is 1.19 and 1.24 fold of P2 (CSW+2%GW) and P1 (CSW+1%GW), respectively. The maximum VFA was generated from 3 to 5 days in all processes during the methane production and on 3 days for fermentation to produce hydrogen. VFA generated is afterward used by methanogenic microorganisms to produce methane, resulting in continued VFA reduction in the systems, as shown in Figure 5. For P3, total VFA existing in the first stage was 3,794.21 mg/l consisting of 1,058.55 mg/l acetic acid, 750 mg/l propionic acid, and 1,985.66 mg/l N-butyric acids at 5 days of fermentation, while the second stage had total VFA 960.04 mg/l, containing 543.42 mg/l acetic acid, 360.51 mg/l propionic acid and 51.10 mg/l N-butyric acid at the end of batch operation day 45 as shown in Figure 5C. Additionally, single-digestion of CSW and co-digestion with GW could prove a synergistic effect is generated by adding GW for co-digestion to produce biogas in all processes. P3 could produce maximum methane production. The total energy yield from the P3 process was 11.33 m³ biohytanes/m³ mixed substrate. The biohythane composition in this study contained 43.11% CH₄, 21.45% H₂, and 35.43% CO₂. Mamin et al. [15] and Khongkliang et al. [25] reported that the composition of biohythane (hydrogen and methane) obtained from two-stage anaerobic digestion of palm oil mill effluent (POME) and starch processing effluent is 51% CH₄, 14% H₂, 35% CO₂, CH₄ is reported to be 55%, 10% H₂ and 35% CO₂. This is very similar to his H₂ composition results from this study, indicating that it is significantly lower. As a result, GW could increase the potential in hydrogen and methane production from CSW by using the P3 process. The result indicates that 2-stage anaerobic co-digestion with GW under mesophilic condition (P3) could enable it to operate under high VFA levels compared to the thermophilic condition, which has a higher cost in operation. So, P3 is one of the attractive choices for increasing the potential to produce hydrogen and methane in the canned sardine industry. Furthermore, the initial temperature of CSW is in the mid-temperature range, so operation in thermophilic conditions is not suitable for CSW.

For kinetic analysis, a modified Gompertz model was used to explain the biogas production. The parameters from the optimum process are summarized and compared with experimental and simulation results using the modified Gompertz model. The parameters from the optimum process are outlined in Table 2. Experimental and simulation results of the modified Gompertz model are shown in Figure 6. For the P3 process, the lag phase time (λ) is 3 days, lower than the 6.65 days of P1. The λ value in P3 is lower than P1, indicating the methanogen could adapt in the 2-stage AD process faster than that in the one-stage AD process under mesophilic conditions, resulting in a maximum methane yield (G_0) was high (303.40 ml CH₄/g COD_r), compared to P1(244.85). Additionally, the modified Gompertz model parameter for hydrogen production in P3 was 1.33 days of λ value and 42.83 ml H₂/g COD_r of G_0 value. In all cases, the maximum production rate (R_{max}) is 21.65, 30.58, and 5.80 ml CH₄/g COD_r-day for P1, P2, and P3, respectively. Although the R_{max} of P3 is significantly lower, the difference in COD loading and R_{max} could not be compared. However, although the P2 process has the smallest λ value (2.55 days), the advantage of P3 is that it could get COD loading higher, generate H₂ gas, and have less cost for heating compared to the P2 process. Thus, biogas production co-digested with GW and CSW under P3 mesophilic AD process is more interesting than P1 and P2 in improving biogas production potential from wastewater from the canned sardine industry. The coefficient of determination (R^2) was higher for the modified Gompertz model during 0.918-0.984 for methane production and 0.976 for hydrogen production, indicating that the modified Gompertz model could simulate satisfactorily for P1, P2, and P3 processes. Figure 7 shows the DGGE profiles of sludge from the 1-stage and 2-stage of the P3 process. The bacteria community structure in the first-stage reactor (H₂) is dominated by *Micrococcus sp.* and *Desulfovibrio sp.* (Figure 7A). Meanwhile, the archaea community in the 2-stage reactor (CH₄) is dominated by *Methanosaeta sp.*, *Methanoculleus sp.*, and *Methanosarcina sp.*, as shown in Figure 7B.

Table 2. The modified Gompertz model parameter values at various process

Process	modified Gompertz model parameter (H ₂)				modified Gompertz model parameter (CH ₄)			
	G ₀ (ml H ₂ /g CODr)	R _{max} (ml H ₂ /g CODr-day)	λ (day)	R ²	G ₀ (ml CH ₄ /g CODr)	R _{max} (ml CH ₄ /g CODr-day)	λ (day)	R ²
P1	-	-	-	-	244.85	21.65	6.65	0.957
P2	-	-	-	-	255.21	30.58	2.55	0.984
P3	42.83	1.25	1.33	0.976	303.40	5.80	3.00	0.918

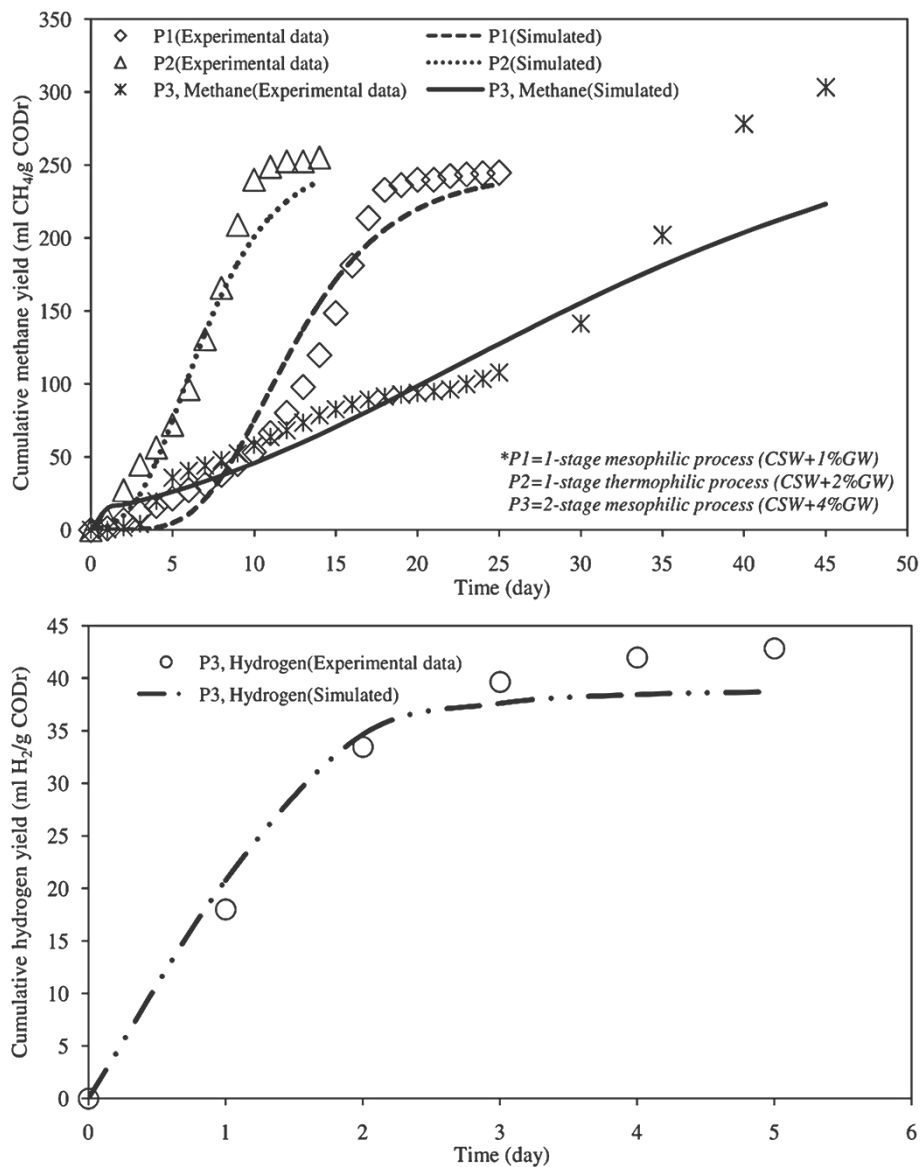


Figure 6. Comparison of the Cumulative methane and hydrogen yield between experimental data and simulation by modified Gompertz model

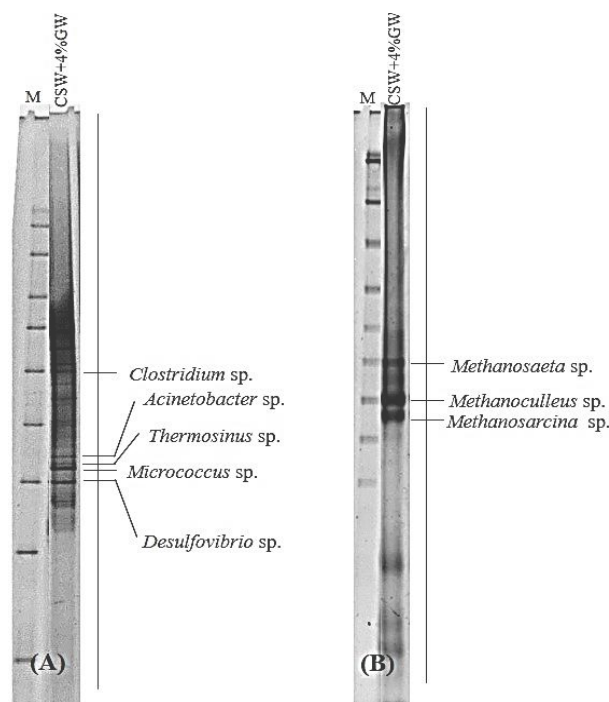


Figure 7. DGGE profiles of 16S rRNA gene fragments for sludge samples from the P3 process of CSW+4%GW, (A) 1- 1-stage fermentation and (B) 2-stage fermentation

4. Conclusions

The results show that two-stage anaerobic co-digestion (P3) with GW under mesophilic conditions can increase hydrogen and methane production by 648.57-fold and 7.75-fold, respectively, compared to CSW-only digestion. The optimal concentration of GW using co-substrate in the P3 process was 4%(v/v). The P3 can handle higher COD concentrations than processes P1 and P2, resulting in a higher organic loading rate (OLR) in the continuous system. So, the P3 process is one of the interesting choices for increasing the potential of hydrogen and methane production from canned sardine wastewater.

5. Acknowledgements

The authors would like to thank Professor Tsuyoshi Imai from the Graduate School of Science and Engineering, Yamaguchi University, Japan, for the opportunity to use the laboratory to do this research.

Author Contributions: Conceptualization, K.R.; methodology, T.S., and K.R.; formal analysis, T.S.; investigation, T.I.; writing—original draft preparation, K.R.; writing—review and editing, K.R.

Funding: The Energy Policy and Planning Office (EPPO) for funding this research.

Conflicts of Interest: The authors declare no conflict of interest.

References

- [1] Intanoo, P.; Chaimongkol, P.; Chavadej, S. Hydrogen and methane production from cassava wastewater using two-stage up-flow anaerobic sludge blanket reactors (UASB) with an emphasis on maximum hydrogen production. *Int J Hydrogen Energy*. **2016**, *41*, 6107-6114.
- [2] Zhang, Q.; Hu, J.; Lee, D.J. Biogas from anaerobic digestion process: Research updates. *Renew Energ*, **2016**, *98*, 108-119.
- [3] Ward, A.J.; Hobbs, P.J.; Holliman, P.J.; Jones, D.L. Optimisation of the anaerobic digestion of agricultural resources. *Bioresour Technol*. **2008**, *99*, 7928-7940.

- [4] Chowdhury, P.; Viraraghavan, T.; Srinivasan, A. Biological treatment processes for fish processing wastewater: A review. *Bioresour Technol.* **2010**, *10*, 439–449.
- [5] Pagliaccia, P.; Gallipoli, A.; Gianico, A.; Montecchio, D.; Braguglia, C.M. Single stage anaerobic bioconversion of food waste in mono and co-digestion with olive husks: Impact of thermal pretreatment on hydrogen and methane production. *Int J Hydrogen Energy.* **2016**, *41*, 905-915.
- [6] Da Silva, C.; AstalSiles, S.; Peces, M.; Campos, J.L.; Guerrero, L. Biochemical methane potential (BMP) test: reducing test time by early parameter estimation. *Bioresour Technol.* **2018**, *71*, 19-24.
- [7] Palenzuela-Rollon, A. *Anaerobic digestion of fish processing wastewater with special emphasis on hydrolysis of suspended solids*. London: Taylor and Francis, **1999**.
- [8] Chen, Y.; Cheng, J.J.; Creamer, K.S. Inhibition of anaerobic digestion process: A review. *Bioresour Technol.* **2008**, *99*(10), 4044-4064.
- [9] Yenigun, O.; Demirel, B. Ammonia inhibition in anaerobic digestion: A review. *Process Biochem.* **2013**, *48*, 901-911.
- [10] Rivero, M.; Solera, R.; Perez, M. Anaerobic mesophilic co-digestion of sewage sludge with glycerol: Enhanced biohydrogen production. *Int J Hydrogen Energy.* **2014**, *39*, 2481-2488.
- [11] Vasquez, J.; Nakasaki, K. Effects of shock loading versus stepwise acclimation on microbial consortia during the anaerobic digestion of glycerol. *Biomass and Bioenerg.* **2016**, *86*, 129-135.
- [12] Kalia, V.C.; Prakash, J.; Houli, S. Biorefinery for glycerol rich biodiesel industry waste. *Indian J Microbiol.* **2016**, *53*(2), 113-125.
- [13] O-Thong, S.; Hniman, A.; Prasertsan, P.; Imai, T. Biohydrogen production from cassava starch processing wastewater by thermophilic mixed cultures. *Int J Hydrogen Energy.* **2011**, *36*, 3409-3416.
- [14] Akyol, C.; Aydin, S.; Ince, O.; Ince, B. A comprehensive microbial insight into single-stage and two-stage anaerobic digestion of oxytetracycline-medicated cattle manure. *Chem. Eng. J.* **2016**, *303*, 675–684.
- [15] Mamimin, C.; Singkhlala, A.; Kongjan, P.; Suraraksa, B.; Prasertsan, P.; Imai, T.; O-thong, S. Two-stage thermophilic fermentation and mesophilic methanogen process for biohydrogen production from palm oil mill effluent. *Int J Hydrogen Energy.* **2015**, *40*, 6319-6328.
- [16] Kafle, G.K.; Kim, S.H.; Sung, K.I. Ensiling of fish industry waste for biogas production: A lab-scale evaluation of biochemical methane potential (BMP) and kinetics. *Bioresour Technol.* **2013**, *127*, 326–336.
- [17] Konjan, P.; O-Thong, S.; Angelidaki, I. Performance and microbial community analysis of two-stage process with extreme thermophilic hydrogen and thermophilic methane production from hydrolysate in UASB reactors. *Bioresour Technol.* **2011**, *102*, 4028-4035.
- [18] Altschul, S.F.; Madden, T.L.; Schäffer, A.A.; Zhang, J.; Zhang, Z.; Miller, W.; David, J.; Lipman, D.J. Gapped BLAST and PSI-BLAST: a new generation of protein database search programs. *Nucleic Acids Res.* **1997**, *25*, 3389–3402.
- [19] APHA. Standard methods for the examination of water and wastewater. 21th ed. Washington DC: USA, **2012**.
- [20] Tian, H.L.; Duan, N.; Lin, C.; Li, X.; Zhong, M.Z. Anaerobic co-digestion of kitchen waste and pig manure with different mixing ratios. *J Biosci Bioeng.* **2015**, *1205*, 1-57.
- [21] Angelidaki, I.; Ellegaard, L. Co-digestion of manure and organic wastes in centralized biogas plants, status and future trends. *Appl Biochem Biotech.* **2003**, *109*, 95-105.
- [22] Switzenbaum, Michael, S.; Eugenio, G.G.; Robert, F.H. Monitoring of the anaerobic methane fermentation process. *Enzyme and Microbial Technology.* **1990**, *12*(10), 722-730.
- [23] Franke-Whittle, I.; Walter, A.; Ebner, C.; Insam, H. Investigation into the effect of high concentrations of volatile fatty acids in anaerobic digestion on mechanic communities. *Waste Manage.* **2014**, *34*, 2080-2089.
- [24] Sreethawong, T.; Chatsirawatana, S.; Rangsuwijit, P.; Chavadej, S. Hydrogen production from cassava wastewater using anaerobic sequencing batch reactor: Effects of operational parameter, COD: N ratio, and organic acid composition. *Int J Hydrogen Energy.* **2010**, *35*, 4092-4102.
- [25] Luo, G.L.; Xie, L.; Zou, Z.; Zhou, Q.; Wang, J.Y. Fermentation hydrogen production from cassava stikkage by mixed anaerobic microflora: Effect of temperature and pH. *Appl Energ.* **2010**, *87*, 3710-3717.
- [26] Khongkhiang, P.; Kongjan, P.; O-Thong, S. Hydrogen and methane production from starch processing wastewater by thermophilic two-stage anaerobic digestion. *Energ Procedia.* **2015**, *79*, 827-832.



Characterization and Development of Venipuncture Practice Rubber Model Based for BCG Economy Framework

Keerakarn Somsuan^{1*}, Siripat Aluksanasuwan², Atthapan Morchang³, Arunothai Wanta⁴, Sittiporn Punyanitya⁵

¹ Cancer and Immunology Research Unit, School of Medicine, Mae Fah Luang University, Muang, Chiang Rai, 57100, Thailand; keerakarn.som@mfu.ac.th

² Cancer and Immunology Research Unit, School of Medicine, Mae Fah Luang University, Muang, Chiang Rai, 57100, Thailand; siripat.alu@mfu.ac.th

³ Cancer and Immunology Research Unit, School of Medicine, Mae Fah Luang University, Muang, Chiang Rai, 57100, Thailand; atthapan.mor@mfu.ac.th

⁴ Cancer and Immunology Research Unit, School of Medicine, Mae Fah Luang University, Muang, Chiang Rai, 57100, Thailand; arunothai.wan@mfu.ac.th

⁵ Innovative Biomaterials and Medical Device Research Group, School of Medicine, Mae Fah Luang University, Muang, Chiang Rai, 57100, Thailand; punyanitya.s@gmail.com

* Correspondence: keerakarn.som@mfu.ac.th

Citation:

Somsuan, K.; Aluksanasuwan, S.; Morchang, A.; Wanta, A.; Punyanitya, S. Characterization and development of a venipuncture practice rubber model based on the BCG economy framework. *ASEAN J. Sci. Tech. Report.* **2024**, *27*(2), 14-20. <https://doi.org/10.55164/ajstr.v27i2.250650>

Article history:

Received: August 23, 2023

Revised: December 16, 2023

Accepted: January 11, 2024

Available online: February 1, 2024

Publisher's Note:

This article is published and distributed under the terms of Thaksin University.

Abstract: The Bio-Circular-Green (BCG) economy framework, which integrates economic, social, and environmental aspects for waste management, holds great promise for fostering growth across various sectors in Thailand. Venipuncture, a critical medical procedure, can lead to complications if not performed correctly. This study uses Thailand para latex resources and calcium carbonate extracted from recycled mollusk shells to develop an educational innovation model for venipuncture procedures. Natural rubber latex (NRL) was obtained from Chiang Rai, Thailand. Preserved latex was heated to obtain 60% concentrated latex, then combined with a sulfur solution, and calcium carbonate powder was added in various ratios. Molding used a specialized mold replicating anatomical features of the antecubital fossa, incorporating three prominent veins. The venipuncture practice rubber model was characterized for pH, moisture content, water absorption, tensile strength, and other properties. The model exhibited neutral pH, low moisture content, and notable resistance and elasticity. This study promotes the sustainable utilization of natural latex resources and recycled mollusk shells in developing innovative medical models within the BCG framework. Additional research is required to enhance the human friendliness and realism of the rubber material used in the venipuncture practice model.

Keywords: Latex; Mollusk shells; Para rubber; Practice model; Venipuncture.

1. Introduction

A Bio-Circular-Green (BCG) economy is a holistic framework that integrates the economic, social, and environmental aspects of production and consumption to implement a waste management system involving self-sustaining cycle strategies (reduction, reuse, and recycling). The BCG model is particularly relevant for Thailand as it promotes efficient utilization of natural resources by focusing on five developing sectors: food, healthcare, sustainable energy, tourism, and the creative economy [1]. The development of medical technologies and procedures continues to improve patient care, management,



and healthcare outcomes [2]. Venipuncture is an invasive technique by healthcare professionals that involves either drug administration or extracting blood from a patient [3]. Poor practices of venipuncture lead to a higher risk of complications, including infection [4], nerve injury [5], and the formation of hematomas [6]. Among these complications, hematoma formation is the most commonly observed issue [6]. Previous studies have been conducted to develop a rubber arm with a fluid system for venipuncture training, aiming to enhance the effectiveness of blood drawing for medical science and nursing students. This innovation can assist students in performing the procedure with confidence by providing a better understanding of the steps involved [7, 8]. The results showed that 72.62% of students appreciated learning the procedure using an artificial arm before performing blood collection from patients [7]. Synthetic polymers for venipuncture practice offer precise structures and customizable properties. However, they can be costly and potentially skin-irritating due to chemical release. Conversely, natural polymers like natural rubber exhibit enhanced biocompatibility. These materials have gained value for artificial blood vessels and muscles due to their beneficial properties when engineered correctly. Therefore, this study utilizes Thailand's para-rubber resources and recycled mollusk shells to develop an innovative educational model for venipuncture procedures. Additionally, we aim to explore the characterization of the para-rubber model and design an initial prototype of a venipuncture model to enhance comprehensive medical education techniques.

2. Materials and Methods

2.1 Materials

The natural rubber latex (NRL) was obtained from Chiang Rai, Thailand. Commercial-grade sulfur, sodium hydroxide, zinc oxide, and methyl paraben were purchased from World Chemical Far East Co., Ltd., Chiang Mai, Thailand. Calcium carbonate was acquired from mollusk shells. The composition includes latex as the primary component, sulfur as the vulcanizing agent, ZnO as an accelerator, and NaOH and paraben as additives. Additionally, CaCO₃ functions as a reinforcing agent.

2.2 Preparation of calcium carbonate from mollusk shells

The fresh mollusk shells were washed with water and soaked in a 50% concentrated H₂O₂ solution for 5 days. The shells obtained were then washed, followed by a 10-day soak in a 20% w/v sodium hydroxide solution. Subsequently, the soaked shells were rinsed with water until they reached a near-neutral pH and dried at 120°C for 16 hours. Afterward, the dried shells were ground using a ball mill for 14 hours and filtered through a 150-mesh sieve to separate coarse and fine powder. The resulting coarse powder underwent multiple cycles of soaking in NaOH solution, drying, and grinding for refinement.

2.3 Preparation of the para rubber

Preserved latex was heated to 85°C for 3 hours to obtain 60% concentrated latex. A 2% w/v sulfur solution was prepared using a 1:1:1 ratio of sulfur, sodium hydroxide, and distilled water and heated at 90°C for 50 minutes. This solution was mixed with the concentrated latex and stirred at 80°C for 30 minutes. Calcium carbonate powder from mollusk shells, particle sizes of 50 to 100 microns, was dispersed in the rubber solution in ratios of 80:20, 70:30, and 60:40. The resulting suspension was stirred at 80°C for 40 minutes. Zinc oxide and methylparaben were added at a concentration of 2 wt% each. After neutralization, the mixture was well mixed at 70°C for 20 minutes. After being placed into molds, the mixes were dried at 70°C for 48 hours and then vulcanized at 140°C for 2 hours after removal from the mold. Subsequently, the rubber model underwent characterization, determination, and the construction of prototypes before the trial phase. A diagram of methods is represented in Figure 1.

2.4 Molding and shaping of the venipuncture practice rubber model.

The venipuncture practice rubber model's molding and shaping process involved using a carefully designed mold that replicated the anatomical features of the antecubital fossa, situated on the anterior aspect of the elbow, complete with veins and skin texture. Three prominent veins were inserted on the model within

this area: the cephalic, median cubital, and basilic veins [3]. During the next step, the rubber compound was poured into the mold, followed by subjecting the mold to a controlled curing process. This curing process facilitated the solidification of the rubber compound into the intended shape, resulting in a highly realistic and anatomically accurate representation suitable for venipuncture training (Figure 1).

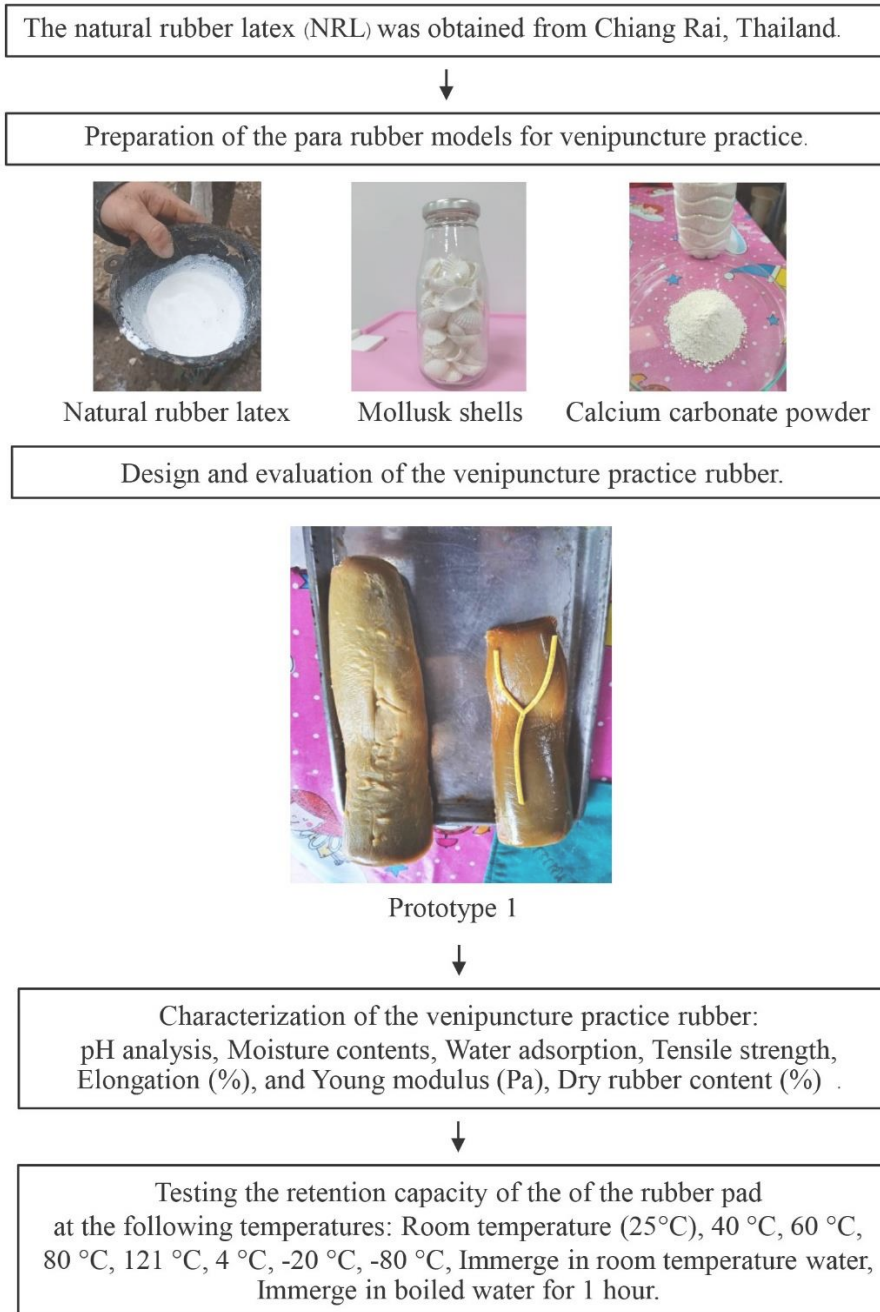


Figure 1. Diagram of developing and characterization of the venipuncture practice rubber model.

2.5 Characterization of the venipuncture practice rubber model

2.5.1 pH analysis

The pH values of the samples were determined using a waterproof pH spear tester (Oakton pH Spear Waterproof Pocket Tester EW-35634-40-Pro, Singapore). The measured ranges ranged from -1 to 15, with a

resolution of 0.01, and the accuracy was within ± 0.01 . Each sample was measured five times, and data were collected to calculate the average values.

2.5.2 Determination of moisture contents

The moisture content was determined using a moisture analyzer (PMB 53, ADAM, Singapore). The samples, weighing approximately 1 to 2 g with a resolution of 0.01% and sensitivity of 0.1 mg, were placed on the moisture analyzer and subjected to temperatures of 0-50°C for 4 minutes. Each sample was tested five times, and data was collected to calculate the average values.

2.5.3 Measurement of water adsorption

The samples were all precisely weighed (W_1) and immersed in distilled water for 24 hours at room temperature. The swollen samples were removed, and the excess water was taken off the surface. Then, the swollen samples were reweighed (W_2). The percent water adsorption of the samples was calculated using the following equations:

$$\text{Water adsorption (\%)} = (W_2 - W_1) / W_1 \times 100$$

2.5.4 Testing of tensile strength, elongation (%), and Young modulus (Pa)

The Universal Material Testing Machine (Instron 5569, US) and ASTM D638M-93 were used to test tensile strength, elongation (%), and Young modulus (Pa) with a 60N load cell. The sample size was 110 × 20 mm. The crosshead speed was set to 5 mm/min. Each sample was tested at least five times in parallel.

2.5.5 Determination of dry rubber content (%)

The dry rubber content of rubber latex was measured following the standard method of ISO 126:2005.

2.6 Assessment of the retention capacity of the rubber pad of the venipuncture practice rubber model

The rubber model was then cut into uniform square shapes. Before commencing the experiment (pre-incubation), the weight and volume of each rubber pad were measured with three repetitions for accuracy. Subsequently, the rubber pads were incubated at different temperatures: ambient room temperature (25°C), 40°C, 60°C, 80°C, 121°C, 4°C, -20°C, -80°C, room temperature water, and boiled water. Each point was incubated for one hour (incubation), and the weight and volume of each rubber pad were measured with three repetitions. Following the temperature incubation phase, the rubber samples were allowed to stabilize at room temperature for one hour (post-incubation), after which their weight and volume were measured, again in triplicate.

3. Results and Discussion

3.1 Characterization of the venipuncture practice rubber model

The physiochemical and mechanical properties of the venipuncture practice rubber model are shown in Table 1. The pH values of the venipuncture practice rubber model were 7.92 ± 0.15 . The pH value was neutral and did not cause skin irritation while being used. The percentage of moisture content value was $0.14 \pm 0.05\%$, indicating that there would be only minimal bacterial growth. The recorded water absorption was $9.12 \pm 0.02\%$, owing to the formation of pores during the preparation of the rubber compound. After the drying procedure, the sample underwent a controlled evaporation process that led to the residual presence of porous regions, thereby giving rise to the occurrence of closed or open pores. Calcium carbonate was added to increase the hardness and tensile strength of the venipuncture practice rubber model (2.54 ± 0.054 MPa). The elongation, Young modulus, and dry rubber content values were $669.5 \pm 1.94\%$, 1.51 ± 0.35 Pa, and 36.37%, respectively. Sulfur increased the hardness of the rubber, and zinc oxide was the catalyst for the cross-linking reaction. These chemical combinations helped the rubber to have less stretch and higher resistance to tensile strength. It confirmed that the dry rubber content of the sample met the quality criteria of field latex. According to a previous study, natural latex had remarkable mechanical characteristics because of its distinctive hierarchical structures, including strong tensile and tear strength, high cracking growth resistance, good elasticity, and low heat buildup. Natural rubber latex particles have a core-shell structure consisting of a polyisoprene hydrophobic core encircled by either a layer of mixed proteins and phospholipids or a layer of lipid monolayers below a protein monolayer [9]. Our results indicated that para rubber is suitable for developing rubber materials used in venipuncture practice.

Table 1. Characterization of the venipuncture practice rubber model.

Physiochemical and mechanical properties	Venipuncture practice Rubber
pH	7.92 ± 0.15
Moisture content (%)	0.14 ± 0.05
Water adsorption (%)	9.12 ± 0.02
Tensile strength (MPa)	2.54 ± 0.054
Elongation (%)	669.5 ± 1.94
Young modulus (Pa)	1.51 ± 0.35
Dry rubber content (%)	36.37

After molding and shaping the venipuncture practice rubber model, the artificial blood was poured into the tubes embedded in the model. We successfully drew artificial blood from the venipuncture practice rubber model in the conducted trials phase. However, it should be noted that this study was a preliminary investigation of the characteristics of the rubber model. The study of qualification and satisfaction surveys to align with human friendliness, realism, and a lifelike blood collection simulation mimicking practical human situations should be investigated in further study.

3.2 The retention capacity of the rubber pad of the venipuncture practice rubber model

The gross appearance of the rubber pad did not change after incubation in different temperature environments (Figures 2 and 3). However, the venipuncture pad changed to a pale color and became bloated when exposed to a temperature of 121°C and immersed in boiled water (Figures 2 and 3). The weight and volume of the rubber pad remained unchanged across the various incubation time points (pre-incubation, incubation, and post-incubation) under different temperature exposures, except for incubation of rubber in boiled water (> 200 °C) (Figures 4A and 4B). The rubber pad displayed a notable retention capacity and returned to its original state after exposure to various temperatures. As seen in previous studies, the hyperelastic mechanical response and deformation of rubber were influenced by temperature [10, 11]. In Thailand, rubber models used for medical and health studies were frequently employed in challenging environments with varying temperatures. Fluctuations in temperature due to seasonal changes can lead to significant changes and deformity of the mechanical characteristics of rubber, especially in the summer. Consequently, the effects of temperature on the mechanical properties of the rubber model should be a significant point of concern in developing the rubber model. Understanding how weight and volume change with temperature variations would help refine the model's design and manufacturing, ensuring optimal performance and quality during use. A limitation of our study was the lack of a scanning electron microscope to further examine the mechanical properties and fracture mechanism of rubber pads under different temperature exposures.

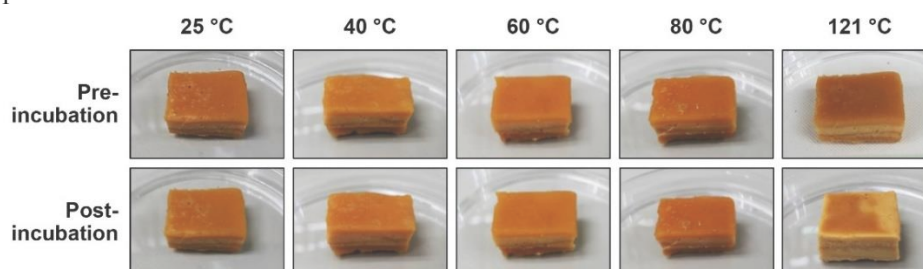


Figure 2. Testing the retention capacity of the rubber pad at various temperatures: 25°C, 40 °C, 60 °C, 80 °C, 121 °C, before and after incubation for 1 hour.

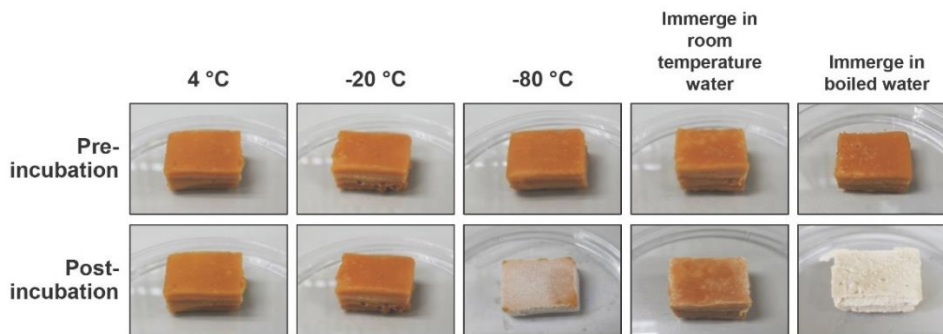


Figure 3. Testing the retention capacity of the rubber pad at various temperatures: 4 °C, -20 °C, -80 °C, after immersion in room temperature water, in boiled water, before and after incubation for 1 hour.

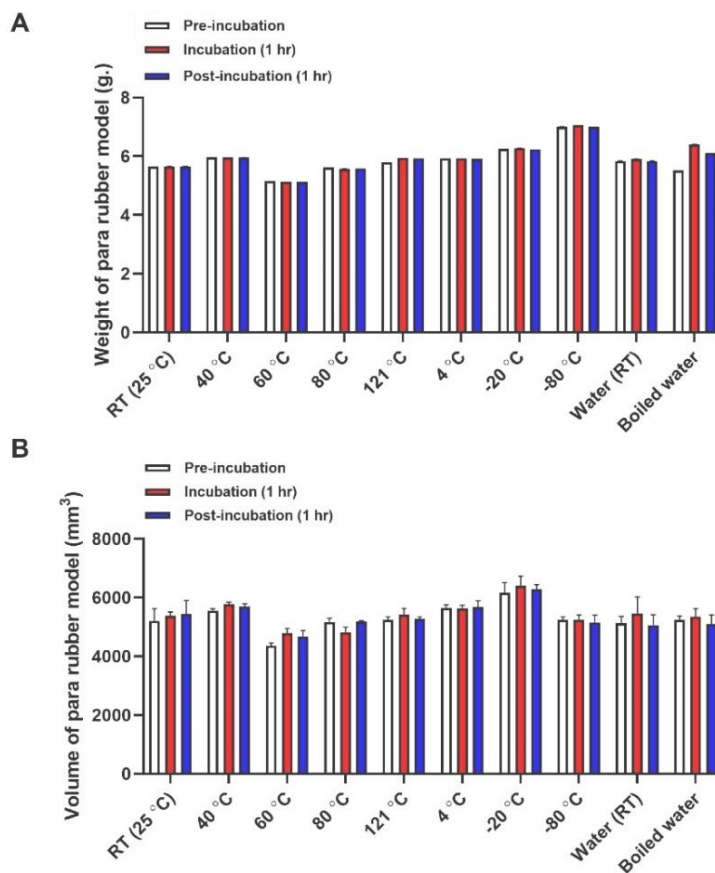


Figure 4. The graph of weight and volume changes of the rubber pad at various temperatures (A and B). Pre-incubation means the initiation time point that measures the weight and volume of the rubber pad. Incubation means the time after incubating the rubber pad at various temperatures for 1 hour (hr.). The rubber pad was then measured to establish its weight and volume. Post-incubation means the time after incubation, leaving the rubber pad at room temperature for 1 hour (hr.) and immediately measuring its weight and volume—RT; room temperature.

4. Conclusions

In conclusion, the venipuncture practice rubber model was characterized by favorable physiochemical and mechanical properties. The model exhibited neutral pH, low moisture content, and notable resistance and elasticity. The model's retention capacity was evident, maintaining its weight and volume across varying temperatures, except for exposure to extreme conditions. Our research suggested that para rubber can create materials specifically for venipuncture procedures. However, this study needs further improvement to enhance human friendliness and realism, aligning the model more closely with lifelike blood collection simulations in practical scenarios.

5. Acknowledgements

The School of Medicine, Mae Fah Luang University, supported all facilities and resources. We want to thank Dr. Roger Timothy Callaghan, MD., from the UK, for his assistance with English language preparation.

Author Contributions: Conceptualization, K.S. and S.B.; methodology, K.S., and S.B.; validation: K.S. and S.B.; formal analysis, K.S. and S.B.; investigation, K.S., S.A., A.M., A.W. and S.B.; resources, S.B.; data curation, K.S.; writing—original draft preparation, K.S. and S.B.; writing—review and editing, K.S.; visualization, K.S.; supervision, S.B.; funding acquisition, S.B. All authors have read and agreed to the published version of the manuscript.”

Funding: This research received no external funding.

Conflicts of Interest: The authors declare no conflict of interest.

References

- [1] Cheng, H.Y.; Lu, C.Y.; Huang, L.M.; Lee, P.I.; Chen, J.M.; Chang, L.Y. Increased frequency of peripheral venipunctures raises the risk of central-line associated bloodstream infection in neonates with peripherally inserted central venous catheters. *Journal of Microbiology, Immunology and Infection*. **2016**, *49*(2), 230-236. <https://doi.org/https://doi.org/10.1016/j.jmii.2014.06.001>
- [2] Edyvean, R.G.J.; Apiwatanapiwat, W.; Vaithanomsat, P.; Boondaeng, A.; Janchai, P.; Sophonthammaphat, S. The Bio-Circular Green Economy model in Thailand-A comparative review. *Agriculture and Natural Resources*. **2023**, *57*(1), 51–64. <https://li01.tci-thaijo.org/index.php/anres/article/view/258253>
- [3] Fu, X.; Wang, Z.; Ma, L.; Zou, Z.; Zhang, Q.; Guan, X. Temperature-Dependence of Rubber Hyperelasticity Based on the Eight-Chain Model. *Polymers*. **2020**, *12*(4), 932. <https://doi.org/10.3390/polym12040932>
- [4] Horowitz, S.H. Venipuncture-Induced Nerve Injury. *Journal of Neuropathic Pain & Symptom Palliation*. **2005**, *1*(1), 109-114. https://doi.org/10.3109/J426v01n01_17
- [5] Jarintanan, F.; Chanprasert, K.; kongwan, W.; Ratanawiboolsook, N.; Pawinwongcha, J.; Liemmanee, W. Rubber arm with fluid system for venipuncture training, new model in clinical skills tutors. *Progress in Applied Science and Technology*. **2016**, *6*(1), 212-220. <https://ph02.tci-thaijo.org/index.php/past/article/view/243173>
- [6] Kimori, K.; Konya, C.; Matsumoto, M. Venipuncture-Induced Hematomas Alter Skin Barrier Function in the Elderly Patients. *SAGE Open Nursing*. **2018**, *4*, 2377960818782050. <https://doi.org/10.1177/2377960818782050>
- [7] Lew, K. 3.05 - Blood Sample Collection and Handling. In J. Pawliszyn (Ed.), *Comprehensive Sampling and Sample Preparation* (pp. 95-121). Academic Press. **2012**, <https://doi.org/https://doi.org/10.1016/B978-0-12-381373-2.00068-5>
- [8] Rey, T.; Chagnon, G.; Le Cam, J.B.; Favier, D. Influence of the temperature on the mechanical behaviour of filled and unfilled silicone rubbers. *Polymer Testing*. **2013**, *32*(3), 492-501. <https://doi.org/10.1016/j.polymertesting.2013.01.008>
- [9] Saengpayab, Y.; Kongsri, W.; Chongsereechooen, E.; Pratummasoot, N.; Akkarapattanapong, V.; Jarintanan, F. Venipuncture training assists using electrical sensors in a rubber arm system. *Journal of Physics: Conference Series*. **2021**, *1719*(1), 012025. <https://doi.org/10.1088/1742-6596/1719/1/012025>
- [10] Thimbleby, H. Technology and the future of healthcare. *J Public Health Res*. **2013**, *2*(3), e28. <https://doi.org/10.4081/jphr.2013.e28>
- [11] Wei, Y.; Zhang, H.; Wu, L.; Jin, L.; Liao, S. A review on characterization of molecular structure of natural rubber. *MOJ Poly Sci*. **2017**, *1*(6), 197-199. <https://doi.org/10.15406/mojps.2017.01.00032>



Pyrolysis of Latex Sediment from Concentrated Latex Industry and Properties of Pyrolytic Products

Fareeda Wongdaeng^{1,5,6}, Saowapa Chotisuwan^{2,5}, Rattana Jariyaboon^{3,5}, and Prawit Kongjan^{4,5*}

¹ Faculty of Science and Technology, Prince of Songkla University, Pattani, 94000, Thailand; fareeda_b439@hotmail.com

² Faculty of Science and Technology, Prince of Songkla University, Pattani, 94000, Thailand; saowapa.c@psu.ac.th

³ Faculty of Science and Technology, Prince of Songkla University, Pattani, 94000, Thailand; rattana.sa@psu.ac.th

⁴ Faculty of Science and Technology, Prince of Songkla University, Pattani, 94000, Thailand; prawit.k@psu.ac.th

⁵ Bio-Mass Conversion to Energy and Chemicals (Bio-Mec) Research Unit, Faculty of Science and Technology, Prince of Songkla University, Pattani, 90112, Thailand

⁶ Topglove Technology Co.,Ltd. 188, Moo 5, Tambon Phangla, Amphur Sadao, Songkhla 90170, Thailand

* Correspondence: prawit.k@psu.ac.th

Citation:

Wongdaeng, F.; Chotisuwan, S.; Jariyaboon, R.; Kongjan, P. Pyrolysis of latex sediment from concentrated latex industry and properties of pyrolytic products. *ASEAN J. Sci. Tech. Report.* **2024**, *27*(2), 21-28. <https://doi.org/10.55164/ajstr.v27i2.250798>.

Article history:

Received: September 3, 2023

Revised: December 2, 2023

Accepted: January 11, 2024

Available online: February 1, 2024

Publisher's Note:

This article is published and distributed under the terms of the Thaksin University.

Abstract: Concentrated latex is an intermediate rubber product in Thailand. It is an important industry that generates income for the country and its southern region. The main products of the latex factory were concentrated latex and skim blocks. The industrial waste from the concentrated latex factory is called latex sediment. It appears to be a white mixed light-yellow sludge or a dark brown color, contains magnesium compounds, and phosphorus is an important element. Therefore, finding appropriate measures for rubber production and environmentally friendly industrial waste management is important. Therefore, this study investigates the pyrolysis of latex sediment as an alternative to industrial waste management. Pyrolysis of 100 g of latex sediment was performed at 300 °C, 500 °C, and 700 °C. From the experiment, it was found that the properties of the liquid product from the pyrolysis process at 500 °C were alkaline, with a pH of 9.45. However, acetic acid was the highest amount of organic substance in the liquid product. Substances in the amine and amide groups were also observed, a base result for the liquid product exhibiting an alkaline value. The pH is an important factor in the decomposition of organic substances under anaerobic conditions. Therefore, a 1 wt% liquid product was used in a volume of 13.5 mL, which is the most appropriate amount because it uses the least amount of liquid product to adjust the alkalinity of the skim latex serum before entering the anaerobic fermentation system. Pyrolysis is an environmentally friendly option for managing factory latex sediments for sustainable production and creating a good image for the organization.

Keywords: Pyrolysis; Latex Sediment; Concentrated latex; Skim latex serum



1. Introduction

Thai rubber products will expand from 2021 to 2023 in line with the related industries likely to grow. In addition, exports of concentrated latex still have the opportunity to grow as demand from the world market expands. Concentrated latex is an intermediate rubber product in Thailand. This important industry generates income for the country and southern region [1]. Since 2003, Thailand has been the world's largest producer of natural rubber. In 2011, Thailand produced latex for the first time. Approximately 3.4 million tons of fresh latex is tapped and collected for processing into primary rubber

products such as concentrated latex, skim block rubber, and smoked rubber sheets. The primary rubber products are then processed into final rubber products such as condoms and gloves. The concentrated latex produced in Thailand is mostly exported to European countries, such as China, India, and Malaysia [2]. Concentrated latex is an intermediate rubber product in Thailand. The main products from the concentrated latex factory were concentrated latex and skim block rubber. Two types of waste are generated from the production processes of such rubber products.

1) Wastewater generated from the production of concentrated latex and skim blocks. The wastewater from both production processes is treated and collected into the wastewater treatment systems of all factories. During the anaerobic decomposition treatment process, biogas was produced, which needed to be disposed of by combustion at the flare system. It cannot be utilized as biofuel gas due to the low production rate of biogas and the high concentration of H₂S (20,000-50,000 ppm). Installing a biogas quality improvement system to eliminate H₂S is not cost-effective.

2) Waste from the production process of a factory is called latex sediment, which appears to be white, light-yellow, or dark brown sediment containing magnesium and phosphorus compounds as important elements. This is caused by adding chemicals to field latex in making latex concentrate, causing the magnesium ions in the latex to precipitate at the bottom of the tank. There are also organic and inorganic impurities, such as rubber, flour, dust, fat, protein, nitrogen compounds, and metal ions. The rate of latex sediment generation per ton of concentrated latex produced was calculated as a proportion of 0.6-50.0 kg latex sediment per ton of concentrated latex. Latex sediment is classified as a non-hazardous waste. It can be utilized directly as a raw material for improving soil or as latex sediment as a source of magnesium for plant growth [3]. The research study of [4] found that this latex sediment contains nitrogen, phosphorus, and potassium, which can be used as liquid and granular fertilizers. Alternatively, producing other materials for various uses could be further improved.

Since natural rubber and concentrated latex are majorly exported products of Thailand, information on sustainable production is necessary. Therefore, it is challenging for Thai rubber entrepreneurs to find appropriate measures to produce environmentally friendly rubber in many respects, including water pollution, odor problems, and industrial waste [2]. Latex sediment, an industrial waste, can be used for soil improvement. However, utilization of this latex sediment is not yet widespread. Therefore, the latex sediment generated by the company was granted permission to remain in the factory area while waiting to be transported to the fertilizer producers. As the production capacity of concentrated latex is likely to increase, the amount of latex sediment accumulates increasingly in the company's area. Therefore, improper management of latex sediment may cause increased pollution due to various microbial groups' biodegradation of organic substances in latex sediment. Waste management for maximum benefit and environmental friendliness is necessary for the concentrated latex industry to achieve sustainable production.

This study aimed to investigate the pyrolysis of latex sediment from concentrated latex industries and studied the alkalinity adjustment of skim latex serum from the skim block production process with liquid products from the pyrolysis process.

2. Materials and Methods

2.1 Material preparation

Latex sediment was collected from a concentrated latex industry in Songkhla Province, Thailand. The samples were pre-treated by drying at 105 °C for 24 h. [5] All chemicals in this work were of analytical grade and used without further purification.

2.2 Pyrolysis method

The equipment was set up according to the schematic diagram of the pyrolysis system shown in Figure 1. Initially, 100 g of the pre-treated sample was placed in a furnace tube and then heated for 1 h at 300 °C, 500 °C, and 700 °C. The system was operated at a heating rate of 20 °C/min, nitrogen gas flow of 1 L/min, as shown in Table 1, and a controlled cooling bath at 4 °C cooling temperature. The condensed pyrolysis liquid was collected using a glass liquid collector equipped with a condenser.

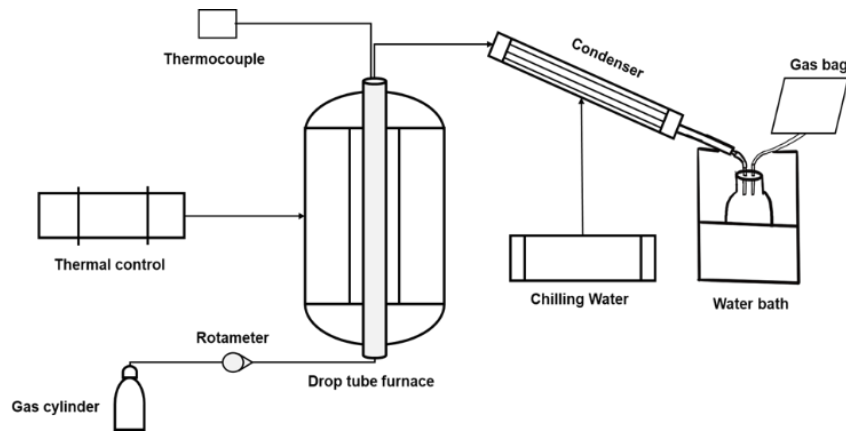


Figure 1. Schematic diagram of the pyrolysis system.

Table 1. Condition of pyrolysis process.

Conditions	Temperature (°C)		
	300	500	700
Initial sample (g)	100	100	100
Reaction time (hr.)	1	1	1
Heat rate (°C /min)	20	20	20
Flow rate (L/min)	1	1	1

2.3 Characterization method

The composition of the latex sediment before pretreatment was analyzed for moisture, total solids, volatile solids, and ash content, as shown in Table 2.

Table 2. Latex sediment composition analysis.

Parameter	Analytical methods/Equipment
Moisture	ASTM Standard D 3173-11
Total Solid (TS)	APHA, AWWA and WEF (1998)
Volatile Solid (VS)	APHA, AWWA and WEF (1998)
Ash Content	ASTM Standard D 3174-12

The pyrolytic liquid product was analyzed for pH, chemical oxygen demand (COD), and chemical compounds, as shown in Table 3. This work analyzed the chemical compounds using a gas chromatograph-mass spectrometer (7890B) and a mass spectrometer (5977AMSD), Agilent, USA.

Table 3. The pyrolytic liquid product analysis.

Parameter	Analytical methods/Equipment
COD (g/l)	ASTM Standard D 7544-12
pH	ASTM Standard D 7544-12
Chemical compound	ASTM Standard D 3173

2.4 The pyrolytic liquid product application

The pyrolytic liquid product was used to adjust the pH of skim latex serum before entering the wastewater treatment system, as shown in Table 4. The experiment began with pyrolytic liquid product samples were prepared by diluting with distilled water at concentrations of 1%, 3%, and 5%, and then used as a titrant in skim latex serum titration to determine the appropriate amount of liquid product for pH adjustment. Skim latex serum samples were prepared by adding sulfuric acid to 1000 g of skim latex to coagulate rubber. The rubber was then separated from skim latex serum.

Table 4. Experiment on skim latex serum pH adjustment.

Pyrolytic product	Vol. of skim latex serum (mL)	pH final
1% Liquid product	100	6.8
3% Liquid product	100	6.8
5% Liquid product	100	6.8

3. Results and Discussion

3.1 Composition of latex sediment

Sample of latex sediment from a concentrated latex factory in Songkhla Province. The two points where latex sediment was collected are the sludge sump pit and latex sediment collection area. The sludge sump pit collects latex sediment from the fresh latex receiving process and concentrated latex production department. The latex sediment was a white light-yellow solid. There is high moisture because the washing water from the production process flows into the pond at all times, as shown in Figure 2. The latex sediment was generated by adding ammonia to the latex field. This causes Mg to precipitate after leaving the latex overnight. The other part is from the centrifuge or disc centrifuge used to produce concentrated latex. The latex sediment collection area is wide open, with gutters around the storage area to accommodate latex sediment leachate and a pump system to transfer leachate into the factory wastewater treatment system. The latex sediment has less moisture because it is exposed to the sun, as shown in Figure 3.

**Figure 2.** Latex sediment from the sludge sump pit.**Figure 3.** Latex sediment from latex sediment collecting area**Table 5.** Compositions of latex sediment.

Parameter	Value	
	Sludge sump pit	Latex sediment collecting area
Moisture content (%w/w)	67.07 ± 3.78	62.78 ± 0.57
Total solid TS (%w/w)	38.20 ± 0.26	36.82 ± 0.14
Volatile solid VS (%w/w)	14.08 ± 0.14	14.40 ± 0.05
Ash (%w/w)	24.11 ± 0.18	22.42 ± 0.01

From Table 5, latex sediment from the concentrated latex production plant in January 2022 in the sludge sump pit had moisture, total solids, volatile solids, and ash content of the latex sediment equal to 67.07 (%w/w), 38.20 (%w/w), 14.08 (%w/w) and 24.11 (%w/w), respectively. Simultaneously, the latex sediment collecting area had moisture, total solids, volatile solids, and ash content of the latex sediment equal to 62.78 (%w/w), 36.84 (%w/w), 14.40 (%w/w) and 22.42 (%w/w), respectively. The experiment was able to criticize that latex sediment contained the least amount of volatile solids; therefore, the products obtained from pyrolysis had a low chance of being liquid and obtained the most solid product owing to the presence of inorganic substances as the main components in the latex sediment. At the latex sediment sampling site, the humidity of the latex sediment was higher in the sludge sump pit than in the latex sediment collecting area. Therefore, latex sediment in the latex sediment collection area is more appropriate for factory pyrolysis than latex sediment from the latex sediment storage tank.

3.2 Product yield

The pyrolysis experiments were conducted at different temperatures (300, 500, and 700 °C) for 1 h with a nitrogen gas flow rate of 1 L/min and a heating rate of 20 °C/min. The products have three phases: solid, liquid, and gas. The three product phases yielded unequal proportions at different temperatures. The products obtained by pyrolysis at various temperatures are listed in Table 6. Pyrolysis at 300 °C yielded the most solid product and the lowest amount of liquid products, 71 wt% and 19 wt%, respectively. Most of the gas obtained was nitrogen from the pyrolysis process. Pyrolysis at 500 °C showed that the highest amount of liquid product was 33 wt%, followed by 25 wt% at 700 °C. The liquid product obtained from pyrolysis was the main product required for this research. Therefore, the study of the conditions used in pyrolysis The most liquid product was sludge pyrolysis at 500 °C for 1 h.

Table 6. Product yield of pyrolysis of latex sediment at difference temperatures.

Temperature °C	Sample (g)	Product yields (wt%)		
		Solid product	Liquid product	Syngas
300	100.29 ± 0.08	71.39 ± 1.05	19.05 ± 0.34	9.85 ± 0.84
500	100.39 ± 0.14	56.58 ± 0.48	32.86 ± 0.74	10.95 ± 0.66
700	100.99 ± 0.07	47.94 ± 0.53	25.39 ± 0.65	27.66 ± 1.21

3.3 Properties of the pyrolytic liquid product

The liquid from the pyrolysis at 500 °C was a dark brown solution with a pungent odor. There were two layers: an aqueous phase and an organic phase. Some properties are shown in Table 7 and Figure 4. The pH value in this study was 9.45. This contradicts the research of [6] and [7], in which liquid products were acidic with pH equal to 4.50 and 2.40, respectively, possibly due to different starting materials. Consequently, the chemical compositions of the products were different. From Table 8, It was found that the highest organic substance in the liquid product was acetic acid, but substances in the amine and amide groups were also found, with the property of being a base. As a result, the liquid part of the product has high pH.

From the analysis of the COD value of the product, it was found that the COD value obtained was 26.75 g/L, which is similar to the research of [5], who studied various properties and compared the volume of methane accumulated from the decomposition process between wastewater and pyrolysis liquid from sludge pyrolysis at temperatures of 250, 350, 450, and 550 °C at the ratio (S/I) 30%:70% (by volume) from the mesophilic group. It was found that the highest volume of methane gas produced was at temperatures of 250 °C, 350 °C, 450 °C, and 550 °C, where the methane yields were 461.0 mL/g-VS, 366.1 mL/g-VS, 233.1 mL/g-VS and 207.8 mL/g-VS were inconsistent with the preliminary properties study. These include total solids, volatile solids, and COD. Because the highest amount of organic matter is found at 550 °C, the highest methane gas production should be obtained. Increased organic matter may inhibit microorganisms that produce methane gas. Another reason is the pH of the system because, at a temperature of 550 °C, there is a pH as high as 8.88, which is not suitable for the growth of microorganisms. Because acid-producing and methane-producing microorganisms can work together well, the pH value must be maintained within an

appropriate range of approximately 6.8-7.2 [8]. Therefore, it can be concluded that using liquid products in fermentation systems for direct anaerobic treatment may not be appropriate as it may be toxic to the system.

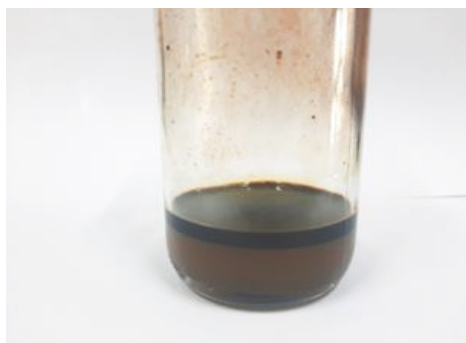


Figure 4. Pyrolytic liquid products at 500 °C.

Table 7. Properties of pyrolytic liquid products.

Properties	Asadullah et al. (2007) at 500 °C	Sara B. (2018) at 500 °C	Lutfiyah S. (2018) at 550 °C	This study at 500 °C
pH	4.50	2.40	-	9.45
COD (g/L)	-	-	23.83	26.75

Table 8. Identified compounds in latex sediment pyrolytic liquid at 500°C.

Compound Name	Formula	%Area
Anhydrosecoisolariciresinol	C ₂₀ H ₂₄ O ₅	0.23
Pyridine	C ₅ H ₅ N	2.96
2,3-Dimethylpyridine	C ₇ H ₉ N	0.74
3-Methylpyridine	C ₆ H ₇ N	1.86
2,3-Dimethylpyridine	C ₇ H ₉ N	0.92
N-(2-Aminoethyl)-N-methyl ethylenediamine	C ₅ H ₁₅ N ₃	0.39
Acetic acid	C ₂ H ₄ O ₂	7.20
Pyrrole	C ₄ H ₅ N	3.30
Isobutyric acid	C ₄ H ₈ O ₂	0.52
Butanoic acid	C ₄ H ₈ O ₂	0.45
4-Methylhex-5-en-4-olide	C ₇ H ₁₀ O ₂	1.58
Acetamide	C ₂ H ₅ NO	3.29
Propionamide	C ₃ H ₇ NO	0.90
2-Pyridinamine	C ₅ H ₆ N ₂	1.09
(3S,4S)-3-fluoro-2-phenylheptan-4-ol	C ₁₃ H ₁₉ FO	0.54
2-Pyrrolidinone	C ₄ H ₇ NO	1.95
3,4,5-Trimethylpyrazole	C ₆ H ₁₀ N ₂	2.04
1,2,3-Propanetriol	C ₃ H ₈ O ₃	4.55
3-Pyridinol	C ₅ H ₅ NO	3.57
2-Methoxy-6-methyl pyrazine	C ₆ H ₈ N ₂ O	0.95
Parthenin	C ₁₅ H ₁₈ O ₄	0.45
Benzeneacetamide	C ₈ H ₉ NO	0.06
Dibutylformamide	C ₉ H ₁₉ NO	0.60
5,5-Dimethylhydantoin	C ₅ H ₈ N ₂ O ₂	2.40
5-Ethyl-5-methylhydantoin	C ₆ H ₁₀ N ₂ O ₂	1.28
N,N-Dipropyl-1-butanamine	C ₁₀ H ₂₃ N	0.74

Table 8. Identified compounds in latex sediment pyrolytic liquid at 500°C (continued).

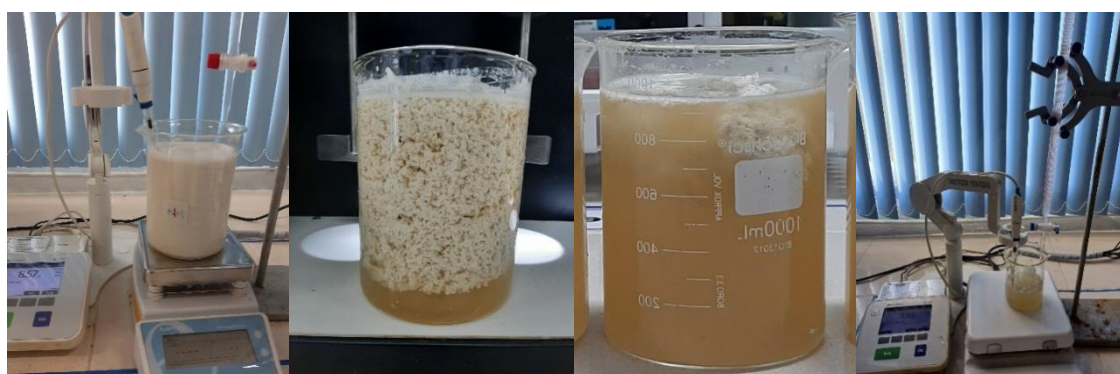
Compound Name	Formula	%Area
5-Ethyl-5-methylhydantoin	C ₆ H ₁₀ N ₂ O ₂	1.28
N,N-Dipropyl-1-butanamine	C ₁₀ H ₂₃ N	0.74
5-Isopropyl-2,4-imidazolidinedione	C ₆ H ₁₀ N ₂ O ₂	5.12
5-Isopropyl-2,4-imidazolidinedione	C ₁₁ H ₁₈ N ₂ O ₂	0.43
5-Isopropyl-2,4-imidazolidinedione	C ₆ H ₁₀ N ₂ O ₂	1.44
3-Isobutylhexahydropyrrolo[1,2-a]pyrazine-1,4-dione	C ₁₁ H ₁₈ N ₂ O ₂	0.69
N,N'-Methylenebisacrylamide	C ₇ H ₁₀ N ₂ O ₂	0.44

3.4 The alkalinity of skim latex serum was adjusted using liquid products from the pyrolysis process.

The pH is an important factor in organic decomposition systems under anaerobic conditions. The optimum pH range was approximately 6.8-7.2. If the pH value is higher or lower, the system performance will decrease rapidly; if the pH value is lower than 6.6 or higher than 7.6, the system performance will quickly decrease [8]. From a study of the use of the liquid product to adjust the alkalinity of skim latex serum before entering the anaerobic fermentation system, as shown in Figure 5, it was found that skim latex serum from the skim block production process had a pH of 4.95, which has the condition somewhat acidic and is toxic to anaerobic fermentation systems. Adjusting the alkalinity of skim latex serum from a pH of 4.95 to 6.80 before entering the organic decomposition system under anaerobic conditions is necessary and extremely important. From the experiment, as shown in Table 9, it was found that using the liquid product at 1 wt% liquid product (13.5 mL) was the most appropriate amount because it used the least amount of liquid product to adjust the alkalinity of skim latex serum.

Table 9. Pyrolytic liquid products application.

Pyrolytic product	Vol. of skim latex serum (mL)	pH initial	pH final	Vol. of pyrolytic product (mL)
1% Liquid product	100.01 ± 0.02	4.95 ± 0.00	6.80 ± 0.01	13.53 ± 0.15
3% Liquid product	100.04 ± 0.01	4.95 ± 0.00	6.81 ± 0.02	12.20 ± 0.20
5% Liquid product	100.02 ± 0.02	4.95 ± 0.00	6.81 ± 0.01	11.17 ± 0.15

**Figure 5.** Preparation of skim latex serum and adjustment of alkalinity of serum water with liquid products from pyrolysis at a temperature of 500 °C.

As shown in Figure 5, serum was prepared from 1,000 grams of latex, and sulfuric acid was added to coagulate the rubber. Skim latex serum was collected after coagulation. The product was obtained as a yellow

liquid. Has a relatively low pH. Skim latex serum from the skim block production plant was released into a stabilization pond before entering the anaerobic digester. This can result in a rapid decrease in the pH of the digester. The factory solves this problem by adjusting the alkalinity condition by adding chemicals such as lime because the cost is lower than that of sodium bicarbonate and sodium hydroxide; however, the factory requires a large amount of water to dilute the lime. It was found that lime did not dissolve completely and precipitated. When entering the anaerobic digester, the sediment accumulates at the bottom of the pond, causing the pond capacity to decrease, and the amount of lime solution used to adjust the pH appropriately requires a large amount. This increases the amount of wastewater that wastes energy during treatment. Therefore, using a liquid product from the pyrolysis of the latex sediment at a temperature of 500 °C is an option to adjust the alkalinity of the wastewater appropriately to increase the efficiency of the anaerobic digester. This could be a beneficial guideline for managing and utilizing sediment residue generated from the concentrated latex production process.

4. Conclusions

The batch process of pyrolysis of latex sediment from concentrated latex industries at temperatures ranging from 300-700°C was successfully demonstrated. The alkaline pH of the pyrolytic liquid was around 9.45. Therefore, the liquid pyrolytic product is suggested to be added to acidic serum wastewater for pH improvement before feeding to the anaerobic digestion system.

5. Acknowledgements

The authors thank the financial support from the Research Grant for Master Thesis, Graduate School and Faculty of Science and Technology, Prince of Songkla University.

Author Contributions: F.W. conducted the research, analyzed the data, and wrote the paper; S.C., R.J., and P.K. validated the results and reviewed a manuscript; S.C., R.J., and P.K. reviewed the manuscript and original draft preparation; all authors had approved the final version.

Funding: This research was supported by a Thesis Research Grant for graduate students, Department of Applied Chemistry, Faculty of Science and Technology, Prince of Songkla University.

Conflicts of Interest: The authors declare no conflict of interest.

References

- [1] Wichakit, S. *Thai rubber industry Growth trends in 2022*. https://www.v-servelogs.com/media/vserve2017/file_pdf/22020160904_NA-JAN2022-Siwakorn.pdf. 2022.
- [2] Jawjit, W.; Pavasant, P.; Kroeze, C. Evaluating environmental performance of concentrated latex production in Thailand. *Journal of Cleaner Production*, 2015; 98, 84-91. (Jawjit, 2015).
- [3] Chinnawong, P.; Dhanaraks, K.; Siriratpiriya, O. Effect of rubber latex sludge used as magnesium source for growth of oil palm in main nursery stage. *The 15th Graduate Research Conferences*. 776-782. Khon Kaen University. (Phiromkhan, 2014). 2014.
- [4] Korwutthikulrangsri, S.; Chaisuksan, Y.; Niyomdech, S.; Saengkha, P. *Autho Modification of concentrated latex sludge using effective microorganisms*. Rubber Industry Development Project Set, TRF. Project code RDG5050102. 2009.
- [5] Saeseng, L. *Efficient biogas production from organic wastes in concentrated latex factory by integrated pyrolysis and anaerobic digestion* [Master's thesis]. Prince of Songkhla University. 2018.
- [6] Asadullah, M.; Rahman, M.A.; Ali, M.M.; Rahman, M.S.; Motin, M.A.; Sultan, M.B.; Alam, M.R. Production of bio-oil from fixed bed pyrolysis of bagasse. *Fuel*. 2007; 86, 2514-2520.
- [7] Benmad, A. *Production and characterization of bio-fuel from sugarcane bagasse by using pyrolysis and pelletization* [Master's thesis]. Prince of Songkhla University. 2018.
- [8] Sohgratok, N. *Biogas production from decanter cake of plam oil mill withwastewater from frozen seafood industry* [Master's thesis]. Prince of Songkhla University. 2012.



Income and Expenditure Analysis of Selected Lowland Rainfed Rice Farmers in Tubog, Cawayan, Masbate

Roger Y. Ibañez Jr.^{1*}, Jacob Frederick P. Velza², Restiel V. Gaylan³, Jonna Mae B. Catimpuhan⁴

¹ Faculty of Cawayan Campus, Dr. Emilio B. Espinosa Sr. Memorial State College of Agriculture and Technology, 5405, Philippines; jacobfrederickvelza@gmail.com

² Faculty of Cawayan Campus, Dr. Emilio B. Espinosa Sr. Memorial State College of Agriculture and Technology, 5405, Philippines; ryibanez@debesmscat.edu.ph

³ Student of Cawayan Campus, Dr. Emilio B. Espinosa Sr. Memorial State College of Agriculture and Technology, 5405, Philippines; restielgaylan@gmail.com

⁴ Student of Cawayan Campus, Dr. Emilio B. Espinosa Sr. Memorial State College of Agriculture and Technology, 5405, Philippines; jonnamacatimpuhanb@gmail.com

* Correspondence: ryibanez@debesmscat.edu.ph

Citation:

Velza, J.F.; Ibañez Jr., R.; Gaylan, R.; Catimpuhan, J. Income and Expenditure Analysis of Selected Lowland Rainfed Rice Farmers in Tubog, Cawayan, Masbate. *ASEAN J. Sci. Tech. Report*. 2024, 27(2), 29-38. <https://doi.org/10.55164/ajstr.v27i2.246626>.

Article history:

Received: June 16, 2023

Revised: December 1, 2023

Accepted: January 23, 2024

Available online: February 1, 2024

Publisher's Note:

This article is published and distributed under the terms of Thaksin University.

Abstract: This study investigated the rice income and expenses of lowland rain-fed farmers in Barangay Tubog to ascertain whether these farmers could generate profits. A survey questionnaire was utilized to collect the data. The findings indicated that rice farmers earned an average annual income of P11,571.43. Conversely, their agricultural costs amounted to an average of P15,681.68 per cropping season. The study revealed that farmers needed more awareness regarding the recommended fertilizer application rates for a given farm area. Consequently, they incurred higher expenses on inputs, which harmed their income. Specifically, the average total cost of land preparation was found to be P3,084.09. The labor cost averaged P3,050.00, while the total expenses on fertilizer per cropping season averaged P5,812.42. Furthermore, the average total cost of pesticides per cropping season was approximately P1,258.42, and the average total milling cost amounted to P1,756.75. Overall, the entire agricultural expenses averaged P15,681.68 per cropping season. In terms of household expenses, the average was calculated to be P12,626.47. The researchers discovered that lowland rain-fed rice farmers in Barangay Tubog incurred higher expenses while generating lower income due to limited production output. This is likely due to some factors, including outdated farming practices, lack of access to credit, and the high cost of inputs. These findings suggested a need for government intervention to support lowland rain-fed rice farmers in Barangay Tubog. This could include providing farmers access to improved farming technologies, credit, and market linkages.

Keywords: Expenditure; income; inputs; lowland; rain-fed

1. Introduction

Agriculture is crucial to society because it sustains the local economic system. Also, it offers a large percentage of the population opportunities for employment [1]. Based on the data from Trading Economics [2], workers in the service sector share 58.8 percent of the total employment in the Philippines, followed by agriculture, which shares about 22.5 percent as of 2021. Agriculture is one of the primary sources of income for most Filipinos. 13.73 percent of the total population is the labor force in agriculture, composed of the farming and fishing sub-sector [3].



For most Filipinos, rice is their primary food source and staple crop. 2.5 million families, or 2.1 million farmers, are employed in the rice industry [4]. Rice output in the nation grew between 2018 and 2020, rising to 19.32 million metric tons in 2020 from 19.07 million metric tons in 2018, indicating an average annual rise of 0.7 percent. Central Luzon continuously produced the most rice from 2018-2020, with 19.0 percent of the national annual rice produced or 3.62 million metric tons or 18.8 percent. Irrigated farms, which accounted for 68.5 percent of the total harvest area in 2018, 70.1 percent in 2019, and 68.9 percent in 2020, provided most of the harvest areas across the three years. The share of the rain-fed regions dropped from 29.3 percent in 2018 to 28.8 percent in 2020. In upland farms, harvest areas ranged from 2.0 percent to 2.20 percent in 2018-2020. The Bicol region ranked fifth, having produced the most rice in 2018, amounting to 1.35 million metric tons or 7.1 percent of the share total, ranked sixth in 2019, amounting to 1.19 million metric tons or 6.3 percent, and ranked fifth in 2021, amounting to 1.29 million metric tons or 6.7 percent [20]. Farming is a good source of income; some even get rich because of entering this sector. The average net return for rice farmers is P16,832.00, earning P140.00 for every P100.00 spent. A farm with ten (10) hectares can expect a net income of P 600,000.00 to P 800,000.00 per year [5].

Due to some factors, especially the expenses and demand of the farm, there are some effects on the farm's income. Seeds, fertilizers, pesticides, and labor utilization are some of the most significant expenses the farmers need to provide for the demand of their farms. In rice production, the average quantity of seeds was estimated at 91.94 kilograms. Fertilizer averaged 214.76 kilograms per hectare for inorganic and 11.52 kilograms for organic. The usage of pesticides ranged from 0.03 liters for fungicides to 0.82 liters for insecticides, and the average labor utilization was 61.61 man-days per hectare [6]. But in 2013, the average variable costs of producing rice amounted to P35,675 per hectare or 85 percent of the total cost; 32 percent of the total variable cost was labor, and 15 percent averaged, or P6,386 per hectare, is the fixed cost. In irrigated farms, the average cost of production was P46,513 per hectare, while P33,888 per hectare in non-irrigated farms. There were P20,688 net returns in irrigated rice farms and P9,755 per hectare in non-irrigated rice farms, considering the cash and non-cash expenses of the farms [7]. Based on the recent data of the Registry System for Basic Sectors in Agriculture (RSBSA), there are 179 registered farmers in Tubog, Cawayan, Masbate; 36 of these are just registered but do not engage in farming, and five farmers transfer to nearby municipalities.

Nowadays, farmers do not just focus on one income source but tend to enter other jobs to support their household expenses. According to Hartoyo & Shara [4], the higher the household income, the higher the household expenditure. According to PhilRice, farmers' income depends on the farm yield, labor cost, and farm inputs. The objectives of this study are to (1) Determine the demographic profile of the farmers in Tubog, Cawayan, Masbate; (2) Determine the income of lowland rain-fed rice farmers in Tubog, Cawayan, Masbate; (3) Determine the household and agricultural expenditure of lowland rain-fed rice farmers in Tubog, Cawayan, Masbate, and how it influences the income received by the farmers; (4) To determine whether or not the farms are profitable. There is no significant problem regarding their incomes;

2. Methodology

2.1 Research Design and Sampling

The present study employed a descriptive research approach, aiming to provide a comprehensive description of a specific population's characteristics. Descriptive research gathers data that enables the investigation of various aspects related to the "what," "when," and "how" questions concerning a particular population or group [8]. Data collection involved observations within the research area and structured interviews with the respondents using questionnaires. The study focused on 44 actively engaged lowland rainfed rice farmers in Tubog, Cawayan, and Masbate. The selection of this area was based on the presence of active farming activities and its suitability for the study's objectives. The sample group comprised lowland rice farmers residing in Barangay Tubog, Cawayan, and Masbate. The researchers employed Slovin's formula to calculate this study's required number of respondents. With a population size of 1,265, the researchers determined the appropriate sample size considering the desired percent margin of error, resulting in a sample of 44 respondents. Respondents were selected based on their suitability for providing the sought-after information. Convenience sampling, a non-probability sampling technique, was utilized, whereby the sample units were selected based on the researcher's ease of access [9].

2.2 Data Collection and Statistical Analysis

The data collection process involved a structured questionnaire to gather relevant participant information. The questionnaire was carefully constructed to capture key aspects such as the farmers' sources of income, estimated annual income, production practices, production volume, and estimated expenses. Using a structured questionnaire, the researchers aimed to ensure consistency in data collection and facilitate systematic information collection. The questionnaire was administered to 44 lowland rainfed rice farmers in Barangay Tubog, Cawayan, Masbate. The researchers chose this sample size based on applying Slovin's formula, which considers the desired percent margin of error and the total population size of 1,265. This sample was considered representative of the larger population of interest. The researchers conducted face-to-face interviews, following a structured approach, to gather the required data. This approach allowed for further clarification of questions and ensured that respondents provided accurate and complete responses. The interviews were conducted consistently to minimize potential biases or variations in data collection. After the data collection, the researchers proceeded with the statistical analysis of the collected data. Descriptive statistics were employed to summarize and describe the key variables of interest. Frequency counts were used to determine the number of occurrences of specific responses or categories within each variable. Percentages were calculated to express the proportion of respondents who provided particular answers or fell into specific categories. Mean values were calculated to give an average representation of numerical variables, such as estimated annual income or production volume. These descriptive statistics allowed the researchers to gain insights into the characteristics, patterns, and trends present within the collected data.

3. Results and Discussion

3.1 The Characteristics of Farmer Respondents

The characteristics of farmer respondents in this study were sexual identity, quantity of families, marital status, level of education, and employment status. Based on the data gathered, most farmers were male (52%) and were the head of the family, responsible for cultivating the land to provide food for their families. It is consistent with Velza et al.'s study that the male does the direct farming operation [10]. The same table (Table 1) shows that 39% of the households had between one and three children, 43% had four to six children, 16% had seven to nine children, and 2% had ten or more children. It was noted that the average number of persons in a household was 4.2; number of household members is one of the determinants of the ability of the family to support their members in all aspects of their needs; thus, it is necessary for the farmers to carefully plan their family size base on their financial ability [11]. Moreover, the size of the farmers' families influenced their expenditures, and if the size of a family is large, its expenses will be higher [12].

Based on the marital status, 98% of the farmers were married, while 2% were widows. Regarding education, 68% of the farmers were elementary graduates, 14% completed secondary education, 11% had incomplete primary education, and only 3% reached high school. The lack of formal education among farmers may impact their productivity, particularly in adopting modern agricultural technologies [13]. Low education levels, large family size, and limited access to agricultural inputs were identified as factors affecting rice production [14]. Thus, providing informal education, such as training and seminars, could help improve farmers' knowledge and encourage the adoption of new technologies [15]. Regarding farming experience, 39% of farmers had cultivated their land for 11-20 years, followed by 16% farming for 0-10 years. Additionally, 14% of the farmers had dedicated 41-50 years to agriculture, while 11% had experience ranging from 31-40 and 51-60 years. Only 9% of the farmers had been farming for 21-30 years. The length of farming experience is one of the determinants of the success or failure of farming; thus, farmers must gain more experience and insights in their agriculture to learn more and be more productive. Regarding the farm size, most farmers (57%) had a farm size of 1-3 hectares, with an estimated average rice harvest of 19.8 sacks per year. The farmers' yield from their production is much lower because, according to PhilRice [16], an average yield of 3.29 metric tons of rice is expected per hectare. The study identified 16% of the farmers as small, while others were considered significant, with land holdings of 4-10 hectares or more. It was found that larger farms tend to generate higher income [14], and the size of the farm is a key factor affecting the farmer's income; moreover, economic of scale is one of the limiting factors for economic production in rice farming and in this location, it seems that agronomic production (rice) is small. [18]. Regarding farming capital, 57% of the farmers borrowed

money from various sources, while 43% used their funds to support rice production. Regarding land ownership, 57% of the farmers owned their land, 30% were tenants, and 14% rented the land for agricultural activities.

In general, the characteristics of farmer respondents, including their family size, marital status, education level, farming experience, farm size, capital sources, and land ownership, were identified in this study. These characteristics are significant in farmers' decision-making processes and overall farming activities. The findings highlight the need for educational interventions and support to enhance farmers' knowledge and productivity, particularly in adopting new technologies.

Table 1. Socio-demographic profile of farmers in barangay Tubog

Variable	Frequency (44)	Percentage (%)
Gender		
Male	23	52
Female	21	48
Number of children		
1-3	17	39
4-6	19	43
7-9	7	16
10 and above	1	2
Marital Status		
Single	0	0
Married	43	98
Separated	0	0
Widow	1	2
Educational attainment		
Graduate of Elementary	30	68
Primary level	5	11
Secondary Level	3	7
Graduate of high school	6	14
Occupation		
Farming	44	100
Year in farming		
0-10 years	7	16
11-20 years	17	39
21-30 years	4	9
31-40 years	5	11
41-50 years	6	14
51-60 years	5	11
Farm size		
Below 1 ha	16	36
1 ha – 3 ha	25	57
4 ha – 9 ha	2	5
Above 10 ha	1	2
Sources of capital in farming		
Borrowed	25	57
Owned	19	43

System of Land Ownership		
Owned	25	57
Tenant	6	14
Rented	13	30

3.2. Economic Analysis of Agricultural Production

The analysis of farmers' yields and income on their rice production is shown in Table 2. The findings revealed that 66% of the farmers harvested only 1-20 bags of rice per cropping, while 25% harvested 21-40 bags per cropping, 7% of the farmers gathered around 41-60 bags, and only 2% of the farmers achieved a harvest of 81-100 bags. It is shown that most of the farmers' respondents are low-yielding or low-production, which will be converted into cash. It shows that farmers in barangay Tubog will earn a low income because of their low production. The table below indicates farmers received P10,500 for every 1-20 bags harvested, P30,500 for every 21-40 bags harvested, P50,000 for every 41-60 bags harvested, P70,500 for every 61-80 bags harvested, and P90,500 for every 81-100 bags produced. These results demonstrated that the amount of yield harvested directly impacted the income received by the farmers since the higher the yield, the higher the revenue [19].

Furthermore, the table provided information on farmers' annual incomes. It revealed that most (100%) farmers generated their income from farming. Notably, 27% of the farmers had an income of P20,000 and above, equivalent to a monthly income of P1,666.67. On the other hand, 23% earned P5,001 to P8,000 and P17,000 to P20,000. Additionally, two or 5% of the farmers earned P8,001 to P11,000, and two earned P14,001 to P17,000. Based on the study by Reyes [20], farmers in the research location were considered poor for having an income of less than P10,957.

Based on these results, it was evident that the farmers in barangay Tubog belonged to 31.6% of farmers experiencing poverty, as per the data from the PSA in 2018 [7]. Furthermore, the income derived from rice harvests in barangay Tubog, Cawayan, Masbate fell significantly below the average base salary of farmers in the Philippines, which averaged to P9,833 monthly [21].

Table 2. Economic analysis of harvested produce of farmers in barangay Tubog

Variables	Income	Frequency (44)	Percentage (%)
<i>Estimated yield per cropping</i>			
1-20 bags	10,500	29	66
21-40 bags	30,500	11	25
41-60 bags	50,500	3	7
61-80 bags	70,500	0	0
81-100 bags	90,500	1	2
<i>Annual Income</i>			
5,000 and below		8	18
5,001-8,000		10	23
8,001-11,000		2	5
11,001-14,000		0	0
14,001-17,000		2	5
17,001-20,000		10	23
Above 20,001		12	27

3.3. Estimated pre-planting and planting expenses

The results of the study on pre-planting and planting expenses of rice farmers are presented in Table 3. Based on the farmers' estimates, the cost of land preparation varied among respondents. Most farmers (61%) reported an estimated cost of land preparation ranging from 501 to 2,500. A smaller percentage of respondents

(14%) indicated a higher estimated cost of land preparation, falling within the range of 4,501 to 6,500. Another 11% of farmers reported their land preparation cost around 2,501 to 4,500, while 7% stated a cost of 8,501 to 10,500. Only 2% of farmers mentioned a land preparation cost of 500 and below. Therefore, the Philippine government implemented the Rice Competitiveness Enhancement Program to compete with neighboring countries regarding rice production. The cost of production for their rice is relatively low compared to the cost of rice in the country.

Table 3. Pre-planting and Planting Expenses of rice farmers

Variables	Frequency	Percentage (%)
<i>Estimated cost for land preparation</i>		
500 and below	1	2
501-2,500	27	61
2,501-4,500	5	11
4,501-6,500	6	14
6,501-8,500	2	5
8,501-10,500	3	7
<i>Estimated labor cost/cropping</i>		
5,000 and below	39	89
5,001-8,000	0	0
8,001-11,000	3	7
11,001-14,000	0	0
14,001-17,000	1	2
17,001-20,000	0	0
Above 20,000	1	2
<i>Estimated total cost of fertilizer</i>		
5,000 and below	28	64
5,001-8,000	7	16
8,001-11,000	4	9
11,001-14,000	0	0
14,001-17,000	4	9
17,001-20,000	0	0
Above 20,000	1	2
<i>Estimated total cost of pesticides</i>		
Not practicing	6	14
500 and below	11	25
501-1,000	15	34
1,001-1,500	2	5
1,501-2,000	1	2
2,001-2,500	0	0
2,501-3,000	6	14
3,001-3,500	2	4
3,501-4,000	0	0
4,001-4,500	0	0
4,501 and above	1	2

Regarding labor costs, 89% of the farmers reported a cost of 5,000 and below. The frequency distribution in Table 3 shows that most respondents (39%) had an estimated labor cost below or equal to 5,000.

A small percentage of farmers (7%) reported a labor cost ranging from 5,001 to 8,000. No respondents reported labor costs falling within 8,001 to 11,000, 11,001 to 14,000, 14,001 to 17,000, 17,001 to 20,000, or above 20,000. Labor cost is the cost in rice production that most farmers responded to with high cost, similar to the study of Bordey [19]. Regarding fertilizer expenses, the study found that most farmers used synthetic fertilizers, particularly Complete fertilizer, Urea, and Ammonium phosphate. Despite the increasing price of Urea, it remained the most commonly used fertilizer among farmers. More than half (64%) of the farmers reported a fertilizer cost of 5,000 and below. The estimated total cost of fertilizer varied among respondents, with 16% stating a cost range of 5,001 to 8,000, 8,001 to 11,000, and 14,001 to 17,000, the same percentage (9%), while 2% of farmers reported a cost above 20,000. On average, the estimated cost of fertilizer was approximately 5,812.42 pesos. Regarding pesticide costs, the study found that 14% of farmers did not practice the application of pesticides on their farms. Among those who used pesticides, the cost varied. The majority (34%) reported a cost range of 501 to 1,000, followed by 25% who said a cost of 500 and below. The same percentage (14%) of farmers had a cost range of 2,501 to 3,000. A smaller percentage (5%) reported a cost of 1,001 to 1,500, while 4% stated a cost range of 3,000 to 3,500. Additionally, 2% of farmers reported costs of 4,001 to 4,500 and 4,501 and above for purchasing pesticides. The study's findings highlight that fertilizer expenses constitute the highest costs for farmers. This aligns with the results of a previous study by Turlley [6] and corroborates the data from the PSA in 2021, which indicated that farmers spent more on labor followed by fertilizer [22]

3.4 Estimated post-harvest expenses

In the study, the post-harvest expenses of rice farmers were examined (Table 4). The table presented the variable frequencies and percentages of estimated transport, milling, and drying costs per cropping. Regarding estimated transport costs per cropping, most farmers (84%) reported expenses of 500 and below. A smaller portion (14%) spent between 501 and 4,500, while only 2% of farmers had expenses of 4,501 and above. This result is opposite to the situation published by DA, in which the cost of transportation is high. Concerning estimated milling and drying costs per cropping, a mere 9% of farmers incurred expenses of 500 and below. The majority (89%) paid between 501 and 5,001, while there were no reported costs for the ranges of 5,001-10,000 and 10,001-15,000. However, 2% of farmers had high expenses of 15,001 and above. It is worth noting that the milling cost was estimated to be P2.50 per kilogram. The findings indicate that the majority of farmers (89%) paid within the range of 501-5,001 for milling. Meanwhile, a smaller proportion (9%) had lower costs of 500 and below, and a mere 2% faced higher charges of 15,001 and above in Tubog. These results suggest that rice farmers still allocate significant money for transportation and milling costs, which can impact their overall income. This is consistent with Bordey's study, which found that milling costs significantly affect rice production expenditures [19].

Table 4. Post-harvest Expenses of the farmers

Variables	Frequency	Percentage (%)
<i>Estimated transport cost/cropping</i>		
500 and below	37	84
501-4,500	6	14
4,501 and above	1	2
<i>Estimated milling and drying cost/cropping</i>		
500 and below	4	9
501-5,000	39	89
5,001-10,000	0	0
10,001-15,000	0	0
15,001 and above	1	2

3.5 Farmers household expenditures

A study showed that most farmers' household expenses were allocated to various categories, including food, electric bills, water, education, health, vices, clothes, and other miscellaneous items. However, the largest household expenses were spent on production costs and food. Table 5 summarizes the average monthly expenses for each expenditure category. Food accounted for an average expenditure of P2,122.73,

representing 17% of the total household expenses. The electric bill amounted to an average of P817.41, accounting for 6% of the expenses. Water expenses were relatively lower, with an average of P313.33, representing 3% of the total. Education expenses constituted the highest percentage, with an average of P4,225.00, accounting for 33% of the expenses. Health expenses averaged P607.04, representing 5% of the total. Vices, including alcohol and cigarettes, accounted for an average of P502.08, comprising 4% of the expenses. Clothes expenses totaled P788.88, also representing 6% of the total. Lastly, other expenses, including feed for farm animals and other miscellaneous items, averaged P3,250.00, accounting for 26% of the total [23].

Farmers had to divide their income to cover these household expenses. Education became the highest routine expenditure, constituting 33% of their income. Additionally, farmers allocated P3,250.00 per month, or 26% of their income, for other expenses such as farm animal feed and miscellaneous items. Farmers also utilized their income to supplement their food supply to purchase goods not produced on their farms. On average, they spent around P2,122.73 on food, representing 17% of their income. In addition to food, farmers allocated a portion of their income towards paying the monthly electric bill, averaging P817.41 or 6% of their income. The same proportion (6%) was dedicated to purchasing clothes for their children and themselves. Due to limited income, farmers could only allocate an average of P607.00 per month or 5% of their income for health expenses. Furthermore, farmers used a portion of their income, approximately P502.00 per month or 4%, to cover their vices, which included alcohol and cigarettes. Based on farmers' expenditures, the income from rice alone is not enough to cover their family's monthly expenses, making them sort from other sources of income and mostly leave rice farming to focus on other sources of income.

Table 5. Farmers household expenditure

Expenditure Category	Average Household Monthly Expenses	Percentage (%)
Food	2,122.73	17
Electric bill	817.41	6
Water	313.33	3
Education	4,225.00	33
Health	607.04	5
Vices	502.08	4
Clothes	788.88	6
Other	3,250.00	26
TOTAL	12,626.47	

The table below (Table 6) provides insights into the profitability of farms. The average annual income of farmers was reported to be P11,571.43. However, this income fell short of meeting household expenses, which averaged P12,626.47, and agricultural expenses, which averaged P15,681.82. These findings indicate that farming alone cannot satisfy a family's basic needs. As a result, farmers must seek alternative livelihoods to ensure their survival [24]. The study demonstrates that farmers' household expenses primarily consist of production costs and food. Education became the most significant routine expenditure, followed by other miscellaneous expenses. The need for additional income sources beyond farming alone highlighted the fact that the average annual income of farmers was not enough to cover both household and agricultural expenses.

Table 6. Profitability of the farmers' farms

Income in Farming	Amount
Average Income	11, 571.43
Expenditures	
Household Expenses	12,626.47
Agricultural Expenses	15,681.82
Total Expenditures	28,308.29

4. Conclusions

Most farmers in barangay Tubog were male, married, and served as the head of the family. They had a relatively low level of education, with most having only completed elementary school. Farmers had large families, and the size of the family influenced their expenditures, as larger families required more financial resources. Farmers in barangay Tubog had significant farming experience, with most cultivating their land for 11-20 years. Most farmers had a farm size of 1-3 hectares, and their average rice harvest was significantly lower than the expected average yield per hectare. Small farmers constituted 16% of the respondents, while the rest were considered large farmers with land holdings of 4-10 hectares or more. Farmers primarily relied on borrowed capital, and a majority owned their land. However, significant percentages were tenants or rented land for agricultural activities. The yield of their rice harvest directly influenced the income of farmers. The higher the yield, the higher the income. The annual income of farmers in barangay Tubog fell significantly below the average base salary of farmers in the Philippines, indicating that a substantial portion of farmers were experiencing poverty. The cost of land preparation varied among respondents, with the majority reporting an estimated cost ranging from 501 to 2,500 pesos. Labor costs were relatively low, with most farmers reporting 5,000 pesos and below. Fertilizer expenses constituted the highest costs for farmers, followed by labor costs. Synthetic fertilizers, particularly Urea, were commonly used by farmers. Pesticide costs varied among farmers, with a significant portion not practicing the application of pesticides. Among those who used pesticides, most reported costs ranging from 501 to 1,000 pesos.

5. Acknowledgements

First and foremost, the researchers would like to thank God for His guidance and blessing until the research is completed. To the rice farmers of Barangay Tubog, Cawayan, Masbate for their cooperation, especially in answering the interviews. They serve as the main characters of this study. The researchers genuinely appreciate their time and effort because this study was only possible with their cooperation. To the Barangay captain of Tubog, Cawayan, Masbate, Hon. Isagani P. Pelayo, for his full support and warm welcome to their barangay. His few suggestions and comments helped make the interview much faster.

Author Contributions: JFPV: Conceptualization, methodology, validation, RVG, and JMBC; formal analysis, investigation, resources, data curation; writing—original draft preparation, RYIJ; writing—review, editing, and visualization. All authors have read and agreed to the published version of the manuscript.

Funding: This research received no external funding.

Conflicts of Interest: The authors declare no conflict of interest.

References

- [1] Dane, K. *Why Agriculture is Important and its Role in Everyday Life*. 2022. <https://agriculturegoods.com/why-is-agriculture-important/>
- [2] Trading Economics. *Philippines-Employment in Services (% of total Employment)*. 2022. <https://tradingeconomics.com/philippines/employment-in-services-percent-of-total-employment-wb-data.html>
- [3] Food Agriculture Organization. *Farm and Household and Their Relation to Farm Size*. 2012. <https://www.fao.org/3/Y4890E/y4890e0p.htm?fbclid=IwAR3WWE0JzgKcJtuf1zizmKFgKMKC3PboyUfkcPZLO3lwLKqij7a-dZQFCc>

- [4] Hartoyo, B.; Shara, D. Analysis of income and expenditure of farmers' households in rain-fed area of Boyolali district. *IOP Conference Series: Earth and Environmental Science*. **2021**. 653.012007. <https://doi.org/10.1088/1755-1315/653/1/012007>.
- [5] Panay News. *5 reasons to farm in the Philippines*. **2022**. https://www.panaynews.net/5-reasons-to-farm-rice-in-thephilippines/?amp=1&fbclid=IwAR1j62MnXOapaXj7WXTMkcWTTz1-HW7ImPn3Em4oYTwaZcX7X92ca_LM1Czk
- [6] Turlley, L. O. *Historical Farm Income and expenses*. **2022**. <https://agecon.ca.uky.edu/historical-farm-incomeandexpenses#:~:text=Fertilizer%20and%20rent%20are%20ost, costs%20for%20all%20grain%20farms>.
- [7] Philippine Statistics Authority. *2013 Costs and Returns Survey (CRS) of Palay Production*. **2015**. https://psa.gov.ph/sites/default/files/crs_palay2013.pdf
- [8] Voxco. *Descriptive Research: Definition, Methods & Examples*. **2021**. <https://www.voxco.com/blog/descriptive-research/>
- [9] Nikolopoulou, K. *What is convenience sampling?*. (n,d). <https://www.scribbr.com/methodology/convenience-sampling/>
- [10] Velza, J.F.P.; Ibañez Jr.; R.Y.; Clores, N.R.; Valler, D.L. Socio-demographic characteristics and perceived constraints of the farmers to crop production in selected barangays of Cawayan, Masbate, Philippines. *International Research Journal of Science, Technology, Education, and Management*. **2023**, 3(1), 16-30. <https://doi.org/10.5281/zenodo.7772805>
- [11] Philippine Statistics Authority. *Philippines National Demographic and Health Survey 2017*. **2018**. https://psa.gov.ph/sites/default/files/PHILIPPINE%20NATIONAL%20DEMOGRAPHIC%20AND%20HEALTH%20SURVEY%202017_new.pdf
- [12] Family Economics and Consumer Education. *Factors affecting Budget*. **2012**. <https://ecourseonline.iasri.ers.in.mod/page/view.php?id=25949>.
- [13] Serin, V.; Bayyurt N.; Civan A. Effects of Formal Education and Training on Farmers Income. *European Journal of Social Science*. **2009**. https://www.researchgate.net/publication/253741425_Effects_of_Forma Education_and_Training_on_farmers_income.
- [14] Hoda, A.; Terway P. *Credit policy for Agriculture in India - An evolution: Supporting Indian Farms the Smart way: Rationalising subsidies and Investments for Faster, Inclusive and Sustainable Growth*. **2015**. <https://hdl.handle.net/11540/11012>.
- [15] Oduro-ofori, E.; Anokye, P.A.; Naa, A.; Elfreda, A. Effects of Education on the Agricultural Productivity of Farmers in Offinso Municipality. *International Journal of Development Research*. **2015**, 6(9), 1951-1960. <http://www.journalijdr.com>
- [16] PhilRice. Yield per hectare. *Philrice*. **2022**. <https://www.philrice.gov.ph/ricelytics/estiyields>
- [17] Noack, F.; Larsen, A. The contrasting effects of farm size on farm incomes and food production. *Environmental Research Letters*. **2019**, 14(8), 084024. <https://doi.org/10.1088/1748-9326/ab2dbf>
- [18] Maniriho, A.; Musabanganji, E.; Lebailly, P. Factors Affecting Farm Performance among Small-Scale Farmers in the Volcanic Highlands of Rwanda: What is the Role of Institutions?. *Asian Journal of Agriculture and Rural Development*. **2021**, 11(4), 262-268. <https://doi.org/10.18488/journal.ajard.2021.114.262.268>
- [19] Bordey, F.H. *The Impacts of Research on Philippine Rice Production*. PhD dissertation. University of Illinois. **2010**. Retrieved December 1, 2023, from <https://core.ac.uk/download/pdf/4824594.pdf>
- [20] Reyes, S. How much does the middle class contribute to taxes?. *Philippine Institute for Development Studies*. **2022**. https://pidswebs.pids.gov.ph/CDN/document/1657498942_62cb6d3eddf17.pdf
- [21] Indeed. *Farmer salary in Philippines*. **2023**. <https://ph.indeed.com/career/farmer/salaries>.
- [22] Philippine Statistics Authority. *2016-2020 Crop Statistics of the Philippines*. **2021**. <https://psa.gov.ph/sites/default/files/Crops%20Statistics%20of%20the%20Philippines%202016-2020.pdf>
- [23] Foronda, V. Agricultural Biodiversity Conservation Towards Sustainable Rice-based Farming Systems. *Journal of Development Sustainable Agriculture*. **2007**, 2, 167-191.
- [24] Food and Agriculture Organization of the United Nations Rome. *The economic lives of smallholder farmers. An analysis based on household data from nine countries*. **2015**. <https://www.fao.org/3/i5251e/i5251e.pdf>



Environmental Impact Assessment of Onshore Wind Power Plants: A Case Study of a 50 MW Wind Power Plant in Northeastern Thailand

Sunisa Kongprasit¹, Somphol Chiwamongkhonkarn², Fida Ali³, Pongsak Makhampom⁴, Yves Gagnon⁵ and Jompob Waewsak^{6*}

¹ Faculty of Science and Digital Innovation, Thaksin University, Phatthalung, 93210, Thailand; sunisa@tsu.ac.th

² Research Center in Energy and Environment (RCEE), Division of Physics, Faculty of Science and Digital Innovation, Thaksin University Phatthalung, 93210, Thailand; dung_ding19@hotmail.com

³ Research Center in Energy and Environment (RCEE), Division of Physics, Faculty of Science and Digital Innovation, Thaksin University, Phatthalung, 93210, Thailand; engr.fidaali16@gmail.com

⁴ Faculty of Engineering, Thaksin University, Phatthalung, 93210, Thailand; 602995011@tsu.ac.th

⁵ Université de Moncton, Edmundston (NB), Canada; yves.gagnon@umoncton.ca

⁶ Research Center in Energy and Environment (RCEE), Division of Physics, Faculty of Science and Digital Innovation, Thaksin University, Phatthalung, 93210, Thailand; jompob@tsu.ac.th

* Correspondence: jompob@tsu.ac.th

Citation:

Kongprasit, S.; Chiwamongkhonkarn, S.; Ali, F.; Gagnon, Y.; Waewsak, J. Environmental impact assessment of onshore wind power plants: A case study of a 50 MW wind power plant in northeastern Thailand. *ASEAN J. Sci. Tech. Report.* **2024**, *27*(2), 39-57. <https://doi.org/10.55164/ajstr.v27i2.252058>

Article history:

Received: December 13, 2023

Revised: January 16, 2024

Accepted: January 26, 2024

Available online: February 29, 2024

Publisher's Note:

This article is published and distributed under the terms of the Thaksin University.



Abstract: This research aims to assess the environmental feasibility of a wind power plant by investigating its noise disturbances, shadow flicker, and zones of visual influence. The model is applied as a case study for a 50 MW wind power plant, located in the Nakhon Ratchasima province of northeastern Thailand. The acoustic noise emissions were analyzed using the sound propagation and absorption models under the wind conditions on the site studied. The shadow flicker around each wind turbine generator, in terms of the number of hours per year, was also simulated along with the analysis of the zones of visual influence according to the number of wind turbines that can be seen by an observer from a certain distance. The results show a maximum sound level of 47 dBA, within the allowed limits of the 50 dBA legislation of the Department of Pollution Control of the Royal Thai Government. Similarly, the shadow flicker within 1 km of the wind turbines is 10 hours/year, well below the international standard of 30 hours/year. Results of the zones of visual influence indicate that between 15 and 20 turbines are visible from observation points surrounding the potential wind power plant. The results applied to this case study suggest that the potential wind power plant is well-suited regarding its environmental impacts and should typically not incur negative impacts for the local communities. Studies like these are vital to gaining the trust of the communities living near wind power plants to address their concerns and minimize opposition.

Keywords: Onshore Wind Power Plant; Noise Emission; Shadow Flicker; Zone of Visual Influence; Public Opposition.

1. Introduction

Renewable energy sources, such as solar and wind energy, are steadily replacing conventional fossil fuels as the primary source of electricity generation. Renewable energy is predicted to be the world's top electricity generation

source within three years [1]. According to a recent International Energy Agency (IEA) report on renewables, solar PV capacity will surpass gas and coal as primary energy sources by 2027. Similarly, wind generation capacity will double during this period, with offshore wind power plants contributing the bulk of the share [2]. This steady shift towards renewables is primarily due to global warming caused by greenhouse gas emissions, which led world leaders to pledge a reduction in global carbon footprint under the Paris Agreement [3]. In addition, the volatility in energy markets, notably caused by events such as the Russia-Ukraine war, has also pushed the adoption of renewables on fast tracks, especially in the European market, which heavily depends on Russian natural gas for its needs.

Thailand, an emerging economy in the ASEAN, also heavily relies on fossil fuels for its energy demands. Electricity generation is dominated by natural gas, accounting for the highest share of the Electricity Generating Authority of Thailand (EGAT), the largest producer of electricity in the country, followed by coal [4]. Thailand imports most of its natural gas and oil, with gulf gas leading the share [5], making it heavily dependent on energy imports. However, Thailand has ambitious plans to diversify its energy mix by increasing the share of renewable energy in electricity generation. Currently, renewables, including large hydropower, contribute almost 13% of the country's total electricity generation capacity [5], but the country plans to continue to increase this share.

With its power development plan (PDP 2015-2036), Thailand aims to reduce the share of fossil fuels in power generation by 30 to 40%, offsetting it by increasing the renewable energy share to 20% by 2036 [6]. Another more ambitious plan formulated by Thailand's Energy Policy and Planning Office (EPPO) aims to achieve a 50% renewable energy share to reach the carbon neutrality target by 2065 - 2070 [7]. Thailand has a total renewable electricity generation capacity of 23,856 GWh, with solar PV and wind energy contributing the highest share, 21% and 17 %, respectively. Following the global trend, both of these sources will be major contributors to the expansion of renewable energy in the country.

Thailand has an excellent onshore wind capacity that can be developed to improve the share of renewable energy in the country. Currently, the installed onshore wind capacity of Thailand reaches 1,500 MW (1.5 GW), making up 17% of the total renewable energy-based power generation in 2021 [5, 8]. However, the country has the potential to install between 13 and 17 GW of onshore wind power capacity if given the proper regulatory and policy framework [9].

Several studies have been carried out in different parts of Thailand to assess onshore wind power potential, showing encouraging results. Using the Wind Atlas Analysis and Application Program (WAsP), the wind potential assessment of Hat Yai city in Songkhla province, with its 3.5 m/s mean annual wind speed at 10 m above ground level (agl), is estimated at 2,731 MWh of wind energy generation [10]. With its mean annual wind speed of 8 m/s at 120 m agl and employing atmospheric and computational fluid dynamics (CFD) wind flow modeling, a wind power potential of 300 MW was estimated in southern Thailand [11]. In a similar study, using CFD wind flow modeling at 120 - 125 m agl, potential wind power plant sites along the Andaman coast of Thailand could generate 18 to 36 GWh/year [12]. Finally, using wind shear coefficients, the technical power potential for elevations between 65 and 120 m agl of Koh Phangan, Thailand, could reach between 10 and 20 MW [13]. These studies suggest that Thailand has good potential for developing its onshore wind energy. However, developing onshore wind power plants face challenges ranging from techno-economic aspects to socio-environment issues.

Wind turbine generators can cause noise and visual disturbances in their immediate vicinity. An international panel of experts, working under a mandate of the Government of Canada, identified through a thorough assessment of the scientific literature that the evidence is sufficient to establish a causal relationship between exposure to wind turbine noise and annoyance. At the same time, there is limited evidence to establish a causal relationship between exposure to wind turbine noise and sleep disturbances [14]. Further, the evidence suggests a lack of causality between exposure to wind turbine noise and hearing loss. In contrast, the evidence was inadequate to come to any conclusion about the presence or absence of a causal relationship between commonly claimed health impacts and exposure to wind turbine noise [14].

Nonetheless, the negative impacts of large onshore wind power plants, such as visual and noise disturbances, land use conflicts, etc., pose significant challenges to the acceptance of wind energy [15]. While large wind turbines have been well accepted in unattractive landscapes, they have faced negative social acceptance in high aesthetic quality landscapes, suggesting the visual factor is important [16]. For example, it is documented that noise and visual disturbances were considered major factors by some local community

groups in Australia opposing the development of wind energy in their area [17]. Hence, noise and visual disturbances are the primary concerns of the local communities that need to be well addressed while developing a wind power project in an area.

This study specifically focuses on assessing noise disturbances, shadow flicker, and zones of visual influence of a potential 50 MW wind power plant in the Nakhon Ratchasima province of northeastern Thailand. While the methodology of this study is independent of the location, it aims to investigate and identify the social acceptance barriers for onshore wind energy in general and specifically in Thailand.

2. Materials and Methods

2.1 Study Area

The potential wind power plant investigated is located in the Nakhon Ratchasima province of northeastern Thailand, as shown in Figure 1. The province of Nakhon Ratchasima is the most important economic hub of the northeastern region, supporting many economic activities, including tourism. Being an economic hub with a good wind resource, Nakhon Ratchasima province is home to many of Thailand's current utility-scale wind power plants, including the 90 MW KR-I wind power plant and the 103 MW first Korat wind power plant. Considering its pleasant climate, the region is also a tourist destination. The rainy season lasts almost nine months, from February to November, with September being the month with the most rain. The period of late November to early February is considered the most ideal time for tourism [18]. Thus, along with tourism, renewable energy, and notably wind energy, is vital in supporting the economic activities of this region.

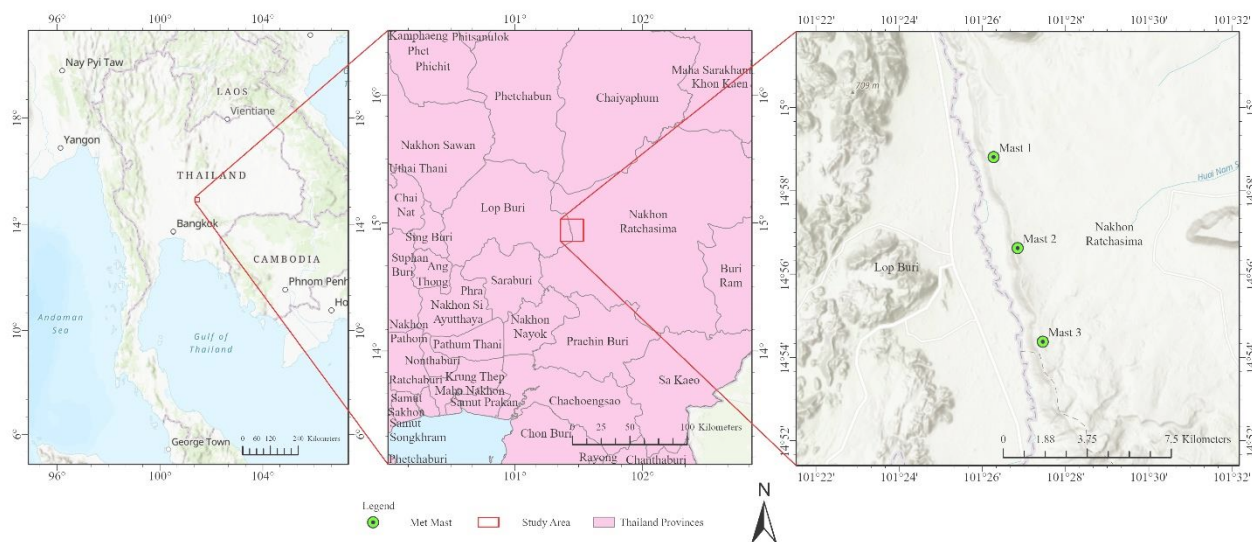


Figure 1. The study area is located in the Nakhon Ratchasima province of northeastern Thailand.

2.2 Microscale Computational Fluid Dynamics Wind Flow Modeling

The computational fluid dynamics (CFD) wind flow modeling, with a 90 m resolution, was applied for the wind speed prediction over a 10 x 10 km² grid, while met masts of 90 m (1 mast) and 125 m (2 masts) spread across three locations, were used to validate the numerical modeling. The positions of the three met masts are indicated in Figure 1, while their characteristics are presented in Table 1.

CFD wind flow modeling is widely used to simulate wind flow caused by the local terrain characteristics and topography and is quite helpful for developing wind energy in complex terrains [11,19]. The main inputs in CFD wind flow modeling consist of boundary conditions, i.e., terrain feature (Digital Elevation Model (DEM)) and roughness, as well as initial conditions, i.e., wind climatology in the form of wind speeds and directions at typical points of measurement in the study area. In this analysis, the ASTER Global Digital Elevation Model (GDEM) V2 provided by the USGS was used to represent the terrain feature of the

study area. The roughness was interpreted using the Land Cover Land Use (LCLU) data from the Land Development Department of Thailand [20]. The 3D DEM and roughness of the study area are presented in Figure 2.

The standard k-epsilon turbulent model was applied to execute the CFD wind flow modeling under neutral air stability conditions and air density of 1.225 kg/m^3 using the GCV solver in the WindSim simulation tool. The CFD wind flow modeling output was the spatial wind resource distribution at 137 m agl, corresponding to the hub height of the wind turbine generators used in this investigation. The distribution of the climatic wind speeds, at 90 m and 125 m agl, at the positions of the three met masts used in the CFD simulations are shown in Figure 3. This figure shows similar wind profiles for each met mast position, with average annual wind speeds of 5.81, 5.75, and 6.07 m/s, respectively, making the study area suitable for developing wind energy. Figure 4 shows the layout of the potential wind power plant and the positions of the wind turbines in the study area.

Table 1. Characteristics and period of wind measurements of the three met masts used in the study area.

Met Mast	Representative Period	Measurement Height (m agl)	Representative Period (Months)	Mean Annual Wind Speed (m/s)
KWE_Mast1	11/12/2013 (00:00) - 22/11/2016 (07:00)	125	15.0	5.81
KWE_Mast2	12/12/2013 (00:00) - 13/01/2017 (00:00)	90	14.9	5.75
KWE_Mast3	23/12/2013 (00:00) - 16/11/2016 (00:00)	125	14.9	6.07

2.3 Noise Level Measurement

One of the major barriers being faced by onshore wind power plants is their acoustic noise emissions. The acoustic footprint of large wind power plants is often the cause of concern for the residents in the vicinity, and addressing this problem is essential for the sustainable development of onshore wind energy.

The noise model of the GH WindFarmer simulation model [22] was used to model the acoustic noise emissions of the potential 50 MW wind power plant. This model designs wind power plants within the legal noise levels. The noise model calculates the attenuation for a single representative frequency and assumes hard ground surfaces.

The noise model in GH WindFarmer calculates the noise propagation at a fixed reference frequency of 500 Hz. The continuous octave-band sound pressure level at a receiver location (L_{ft}) is calculated using Eq. (1).

$$L_{ft} = L_W + D_c - A \quad (1)$$

L_W is the sound power level in dBA produced by each turbine, taking the turbine as a point source, and D_c is the directivity correction in dBA. For the case of an assumed omni-directional point sound source (i.e., a wind turbine), $D_c = 0$ dBA. The directivity of the wind turbine noise is considered when measuring the sound power level. Thus, A is the attenuation that occurs during the propagation from the point sound source to the receiver in dBA, calculated using Eq. (2).

$$A = A_{div} + A_{atm} + A_{gr} + A_{bar} + A_{misc} + A_{met} \quad (2)$$

Where A_{div} is the attenuation due to geometrical divergence, A_{atm} is the attenuation due to atmospheric absorption, A_{gr} is the attenuation due to the ground effects, A_{bar} is the attenuation due to barriers, A_{misc} is the attenuation due to other effects such as foliage and areas of buildings, and A_{met} is the attenuation due to the meteorological impacts. In this investigation, there are no barriers or areas of buildings. Also, the attenuation due to the foliage of the trees is usually small. Consequently, the A_{misc} was not taken into consideration. Also, the meteorological effects are neglected since the meteorological conditions are unchanged.

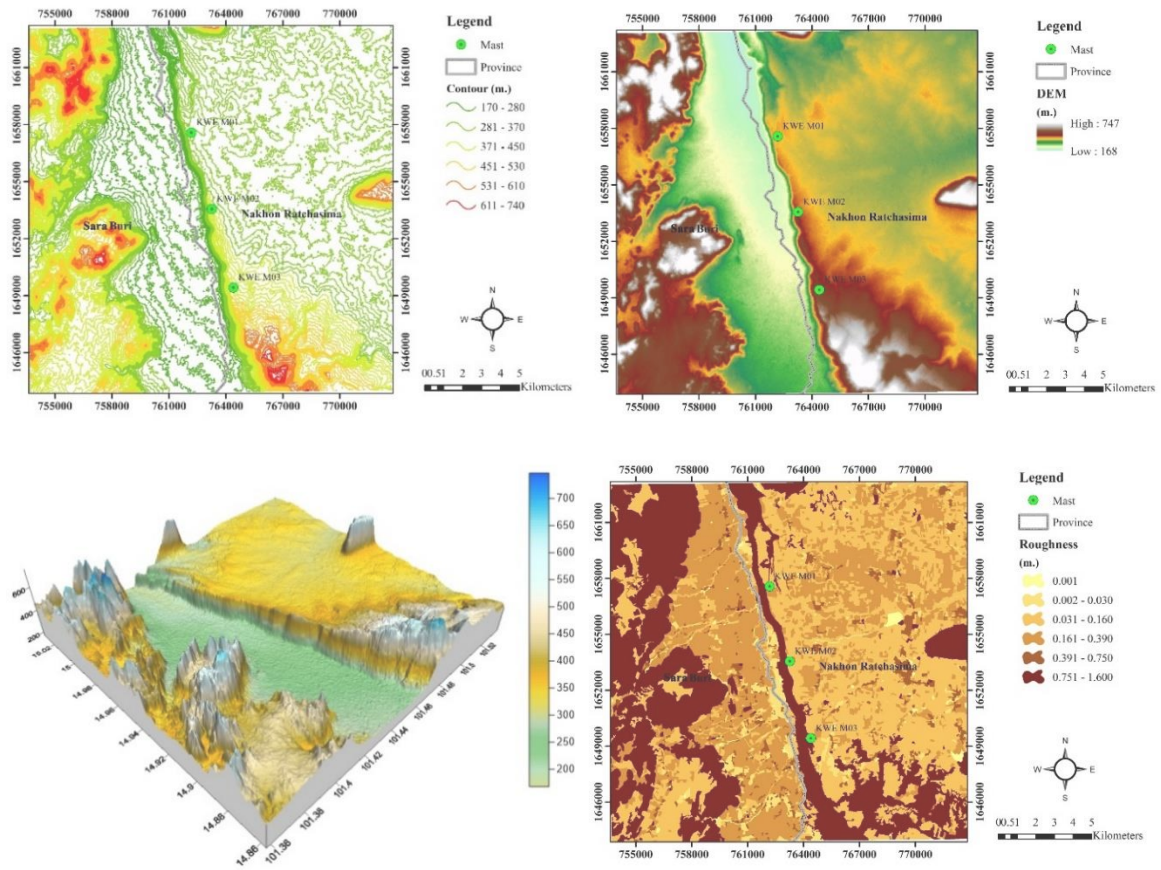


Figure 2. Contour map (upper left), 2D GDEM (upper right), 3D GDEM (lower left) and roughness (lower right) of the study area. (Source: NASA-ASTER [21])

2.3.1 Geometrical Divergence (A_{div})

The geometrical divergence attenuation A_{div} accounts for the spherical spreading in the free field from a point sound source over hard ground and is calculated using Eq. (3).

$$A_{div} = [20\log(d)+11]dB \tag{3}$$

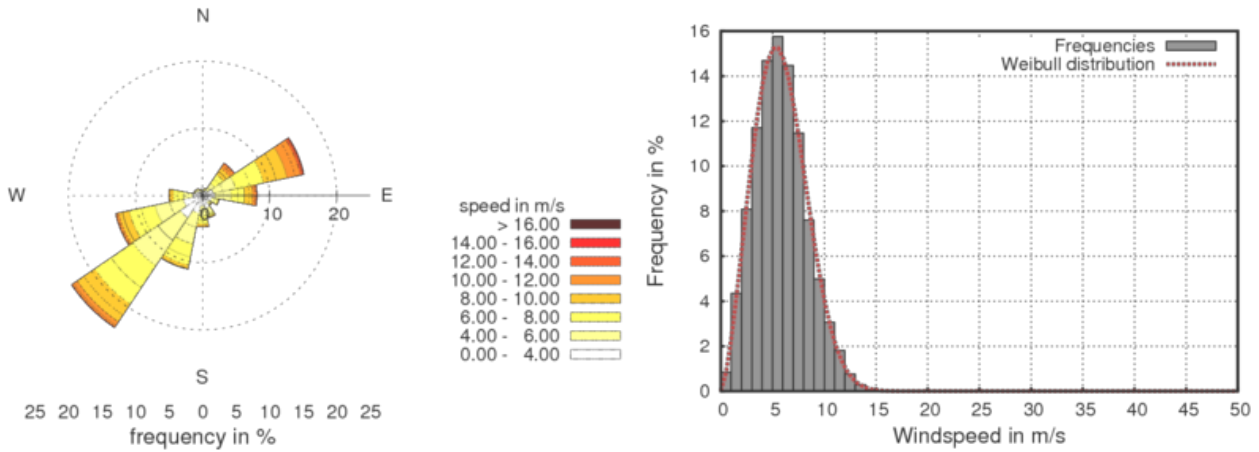
Where d is the 3-dimensional distance between the source and the receiver.

2.3.2 Atmospheric Attenuation (A_{atm})

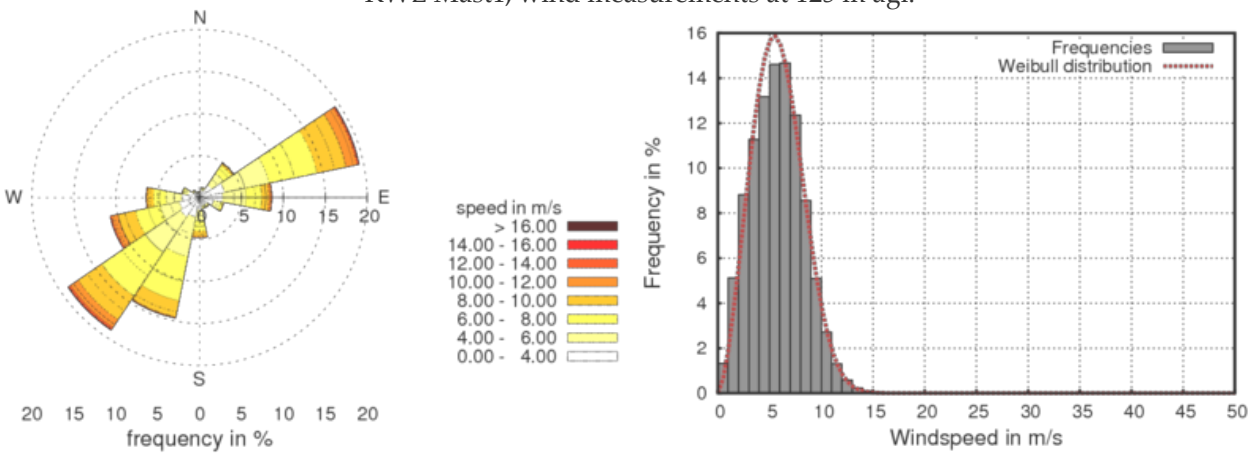
The attenuation due to atmospheric absorption A_{atm} is calculated using Eq. (4).

$$A_{atm} = [\alpha d/1000] \tag{4}$$

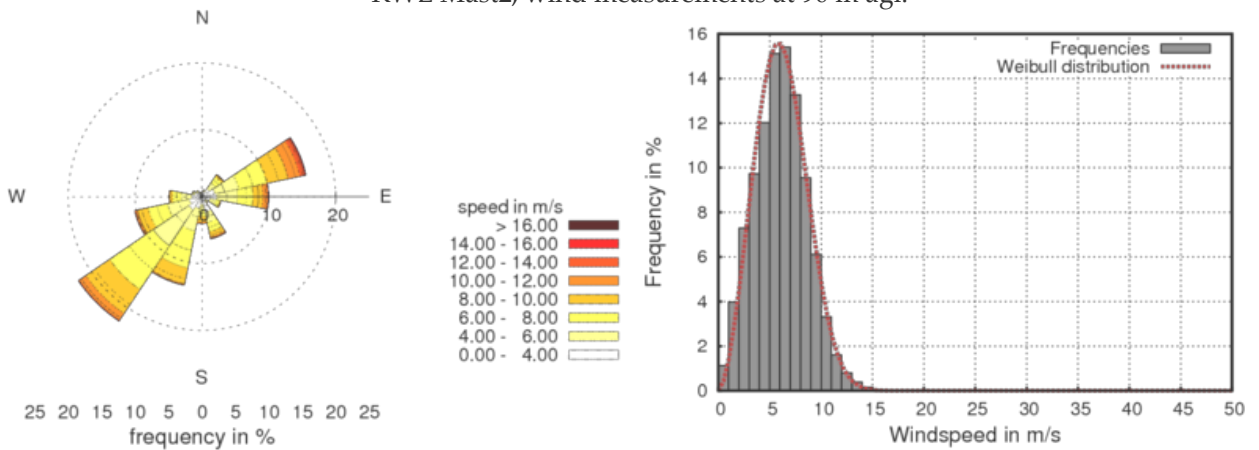
Where α is the atmospheric attenuation coefficient in dBA/km for each octave band.



KWE Mast1, wind measurements at 125 m agl.



KWE Mast2, wind measurements at 90 m agl.



KWE Mast3, wind measurements at 125 m agl.

Figure 3. Distribution of the wind speeds, at 90 m and 125 m agl, at the positions of the met masts used in this study.

2.3.3 Ground Attenuation (A_{gr})

The total ground attenuation A_{gr} is the sum of the ground attenuation in the source region (A_s), the middle region (A_m), and the receiver region (A_r). In the source and receiver regions, the ground attenuation is -1.5 dB. The ground attenuation in the middle region is given by Eq. (5).

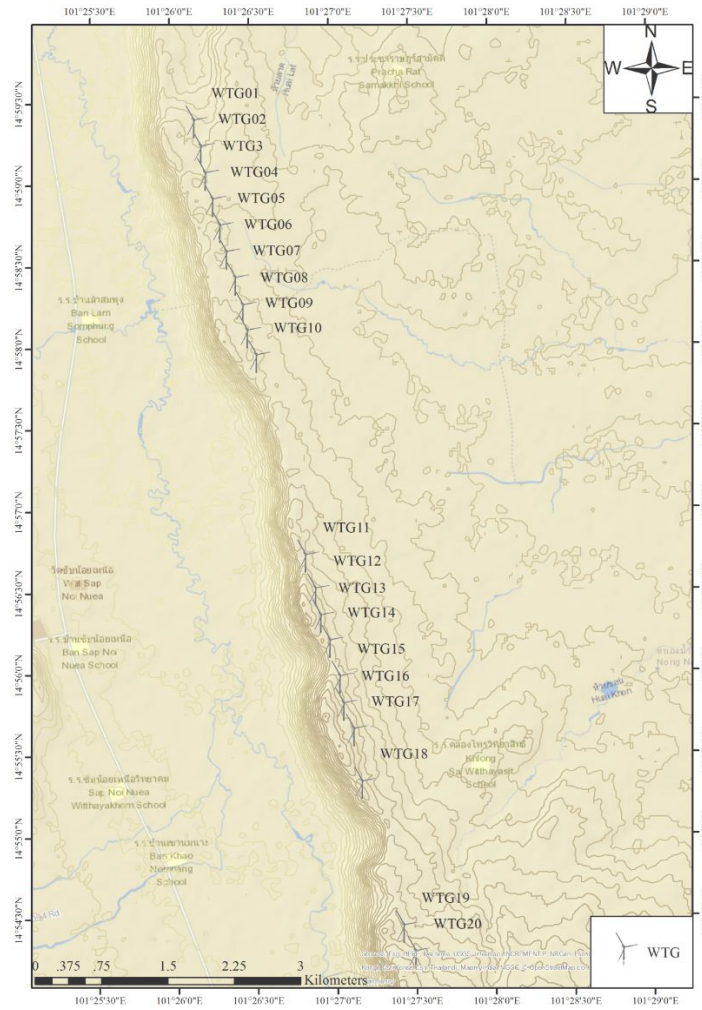


Figure 4. Layout of the potential wind power plant and the positions of the wind turbines in the study area.

$$A_m = -3qdB \tag{5}$$

$$q = \begin{cases} 1 - \frac{30(h_s + h_r)}{dp} & \text{When } dp > 30(h_s + h_r) \\ 0 & \text{When } dp < 30(h_s + h_r) \end{cases} \tag{6}$$

Where h_s is the hub height of the wind turbine, h_r is the height of the receiver above ground, and dp is the distance from the wind turbine base to the receiver base projected onto the ground plane.

Finally, for multiple wind turbines, the combined sound pressure level for all the turbines 1 to n at a point must be calculated using Eq. (7).

$$L_{total} = 10 \log \left[10^{\frac{Lft1}{10}} + 10^{\frac{Lft2}{10}} + 10^{\frac{Lft3}{10}} + \dots + 10^{\frac{Lftn}{10}} \right] \tag{7}$$

In this work, the noise levels emitted by the 20 turbines composing the potential 50 MW wind power plant were analyzed and mapped using the above set of equations.

2.4 Shadow Flicker

The moving shadow caused by the rotation of a wind turbine rotor and blades is known as shadow flicker, and it can annoy the residents in the vicinity of a wind power plant [23]. Therefore, it is important to properly understand and address this issue to minimize the probability of opposition to wind power plant developments. The WindFarmer model [22] calculates the shadow flicker of a wind turbine using a multi-step calculation process considering many input parameters. The shadow flicker module simulates the path of the sun over one year and assesses the shadow flicker at different time intervals at multiple positions. This assessment can help turbine controllers plan the operations of the wind turbines to avoid the worst shadow flicker timing to minimize annoyance to the nearby residents.

Before the actual calculation of shadow flicker, the position of the sun at any time of the year needs to be determined. The WindFarmer model uses the following methods for determining the position of the sun [22].

2.4.1 Calculating the Hour Angle

The Hour Angle is the angular displacement of the sun, from the west or the east, of the local meridian due to the rotation of the earth on its axis at $15^\circ/\text{hour}$. To calculate the hour angle, one needs to calculate the following variables.

2.4.2 Julian Date

The Julian Date (JD) is the difference in days between the current Julian day and the Julian day at noon on January 1, 2000, and is given by Eq. (8).

$$JD = 2432916.5 + 365 \times \text{delta} + \text{leap} + \text{day} + \text{hour}/24 \quad (8)$$

Where $\text{delta} = \text{year} - 1949$, $\text{leap} = \text{int} \left[\text{delta}/4 \right]$, it is defined as the integer portion of the argument.

2.4.3 Elliptic Coordinates

The elliptical coordinates are calculated using Eqs. (9 – 13).

$$n = JD - 2451545.0 \quad (9)$$

$$L = 280.460 + 0.9856474 \times n ; (0^\circ \leq L < 360^\circ) \quad (10)$$

$$g = 357.528 + 0.9856003 \times n ; (0^\circ \leq g < 360^\circ) \quad (11)$$

$$l = L + 1.915 \times \sin(g) + 0.020 \times \sin(2g) ; (0 \leq l < 360^\circ) \quad (12)$$

$$\text{ep} = 23.439 - 0.0000004 \times n \quad (13)$$

Where L is the mean longitude, g is the mean anomaly, l is the ecliptic longitude, and ep is the obliquity of the ecliptic.

2.4.4 Celestial Coordinates

The celestial coordinates are the coordinates that define the position of objects in the celestial sphere or the set of numbers that pinpoint the position of objects in the sky. These coordinates are calculated by using Eq. (14 – 15).

$$\tan(\text{ra}) = \cos(\text{ep}) \times \sin(l) / \cos(l) \quad (14)$$

$$\sin(\text{dec}) = \sin(\text{ep}) \times \sin(l) \quad (15)$$

Where ra is the right ascension, and dec is the declination.

2.4.5 Greenwich Mean Sidereal Time (gmst)

The Greenwich mean sidereal time (gmst) is given by Eq. (16).

$$\text{gmst} = 6.697375 + 0.0657098242 \times n + \text{hour (UTC)} ; (0 \leq \text{gmst} < 24\text{h}) \quad (16)$$

2.4.6 Local mean sidereal time (lmst)

The local mean sidereal time (lmst) from a given gmst, the East longitude must be added to the gmst using Eq. (17).

$$\text{lmst} = \text{gmst} + \text{east. longitude} / 15 \quad (17)$$

2.4.7 Hour Angle

The hour angle (ha) is calculated using Eq. (18).

$$\text{ha} = \text{lmst} - \text{ra} ; (-12\text{h} < \text{ha} \leq 12\text{h}) \quad (18)$$

2.4.8 Azimuth and Elevation

Finally, the sun's position definition parameters of azimuth (az) and elevation (el) are calculated using Eq. (19 – 20).

$$\sin(\text{el}) = \sin(\text{dec}) \times \sin(\text{lat}) + \cos(\text{dec}) \times \cos(\text{lat}) \times \cos(\text{ha}) \quad (19)$$

Where lat is the latitude and then the azimuth angle az can be calculated, which is measured from the north (0°):

$$\sin(\text{az}) = -\cos(\text{dec}) \times \sin(\text{ha}) / \cos(\text{el}) ; (0^\circ < \text{az} < 360^\circ) \quad (20)$$

2.4.9 Occurrence of Shadow Flicker

Once the sun position and elevation are calculated, the shadow flicker is determined by the position (P) of the wind turbine, and the position of the sun (elevation angle and azimuth angle). Figure 5 illustrates the method and concept used by WindFarmer [22]. The model calculates the minimum distance from the wind turbine hub to any point (S) on the line between the sun and the point of interest (A).

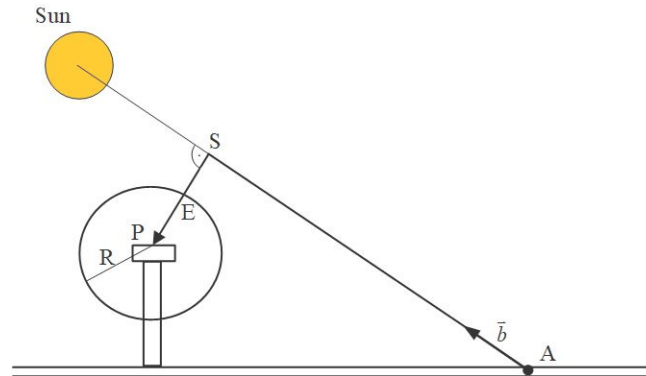


Figure 5. Conceptual model of the shadow flicker calculation in WindFarmer [22].

The points A, P, and S are represented by their vectors, \vec{A} , \vec{P} and $\vec{S} = \vec{a} + \lambda_s \vec{b}$. The vector \vec{b} is a unit vector pointing from the receptor to the middle of the sun and is given by Eq. (21).

$$\vec{b} = \begin{pmatrix} \cos(\text{el}) & \sin(\text{az}) \\ \cos(\text{el}) & \cos(\text{az}) \\ \sin(\text{el}) & \end{pmatrix} \quad (21)$$

For the vector AS to be perpendicular to the vector PS, we require $\vec{b} \cdot (\vec{S} - \vec{P}) = 0$. This will lead to vector SP, perpendicular to the vector AS given in Eq. (22).

$$\vec{SP} = \vec{a} + \frac{\vec{b} \cdot (\vec{P} - \vec{a})}{\vec{b} \cdot \vec{b}} \vec{b} - \vec{P} \quad (22)$$

WindFarmer compares the norm of the vector PS with the radius R of the turbine. This is repeated in time intervals of 1 minute through one year to detect if the shadow is produced at the point of analysis at each time. The model counts the minutes/day and the hours/year of shadow flicker caused by each wind turbine. The terrain features are also considered in the calculation to check for terrain features blocking the line of sight between the wind turbine and the receptor.

The rotor position is very important in the shadow flicker calculations as it is the source of the shadow. The rotor offset is calculated using Eq. (23).

$$\text{Rotor offset} = (1/2)\text{tower to diameter} + \text{tower position} + \text{disc depth} \quad (23)$$

Where tower position and disc depth are defined in the 3D Designer module of the Turbine Studio software.

Finally, employing the above shadow flicker calculation method, the shadow flicker of the wind power plant was calculated and presented for each wind turbine and all positions in the vicinity of the wind power plant.

2.5 Zones of Visual Influence (ZVI)

The zones of visual influence (ZVI) determine the visibility, suggesting the number of wind turbines that can be seen from certain distances from the wind power plant. In much research, the visual impacts of large wind turbines have been studied, and the findings show them to be directly related to the aesthetic value of the landscape. Large wind turbines in high aesthetic value areas face significant public opposition, while those in low aesthetic value areas are generally accepted quite well [25].

In this study, the ZVI assessment of the 50 MW wind power plant was also done using the WindFarmer model [22]. This model uses the line-of-sight algorithm, which checks the line of sight at regular intervals against the terrain height at each point of interest. This method offers a good degree of accuracy in comparison to other methods.

2.5.1 Standard ZVI Calculation

The standard ZVI calculates the number of wind turbines visible from the point of observer A, as shown in Figure 6, with the visibility defined as either where the hub is visible or, more sensitively, where the tip of the blade is visible.

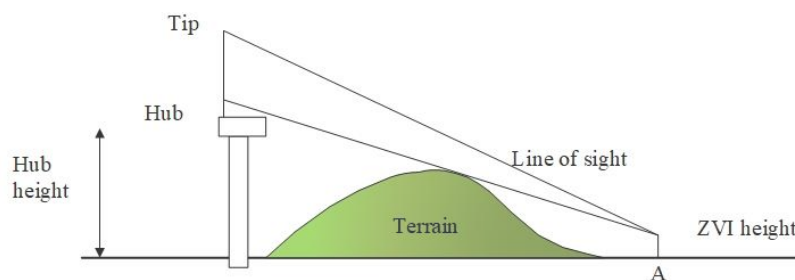


Figure 6. Standard calculation of the zones of visual influence [22].

In addition to the standard ZVI calculation, WindFarmer also calculates other ZVI parameters to assess the visual impacts of wind power plants on landscapes fully.

2.5.2 Vertical Subtended Angle

The vertical subtended angle addresses how large the wind turbines are in the observer's field of view. Wind turbines on elevated positions like hilltops will usually be visible from great distances, and the severity of the visibility declines with the distance. Figure 7 explains the vertical subtended angle calculation.

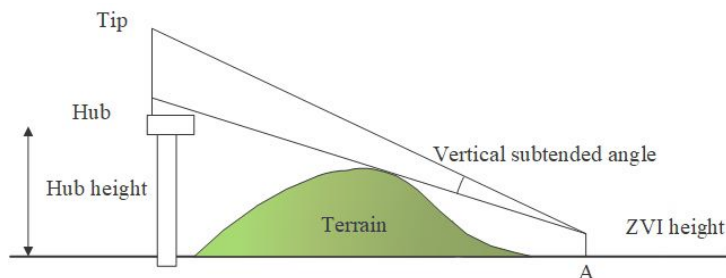


Figure 7. Conceptual representation of the vertical subtended angle [22].

2.5.3 Horizontal Subtended Angle

Similar to the vertical subtended angle, the horizontal subtended angle calculates the observer's horizontal field of view from the point of observation, as shown in Figure 8.

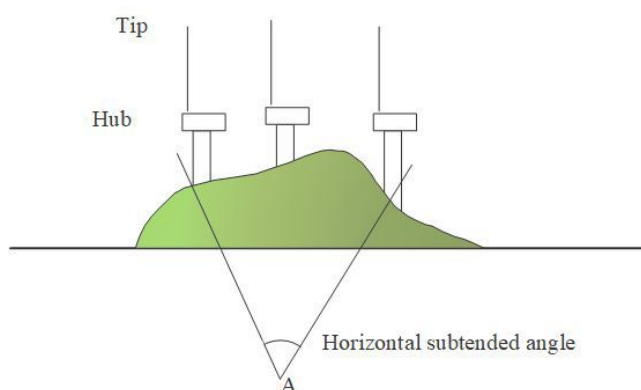


Figure 8. Conceptual representation of the horizontal subtended angle [22].

2.5.4 Visibility of the Site

Finally, using the calculations discussed above, the visibility of the site is determined. The visibility of the site determines the number of wind turbines visible from the point of observation. This work investigates and presents the number of wind turbines visible from different observation distances of the 50 MW wind power plant.

3. Results and Discussion

The microscale wind resource map at 137 m agl (10 × 10 km² grid, with a resolution of 90 m), including the positions of the 20 wind turbines at the location of the potential 50 MW wind power plant, is presented in Figure 9. It can be seen that the wind speeds over the study area varied in the range of 4 to 8 m/s. However, the wind speeds near the wind turbines range from 5 to 7 m/s.

This section presents and discusses the results of the noise levels, the shadow flicker, and the zones of visual influence. Many studies carried out by governments and organizations worldwide have suggested safe noise levels for wind power plant operations. In its report, the Environmental Protection Agency of Europe [24] has defined a 45 dBA or a maximum increase of 5 dBA above background noise at nearby noise-sensitive locations as allowed sound levels for normal places. Otherwise, in low-noise environments where background noise is less than 30 dBA, the allowed limit is 35 to 40 dBA.

Similarly, a report from the Energy Department of South Africa defines 35 to 40 dBA as the allowed operating sound levels for wind power plants [25]. For its part, the South Australian state government has allowed noise levels of 35 dBA for rural areas and 40 dBA for other areas, or in general, the noise level should not exceed more than 5 dBA compared to the background noise of the area [26].

In Thailand, the Department of Pollution Control has defined an acceptable noise level of 50 dBA or a noise level that is less than 10 dBA above the background noise [27]. Hence, a noise level of 35 to 50 dBA is generally allowed in various jurisdictions.

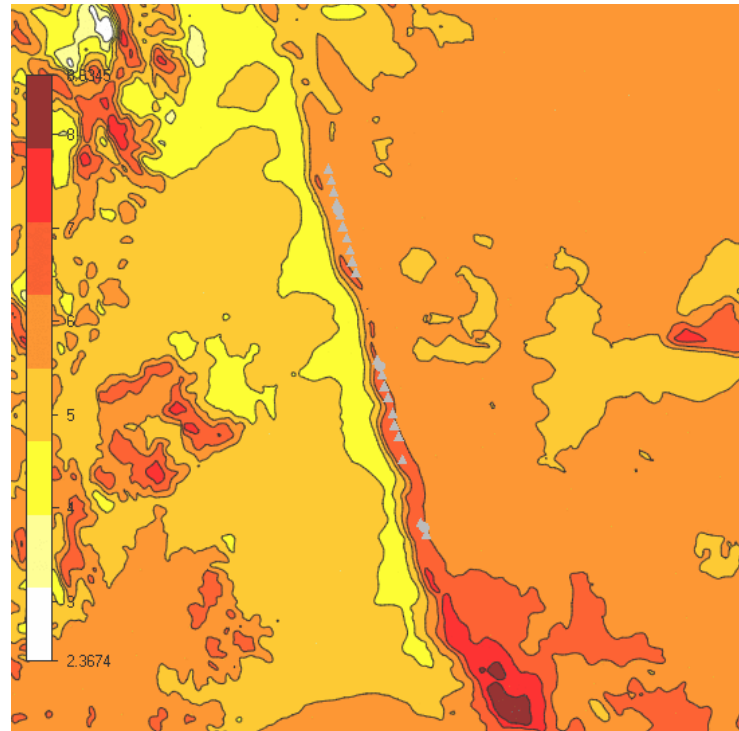


Figure 9. Microscale wind resource map at 137 m above ground level ($10 \times 10 \text{ km}^2$ grid, with a resolution of 90 m), including the positions of the 20 wind turbines at the location of the potential 50 MW wind power plant.

Figure 10 presents the noise emission contours for the potential 50 MW wind power plant in northeastern Thailand. It was found that the maximum noise occurred at less than 50 dBA. It can also be observed that the noise emissions are higher near each wind turbine. Thus, the noise emission levels reduce significantly with the distance of each wind turbine. This is because the noise emitted by the operation of a wind turbine under varied wind resources is attenuated by geometrical divergence, atmospheric absorption, ground effects, barriers, and other effects like foliage and areas of buildings, as well as due to the meteorological impacts.

Table 2 shows the noise produced by each wind turbine of the potential 50 MW wind power. In contrast, Table 3 illustrates the noise levels and the area affected by certain noise levels compared to the $10 \times 10 \text{ km}^2$ computational grid. The wind turbines produce between 46.5 - 47.5 dBA noise levels, well below the allowed level of 50 dBA in Thailand. Apart from this, most of the area around the potential wind power plant is affected by relatively low noise levels, and only a small area of 5.9 km^2 (1.3% of the area studied) is in the range of 41 - 50 dBA.

Similar to the noise emission levels, the shadow flicker is another important aspect affecting the social acceptance of a wind power plant. Few countries and states have introduced legislation to limit the shadow flicker caused by wind farms. Governments in Australia, England, Ireland, and many other countries require that the shadow flicker of wind power plants be below 30 hours/year and 30 minutes/day [28, 29]. So far, Thailand has not introduced any specific legislation for shadow flickering of wind power plants. Table 2 also shows the shadow flicker of each wind turbine on an annual basis. In contrast, Table 4 shows the area affected by the shadow flicker of the potential wind power plant in comparison to the $10 \times 10 \text{ km}^2$ computational grid. While the majority of the area studied has no shadow flicker (73.7% of the area studied) or less than 10 hours per year (11.9% of the area studied), shadow flicker of an individual wind turbine is in the range of 50 hours/year for nearly 10% of the area studied. Less than 2% of the area studied has shadow flicker above 100 hours per year. Figure 11 summarizes the shadow flicker in graphical form, confirming that the shadow flicker for all wind turbines is well within the 1000 m buffer zones established for each wind turbine. Thus, the shadow flicker should have limited impacts on the population.

Finally, the visual impact of wind energy developments is highly related to the quality of the landscape and the perception of the residents living around it. Wind energy developments face opposition in

high-value aesthetic landscapes and are well-accepted in areas with lower aesthetic values. Similarly, some people feel annoyed due to the wind turbines obstructing the field of view, while others consider it a positive addition to the landscape. Table 2 provides the zone of visual influence for each wind turbine, while Figure 12 shows different areas with the number of wind turbines visible. Generally, between 15 and 20 turbines are visible from observation points surrounding the potential wind power plant.

Table 2. Noise emission levels, shadow flicker, and zones of visual influence of the potential 50 MW wind power plant.

Turbine	Noise (dBA)	Shadow Flicker (hours/year)	Zone of Visual Influence (Turbine)
WTG 1	47.10	102.4	17
WTG 2	47.57	87.4	15
WTG 3	47.69	78.4	20
WTG 4	47.72	93.9	20
WTG 5	47.73	140.0	20
WTG 6	47.72	88.8	20
WTG 7	47.68	83.0	20
WTG 8	47.70	133.8	20
WTG 9	47.66	71.8	20
WTG 10	47.12	62.5	20
WTG 11	46.81	60.0	12
WTG 12	47.35	85.0	20
WTG 13	47.60	116.0	20
WTG 14	47.42	95.8	15
WTG 15	47.41	124.5	20
WTG 16	47.52	136.3	20
WTG 17	47.18	98.9	20
WTG 18	46.50	74.9	10
WTG 19	46.79	50.8	20
WTG 20	46.82	85.7	20

Table 3. The area is affected by the noise emissions of the potential 50 MW wind power plant compared to the 10 x 10 km² computational grid.

Noise (dB(A))	Area (km ²)	%
> 0	17.66	4.4
1.0 - 10.0	131.24	32.8
11.0 - 20.0	150.22	37.6
22.0 - 30.0	69.91	17.5
31.0 - 40.0	25.80	6.5
41.0 - 50.0	5.89	1.3

Table 4. The area affected by shadow flicker of the potential 50 MW wind power plant.

Shadow Flicker (hours/year)	Area (km ²)	%	Cumulative (%)
No shadow flicker	73.7	73.7	73.7
0.1 - 10	11.9	11.9	85.6
10.1 - 100	9.7	9.7	95.3
100.1 - 200	2.8	2.8	98.1
200.1 - 300	1.1	1.1	99.2
300.1 - 400	0.5	0.5	99.7
400.1 - 500	0.3	0.3	100
500.1 - 600	0.02	0.02	100
Total Area	26.3	100.0	100

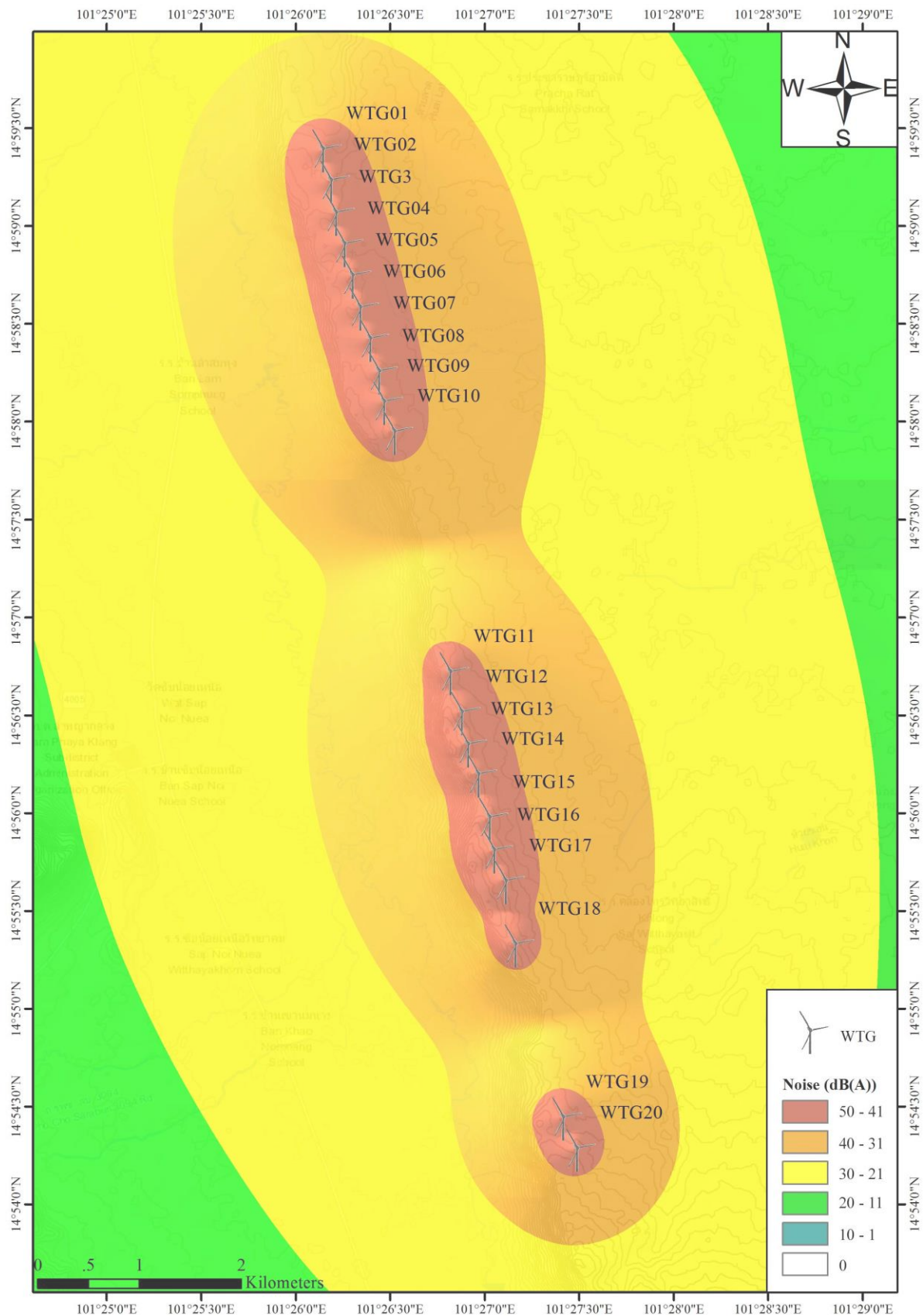


Figure 10. Noise emission contours of the 20 wind turbines composing the potential 50 MW wind power plant.

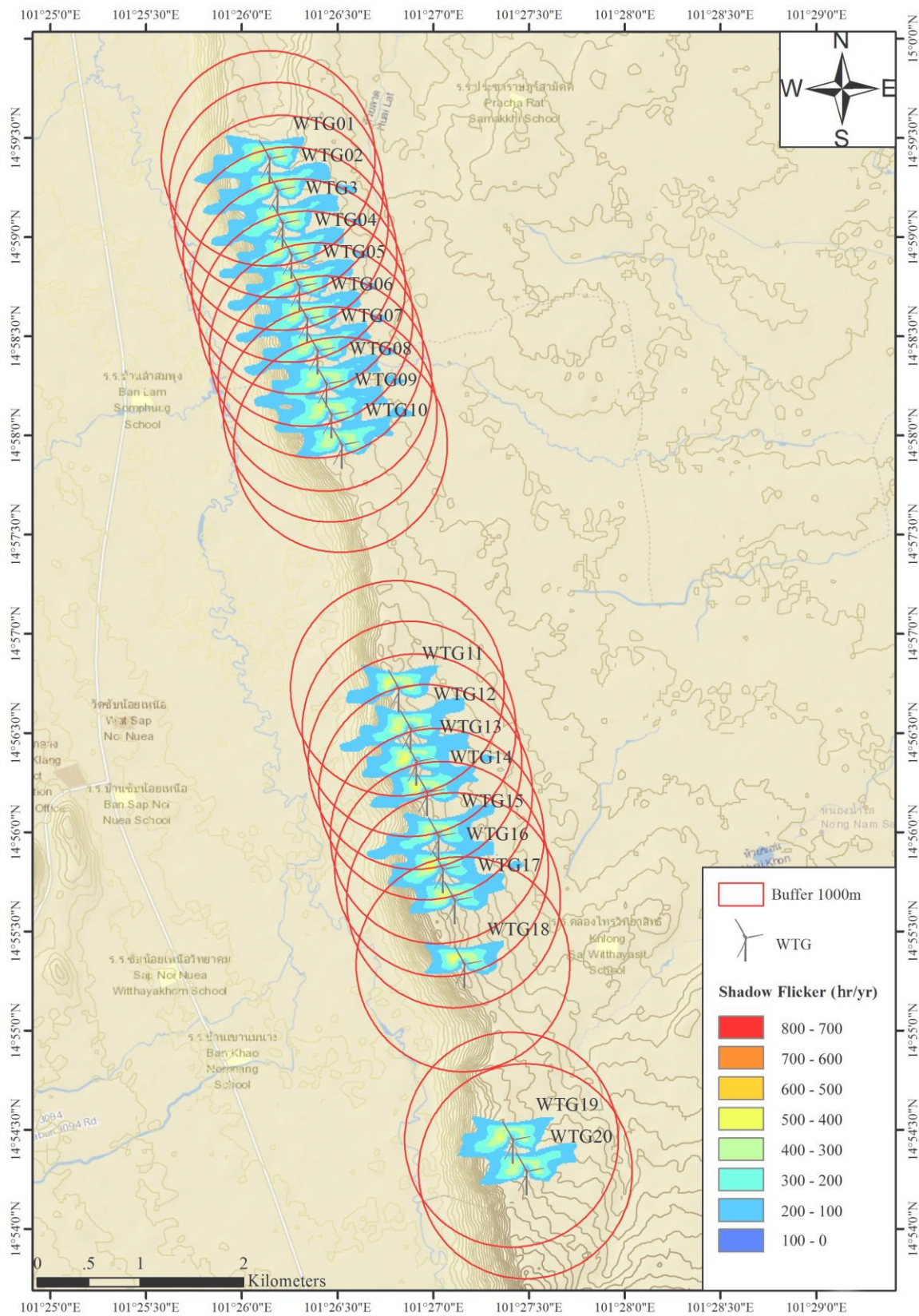


Figure 11. Shadow flicker of the potential 50 MW wind power plant.

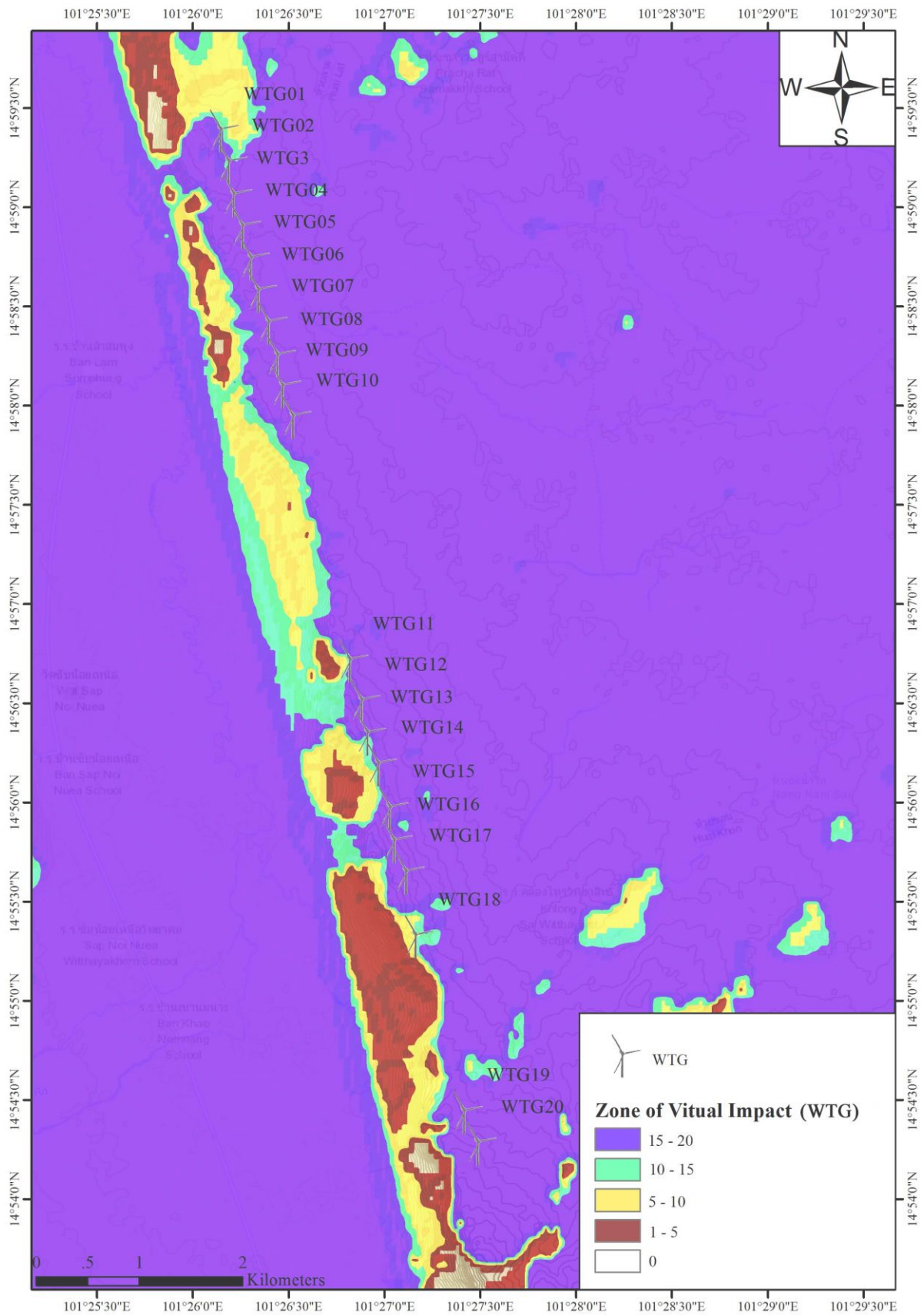


Figure 12. Zone of visual influence of the potential 50 MW wind power plant.

4. Conclusions

Onshore wind power plants are important renewable energy sources and will be crucial for countries like Thailand to transition to green, non-GHG-emitting energy. But despite being the most popular renewable energy source, onshore wind power plants are susceptible to public opposition due to their environmental impacts. Onshore wind power plants face acceptance issues due to noise and shadow flicker disturbances they cause in their vicinity. In addition, their visual impacts are also considered undesirable, especially in highly aesthetic-valued areas where it is believed to have a profound effect on the land value. Therefore, it is vital to fully understand and address these issues while developing a wind power plant in an area to avoid conflicts and develop wind resources sustainably. This research aimed to assess the noise emission levels, the shadow flicker, and the visual impacts of a potential 50 MW wind power plant located in the Nakhon Ratchasima province of northeastern Thailand.

The WindFarmer simulation model [22] assessed the noise emission levels, the shadow flicker, and the zones of visual influence of the wind power plant. With noise levels of 46.5 to 47.5 dBA, the wind power plant would be well within the allowable range of 50 dBA. Similarly, it also has a good shadow flicker profile of less than 10 hours/year for most of the area surrounding the site, way below the value of 30 hours/year seen in other jurisdictions. Finally, the results of the zones of visual influences indicate that between 15 and 20 wind turbines are visible from observation points surrounding the potential wind power plant. The results applied to this case study suggest that the potential wind power plant is well-suited regarding its environmental impacts and should typically not incur negative impacts for the local communities. Studies like these are vital to gaining the trust of the communities living near wind power plants to address their concerns and minimize opposition.

On a broader scale, the method used in this study can be employed in any other part of the world to assess and better plan the development and installation of onshore wind power plants. Beyond the technical, economic, and environmental aspects of wind power plants, future investigations should look at the impacts of wind turbines and wind power plants on biodiversity and the social acceptance of wind power plants. Understanding these issues better should identify mitigation strategies in wind energy development as an important component of the energy transition.

5. Acknowledgements

The authors would like to thank the Research and Development Institute and the Research Center in Energy and Environment (RCEE) of Thaksin University for their financial support of this work under the framework of an International Collaborative Research Project.

Author Contributions: Conceptualization, K.S. and W.J.; methodology, K.S.; software, C.S.; validation, K.S.; formal analysis, M.P.; investigation, K.S. and W.J.; writing-original draft preparation, K.S.; writing-review and editing, A.F. and G.Y.; visualization, W.J.; supervision, W.J. and G.Y.; All authors have read and agreed to the published version of the manuscript.

Funding: The authors thank the private company for their financial support and the data used in this work. The private company was not involved in the research work or in preparing and submitting this publication.

Conflicts of Interest: There is no conflict of interest.

References

- [1] International Energy Agency (IEA). *Electricity Market Report 2023*. 2023. <https://www.iea.org/reports/electricity-market-report-2023>. (accessed April 25, 2023)
- [2] International Energy Agency (IEA). *Renewables 2022: Analysis and Forecast to 2027*. 2022. <https://www.iea.org/reports/renewables-2022> (accessed May 2, 2023).
- [3] United Nations Framework Convention on Climate Change (UNFCCC). *Adoption of the Paris Agreement - Paris Agreement Text English*, 2015. https://unfccc.int/sites/default/files/english_paris_agreement.pdf. (accessed May 1, 2023).

- [4] Electricity Generating Authority of Thailand (EGAT). *Annual Report 2021 Electricity Generating Authority of Thailand*. 2022. https://www.egat.co.th/home/en/wp-content/uploads/2022/06/EGAT-Annual-2021-EN_2022-06-22.pdf. (accessed May 3, 2023).
- [5] Energy Regulatory Commission (ERC). *Annual Report - Energy Regulatory Commission of Thailand*. 2021. <https://www.erc.or.th/en/annual-report/3749> (accessed May 3, 2023).
- [6] Energy Policy and Planning Office (EPPO). *Thailand Power Development Plan (2015-2036)*. 2015. https://www.eppo.go.th/images/POLICY/ENG/PDP2015_Eng.pdf. (accessed April 25, 2023).
- [7] Energy Policy and Planning Office (EPPO). *Meeting Resolution on Energy Saving Methods No. 2/2021 (No. 154)*. 2021. <https://www.eppo.go.th/index.php/th/component/k2/item/17213-nepc-prayut04-08-64>. (accessed April 30, 2023).
- [8] International Renewable Energy Agency (IRENA). *Renewable Energy Outlook – Thailand*. 2017. https://www.irena.org//media/Files/IRENA/Agency/Publication/2017/Nov/IRENA_Outlook_Thailand_2017.pdf (accessed April 10, 2023).
- [9] Global Wind Energy Council (GWEC). *An Industry Perspective on Strengthening Onshore Wind Development in Thailand*. 2019. <https://ec.europa.eu/eurostat/statistics-> (accessed April 29, 2023).
- [10] Kamdar, I.; Taweekun, J. Assessment of Wind Energy Potential of Hat Yai (Songkhla), Thailand. *IOP Conference Series: Materials Science and Engineering*. 2021, 1163(1), 012001. <https://doi.org/10.1088/1757-899X/1163/1/012001>
- [11] Waewsak, J.; Chancham, C.; Chiwamongkhonkarn, S.; Gagnon, Y. Wind Resource Assessment of the Southernmost Region of Thailand Using Atmospheric and Computational Fluid Dynamics Wind Flow Modeling. *Energies*. 2019, 12, 1899. <https://doi.org/10.3390/EN12101899>.
- [12] Niyomtham, L.; Lertsathittanakorn, C.; Waewsak, J.; Gagnon, Y. Mesoscale/Microscale and CFD Modeling for Wind Resource Assessment: Application to the Andaman Coast of Southern Thailand. *Energies*. 2022, 15, 3025. <https://doi.org/10.3390/EN15093025>.
- [13] Werapun, W.; Tirawanichakul, Y.; Waewsak, J. Wind Shear Coefficients and their Effect on Energy Production. *Energy Procedia*. 2017, 138, 1061-1066. <https://doi.org/10.1016/J.EGYPRO.2017.10.111>.
- [14] Council of Canadian Academes, 2015. "Understanding the Evidence: Wind Turbine Noise". Ottawa (ON), Canada: The Expert Panel on Wind Turbine Noise and Human Health, Council of Canadian Academes, 180 p. (Experts Panel (alphabetical order): H.W Davies, Y. Gagnon, C. Giguère, T.L. Guidotti (Chair), S. Grace, R.V. Harrison, B. Howe, D.A. Johnson, K. Persson Wayne, J.D. Roberts). <https://cca-reports.ca/reports/understanding-the-evidence-wind-turbine-noise/> (accessed April 29, 2023).
- [15] Huber, S.; Horbaty, R.; Ellis, G. *Social Acceptance of Wind Power Projects: Learning from Trans-National Experience*, 5th ed.; Palgrave Macmillan UK: London, England. 2012, 215-278. https://doi.org/10.1057/9781137265272_11
- [16] Molnarova, K.; Sklenicka, P.; Stiborek, J.; Svobodova, K.; Salek, M.; Brabec, E. Visual Preferences for Wind Turbines: Location, Numbers and Respondent Characteristics. *Applied Energy*. 2012, 92, 269–278. <https://doi.org/10.1016/j.apenergy.2011.11.001>.
- [17] Hall, N.; Ashworth, P.; Devine-Wright, P. Societal Acceptance of Wind Farms: Analysis of Four Common Themes across Australian Case Studies. *Energy Policy*. 2013, 58, 200–208. <https://doi.org/10.1016/j.enpol.2013.03.009>.
- [18] Weather Spark. *Nakhon Ratchasima Climate, Weather by Month, Average Temperature (Thailand)*. <https://weatherspark.com/y/114253/Average-Weather-in-Nakhon-Ratchasima-Thailand-Year-Round> (accessed May 1, 2023).
- [19] Niyomtham, L.; Waewsak, J.; Kongruang, C.; Chiwamongkhonkarn, S.; Chancham, C.; Gagnon, Y. Wind Power Generation and Appropriate Feed-in-Tariff under Limited Wind Resource in Central Thailand. *Energy Reports*. 2022, 8, 6220–6233. <https://doi.org/10.1016/j.egy.2022.04.068>.
- [20] https://liddcatalog.ldd.go.th/dataset/lidd_21_01 (accessed December, 11 2022).
- [21] <https://asterweb.jpl.nasa.gov/gdem.asp> (accessed December, 11 2022).
- [22] GH and Partners. *GH WindFarmer: Theory Manual*. <http://www.ccpo.odu.edu/~klinck/Reprints/PDF/garradhassan2009.pdf>. (accessed May 10, 2023).
- [23] Haac, R.; Darlow, R.; Kaliski, K.; Rand, J.; Hoen, B. In the Shadow of Wind Energy: Predicting Community Exposure and Annoyance to Wind Turbine Shadow Flicker in the United States. *Energy Research & Social Science*. 2022, 87, 102471. <https://doi.org/10.1016/j.er ss.2021.102471>.

- [24] Environmental Protection Agency Office of Environmental Enforcement (OEE). *Guidance Note on Noise Assessment of Wind Turbine Operations at EPA Licensed Sites (NG3)*. 2011. https://www.epa.ie/publications/monitoring--assessment/noise/Wind_Turbine_web.pdf. (accessed May 11, 2023).
- [25] Powered by Wind. *Noise Levels of Wind Farms*, 2018. <http://www.poweredbywind.co.za/dl/english/factsheet5.pdf>. (accessed May 5, 2023).
- [26] Corke, T.; Nelson, R. *Wind Farms Environmental Noise Guidelines*. 2018. <https://doi.org/10.1201/b22301-8>. (accessed May 8, 2023).
- [27] Waewsak, J.; Kongruang, C.; Gagnon, Y. Assessment of Wind Power Plants with Limited Wind Resources in Developing Countries: Application to Ko Yai in Southern Thailand. *Sustainable Energy Technologies and Assessments*. 2017, 19, 79-93. <https://doi.org/10.1016/j.seta.2016.12.001>.
- [28] Poli, S. *Annex D Shadow Flicker Assessment Cañadon Leon Windfarm*. 2019. https://www3.dfc.gov/Environment/EIA/canadon/Supp_ESIA_ANNEX_D.pdf. (accessed May 10, 2023)
- [29] Brinckerhof, P. *Update of UK Shadow Flicker Evidence Base*. 2011. https://assets.publishing.service.gov.uk/government/uploads/system/uploads/attachment_data/file/48052/1416-update-uk-shadow-flicker-evidence-base.pdf. (accessed May 12, 2023).



Prevalence, Virulence Profiles, and Genetic Relatedness of *Escherichia coli* O45 from Raw meats, Southern Thailand

Pharanai Sukhumungoon^{1*}, Aphisara Sae-lim², Fadeeya Hayeebilan³ and Pattamarat Rattanachuay⁴

¹ Division of Biological Science, Faculty of Science, Prince of Songkla University, Songkhla, 90110, Thailand; pharanai82@gmail.com

² Division of Biological Science, Faculty of Science, Prince of Songkla University, Songkhla, 90110, Thailand; aphisara.sae@gmail.com

³ Division of Biological Science, Faculty of Science, Prince of Songkla University, Songkhla, 90110, Thailand; fadeeyah.h@psu.ac.th

⁴ Department of Science, Faculty of Science and Technology, Prince of Songkla University, Pattani, 94000, Thailand; pattamarat.r@gmail.com

* Correspondence: pharanai82@gmail.com

Citation:

Sukhumungoon, P.; Sae-lim, A.; Hayeebilan, F.; Rattanachuay, P. Prevalence, Virulence Profiles, and Genetic Relatedness of *Escherichia coli* O45 from Raw meats, Southern Thailand. *ASEAN J. Sci. Tech. Report.* **2023**, *27*(2), 58-71. <https://doi.org/10.55164/ajstr.v27i2.252140>

Article history:

Received: December 22, 2023

Revised: February 7, 2024

Accepted: February 26, 2024

Available online: February 29, 2024

Publisher's Note:

This article is published and distributed under the terms of the Thaksin University.

Abstract: Non-O157 Enterohaemorrhagic *Escherichia coli* (EHEC) has become a major public health concern all around the globe. This study investigated the *E. coli* serogroup O45 from raw meats in southern Thailand using the immunomagnetic separation approach (IMS). Forty-nine *E. coli* O45 strains were obtained from 13 positive meat samples (13/105), showing the prevalence of O45 contamination as 12.4%. They were not members of EHEC. Exploration of other virulence genes exhibited that *fimH*, responsible for bacterial adherence, was found in all strains, while *astA* encoding for EAST-1 toxin was 63.2% of the strains. Moreover, *lpf* encoding long polar fimbriae was found as 30.6%. Phylogenetic group analysis revealed that the majority of *E. coli* O45 belonged to group D (88%), followed by group A (8%) and group B1 (4%). However, none belonged to group B2. The intactness of *stx*₂-phage integration sites showed that *sbcB* was occupied by prophages at the highest rate, followed by the Z2577 site. Antimicrobial susceptibility assay demonstrated relatively high bacterial resistance to cephalothin (78%), streptomycin (51%), cotrimoxazole (39%), tetracycline (31%), and chloramphenicol (23%). Furthermore, multi-drug resistant ability was uncovered in O45 strains at 49%. DNA profiling of *E. coli* O45 by BOX-PCR analyzed at 80% genetic similarity revealed 5 distinguishable clusters. More importantly, the strains from different samples and time intervals showed identical DNA fingerprints, suggesting that they may have originated from the same bacterial clone.

Keywords: *Escherichia coli*, O45, raw meat, Thailand, EHEC

1. Introduction

Diarrheal disease plays an important role as a public health problem, accounting for about 11% of child deaths worldwide, making diarrhea the second leading cause of mortality among children under 5 years of age [1]. Among the diarrheagenic *E. coli* (DEC) group, enterohaemorrhagic *E. coli* (EHEC) is the most important pathotype in human infections, showing the most devastating effect on the host. Only < 100 cells of EHEC are enough to cause illness [2].

EHEC, containing the cardinal virulence factors Shiga toxins (Stxs), is capable of causing food poisoning outbreaks in both the western and eastern hemispheres [3-5]. The symptoms of patients infected by EHEC vary from bloody diarrhea to renal failure and death [6]. Renal failure occurs when Stx is internalized into kidney cells through the cellular membrane-specific receptor



globotriaosylceramide (Gb3). After one adenine residue from 28S ribosomal RNA of 60S ribosomal subunit is removed, it inhibits protein synthesis [7].

Even though the EHEC serotype O157:H7 is the most crucial, EHEC in serotypes other than O157:H7 has recently attracted attention and is involved with severe human diseases [8]. There are 6 important EHEC serotypes (also called the big six) that have been demonstrated to carry *stx* genes, O26, O45, O103, O111, O121, and O145. These EHEC serotypes show a striking ability to cause sporadic infections and outbreaks in many countries worldwide. Although EHEC O45 infections were less found than serotype O157, the strain that carries *stx* is also thought to cause severe morbidity and mortality.

Natural reservoir hosts of EHEC are ruminants, especially cattle, that carry EHEC in their gut without pathological symptoms [9]. There are many routes of EHEC transfer from animals to humans, and the contamination through raw meats during slaughtering processes is one of the potential routes transferring EHEC to humans. Thus, raw meats, especially beef, are the important EHEC vehicles [10].

Although several EHEC serotypes are well-studied, a lack of information regarding the prevalence and characteristics of EHEC serotype O45 is documented in Thailand. Thus, this study aimed to investigate its prevalence, virulence profile, antimicrobial susceptibility, and the genetic similarity of EHEC O45 strains from meats marketed in southern Thailand. The data obtained in this study could provide information on possible infections and outbreaks of EHEC O45 in the southern area of Thailand and neighboring countries. This is essential from a public health standpoint.

2. Materials and Methods

2.1 Sample collection and immunomagnetic separation (IMS) of *E. coli* O45 from raw meats

To obtain *E. coli* O45 from raw meats, the IMS technique was carried out as previously described [11]. Raw meat samples, e.g., beef, chicken, and pork, were collected from 8 fresh markets throughout Hat-Yai City, Songkhla province, Thailand, and processed within 2 hours after collection. Briefly, 50 g of raw meat was homogenized with 450 ml of tryptic soy broth (TSB) for 1 minute. The liquid phase was obtained aseptically in a sterile bottle and incubated at 37°C for 6 hours statically. Afterward, 1 ml of the enriched culture was transferred to a 1.5 ml sterile tube and mixed with 15 µl O45-specific immunomagnetic beads (Dynabeads, Thermo Scientific, USA) for 30 minutes with a gentle tube inverted every 5 minutes. The magnetic concentrator harvested the immunomagnetic beads-bacteria complex and washed it with 500 µl of phosphate buffer saline, pH 7.4 (PBS). Subsequently, it was re-suspended in 100 µl PBS, streaked on eosin methylene blue (EMB) agar, and incubated at 37°C for 18 hours. For further analyses, ten to twenty green metallic sheen colonies were selected and kept at -80°C (using 10% (v/v) glycerol as a cryoprotectant).

2.2 Genomic DNA preparation

Bacterial genomic DNA (gDNA) was extracted using boiling [12]. In brief, a single bacterial colony was grown in 3 ml of TSB at 37°C for 3 hours with aeration (150 rpm orbital shaking). One ml of bacterial culture was boiled for 10 minutes, immediately immersed on ice for 5 minutes, then centrifuged at 11,000 g for 5 minutes. To prepare the PCR template, a ten-fold dilution of boiled supernatant was carried out using sterile deionized water (10-µl boiled supernatant: 90-µl sterile deionized water).

2.3 Identification of *E. coli* O45

For the identification of *E. coli* O45, PCR targeting the *wzy*O45 gene was performed. A 25-µl PCR reaction mixture was composed of 3.0 mM MgCl₂, 0.1 mM of dNTPs, 0.4 µM of forward and reverse primers (Table 1), 1X GoTaq Flexi green buffer, 0.5 unit of GoTaq DNA polymerase (Promega, USA) and 2 µl of DNA template. Thirty-five cycles composing denaturation at 94°C for 1 min, annealing at 50°C for 1 min, and extension at 72°C for 1 min were carried out in T100™ Thermal Cycler (Bio-Rad, Hercules, CA, USA). Amplicons were analyzed in 1.0% agarose gel electrophoresis, stained with ethidium bromide, and visualized under the WSE-5200 Printgraph 2M gel imaging system (ATTO Corp., Tokyo, Japan). The *uidA* gene specific for *E. coli* was also performed to confirm the being of *E. coli*.

2.4 *E. coli* pathotype classification and detection of virulence genes

Pathotype classification was investigated since *E. coli* in serogroup O45 tend to be a member of enterohaemorrhagic and Shiga toxin-producing *E. coli* (STEC). Indicator genes for 6 DEC categories were examined by PCR as following criteria, *stx+eae* for EHEC; *bfp+eae* for typical enteropathogenic *E. coli* (tEPEC) or *eae* alone for atypical enteropathogenic *E. coli* (aEPEC); *est/elt* for enterotoxigenic *E. coli*, ETEC; *aggR* for enteroaggregative *E. coli*, EAEC; *ipaH* for enteroinvasive *E. coli*, EIEC; *daaE* for diffusely adherent *E. coli*, DAEC (Table 1). Thermal cycling conditions were as follows: pre-heated at 95°C for 3 minutes followed by 35 cycles of denaturation at 94°C for 1 minute, annealing at 40°C (for *est*), 50°C (*elt*, *aggR*, *stx2*), 55°C (*stx1*, *eae*, *daaE*), 60°C (for *ipaH*), and extension at 72°C for 1 minute except for *eae* for 70 seconds. The reactions were finalized at 72°C for 5 minutes. Amplicons were analyzed as described above. Other *E. coli* virulence genes of *astA*, *agn43*, *cnf1*, *hlyA*, *fimH*, and *lpf* were investigated using PCR with appropriate primer pairs (Table 1). PCR components and conditions were the same as mentioned above except the annealing temperature as follows: 50°C (for *astA*), 55°C (*fimH*, *lpf*), 58°C (*cnf1*, *hlyA*), and 67°C (for *agn43*) for 1 minute.

2.5 Phylogenetic group classification of *E. coli* O45

The phylogenetic group might indicate the virulence capability of *E. coli* to some extent. Therefore, *E. coli* O45 was investigated for their phylogenetic groups in this study. Determination of the phylogenetic group was performed as described previously [23]. PCR targeting *chuA*, *yjaA*, and TspE4.C2 fragment was employed. The thermal cycling condition was pre-heated at 95°C for 3 minutes, followed by 35 cycles of denaturation at 94°C for 50 seconds, annealing at 54°C for 50 seconds, and extension at 72°C for 30 seconds. The reaction was finalized at 72°C for 5 minutes. PCR products were analyzed as described above. Bacterial phylogenetic group classification was interpreted, followed by Clermont et al. [23].

2.6 Investigation of *stx2*-phages occupancy in *E. coli* O45

Five *E. coli* genes, *sbcB*, *wrbA*, *yecE*, *yehV*, and Z2577, are essential sites for *stx2*-phages to insert [32]. Thus, the intactness of all 5 genes was investigated by PCR using the components and condition described above except the different primers (Table 1) with the following annealing temperatures: 47°C for *wrbA*, 50°C for *sbcB* and *yehV*, 53°C for Z2577, and 60°C for *yecE*. The PCR products were analyzed by agarose gel electrophoresis as described above. If the *stx2* phage occupied a particular locus, PCR amplification was not allowed because of the large *stx2* phage genome.

2.7 Antimicrobial susceptibility assay

The disk diffusion method explored the antimicrobial susceptibility profile [33]. Briefly, a single colony was grown in 3 ml of Mueller-Hinton broth (MHB) at 37°C for 3 hours with aeration. Then, the culture was centrifuged at 8,000 g for 30 seconds to obtain the cell pellet. The solution was adjusted to 0.5 McFarland turbidity standards (approximately 1.5×10^8 cfu/ml) by densitometer (Biosan, Latvia) using 0.85% (w/v) sodium chloride solution (NSS). The adjusted bacteria were swabbed on the surface of Mueller-Hinton agar (MHA). Ten crucial antimicrobial agents, amikacin (30 µg), cephalothin (30 µg), chloramphenicol (30 µg), fosfomicin (200 µg), gentamicin (10 µg), imipenem (10 µg), kanamycin (30 µg), streptomycin (10 µg), tetracycline (30 µg) and trimethoprim/sulfamethoxazole (25 µg) were applied. The plates were incubated at 37°C for 18 hours. Vernier caliper measured clear zone and interpreted followed CLSI [33].

Table 1. Oligonucleotide primers used in this study

Gene	Virulence factor	Primer name	Sequence (5' to 3')	T _m (°C)	Amplicon size (bp)	References
<i>wzyO45</i>	O45 antigen	Forward- 5'O45	GGCTCATCATTTGGTGTCTTG	55	404	[13]
		Reverse- 3'O45	ATAAGGATTTTCAGGCCCCCTG	54		
<i>stx1</i>	Shiga toxin 1	Forward- EVT-1	CAACACTGGATGATCTCAG	49	350	[11]
		Reverse- EVT-2	CCCCCTCAACTGCTAATA	48		
<i>stx2</i>	Shiga toxin 2	Forward- EVS-1	ATCAGTCGTCACCTCACTGGT	52	404	[11]
		Reverse- EVS-2	CCAGTTATCTGACATTCTG	47		
<i>eae</i>	Intimin	Forward- AE-19	CAGGTCGTCGTCTGTCTAAA	55	1,087	[14]
		Reverse- AE-20	TCAGCGTGGTTGGATCAACCT	55		
<i>elt</i>	Heat-labile enterotoxin	Forward- TW20	GGCGACAGATTATACCGTGC	54	450	[15]
		Reverse- JW11	CGGTCTATATATCCCTGTT	50		
<i>est</i>	Heat-stable enterotoxin	Forward- JW14	ATTTTACTTCTCTATTAGTCTT	45	190	[15]
		Reverse- JW7	CACCCGGTACAAGGCAGGATT	56		
<i>ipaH</i>	Enteroinvasive mechanism	Forward- ipaIII	GTTCTTGACCCGCTTCCGATACCGTC	64	603, 619	[16]
		Reverse- ipaIV	GCCGGTCAGCCACCCCTCTGAGAGTAC	66		
<i>daaE</i>	F1845 fimbriae	Forward-daaF-F	GAACGTTGGTTAATGTGGGGTAA	54	542	[17]
		Reverse-daaF-R	TATTCACCGGTCGGTATCAGT	53		
<i>aggR</i>	Transcriptional activator of AAF/I	Forward-AggR-1	CAGAATACATCAGTACACTG	48	433	[18]
		Reverse- AggR-2	GAAGCTTACAGCCGATATAT	48		
<i>bfpA</i>	Bundle forming pili	Forward- EP-1	AATGGTCTTGGCTTGCTGC	56	326	[19]
		Reverse- EP-2	GCCGCTTATCCAACCTGGTA	54		

Table 1. Oligonucleotide primers used in this study (continued)

Gene	Virulence factor	Primer name	Sequence (5' to 3')	T _m (°C)	Amplicon size (bp)	References
<i>agn43</i>	Antigen 43	Forward- 1-Kpn	GAACCTGTCTGGTACCGATGCCCTCCC	66	≈900	[20]
		Forward- 2-Bam	CGGGATCCGTTGCCACTGTACCGGGCTTGACGACC	73		
<i>fimH</i>	Type 1 fimbriae	Forward- <i>fimH</i> -F	TGCAGAACGGATAAGCCGTGG	56	508	[21]
		Reverse- <i>fimH</i> -R	GCAGTCACTGCCCTCCGGTA	60		
<i>astA</i>	EAST1	Forward- EAST11a	CCATCAACACAGTATATCCGA	51	111	[22]
		Reverse- EAST11b	GGTCGGAGTGACGGCTTTGT	58		
<i>chuA</i>	Heme transport	Forward- chuA1	GACGAACCAACGGTCAGGAT	54	279	[23]
		Reverse- chuA2	TGCCGCCAGTACCAAAAGACA	54		
<i>yjaA</i>	Unknown	Forward- yjaA1	TGAAGTGTGAGGAGACGCTG	54	211	[23]
		Reverse- yjaA2	ATGGAGAATGCGTTCCTCAAC	52		
<i>TspE4.C2</i>	Unknown	Forward- TspE4.C2-1	GAGTAAATGTCGGGGCAATCA	52	152	[23]
		Reverse- TspE4.C2-2	CGCGCCAACAAGTATTACG	52		
<i>uidA</i>	β-glucuronidase	Forward- uidA -F	ATCACCGTGGTGACGCAATGTCGC	61	486	[24]
		Reverse- uidA -R	CACCACGATGCCATGTTTCATCTGC	59		
<i>cnf1</i>	Cytotoxic necrotizing factor-1	Forward- cnf1-F	GGCGACAAAATGCAGTATTGCTTGG	57	552	[22]
		Reverse- cnf1-R	GACGTTGGTTCGGGTAATTTTGGG	57		

Table 1. Oligonucleotide primers used in this study (continued)

Gene	Virulence factor	Primer name	Sequence (5' to 3')	T _m (°C)	Amplicon size (bp)	References
<i>lpf</i>	Long polar fimbriae	Forward- lpf A1-F	GGTCGTTTTTGCCCTTAACCGC	54	≈500	[25]
		Reverse- lpf A1-R	AGGTTGAAAATCGACCTGCGC	54		
<i>wrbA</i>	Quinone oxidoreductase	Forward- wrbA1	ATGGCTAAAAGTTCTGGTG	46	600	[26]
		Reverse- wrbA2	CTCCTGTTGAAGATTAGC	46		
<i>yecE</i>	Unknown	Forward- EC10	GCCAGCGCCGAGCACAATA	60	400	[27]
		Reverse- EC11	GGCAGGCAGTTGCAGCCAGTAT	59		
<i>sbcB</i>	Exonuclease I	Forward- sbcB1	CATGATCTGTGCCACTCG	51	1,800	[28]
		Reverse- sbcB2	AGGTCGTCCGTTTCCACTC	54		
<i>yehV</i>	Transcriptional regulator	Forward- Primer A	AAGTGGCGTTGCITTTGTGAT	50	340	[29]
		Reverse- Primer B	AACAGATGTGTGGTGAGTGCTCG	55		
Z2577	Oxidoreductase	Forward- Z2577F	AACCCCATTTGATGCTCAGGCTC	57	909	[30]
		Reverse- Z2577R	TTCCCATTTTACACTTCCTCCCG	53		
<i>hlyA</i>	α-hemolysin	Forward- hly1	AACAAGGATAAGCACTGTTCCTGGCT	56	1,177	[22]
		Reverse- hly2	ACCATATAAGCGGTCATTCCCGTCA	58		
Repetitive sequence	BOXA1R	CTACGGCAAGCGGACGCTGACG	62	variable	[31]	Repetitive sequence

2.8 Genetic relationship of *E. coli* O45

DNA profiling of *E. coli* O45 was investigated by BOX-PCR [34]. Genomic DNA (gDNA) was obtained using a mini-prep spin column (Geneaid, Taipei, Taiwan). BOX-PCR was carried out in a 25- μ l reaction mixture consisting of 0.2 μ M of BOXA1R primer (Table 1), 0.2 mM dNTPs, 1X GoTaq Flexi green buffer, 3.0 mM of MgCl₂, 1.25 units of GoTaq DNA polymerase, and 50 ng of DNA template. The thermal cycler condition was set with an initial denaturation (95°C for 3 minutes) followed by 30 cycles of denaturation at 94°C for 3 seconds and 92°C for 30 seconds, annealing at 50°C for 1 minute, and extension at 65°C for 8 minutes. The amplification products were analyzed using 1.5% agarose gel electrophoresis for 1.5 hours at 90V and imaging as described above. Dendrograms for O45 were constructed using an unweighted pair-group method of arithmetic average (UPGMA) (Bioprofile software, France).

2.9 Statistical analysis

Data were analyzed using SPSS for Windows version 11.0 (SPSS, USA). One-way ANOVA was employed to analyze significant differences in *E. coli* O45 prevalence among meat types. Significance was set at p-value < 0.05.

3. Results and Discussion

3.1 Prevalence of *E. coli* O45 in raw meat samples

1,890 suspected isolates were obtained from 105 meat samples during *E. coli* O45 investigation by IMS. It exhibited that 49 of 1,890 from 13 samples (prevalence of 12.4%) were positive for *E. coli* O45 (Table 2). The rate of IMS-associated O45 detection in this study was in concordance with the work from Sirikaew et al. [32] and Wamaedesa et al. [35] that investigated the presence of *E. coli* O26 and O104 from raw meats by IMS and found the high prevalence of 12% and 17%, respectively. Therefore, these results suggest that *E. coli* in the serogroup O45 exists in southern Thailand in relatively high prevalence. The higher prevalence of *E. coli* O45 in chicken samples (29.6%) over pork (14.3%) and beef (2%) in this study is thought to be varied, depending upon individual study [32]. In this study, IMS was employed to assist in isolating *E. coli* O45 from meat samples. This IMS method is approximately 100-fold more effective than the conventional culture method for isolating target microorganisms [36]. Lozinak et al. [37] investigated the existence of Shiga toxin-producing *E. coli* (STEC) from several food samples, including raw meat in the United States, using real-time PCR and found *E. coli* O45 and O111 from raw chicken. The Ct value of *E. coli* O45 was much lower than *E. coli* O111, suggesting that *E. coli* O45 may be predominant in the culture. Nevertheless, at such contamination rates, the conventional culture method may not isolate *E. coli* O45 from the samples. Therefore, the IMS method using an antibody-coated magnetic bead is an essential process and must be applied for EHEC/STEC isolation.

3.2 Pathotype classification and virulence gene of *E. coli* O45

Even though *E. coli* O45 in this study did not belong to any DEC pathotypes, but they were possibly equipped with some other virulence genes. Thus, *E. coli* O45 strains were examined for their virulence genes, and the results revealed that *fimH* (encoding type 1 fimbrial tip responsible for bacterial adherence) was found in all O45 strains (100%). The *astA* gene encoding for enteroaggregative heat-stable enterotoxin 1 (EAST-1) was 63.2% (31 of 49 isolates). Additionally, *lpf* encoding long polar fimbriae was found at 30.6% (15 of 49 isolates) (Figure 1A). FimH is a virulent factor conferring autoaggregation, leading to the colonization of bacteria by the host [38]. At the same time, the long polar filaments play a crucial role in bacterial adhesion in *E. coli* O157:H7, including other pathogenic *E. coli* strains [39, 40]. These two virulence factors are very important for the early step of bacterial pathogenesis. Our results are in concordance with the study of Tiba et al. [41] and Van et al. [42] that revealed the high prevalence of *fimH* as 97.5% of 162 UPEC strains isolated from patients with cystitis and 92.1% of 38 multidrug-resistant strains isolated from raw meats and shellfishes sold in Vietnam. In addition, EAST-1, widely distributed among diarrheagenic *E. coli*, has been implicated in many outbreaks [43]. This suggests that although some *E. coli* strains are absent in indicative genes for DEC, they may carry other virulence genes responsible for pathogenesis. Hence, the presence of these genes in *E. coli* O45 in our study is noteworthy; they are virulent strains and potentially cause problems after consumption.

Table 2. Prevalence of *E. coli* O45 in raw meats, Hat-Yai, Thailand.

Serotype	Source	Number of positive samples/ Total number of samples (%)	Number of positive isolates/ Total number of isolates (%)
O45	Beef	1/50 ^A (2)	2/933 (0.2)
	Chicken	8/27 ^B (29.6)	41/495 (8.3)
	Pork	4/28 ^{AB} (14.3)	6/462 (0.9)
Total		13/105 (12.4)	49/1,890 (2.6)

Uppercase letters (A, B, AB) indicate significant differences (p -value < 0.05) among 3 types of raw meat in *E. coli* O45.

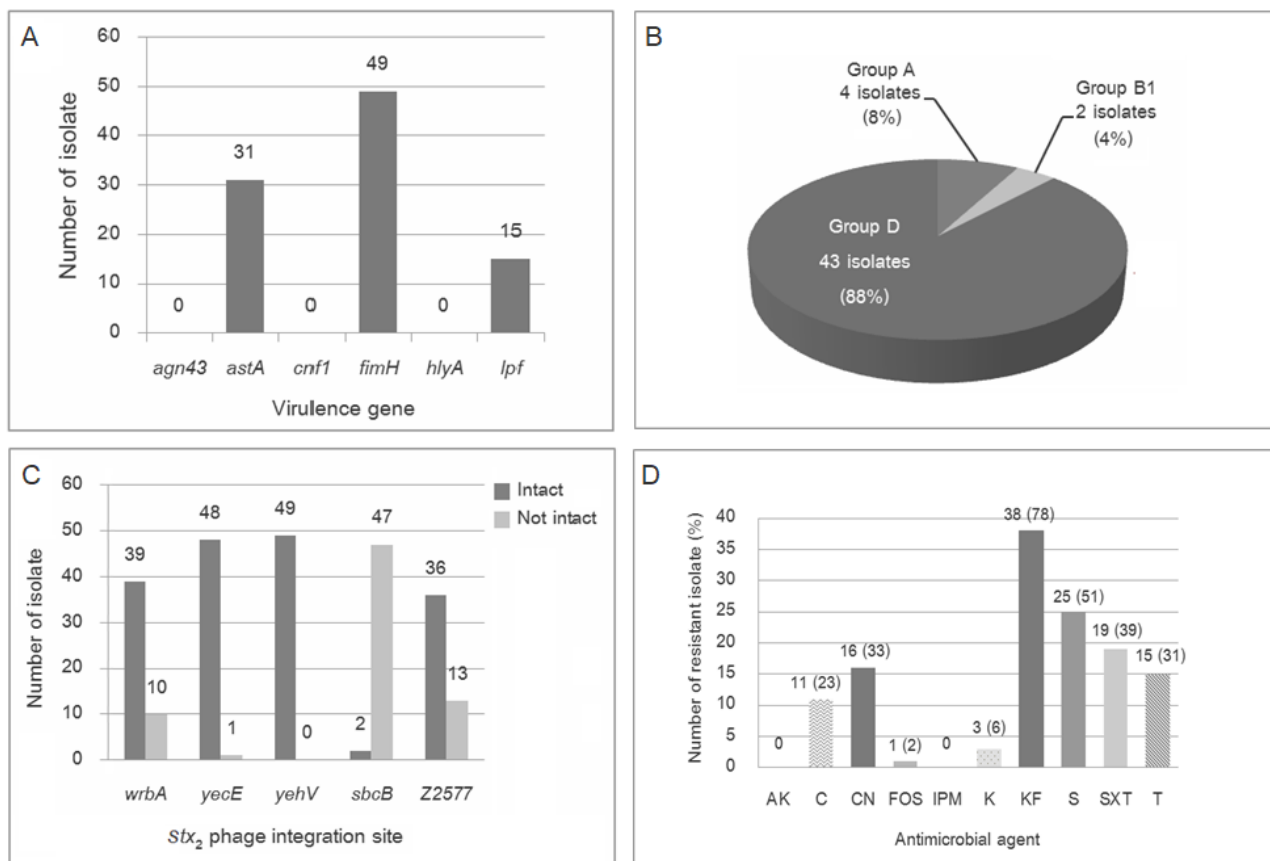


Figure 1. Investigation of virulence genes (A), phylogenetic group classification (B), determination of *stx*₂-phage integration intactness (C), and examination of antimicrobial susceptibility profiles (D) of 49 *E. coli* O45 from meats. AK, amikacin; C, chloramphenicol; CN, gentamicin; FOS, fosfomycin; IPM, imipenem; K, Kanamycin; KF, cephalothin; S, streptomycin; SXT, cotrimoxazole; T, tetracycline.

3.3 Phylogenetic group classification of *E. coli* O45

The phylogenetic group could, in part, indicate the virulence capability of *E. coli*. The results demonstrated that the majority (43 of 49 strains) of *E. coli* O45 belonged to group D (88%) followed by group A (4 of 49 strains, 8%) and B1 (2 of 49 strains, 4%) but none belonged to group B2 (Figure 1B). Based on the phylogenetic group study from Dezfulian et al. [44], they demonstrated that the virulent strains of extraintestinal pathogenic *E. coli* (ExPEC) isolated from animal foods were found mainly to belong to groups B2 and D. In contrast, commensal strains belonged to group A and B1. This criterion was also applied to *E. coli* strains in this current study. Focusing on *E. coli* non-O157 in our previous studies, although some non-O157 groups such as *E. coli* O26 and EAEC O104 were found to be avirulent strains (most of the strains are members of phylogenetic group A and B1, respectively) [32, 35], *E. coli* O45 strains in this present study are thought to

be virulent. This result concurs with aEPEC O145 isolated from the same geographical area belonging to phylogenetic group D [45].

3.4 Investigation of stx2 phages occupancy in *E. coli* O45

The *stx2*-phage carries the *stx2* gene to the genome of *E. coli* through specific integration sites and makes it become EHEC/STEC. Once *stx2*-phage occupies a specific site, no other phages can occupy such a site again. In this study, we investigated the intactness of 5 specific genes reported to be frequently occupied by *stx2*-phage using PCR. The results revealed that in *E. coli* O45, the highest non-intact gene was *sbcB* (47 strains), followed by Z2577 (13 strains) and *wrbA* (10 strains), suggesting that these sites had been occupied by some prophages (Figure 1C). However, *yecE*, and *yehV* were still intact in most O45 strains. A high number of occupied *sbcB* genes in this study is in harmony with our previous work that showed *E. coli* O157:H7 strains from beef had *sbcB* gene occupied [46]. In the study, 41 bovine-origin *E. coli* O157 and non-O157 strains from Thailand from 1998 to 2012 were investigated for intactness of *stx2*-phage integration sites and found that 40 strains (97.56%) revealed the *sbcB* gene occupancy. Integration of prophages is reported to play a key role in *E. coli* O157:H7 evolution and can increase its pathogenesis [47]. Prophage integration occurs through site-specific recombination or transposition. Housekeeping genes or regions close to tRNA genes are uncovered to be the sites for prophage integration [48]. It was reported that prophages preference integration sites in *E. coli* O157:H7 from Spain and sorbitol-fermenting *E. coli* O157: NM (non-motile) are *yehV* and *yecE*, respectively [49, 50]. However, in the current study, *yecE* and *yehV* are still intact in most O45 strains, suggesting the possible integration of *stx2*-phage into these sites, reinforcing the O45 strains to be more powerful.

3.5 Antimicrobial susceptibility of *E. coli* O45

A widespread antimicrobial resistance is a big trouble for public health. In this current study, the results exhibited a high proportion of *E. coli* O45-resistant strains. Most of the strains were found to be resistant to cephalothin (78%), followed by streptomycin (51%), cotrimoxazole (39%), gentamicin (33%), tetracycline (31%), and chloramphenicol (23%), (Figure 1D). Additionally, when focused on the multi-drug resistant (MDR) strains, defined by the capability of resisting at least 3 antimicrobial classes, we found an MDR of 49%, which was considered relatively high. Antimicrobial-resistant capability can be emerged and transferred among bacterial species. The spread of this resistant capability is now becoming a problem worldwide owing to the frequent use of therapy, including prophylaxis and animal growth promotion [51]. The high level of antimicrobial-resistant phenotypes in *E. coli* O45, especially cephalothin, and tetracycline, in this current study is not surprising. Kim & Woo [52] demonstrated the antimicrobial resistance of *E. coli* collected from conventional and organic vegetables. They showed high cephalothin resistance at 67.8% and 71% in organic and conventional vegetables, respectively. In addition, streptomycin, cotrimoxazole, and tetracycline resistance were detected at high rates.

Due to the inexpensiveness of tetracycline, it has been extensively used for prophylaxis and illness therapy of humans and animals. Also, at sub-therapeutic levels, it is used as an animal growth promoter [53]. The study from Vietnam demonstrated that tetracycline was the most frequent antimicrobial resistance in raw meats [42]. More importantly, tetracycline-resistant genes are effectively transferred among bacterial species. Therefore, the ineffectiveness of this antimicrobial agent for treatment should be addressed in the case of infection by *E. coli* from meat consumption.

3.6 Genetic relationship of *E. coli* O45

The genetic relationship of *E. coli* O45 strains in this study was carried out using BOX-PCR as a source tracking tool (Figure 2). It was found that *E. coli* O45 could be distinguished into 5 distinct clusters based on 80% genetic similarity (Figure 3). Dendrogram analysis exhibited identical DNA fingerprints among strains from beef, pork, and chicken collected from different samples and time intervals, suggesting that they were closely related or may have originated from the same bacterial clone. Such a clone may circulate in the Thai environment throughout a period.

In bacterial typing, interspersed repetitive-element PCR (rep-PCR) is extensively employed since repetitive elements dispersed throughout the bacterial genome are highly conserved. Among repetitive elements, BOX elements help generate reliable and reproducible fingerprints. Of the BOX subunits comprising

boxA (57 bp), *boxB* (43 bp), and *boxC* (50 bp), only *boxA* is highly conserved among different bacterial species [31]. Therefore, in this study, a specific nucleotide primer BOXA1R targeting *boxA* was applied in BOX-PCR. A fluorescent-BOX-PCR has also been developed for subtyping *E. coli* and *Bacillus cereus* [54], exhibiting resolution power and discriminatory power higher than traditional BOX-PCR.

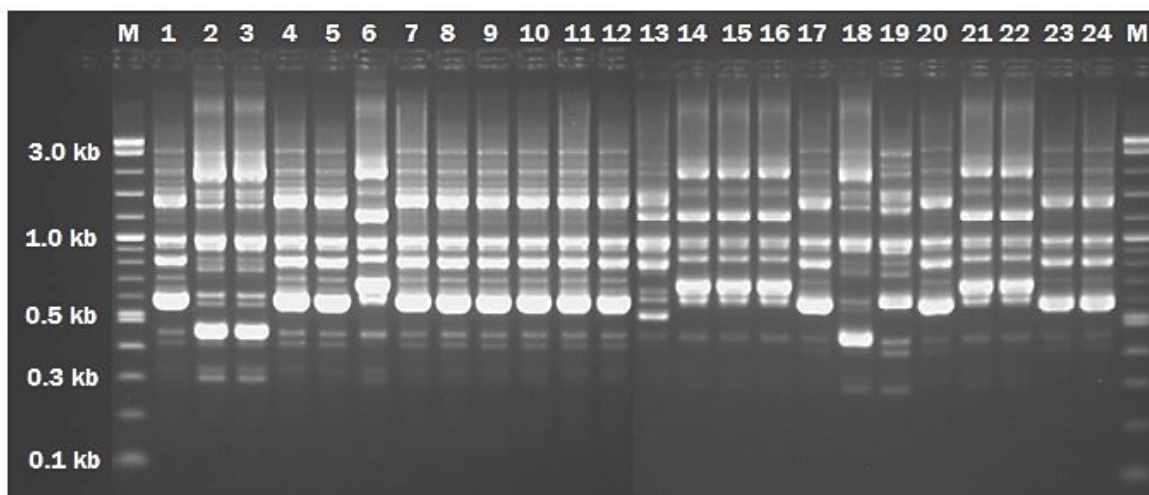


Figure 2. A DNA fingerprint was generated by BOX-PCR of 24 different surrogates of *E. coli* O45 isolated from raw meat samples collected in Hat-Yai, southern Thailand. PCR was performed using primers listed in Table 1 and analyzed by 1.5% agarose gel electrophoresis. Lane M, 2-log DNA markers; lane 1 to 24 are M48.5, C57.1, C57.2, C57.9, C58.18, P60.5, P63.5, C64.5, C64.6, C64.8, C71.6, C72.7, C72.19, P76.4, P76.20, C78.6, C78.10, C78.16, C80.1, C80.4, C80.15, C80.18, C87.1, P95.1, respectively. C, Chicken sample; P, Pork sample; B, Beef sample.

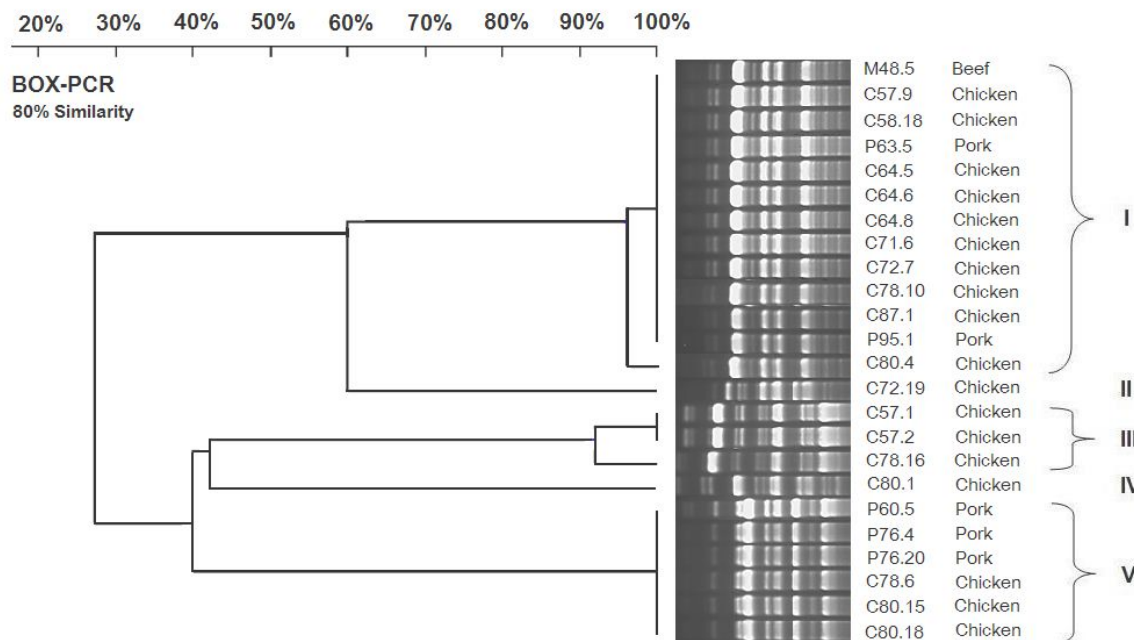


Figure 3. BOX-PCR-based dendrogram of 24 surrogates *E. coli* O45 strains from raw meat samples collected in Hat-Yai, Songkhla, southern Thailand. DNA profiles were generated by BOX-PCR using *boxA*. The dendrogram was constructed using an unweighted pair-group method of arithmetic average (UPGMA) (BioProfile software; Vilber Lourmat, Torey, France) and cut off at 80% similarity.

4. Conclusions

There is a contamination of *E. coli* O45 in meats at high levels. Even though O45 strains in this study are not in the EHEC/STEC group, some contain virulence factors and belong to phylogenetic group D, indicating the potential to cause illnesses. Moreover, they are resistant to numerous antimicrobial agents, and almost half of them show a multi-drug resistant phenotype and the possibility of gaining a *stx2*-phage that makes them more dangerous in the future. These data are important from a public health standpoint.

5. Acknowledgements

We thank the Department of Microbiology, Division of Biological Science, Faculty of Science, Prince of Songkla University for providing the essential facilities.

Author Contributions: Conceptualization, P.S.; methodology, P.S.; software, P.R.; validation, P.S., P.R. and A.S.; formal analysis, P.S. and A.S.; investigation, A.S.; writing—original draft preparation, A.S.; writing—review and editing, P.S. and P.R.; supervision, P.S.; project administration, P.S.; funding acquisition, P.S. All authors have read and agreed to the published version of the manuscript.

Funding: This work was supported in part by Prince of Songkla University (grant no. SCI600588S).

Conflicts of Interest: The authors declare no conflict of interest.

References

- [1] Centers for Disease Control and Prevention. Global diarrhea burden. Available: (Accessed 8 November 2023)
- [2] Kaper, J.B.; Nataro, J.P.; Mobley, H.L.T. Pathogenic *Escherichia coli*. *Nature Reviews Microbiology*. **2004**, *2*, 123-140.
- [3] Michino, H.; Araki, K.; Minami, S.; Takaya, S.; Sakai, N.; Miyazaki, M.; Ono, A.; Yanagawa, H. Massive outbreak of *Escherichia coli* O157: H7 infection in schoolchildren in Sakai City, Japan, associated with consumption of white radish sprouts. *American Journal of Epidemiology*. **1999**, *150*(8), 787-796.
- [4] Dundas, S.; Todd, W.A.; Stewart, A.I.; Murdoch, P.S.; Chaudhuri, A.; Hutchinson, S.J. The central Scotland *Escherichia coli* O157: H7 outbreak: risk factors for the hemolytic uremic syndrome and death among hospitalized patients. *Clinical Infectious Diseases*. **2001**, *33*(7), 923-931.
- [5] Rangel, J. M.; Sparling, P. H.; Crowe, C.; Griffin, P. M.; Swerdlow, D. L. Epidemiology of *Escherichia coli* O157: H7 outbreaks, United States, 1982–2002. *Emerging Infectious Diseases*. **2005**, *11*(4), 603-609.
- [6] Nataro, J.P.; Kaper, J.B. Diarrheagenic *Escherichia coli*. *Clinical Microbiology Reviews*. **1998**, *11*(1), 142-201.
- [7] Karmali, M.; Petric, M.; Steele, B.; Lim, C. Sporadic cases of a haemolytic-uraemic syndrome associated with fecal cytotoxin and cytotoxin-producing *Escherichia coli* in stools. *The Lancet*. **1983**, *321*(8325), 619-620.
- [8] Paton, A.W.; Paton, J.C. *Enterobacter cloacae* producing a Shiga-like toxin II-related cytotoxin associated with a case of hemolytic-uremic syndrome. *Journal of Clinical Microbiology*. **1996**, *34*(2), 463-465.
- [9] Arthur, T.M.; Barkocy-Gallagher, G.A., Rivera-Betancourt, M.; Koohmaraie, M. Prevalence and characterization of non-O157 Shiga toxin-producing *Escherichia coli* on carcasses in commercial beef cattle processing plants. *Applied and Environmental Microbiology*. **2002**, *68*(10), 4847-4852.
- [10] Barkocy-Gallagher, G.A.; Arthur, T.M.; Rivera-Betancourt, M.; Nou, X.; Shackelford, S.D.; Wheeler, T.L.; Koohmaraie, M. Seasonal prevalence of Shigatoxin-producing *Escherichia coli*, including O157: H7 and non-O157 serotypes, and *Salmonella* in commercial beef processing plants. *Journal of Food Protection*. **2003**, *66*(11), 1978-1986.
- [11] Sukhumungoon, P.; Nakaguchi, Y.; Ingviya, N.; Pradutkanchana, J.; Iwade, Y.; Seto, K.; Son, R.; Nishibuchi, M.; Vuddhakul, V. Investigation of *stx2+* *eaec+* *Escherichia coli* O157: H7 in beef imported from Malaysia to Thailand. *International Food Research Journal*. **2011**, *18*(1), 381-386.
- [12] Pannuch, M.; Sirikaew, S.; Nakaguchi, Y.; Nishibuchi, M.; Sukhumungoon, P. Quantification of enteropathogenic *Escherichia coli* from retailed meats. *International Food Research Journal*. **2014**, *21*(2), 547-551.

- [13] Ju, W.; Shen, J.; Li, Y.; Toro, M.A.; Zhao, S.; Ayers, S.; Najjar, M.B.; Meng, J. Non-O157 Shiga toxin-producing *Escherichia coli* in retail ground beef and pork in the Washington DC area. *Food Microbiology*. **2012**, 32(2), 371-377.
- [14] Gannon, V.; Rashed, M.; King, R.K.; Thomas, E. Detection and characterization of the *eae* gene of Shiga-like toxin-producing *Escherichia coli* using polymerase chain reaction. *Journal of Clinical Microbiology*. **1993**, 31(5), 1268-1274.
- [15] Stacy-Phipps, S.; Mecca, J.J.; Weiss, J.B. Multiplex PCR assay and simple preparation method for stool specimens detect enterotoxigenic *Escherichia coli* DNA during infection. *Journal of Clinical Microbiology*. **1995**, 33(5), 1054-1059.
- [16] Sethabutr, O.; Venkatesan, M.; Murphy, G.S.; Eampokalap, B.; Hoge, C.W.; Echeverria, P. Detection of Shigellae and enteroinvasive *Escherichia coli* by amplification of the invasion plasmid antigen H DNA sequence in patients with dysentery. *Journal of Infectious Diseases*. **1993**, 167(2), 458-461.
- [17] Vidal, M.; Kruger, E.; Durán, C.; Lagos, R.; Levine, M.; Prado, V.; Toro, C.; Vidal, R. Single multiplex PCR assay to identify simultaneously the six categories of diarrheagenic *Escherichia coli* associated with enteric infections. *Journal of Clinical Microbiology*. **2005**, 43(10), 5362-5365.
- [18] Tsukamoto, T. PCR methods for detecting enteropathogenic *Escherichia coli* (localized adherence) and enteroaggregative *Escherichia coli*. *Kansenshogaku zasshi*. **1996**, 70(6), 569-573.
- [19] Gunzburg, S.T.; Tornieporth, N.G.; Riley, L.W. Identification of enteropathogenic *Escherichia coli* by PCR-based detection of the bundle-forming pilus gene. *Journal of Clinical Microbiology*. **1995**, 33(5), 1375-1377.
- [20] Danese, P.N.; Pratt, L.A.; Dove, S.L.; Kolter, R. The outer membrane protein, Antigen 43, mediates cell-to-cell interactions within *Escherichia coli* biofilms. *Molecular Microbiology*. **2000**, 37(2), 424-432.
- [21] Johnson, J.R.; Stell, A.L. Extended virulence genotypes of *Escherichia coli* strains from patients with urosepsis in relation to phylogeny and host compromise. *The Journal of Infectious Diseases*. **2000**, 181(1), 261-272.
- [22] Yamamoto, S.; Terai, A.; Yuri, K.; Kurazono, H.; Takeda, Y.; Yoshida, O. Detection of urovirulence factors in *Escherichia coli* by multiplex polymerase chain reaction. *FEMS Immunology and Medical Microbiology*. **1995**, 12(2), 85-90.
- [23] Clermont, O.; Bonacorsi, S.; Bingen, E. Rapid and simple determination of the *Escherichia coli* phylogenetic group. *Applied and environmental microbiology*. **2000**, 66(10), 4555-4558.
- [24] Heininger, A.; Binder, M.; Schmidt, S.; Unertl, K.; Botzenhart, K.; Döring, G. PCR and blood culture for detection of *Escherichia coli* bacteremia in rats. *Journal of clinical microbiology*. **1999**, 37(8), 2479-2482.
- [25] Torres, A.G.; Kanack, K.J.; Tutt, C.B.; Popov, V.; Kaper, J.B. Characterization of the second long polar (LP) fimbriae of *Escherichia coli* O157: H7 and distribution of LP fimbriae in other pathogenic *E. coli* strains. *FEMS Microbiology Letters*. **2004**, 238(2), 333-344.
- [26] Tóth, I.; Schmidt, H.; Dow, M.; Malik, A.; Oswald, E.; Nagy, B. Transduction of porcine enteropathogenic *Escherichia coli* with a derivative of a Shiga toxin 2-encoding bacteriophage in a porcine ligated ileal loop system. *Applied and Environmental Microbiology*. **2003**, 69(12), 7242-7247.
- [27] De Greve, H.; Qizhi, C.; Deboeck, F.; Hernalsteens, J.P. The Shiga-toxin VT2-encoding bacteriophage ϕ 297 integrates at a distinct position in the *Escherichia coli* genome. *Biochimica et Biophysica Acta (BBA)-Gene Structure and Expression*. **2002**, 1579, 196-202.
- [28] Ohnishi, M.; Terajima, J.; Kurokawa, K.; Nakayama, K.; Murata, T.; Tamura, K.; Ogura, Y.; Watanabe, H.; Hayashi, T. Genomic diversity of enterohemorrhagic *Escherichia coli* O157 revealed by whole genome PCR scanning. *Proceedings of the National Academy of Sciences*. **2002**, 99(26), 17043-17048.
- [29] Shaikh, N.; Tarr, P.I. *Escherichia coli* O157: H7 Shiga toxin-encoding bacteriophages: integrations, excisions, truncations, and evolutionary implications. *Journal of Bacteriology*. **2003**, 185(12), 3596-3605.
- [30] Koch, C.; Hertwig, S.; Appel, B. Nucleotide sequence of the integration site of the temperate bacteriophage 6220, which carries the Shiga toxin gene *stx*_{10x3}. *Journal of Bacteriology*. **2003**, 185(21), 6463-6466.
- [31] Versalovic, J.; Schneider, M.; De Bruijn, F.; Lupski, J.R. Genomic fingerprinting of bacteria using repetitive sequence-based polymerase chain reaction. *Methods in Molecular and Cellular Biology* 1994, 5(1), 25-40.

- [32] Sirikaew, S.; Rattanachuay, P.; Nakaguchi, Y.; Sukhumungoon, P. Immuno-magnetic isolation, characterization and genetic relationship of *Escherichia coli* O26 from raw meats, Hat Yai City, Songkhla, Thailand. *Southeast Asian Journal of Tropical Medicine and Public Health*. **2015**, 46(2), 241-253.
- [33] Clinical and Laboratory Standards Institute (CLSI). Performance standards for antimicrobial susceptibility testing; Twenty-third informational supplement M100-S25. Wayne, PA, USA 2015.
- [34] Sukhumungoon, P.; Tantadapan, R.; Rattanachuay, P. Repetitive sequence based-PCR profiling of *Escherichia coli* O157 strains from beef in southern Thailand. *Southeast Asian Journal of Tropical Medicine and Public Health*. **2016**, 47(1), 55-65.
- [35] Wameadesa, N.; Sae-lim, A.; Hayeebilan, F.; Rattanachuay, P.; Sukhumungoon, P. Enteroaggregative *Escherichia coli* O104 from Thai and imported Malaysian raw beef. *The Southeast Asian Journal of Tropical Medicine and Public Health*. **2017**, 48(2), 338-350.
- [36] Chapman, P.; Wright, D; Siddons, C. A comparison of immunomagnetic separation and direct culture for the isolation of verocytotoxin-producing *Escherichia coli* O157 from bovine faeces. *Journal of Medical Microbiology*. **1994**, 40(6), 424-427.
- [37] Lozinak, K.A.; Jani, N.; Gangiredla, J.; Patel, I.; Elkins, C.A.; Hu, Z.; Kassim, P.A.; Myers, R.A.; Laksanalamai, P. Investigation of potential Shiga toxin-producing *Escherichia coli* (STEC) associated with a local foodborne outbreak using multidisciplinary approaches. *Food Science and Human Wellness*. **2016**, 5, 163-168.
- [38] Schembri, M.A.; Christiansen, G.; Klemm, P.; FimH mediated autoaggregation of *Escherichia coli*. *Molecular Microbiology*. **2001**, 41, 1419-1430.
- [39] Fitzhenry, R.; Dahan, S.; Torres, A.G.; Chong, Y.; Heuschkel, R.; Murch, S.H.; Thomson, M.; Kaper, J.B.; Frankel, G.; Phillips, A.D. Long polar fimbriae and tissue tropism in *Escherichia coli* O157:H7. *Microbes and Infection*. **2006**, 8, 1741-1749.
- [40] Jordan, D.M.; Cornick, N.; Torres, A.G.; DeanNystrom, E.A.; Kaper, J.B.; Moon, H.W. Long polar fimbriae contribute to colonization by *Escherichia coli* O157:H7 in vivo. *Infection and Immunity*. **2004**, 72, 6168-6171.
- [41] Tiba, M.R.; Yano, T.; Leite, D.D.S. Genotypic characterization of virulence factors in *Escherichia coli* strains from patients with cystitis. *Revista do Instituto de Medicina Tropical de Sao Paulo*. **2008**, 50(5), 255-260.
- [42] Van, T.T.H.; Chin, J.; Chapman, T.; Tran, L.T; Coloe, P.J. Safety of raw meat and shellfish in Vietnam: an analysis of *Escherichia coli* isolations for antibiotic resistance and virulence genes. *International Journal of Food Microbiology*. **2008**, 124(3), 217-223.
- [43] Nishikawa, Y.; Ogasawara, J.; Helander, A.; Haruki, K. An outbreak of gastroenteritis in Japan due to *Escherichia coli* O166. *Emerging Infectious Diseases*. **1999**, 5, 300.
- [44] Dezfulian, H.; Batisson, I.; Fairbrother, J.M.; Lau, P.C.K.; Nassar, A.; Szatmari, G; Harel, J. Presence and characterization of extraintestinal pathogenic *Escherichia coli* virulence genes in F165-positive *E. coli* strains isolated from diseased calves and pigs. *Journal of Clinical Microbiology*. **2003**, 41, 1375-85.
- [45] Sae-lim, A.; Jearanai, P.; Rattanachuay, P.; Sukhumungoon, P. Prevalence, virulence profiles, and genetic relationship of atypical enteropathogenic *Escherichia coli* O145 from beef, southern Thailand. *Southeast Asian Journal of Tropical Medicine and Public Health*. **2017**, 48(6), 1248-1259.
- [46] Sukhumungoon, P.; Nakaguchi, Y. Shiga toxin 2-converting bacteriophages occupy *shcB* gene as a primary integration site in bovine-originated *Escherichia coli* O157: H7 and non-O157 from Thailand. *Life Science Journal*. **2013**, 10, 2334-2340.
- [47] Ooka, T.; Terajima, J.; Kusumoto, M.; Iguchi, A.; Kurokawa, K.; Ogura, Y.; Asadulghani, M.; Nakayama, K.; Murase, K.; Ohnishi, M. Development of a multiplex PCR-based rapid typing method for enterohemorrhagic *Escherichia coli* O157 strains. *Journal of Clinical Microbiology*. **2009**, 47(9), 2888-2894.
- [48] Schmidt, H.; Zhang, W.L.; Hemmrich, U.; Jelacic, S.; Brunder, W.; Tarr, P.; Dobrindt, U.; Hacker, J.; Karch, H. Identification and characterization of a novel genomic island integrated at *selC* in locus of enterocyte effacement-negative, Shiga toxin-producing *Escherichia coli*. *Infection and Immunity*. **2001**, 69(11), 6863-6873.
- [49] Mellmann, A.; Lu, S.; Karch, H.; Xu, J.G.; Harmsen, D.; Schmidt, M. A.; Bielaszewska, M. Recycling of Shiga toxin 2 genes in sorbitol-fermenting enterohemorrhagic *Escherichia coli* O157: NM. *Applied and Environmental Microbiology*. **2008**, 74(1), 67-72.

- [50] Serra-Moreno, R.; Jofre, J.; Muniesa, M. Insertion site occupancy by *stx2* bacteriophages depends on the locus availability of the host strain chromosome. *Journal of Bacteriology*. **2007**, 189(18), 6645-6654.
- [51] Rasheed, M.U.; Thajuddin, N.; Ahamed, P.; Teklemariam, Z.; Jamil, K. Antimicrobial drug resistance in strains of *Escherichia coli* isolated from food sources. *Revista do Instituto de Medicina Tropical de São Paulo*. **2014**, 56(4), 341-346.
- [52] Kim, S.; Woo, G.J. Prevalence and characterization of antimicrobial-resistant *Escherichia coli* isolated from conventional and organic vegetables. *Foodborne Pathogens and Disease*. **2014**, 11, 815-821.
- [53] Chopra, I.; Roberts, M. Tetracycline antibiotics: Mode of action, applications, molecular biology, and epidemiology of bacterial resistance. *Microbiology and Molecular Biology Reviews*. **2001**, 65, 232-260.
- [54] Brusetti, L.; Malkhazova, I.; Gtari, M.; Tamagnini, I.; Borin, S.; Merabishvili, M.; Chanishvili, N.; Mora, D.; Cappitelli, F.; Daffonchio, D. Fluorescent-BOX-PCR for resolving bacterial genetic diversity, endemism and biogeography. *BMC Microbiology*. **2008**, 8(1), 220.



Induction of Gynogenetic Diploids the Tropical Oyster, *Crassostrea belcheri* 1873 (Ostreids: Ostreidae) from Southern Thailand.

Supatcha Chooseangjaew^{1*}, Nuntaporn Getlekha², Worawut Koedprang³, Chanika Saenge Chooklin⁴, Kattinat Sakulsawasdipan⁵, and Suwat Tanyaros⁶

- ¹ Faculty of Science and Fisheries Technology, Rajamangala University of Technology Srivijaya, Trang, 92150, Thailand; supatcha.c@rmutsv.ac.th
² Faculty of Science and Technology, Muban Chombueng Rajabhat University, Chombueng, Ratchaburi, 70150, Thailand; nanthaphonket@mcru.ac.th
³ Faculty of Science and Fisheries Technology, Rajamangala University of Technology Srivijaya, Trang, 92150, Thailand; worawut2000@hotmail.com
⁴ Faculty of Science and Fisheries Technology, Rajamangala University of Technology Srivijaya, Trang, 92150, Thailand; chanika.sae@gmail.com
⁵ Faculty of Science and Fisheries Technology, Rajamangala University of Technology Srivijaya, Trang, 92150, Thailand; kattinat.s@gmail.com
⁶ Faculty of Science and Fisheries Technology, Rajamangala University of Technology Srivijaya, Trang, 92150, Thailand; stanyaros@gmail.com
* Correspondence: supatcha.c@rmutsv.ac.th

Citation:

Chooseangjaew, S.; Getlekha, N.; Koedprang, W.; Saenge, S.C.; Sakulsawasdipan, K.; Tanyaros, S. Induction of gynogenetic diploids the tropical oyster, *Crassostrea belcheri* 1873 (Ostreids: Ostreidae) from southern Thailand. *ASEAN J. Sci. Tech. Report.* 2024, 27(2), 72-78. <https://doi.org/10.55164/ajstr.v27i2.250804>.

Article history:

Received: September 3, 2023
Revised: February 11, 2024
Accepted: February 26, 2024
Available online: February 29, 2024

Publisher's Note:

This article is published and distributed under the terms of Thaksin University.



Abstract: The induction of diploid gynogenesis in the Tropical oyster, *Crassostrea belcheri* 1873, was carried out through two main experiments: 1) the destruction of spermatozoa DNA using ultraviolet (UV) irradiation, and 2) the induction of gynogenetic diploids. UV light source was placed 30 cm over the sperm for various durations, including 0 (control), 30, 60, 90, and 120 seconds. The study revealed that the highest survival rate was observed in trochophore at 90 minutes ($42.5 \pm 2.50\%$) compared to the normal control *C. belcheri* ($p > 0.05$). Based on cytogenetic study, haploid ($n=10$), diploid ($2n=20$), and aneuploid were observed in all trials, while only diploid ($2n=20$) could be seen in the control group. Diploid gynogenesis was induced using $100 \mu\text{mol}$ 6-DMAP for 10 minutes. The study found that the survival rate and developmental stages in both trochophore and D-shape were gradually decreasing as the duration of UV rays increased. The highest survival rate of trochophore in the control group was $75.20 \pm 4.84\%$, while survival rates in other experimental groups ranged from $52.22 \pm 4.82\%$ to $59.33 \pm 13.57\%$. However, regarding the survival rate of D-shape larvae, their survival rates were relatively low across all trials. They displayed abnormal embryo development, distorted shape, unnatural swimming, and were smaller than normal ($40\text{-}50 \mu\text{m}$). Moreover, haploid ($n=10$), diploid ($2n=20$), triploid ($3n=30$), tetraploid ($4n=40$), and aneuploid were observed in all trials, while only diploid ($2n=20$) could be discovered in the control group. However, gynogenesis in this tropical oyster is still limited at this time. Therefore, suitable conditions for inducing gynogenesis in oysters should be further developed.

Keywords: Gynogenesis; *Crassostrea belcheri*; UV-irradiated sperm; 6-DMAP; UV rays

1. Introduction

Diploid gynogenesis is a biotechnological method of manipulating chromosome sets in marine animals. This production strategy has an advantage over conventional methods as it only produces genetically identical females by destroying DNA in the spermatozoa using the UV irradiation

method [1, 2]. Research on artificial gynogenesis with ultraviolet light-irradiated sperm in the Pacific oyster, *Crassostrea gigas*, has been conducted to study its induction and survival rates [2]. It was found that some aquatic organisms such as *Haliotis discus hannai*, *C. gigas*, *Mulinia lateralis*, *Mytilus edulis*, and *M. galloprovincialis* have higher growth and survival rates in females, which is attributed to their high market demand compared to males [3]. The sexual transformation from male to female can be observed in bivalves and gastropods such as *H. discus hannai*, *C. gigas*, *M. lateralis*, *M. edulis*, *M. galloprovincialis*, and *Chlamys farreri* [4]. It is noteworthy that male *C. belcheri* can become female after its first breeding, and this sex change can occur once or multiple times during a breeding season depending on environmental factors such as temperature and food availability [5].

Some research demonstrated that mature females weigh more than males, indicating a faster growth rate in females [6]. Males also have a higher mortality rate than females, which could be related to changes in the sea [7]. It has been reported that diploid gynogenesis can be achieved in mollusk species such as *Haliotis diversicolor*, *H. discus hannai*, *C. farreri*, *M. edulis*, *M. galloprovincialis*, and *M. lateralis* through cold shock treatment, cytochalasin B, and 6-dimethylaminopurine [8-13]. However, the application of this technique in the economically important *C. belcheri* species in Thailand have not yet been reported. Therefore, this study aimed to apply diploid gynogenesis to this oyster species to promote its production and the aquaculture industry in the country. The successful implementation of this technique will contribute to the production of genetically identical female shellfish.

2. Materials and Methods

In this study, Four females and one male of the mature *C. belcheri* (shell width 12.5 ± 0.2 cm; shell length 11.8 ± 0.3 cm.) were purchased from a farmer farm in Trang Province and were thoroughly washed to remove all dirt from the shell. The oysters were then transferred to a semi-closed recirculation system for cultivation. The oysters were fed with single-cell algae such as *Isochrysis galbana*, *Chaetoceros calcitrans*, and *Tetraselmis suecica* at a rate of 3% calculated by dry meat weight, as described by [14]. The maturity of the oysters was monitored routinely for up to 4 weeks. To examine the maturity of the shellfish, their gametes were collected and analyzed under a light microscope (Motic, Spain) following sampling and dissection, as described by [15].

2.1 Egg preparation

After inducing mature *C. belcheri* broodstock with cold shock at 19 °C to release their gametes, the suspension of eggs at a concentration of 1×10^5 eggs/ml was filtered through a 70-90 μm pore size filter and transferred to a clean container with 25 psu seawater.

2.2 Seminal fluid preparation

The seminal fluid generated in seawater was filtered through a 20-30 μm pore size to eliminate grease and dirt before being stored in a clean, dry container. Next, the fluid was diluted with 0.85% NaCl at a ratio of 1:9 (fluid:0.85% NaCl). To prepare a sample for UV radiation, 1 mL of the diluted fluid was transferred to 15 petri dishes with a diameter of 8 cm each.

2.3 Exposure of the seminal fluid to UV light and gamete fusion (fertilization)

The petri dishes containing the diluted fluid were subsequently exposed to a 30-watt UV lamp at a distance of 30 cm for 0 (control), 30, 60, 90, and 120 seconds. After exposure, the diluted fluid from each petri dish was combined with eggs prepared on filtered cloth about 50-60 μm pore size for 15 to 30 minutes before diploid induction.

2.4 Induction of gynogenetic diploids

1. Diploid gynogenesis induction

At the designated time, 100 μmol of 6-DMAP was added to the sample on each plate and left to incubate for 10 minutes and 30 minutes post-insemination. This concentration and timing of 6-DMAP for treatment was based on that described in the previous research in this oyster [16].

2. Hatchery and nursery

To prevent the larvae from falling to the bottom of the container, they were nurtured in aerated seawater (30 psu) for 24 hours (D-shape stage) at an ambient temperature of about 27 °C following the diploid induction.

3. Data collection

One mL of rearing water was collected at 6-8 hours post-fertilization (trochophore larvae stage) to determine egg hatching and the percentage of haploid larvae. The survival rate and percentage of induced diploid gynogenesis were further examined by metaphase chromosome counting, as described by [17]. The experimental design used in this study was a completely randomized design (CRD) with three replicates.

2.5 Chromosome identification

The oyster larvae, including the trochophore and D-shape stages, were immersed in 0.05% colchicine for 90 minutes. After washing with seawater to remove the chemical, they were treated with 0.075 M KCl for 40 minutes, followed by a fixative for 5 minutes. Next, 15-20 drops of 50% acetic acid were added to 0.2 mL of the sample on a petri dish. After incubation for 20 minutes, the sample was placed on a slide, dried by heating, and stained with 10% Giemsa solution for 40 minutes. Finally, the sample was rinsed with water and examined under a light microscope to determine the metaphase chromosome count.

2.6 Data Analysis

The statistical analysis of all values was performed using a one-way analysis of variance (ANOVA) followed by the New Duncan Multiple Range Test. A p-value of less than 0.05 was considered statistically significant.

3. Results and Discussion

Gynogenesis induction in the tropical oyster *Crassostrea belcheri* (1873) involves two main steps: 1) UV irradiation to inactivate the sperm and 2) gynogenesis induction during the larval stage.

1) Inactivation of sperm chromosomes using UV-irradiated sperm

This experiment was conducted using a UV bulb at a distance of 30 cm, with irradiation periods of 0 (control), 30, 60, 90, and 120 minutes. Afterward, normal eggs were mixed with irradiated sperm. The highest survival rate of trochophore in the control group was found to be $42.58 \pm 12.06\%$. In contrast, the survival rates in the other experimental groups ranged from $32.58 \pm 6.66\%$ to $42.50 \pm 2.50\%$, which were not significantly different ($p > 0.05$), as displayed in Table 1.

Table 1. Survival rate of Trochophore after fertilized eggs with UV irradiated semen.

Periods (Second)	Survival rate (%)
Control	$42.58 \pm 12.06^{\text{ns}}$
30	$32.58 \pm 6.66^{\text{ns}}$
60	$37.17 \pm 9.57^{\text{ns}}$
90	$42.5 \pm 2.50^{\text{ns}}$
120	$36.75 \pm 2.82^{\text{ns}}$

Note: ns= not significant difference ($P > 0.05$)

Previous reports have documented the induction of diploid gynogenesis. For example, [10] investigated gynogenesis induction in the *C. farreri* using a UV intensity of $256 \mu\text{W cm}^{-2} \text{ s}^{-1}$ for 30 seconds. They found that the egg development rate in the control group was 73.3%, but this rate gradually decreased to 33.5% after 30 seconds of exposure. After 60 seconds of irradiation, no development of oocytes was

observed. On the other hand, [2] reported that sperm DNA destruction in *C. gigas* could be achieved with 5-6 minutes of exposure at a UV intensity of $108 \text{ erg mm}^{-2} \text{ min}^{-1}$. In contrast, [16] stated that the use of UV-irradiated sperm from *C. gigas* for 60 seconds at $72 \text{ erg mm}^{-2} \text{ s}^{-1}$ could accomplish sperm DNA destruction to induce gynogenesis. Our study found that embryonic development occurred with an irradiation time of about 25 seconds, but the development rate of D-shape larvae reached 0% in this case. The highest survival rate of trochophore was observed after 90 seconds of UV exposure, which is consistent with the Hertwig effect caused by UV irradiation of sperm in *C. farreri* [10].

Numerous pieces of evidence have been reported on the destruction of genetic material in sperm. It has been postulated that the development of oocytes would decline with increasing duration of irradiation, resulting in a reduction of the breeding rate, such as the case with the Pacific abalone, *H. discus hannai* [18]. Furthermore, the destruction of sperm at various durations depends on several factors, including the density and quantity of sperm, the intensity of the UV light source, and the aquatic animal species being studied.

The destruction of sperm DNA was examined using a chromosome counting technique with simple dyeing. The results showed that the number of chromosomes ranged from 10 to 20, characterized as haploids, aneuploids, and diploids. (Fig 1.)

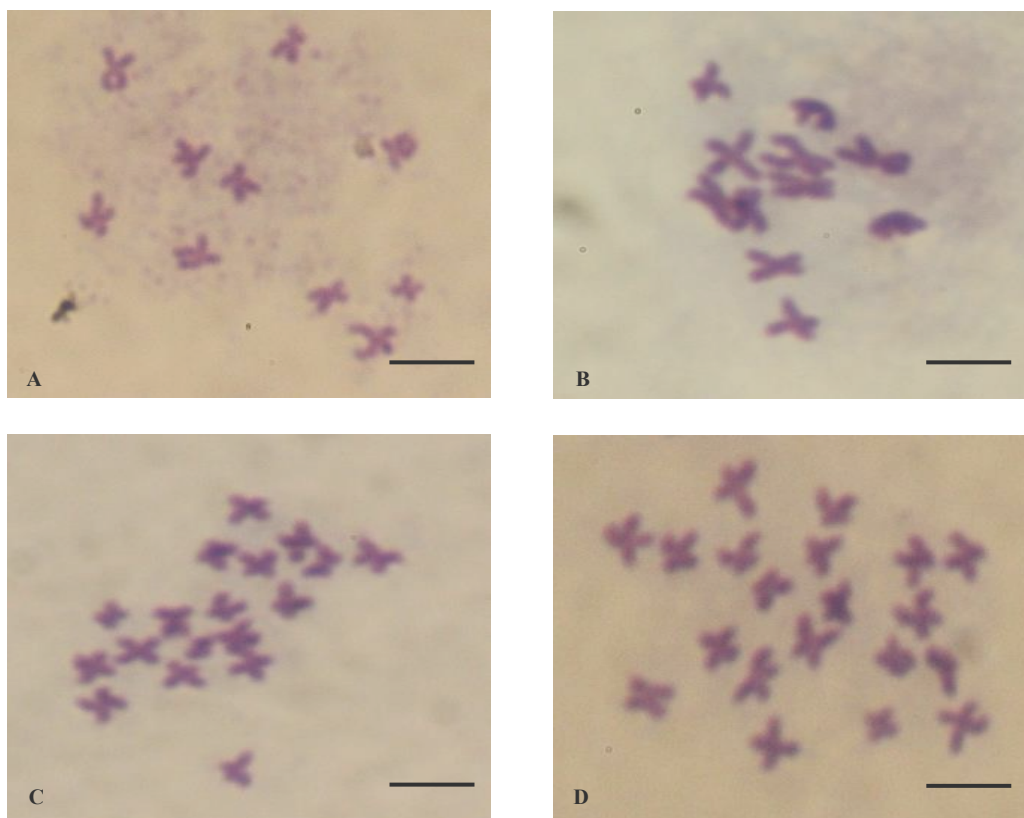


Figure 1. Metaphase chromosome plates of Trochophore after fertilized eggs with UV irradiated sperm: haploid=10 (A), aneuploid 11-18 (B-C) and diploid=20 (D) (scale bars=5 μm).

2) Induction of gynogenetic diploids of larval stage

As mentioned above, the results of the first phase indicated that the genetic material of *C. belcheri* sperm was destroyed, and then it was used to fertilize a normal egg. After that, the sample was treated with $100 \mu\text{M}$ of 6-DMAP for 10 minutes, 30 minutes after fertilization, resulting in the successful production of artificial polyploid in the tropical oyster (*C. belcheri*) [16]. In this study, both trochophore and D-shape larvae were observed, and the survival rate for trochophore in the control group was $75.20 \pm 4.84\%$, but it gradually decreased to $52.22 \pm 4.82 - 59.33 \pm 13.57\%$ in the 6-DMAP-treated group (Table 2).

Table 2. Survival rate of gynogenetic diploid Trochophore and D-shape stages.

Periods (Second)	Survival rate (%)	
	Trochophore	D-shape
Control	75.20 ± 4.84 ^a	23.03 ± 6.05 ^a
30	59.33 ± 13.57 ^{ab}	7.87 ± 2.66 ^b
60	52.22 ± 4.82 ^b	4.67 ± 1.15 ^{bc}
90	52.66 ± 6.42 ^b	0 ^c
120	55.33 ± 10.47 ^b	0 ^c

Means (± SD) in the same column with different superscripts show significant differences ($p < 0.05$)

This result is consistent with a previous study by Pan et al. [10], who stated that the survival rate of the trochophore stage in the control group was 56.3%, gradually falling to 31.3% with 20 seconds of UV intensity. The study also showed that the survival rate of D-shape larvae decreased continually and reached 0% with 15 seconds of UV intensity. The low survival rate could be attributed to the longer duration of UV exposure. [19] conducted a study on gynogenetic diploid induction in *C. gigas* using Cytochalasin B (CB) at a concentration of 0.5 µg/ml, which was found to effectively inhibit cell division during metaphase II when combined with caffeine at a concentration of 10 mM and an incubation temperature of 32°C. The study showed that the highest production of gynogenetic diploid larvae was achieved at 74.6% and 63.7%, with additional production of triploid larvae at 72.7% and 68.1%. However, the D-shape larval survival rate in gynogenetic diploid induction was relatively low compared to triploid and diploid larvae [19]. Previous research on gynogenetic diploid induction in other bivalves, such as *M. edulis*, demonstrated that the highest haploid results were achieved in 15 minutes [11]. *M. galloprovincialis* was operated for 2 minutes at 62 erg/mm² per second [12], and *H. discus hannai* was also studied [9, 20]. However, these studies showed that low production of gynogenetic diploid induction might be due to polar body inhibition in the meiosis II process or damage from UV-irradiated genetic material.

This study found that the survival rate of larvae in the D-shape stage was low after 30 and 60 seconds of exposure to UV-irradiated sperm, whereas no larvae developed to the D-shape stage after 90 and 120 seconds of exposure. In addition, upon examining the overall condition of the larvae that were able to develop up to the D-shape stage, it was discovered that they exhibited a relatively impaired shape, with deformities and smaller sizes of approximately 40-50 µm in comparison to the normal D-shape stage. Some larvae were also found to be non-motile. All surviving larvae were investigated for chromosomal characteristics using conventional staining to quantify the number of chromosomes discovered during gynogenesis induction. It was discovered that haploid (1N), diploid (2N), triploid (3N), and tetraploid (4N) chromosomes could be identified (Fig 2). Additionally, chromosomal characteristics of various aneuploid types were also present. [10] conducted a study to examine the effect of destroying genetic material and inducing diploid gynogenesis on the normal developmental stage of *C. farreri*. The study found that the normal diploid number of chromosomes was 2n=38. However, after 15 seconds of sperm DNA destruction, the number of chromosomes observed was 32, with some being in the form of aneuploidy. Furthermore, 19 haploid chromosomes were discovered within 30 seconds.

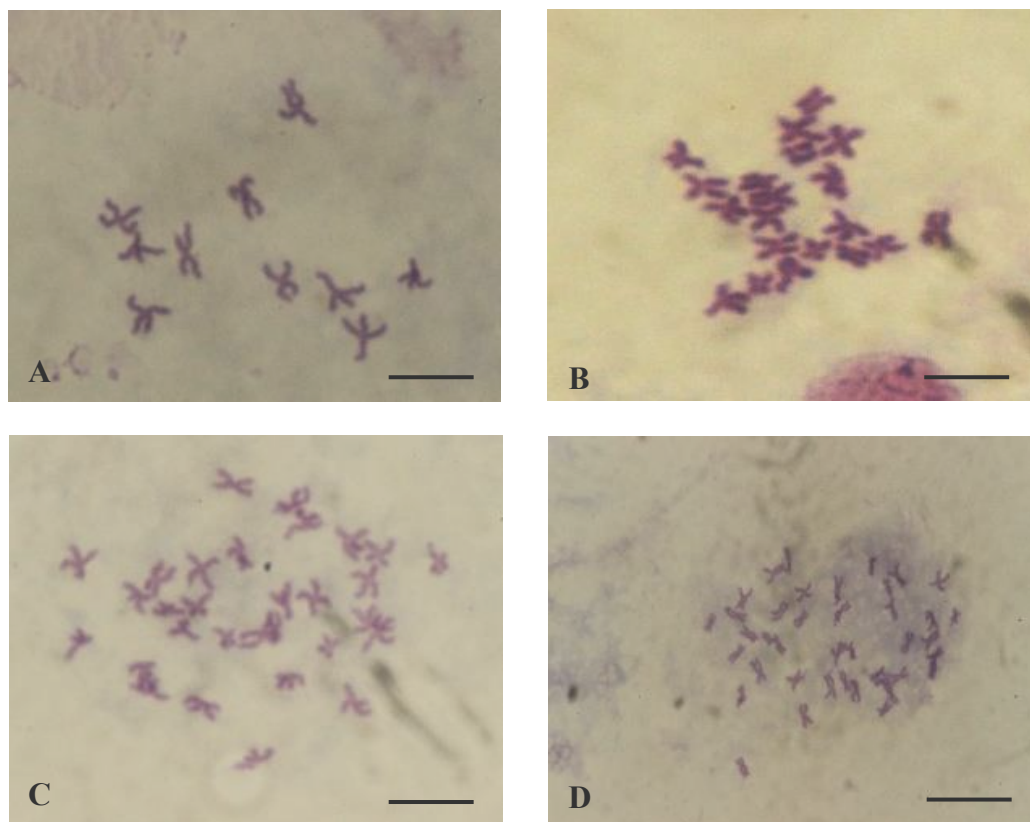


Figure 2. Metaphase chromosome of gynogenetic diploid *C.belcheri*: haploid =10 (A), diploid=20 (B), triploid =30 (C), and tetraploid=40 (D) (scale bars=5 µm).

4. Conclusions

The control group had the highest trochophore survival rate ($42.58 \pm 12.06\%$), which was not significantly different from the 90-second UV exposure group. Additionally, chromosomal characteristics were determined using the conventional staining method, and both 10 and 20 chromosomes and various aneuploid types were observed. The control group had the highest rate of trochophores, indicating diploid gynogenesis ($75.20 \pm 4.84\%$). However, it should be noted that a relatively low survival rate of the D-shaped stage was observed, which may be due to increased stress during development.

5. Acknowledgements

The authors are highly grateful to Rajamangala University of Technology Srivijaya, Trang Campus, for the opportunity to use the laboratory to do this research.

Author Contributions: Conceptualization, S.C., S.T., and W.K; methodology, S.C., and N.G.; formal analysis, S.C., and C.C.; investigation, S.C.; writing—original draft preparation, S.C., and K.S.; writing—review and editing, S.C.

Funding: This research was funded from the university income budget for 2019.

Conflicts of Interest: The authors declare no conflicts of interest.

References

- [1] Yuan, TC.; Liang, Y.; Cai, WR.; Hai, YR.; Ping, WZ. Triploid of *Crassostrea gigas* induced with 6 dimethylaminopurine: blocking polar body I, *J. Fish. China*. **1999**, 2, 128-132.

- [2] Guo, X.; Hershberger, WK.; Cooper, K.; Chew, KK. Artificial gynogenesis with ultraviolet light-irradiated sperm in the Pacific oyster, *Crassostrea gigas*. I. Induction and survival. *Aquaculture*. **1993**, *113*, 201-214.
- [3] Manan, H.; Hidayati, AN.; Lyana, NA.; Amin-Safwan, A.; Ma, H.; Kasan, NA.; Ikhwanuddin, M. A review of gynogenesis manipulation in aquatic animals. *Aquaculture and Fisheries*. **2022**, *7*(1), 1-6.
- [4] Li Q, Kijima A. Segregation of microsatellite alleles in gynogenetic diploid pacific abalone (*Haliotis discus hannai*). *Marine Biotechnology*. **2005**, *7*, 669-676.
- [5] Gosling, E. Bivalve molluscs: biology, ecology and culture: John Wiley & Sons. **2008**.
- [6] Teeraya, C.; Natthapong, T.; Siwa, T. The season of Oyster maturation in Bandon Bay, Suratthani Province. Technical Paper No. 2/2006. Coastal Fisheries Research and Development Bureau, Department of Fisheries, Ministry of Agriculture and Cooperatives. **2006**. 21p. (In Thai).
- [7] Galtsoff, PS. The American oyster *Crassostrea virginica* (Gmelin). US Fish Wildlf. *Serv. Fish. Bull.* **1964**, *64*, 1-480.
- [8] Zhang, Z.; Wang, Y.; Zhang, Z. Induction of gynogenetic diploids in the small abalone, *Haliotis diversicolor supertexta*. *J. Shellfish Res.* **2004**, *23*(4), 1115-1122.
- [9] Fujino K, Arai K, Iwadare K, Yoshida T, Nakajima S. Induction of gynogenetic diploid by inhibiting second meiosis in the Pacific abalone (*Haliotis discus hannai*). *Bull. Jpn. Soc. Sci. Fish.* 1990, *56*: 1755-1763.
- [10] Pan, Y.; Li, Q.; Yu, R.; Wang, R. Induction of gynogenetic diploids and cytological studies in the zhikong scallop, *Chlamys farreri*. *Aquatic Living Resources*. **2004**, *17*, 201-206.
- [11] Fairbrother, JE. Viable gynogenetic diploid *Mytilus edulis* (L.) larvae produced by ultraviolet light irradiation and cytochalasin B shock. *Aquaculture*. **1994**, *126*(1-2), 25-34.
- [12] Scarpa, J.; Komaru, A, Wada KT. Gynogenetic induction in the mussel, *Mytilus galloprovincialis*. *Bull. Natl. Res. Inst. Aquac. (Jpn.)*. **1994**, *23*, 33-41.
- [13] Guo, X.; Allen, S. Sex determination and polyploid gigantism in the dwarf surfclam (*Mulinia lateralis* Say). *Genetics*. **1994**, *138*(4), 1199-1206.
- [14] Helm, M.; Bourne, MN.; Lovatelli, A. *Hatchery culture of bivalves: a practical manual*. **2004**.
- [15] Nowland, SJ.; O'Connor, WA.; Elizur, A.; Southgate, PC. Evaluating spawning induction methods for the tropical black-lip rock oyster, *Saccostrea echinate*. *Aquaculture Reports*. **2021**, *20*, 100676.
- [16] Choo-seangjaew, S.; Tanyaros, S.; Koedprang, W.; Tanomtong, A. Triploid Induction by the use of 6-dimethylaminopurine (6-DMAP) for the Tropical Oyster, *Crassostrea belcheri* (Sowerby, 1871). *Proceedings of the 9th Rajamangala University of Technology International Conference (9th RMUTIC)*. **2018**, 180-188.
- [17] Thomas, P.; Mallia, JV.; Muthiah, P. Induction of triploidy in Indian edible oyster *Crassostrea madrasensis* (Preston) using 6-Dimethylaminopurine. *Asian Fish Sci.* **2006**, *19*(1), 15-20.
- [18] Kijima, A. Effect of irradiation on genetic inactivation of sperm using marketing Tissue culture petri-dish in the Pacific abalone *Haliotis discus hannai*, *Tohoku J. Agric. Res.* **1992**, *42*, 73-81.
- [19] Li, Q.; Osada, M.; Kashihara, M.; Hirohashi, K.; Kijima, A. Induction of gynogenetic diploids and cytological studies in the Pacific oyster, *Crassostrea gigas*. *Aquaculture Science*. **2000**, *48*(2), 185-191.
- [20] Li, Q.; Osada, M.; Kashihara, M.; Hirohashi, K.; Kijima, A. Artificially Induced gynogenetic diploid in the Pacific abalone, *Haliotis discus hannai*. *Fish Genet. Breed. Sci.* **1999**, *28*, 85-94.



Smartphone-Based Spectrophotometer for Facile and Fast Determination of Lipid Peroxidation in Local Fried Food

Trin khawsung¹, Tanyarath Utaipan², Weeraya Treewanjutha^{3*}

¹ Faculty of Science and Technology, Prince of Songkla University, Pattani, 94000, Thailand; trin.k@psu.ac.th

² Faculty of Science and Technology, Prince of Songkla University, Pattani, 94000, Thailand; tanyarath.u@psu.ac.th

³ Faculty of Science and Technology, Prince of Songkla University, Pattani, 94000, Thailand; weeraya.k@psu.ac.th

* Correspondence: weeraya.k@psu.ac.th

Citation:

Khawasung, T.; Utaipan, T.; Treewanjutha, W. Smartphone-based spectrophotometer for facile and fast determination of lipid peroxidation in local fried food. *ASEAN J. Sci. Tech. Report.* 2024, 27(2), 79-89. <https://doi.org/10.55164/ajstr.v27i2.252346>

Article history:

Received: January 10, 2024

Revised: February 27, 2024

Accepted: February 28, 2024

Available online: February 29, 2024

Publisher's Note:

This article is published and distributed under the terms of Thaksin University.

Abstract: During lipid peroxidation in foods, deterioration rancidity occurred, and a toxic by-product also accumulated. The well-known marker of lipid peroxidation in food is malondialdehyde (MDA), suspected to be carcinogenic and mutagenic in humans. MDA level is determined using thiobarbituric acid (TBA) assay. The pink color of the MDA-TBA2 complex after the reaction can be measured spectrophotometrically at 530-540 nm. Several analytical methods, including smartphone-based methods, have been used to determine the MDA-TBA2 complex, such as UV-Vis spectrophotometry and HPLC-DAD. Therefore, this research aimed to determine lipid peroxidation in fried food using a simple smartphone-based spectrophotometer. The device was established using a paper box, LED lamps, and a test tube. Various concentrations of MDA were reacted with TBA reagent and then submitted to the device. RGB intensity data were converted to absorbance values and used to construct linear regression. Results showed that the G value from the smartphone-based spectrophotometer provided consistent results with R² of 0.9869, including 0.93 and 95.17% precision and accuracy, respectively. Then, the developed device was finally used to determine the MDA in local fried food samples. The concentration of MDA in fried foods was successfully determined with high precision (0.96) and accuracy (88.33 %) compared to the traditional UV-Vis spectrophotometric method. Thus, this study provides a practical guideline for developing quick and easy accessibility, portability, and low-cost spectrophotometer for lipid peroxidation assessment in fried food and other future food matrices.

Keywords: Smartphone; Malondialdehyde; Thiobarbituric acid reactive substances; Fried food



1. Introduction

Frying is a fast, simple, and cost-effective cooking method used for producing and preparing food, both on industrial and domestic scales [1]. Fried food has unique sensory characteristics, which consumers highly appreciate. These characteristics include a pleasant flavor, golden-brown color, and crispy texture. During the frying process, the oil used is subjected to high temperatures, which accelerate the formation of lipid oxidation [2]. Mild oxidation of fried food continuously occurs without promoting noticeable sensory changes during processing and storage. The longer fried food is

exposed to high temperatures and atmospheric air, the higher lipid peroxidation and oxidative products are generated [3]. Among the various oxidation products, aldehydes are mostly significant, affecting food flavor and nutritional quality. They are also the main cause of food rancidity during preparation and storage [4-5]. One widely known lipid peroxidation product is malondialdehyde (MDA) [6]. MDA is a final product of lipid peroxidation and is considered a universal lipid oxidation marker of oxidative stress. It had been regarded as a cytotoxic, neurotoxic, mutagenic, and possibly carcinogenic in humans [7]. The thiobarbituric acid (TBA) assay is an empirical method frequently used to measure oxidation in food products. The assay has been utilized due to its simple and quick derivatization of MDA before the detection process [8]. Since free MDA is very low in concentration, thus harsh conditions of acidity and temperature are needed to treat proteins and break down peroxides. One molecule of malonaldehyde reacts with two TBA molecules, forming a pink-colored MDA-TBA₂ complex that absorbs light at 530-540 nm and can be quantified as shown in Fig. 1. However, the reaction is not specific because the other molecules in the sample metric such as ketones, acids, esters, sugars, amino acids, oxidized proteins, and vitamins, can also react with TBA, hence known as TBA-reactive substances or TBARS [9-10]. Meanwhile, the intensity of a pink-colored complex corresponds to the level of lipid peroxidation in the sample.

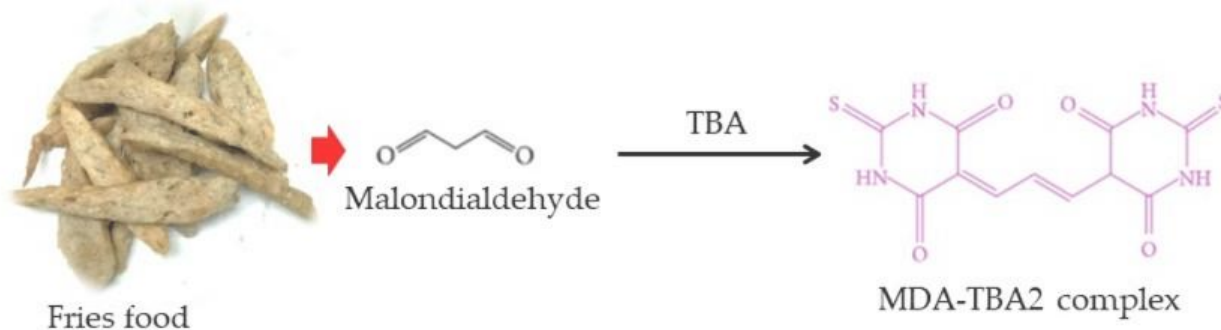


Figure 1. Reaction mechanism of malondialdehyde (MDA) with thiobarbituric acid (TBA) in the presence of acid and heat to produce MDA-TBA₂ colored product [10].

Several analytical methods have been used to determine TBARS, such as spectrophotometrically [11], spectrofluorometrically [12] for screening analysis, and chromatographic, such as HPLC-DAD which is suggested for more specific performance [13], but the longer duration and cost of the analysis will also increase. Spectrophotometry, therefore, is a preferable method for its simplicity, high sample throughput, and low cost. Recently, the use of smartphones has rapidly increased in terms of accessibility for every single person. The capabilities of smartphone technology are more efficient in terms of computational power connectivity, including camera and imaging capability. Smartphone imaging has been increasingly applied across various scientific fields and several applications [14-15]. The RGB (Red-Green-Blue) color system has frequently been used as an alternative for quantitative determinations in analytical chemistry due to its real-time, convenient, and inexpensive [16]. Mostly, smartphone colorimetric data will be converted to analyze concentrations using a high-resolution built-in camera smartphone [17-18].

In this work, the developed smartphone-based spectrophotometer, in combination with Red-Green-Blue (RGB) analysis, was used to trace MDA in the local fried food after a derivatization step with TBA. An in-house smartphone-based spectrophotometer was constructed for field analysis of MDA in fried food samples. The influence of the dimension of the component effective in developing smartphone-based spectrophotometer sensitivity was evaluated and optimized. The reliability of the developed device for MDA in fried food evaluation was compared with the standard UV-Vis spectrophotometry method.

2. Materials and Methods

2.1 Constructing a smartphone-based spectrophotometer

Inside the developed device, there is the sample cell (small test tube, 16 mm x 10 mm, Pyrex, USA.) with base, background panel, and LED board accommodated in a paper box which has a small channel for taking pictures of the solution in a sample cell from outside as shown in Fig. 2.

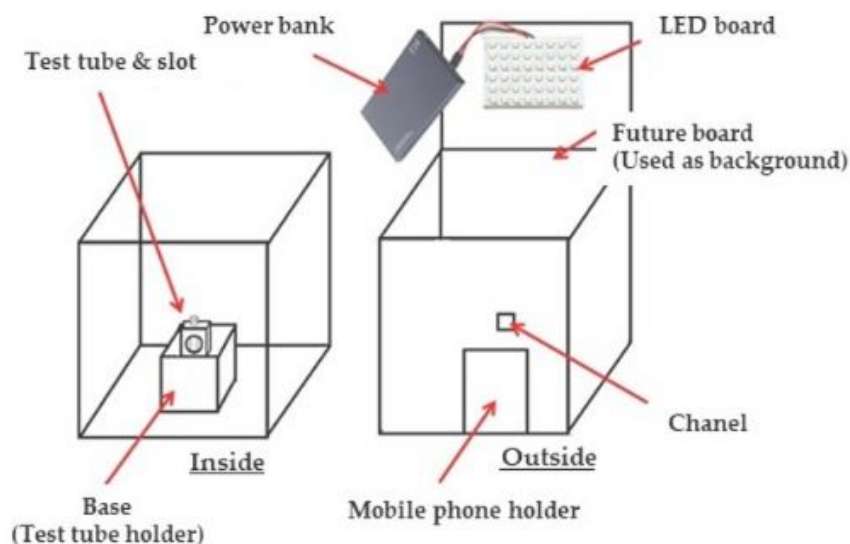


Figure 2. The design of the smartphone-based spectrophotometer to measure RGB value using a flat-palette application.

The dimensions of the device are listed in Table 1. The best distance and position of the sample cell, background, and LED panel were optimized by varying the distance between the camera and sample cell and the distance between the sample cell and the background. The best parameters have been chosen for device construction and further experiments. The digital picture of the MDA-TBA2 solution was captured by a smartphone camera (flat-palette application, Samsung Galaxy S10 Plus, screen is 6.4 inches, 103.8 cm² (88.9% screen-to-body ratio), with a resolution of 1440 x 3040 pixels, 19:9 ratio (522 ppi density), Korea). The image was then decomposed into three color components: red, green, and blue (R, G, and B).

Table 1. Apparatus design of the smartphone-based spectrophotometer.

List	Details
Box	Size 21 cm x 30 cm x 23 cm
White LED light bulbs	Size 5 mm x 18 bulbs
LED board	Size 4.5 cm x 17.5 cm
Test tubes	Size 16 mm x 10 mm
Slot	Size 2.5 cm x 6 cm x 6 cm
Base	Size 5 cm x 10.6 cm x 10 cm
Chanel	Size 1 cm x 2 cm
Phone holder	Size 10 cm x 13 cm
Camera Chanel	Size 1 cm x 2 cm
Feature board	Size 21 cm x 23 cm
Power bank	Capacity 11000 mAh

2.2 Optimization of components of the developed device

The pink solution of the MDA-TBA2 complex was prepared from the derivatization of 100 μ M MDA standard and TBA solution, which was then measured at 532 nm. The red, green, and blue (RGB) colors were detected using a flat-palette application on the smartphone-based spectrophotometer. To achieve the best results, the distance between the camera and the sample cell was varied from 1 to 6 cm. While the LED board was fixed at 3 cm above the sample cell, the background was fixed at 15 cm behind the sample cell. Three different colors (white, blue, and green) of backgrounds were used to find the most appropriate color. The photos were converted to RGB values using the "flat-palette application." Flat-palette is a color manager app that combines useful color scheme ideas and functions, including RGB slider adjustment, center point color extraction, and image color scheme creation. Therefore, the captured image will provide the RGB value, a color commonly seen on a smartphone screen. The RGB obtained values were then converted to absorbance using equation (1) [17].

$$A = -\log\left(\frac{I}{I_0}\right) \quad (1)$$

When

I = R, G, or B value of sample solution

I₀ = R, G, or B value of blank solution

The condition that provided the absorbance comparable to that obtained from a standard UV-Vis spectrophotometer was chosen for further studies.

2.3 Standard curve of MDA-TBA2 complex

The standard solution of TBA was prepared by using 0.375% of TBA dissolved in 15% trichloro acetic acid (TCA). The solution of TBA was prepared freshly before experimenting. BHT stock solution was prepared using 1 g of BHT dissolved in 100 mL of 95% ethanol. Standard solution of MDA (100 mmol/L) was prepared by diluting 99% MDA in 25 mL of distilled water. Then, MDA with concentrations of 1.56, 3.125, 6.25, 12.5, 25, 50, and 100 μ mol/L were prepared. The derivatization of TBA and MDA standard in various concentrations was done by mixing 3.5 mL of 0.375% TBA in 15% TCA and 0.5 mL of MDA standard solutions. The solution was then heated in a water bath at 95°C for 10 min [19]. After cooling, the pink solution was measured at 532 nm using a UV-Vis spectrophotometer. The red, green, and blue (RGB) colors were also measured using pictures from the developed smartphone-based spectrophotometer. All experiments were performed in triplicate.

2.4 Extraction of MDA in fried food samples

Two grams of fried food powder (S1 = fried fish cracker crisps, S2= fried fish cracker sticks, S3= French fries) were taken into a 15 mL test tube, and 5 mL of the glacial acetic acid (50% v/v) was added, followed by 2 mL of BHT (0.01%) for preventing further oxidation [10]. The samples were shaken for one hour and filtered. The filtrate was centrifuged when required.

2.5 Determination of MDA in fried food samples

0.5 mL of sample solution was mixed with 3.5 mL of thiobarbituric acid (TBA), then heated in a water bath at 95°C for 10 min. After the mixture had cooled down at room temperature, the absorbance at 532 nm was measured using the UV-Vis spectrophotometer and developed device. MDA content obtained from the device was compared to MDA content obtained from the UV-Vis spectrophotometer. The limit of detection (LOD), limit of quantification (LOQ), accuracy, precision, and the relative error of the methods were validated. The analysis of all samples was performed in triplicate. The data was expressed as standard deviation (SD).

2.6 Data analysis

Triplicate measurement was done for each standard and sample. All values were displayed as mean \pm SD. LOD, LOQ, precision, accuracy, and error were calculated as compared to the absorbance from the UV-Vis spectrophotometer.

3. Results and Discussion

3.1 The optimization and construction of a smartphone-based device.

The optimization of the device with a smartphone camera was performed to find the best distance between the camera and the sample cell, the sample cell to the background, and the color of the background for TBARS measurement. Several conditions were tested for the analysis of the MDA-TBA2 complex by changing the distance between the camera and the sample cell. Three different backgrounds, white, green, and blue, were also investigated. R G B values after conversion to absorbance using a different camera and sample cell distances and different backgrounds (white, green, and blue) are shown in Table 2. The most efficient distance of each part was selected by considering the similarity of absorbance of the tested MDA-TBA2 complex solution when measured by the UV-Vis spectrophotometer at 532 nm (Abs. = 0.200). The results from Table 2 revealed that the reverse of the green value (G value) gave a positive absorbance value in all backgrounds used and was proportional to the concentration of MDA. However, the closest value to the UV-Vis spectrophotometer was most achieved on a blue background. However, the distance between the camera and sample cell that gives similar absorbance from the UV-Vis spectrophotometer was 3 and 4 cm, with the absorbance value of 0.165 and 0.245, respectively. The results were confirmed additionally, and the values of MDA-TBA2 levels were similar to the previous experiments, whereby 3 cm between the camera and sample cell was chosen. Therefore, the optimum dimensions of the smartphone-based spectrophotometer were 3 cm, 15 cm, and 3 cm for the distance from the camera to the sample cell and from the sample cell to the background and LED panel positions (in the above position), respectively. The absorbance, which was calculated using equation (1) and G value from a flat-palette application on a smartphone-based spectrophotometer, was found to exhibit a correlation with the value obtained from the UV-Vis spectrophotometer because both red chromogen and blue background are absorbing the green light (G value) according to "The light theory of color" [20]. Then, the G value and blue background were used as the analytical signal for further study. The optimum distance of the developed device is shown in Table 3.

3.2 Reaction of standard MDA and the TBA reagent for the standard curve

In this study, the reaction mixture was heated at 95 °C for 10 minutes due to the indicated experimental data that these conditions yield maximal product [10]. In reaction with TBA (TBA assay), MDA forms an intensely pink-colored complex that is easily assessed spectrophotometrically; therefore, this method is frequently used to detect lipid peroxidation in several samples. The pink color of the solution indicated the absorption of the green color wavelength; thus, the red color wavelength was transmitted and then observed. Beer's Law mentioned that the higher the concentration, the lower the light intensity that passes through a chemical solution [21].

The absorbance obtained from the UV-Vis and smartphone-based spectrophotometer increased correspondingly to the MDA concentration, as shown in Table 4. However, the absorbance from the developed device was slightly lower than that obtained from the UV-Vis spectrophotometer. The calibration curve of five points in triplicate ($n=3$) was established in the concentration range of 6.25 to 100 $\mu\text{mol/L}$. Linear regression shows a correlation coefficient (R^2) of 0.9984 with the equation of $y = 0.0144x$ and 0.9865 with an equation of $y = 0.0073x - 0.0532$ for a commercial system and smartphone-based spectrophotometer, respectively, as shown in Fig. 3A and 3B. Meanwhile, the linear regression slope revealed a sensitivity of the method, in which the UV-Vis spectrophotometer provides higher sensitivity (slope = 0.0144) compared to the smartphone-based device (slope = 0.0073). The performance of the commercial UV-Vis spectrophotometer in terms of limit of detection and quantification was 3.352 $\mu\text{mol/L}$ and 10.157 $\mu\text{mol/L}$, respectively, which revealed notably better results. Each run using the smartphone-based spectrophotometer took almost 1 min, compared to less than 5 s for the commercial spectrophotometer. However, this research aimed to provide a handheld device available to everyone to determine the MDA content onsite. Thus, the above performance was acceptable in relation to the robustness, ease of operation, and ultra-low cost of the smartphone-based spectrophotometer. Thus, measuring the concentration of MDA or TBARS in fried food samples can be applicable.

Table 2. The absorbance of MDA-TBA2 complex from R, G, and B values conversion using three different color backgrounds.

Distant between camera and sample cell (cm)	Absorbance (Abs.) value								
	White background			Green background			Blue background		
	Red	Green	Blue	Red	Green	Blue	Red	Green	Blue
1	-0.008 ± 0.001	0.054 ± 0.002	-0.032 ± 0.001	-0.075 ± 0.004	0.060 ± 0.005	-0.015 ± 0.002	-0.102 ± 0.008	0.126 ± 0.000	0.008 ± 0.005
2	0.015 ± 0.002	0.082 ± 0.002	-0.008 ± 0.000	0.104 ± 0.050	0.114 ± 0.021	0.060 ± 0.020	-0.159 ± 0.027	0.139 ± 0.010	0.025 ± 0.003
<u>3</u>	<u>-0.014 ± 0.003</u>	<u>0.039 ± 0.002</u>	<u>-0.036 ± 0.003</u>	<u>-1.652 ± 0.052</u>	<u>0.095 ± 0.041</u>	<u>0.079 ± 0.040</u>	<u>-0.031 ± 0.013</u>	<u>0.165 ± 0.013</u>	<u>0.017 ± 0.002</u>
<u>4</u>	<u>-0.015 ± 0.003</u>	<u>0.035 ± 0.004</u>	<u>-0.038 ± 0.004</u>	<u>-0.134 ± 0.284</u>	<u>0.095 ± 0.025</u>	<u>0.049 ± 0.027</u>	<u>-0.028 ± 0.014</u>	<u>0.245 ± 0.005</u>	<u>0.037 ± 0.004</u>
5	0.010 ± 0.006	0.113 ± 0.017	-0.050 ± 0.001	-0.815 ± 0.027	0.054 ± 0.006	0.000 ± 0.027	-0.195 ± 0.029	0.103 ± 0.016	0.024 ± 0.008
6	-0.016 ± 0.006	0.078 ± 0.009	-0.022 ± 0.003	-0.435 ± 0.088	0.021 ± 0.015	-0.004 ± 0.013	-0.598 ± 0.032	0.136 ± 0.025	0.002 ± 0.010

Data are expressed as mean±SD from triplicate samples.

Table 3. The optimum dimension of the smartphone-based spectrophotometer.

Details	Optimum
Distance between camera to sample cell	3 cm
Distance between sample cell to background	15 cm
Distance of LED panel (from top)	3 cm
R, G, B color	Green
Color of background	Blue

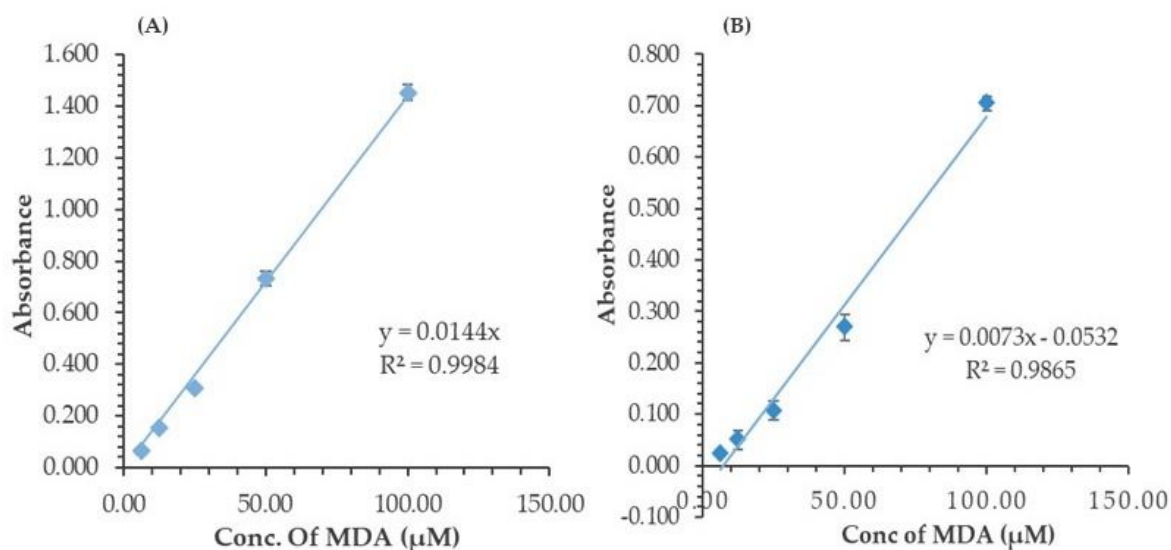


Figure 3. (A) MDA standard curve obtained from the UV-Vis spectrophotometer, (B) MDA standard curve obtained from the smartphone-based spectrophotometer.

Table 4. Absorbances were obtained from the UV-Vis spectrophotometer and the smartphone-based spectrophotometer.

concentration of MDA ($\mu\text{mol/L}$)	Absorbance from UV-Vis spectrophotometer	Absorbance from Smartphone-based spectrophotometer.
6.25	0.063 ± 0.013	0.024 ± 0.005
12.50	0.154 ± 0.008	0.050 ± 0.018
25.00	0.308 ± 0.011	0.107 ± 0.018
50.00	0.735 ± 0.028	0.269 ± 0.026
100.00	1.454 ± 0.029	0.704 ± 0.014

Data are expressed as mean \pm SD from triplicate samples.

The limit of detection (LOD) and quantification (LOQ) were evaluated from the slope and residual standard deviations of the standard curve. The LOD and LOQ can be calculated as described in the following equation: $\text{LOD} = 3.3\sigma/S$ and $\text{LOQ} = 10\sigma/S$, respectively, where σ is the standard deviation of the response, and S is the slope of the calibration curve [22]. Results showed that the LOD and LOQ of the UV-Vis spectrophotometer were $3.352 \mu\text{mol/L}$ and $10.157 \mu\text{mol/L}$ while the LOD and LOQ developed spectrophotometer were $11.490 \mu\text{mol/L}$ and $34.819 \mu\text{mol/L}$. The obtained results are in good agreement with previous studies in the determination of TBARS in fried fast food using a simple spectrophotometric method, which showed that the LOD was $1.758 \mu\text{M}$, while LOQ was $5.859 \mu\text{M}$ [23]. The higher LOD and LOQ of the developed spectrophotometer should be remarked on compared to the commercial system. However, the LOD of MDA by the device achieved $11.490 \mu\text{mol/L}$, which is quite below or lower than the recommended values, whereby the acute toxicity of MDA in the diet is considered not high. Still, the lethal dose of LD_{50} in rats accounts for 632 mg/kg body weight [24]. The analytical performance was also validated for the smartphone-based spectrophotometric method, including accuracy, precision, and error. Three concentrations of MDA (20 , 40 , and $60 \mu\text{mol/L}$) were used for this purpose. Accuracy was reported as the recovery percentage, while the precision and error represented the repeatability of the tested method. Instrumental precision was determined by the replicate ($n=9$) analysis of standard compounds. The accuracy, precision, and error of the developed device were 95.17% , 0.933 , and 4.83% , respectively, as shown in Table 5. Poor color intensity may decrease accuracy when the MDA is used at a lower concentration than $20 \mu\text{mol/L}$. The recoveries ranged from 87 to 95% .

The results exhibited evidence and demonstrated the performance of the device for the analysis of different MDA amounts in different fried food samples.




Table 5. Precision, accuracy, and error of the developed smartphone-based spectrophotometer.

MDA (μM)	Precision	% Accuracy	% Error
20	0.879	87.102	12.898
40	0.926	94.118	5.882
60	0.933	95.169	4.831

3.3 Determination of MDA in fried food samples

To evaluate the performance of the smartphone-based spectrophotometer with real sample matrices, the method was finally applied to analyze MDA in fried food samples found in the local markets. MDA concentrations were determined parallelly between the smartphone-based method and the traditional UV-Vis spectrophotometer. Three samples of street foods were selected since they were popular among consumers and widely consumed. These include fried fish cracker crisps, fried fish cracker sticks, and French fries. The results of this experiment and the short description of these foods are given in Table 6. As determined by spectrophotometry, MDA concentration in fried fish cracker crisps, fried fish cracker sticks, and French fries were 55.84, 53.21, and 58.89 $\mu\text{mol/L}$, respectively. Consequently, MDA concentration in the same samples using the developed device was 63.21, 41.118, and 142.84 $\mu\text{mol/L}$. Zeb and Ullah (2016) revealed that fried fast foods possessed an amount of TBARS in the range of 0.372 ± 0.03 to 2.911 ± 0.13 $\mu\text{mol/g}$ when 50% acetic acid was used as an extraction solvent [10]. Pandey et al. [25] also reported that deep fried Shami kebab possessed the values of TBARS 0.38 to 0.68 mg/kg. The difference may be due to the difference in the laboratory and food preparation, TBARS in sample or frying medium. These results indicate that the methods used in this study, UV-Vis spectrophotometry and the developed device, give similar tendency results to the other works. The precision, accuracy, and error of the device were calculated. The best reliability was found in fried fish cracker crisps (S1), as shown by low error percentage, high precision, and high accuracy percentage. This result was consistent with the color of the reactant. The reactant solution of S1 was pale pink, indicating the expression of TBARS since oxygen can result in oxidative deterioration of the fried fish cracker. Meanwhile, MDA in S3 detected by the device was positively faulty compared to the UV-Vis spectrophotometry due to the yellow color of the reactant, which was derived from the food dye. Thus, the yellow solution's absorption or visible light transmission possibly interfered with the detection system. The precision and accuracy of the device are correlated to the color of the reactant solution. The pink solution shows high precision and accuracy with a lower error percentage. The errors in MDA detection using the device may be due to the color of the solution. The device could determine MDA in fried fish cracker crisps extract (S1) precisely compared to the spectrophotometer result. Fried fish cracker crisps are generally consumed instantly after preparation. Hence, the high amounts of lipids and the packaging process can result in high oxidative deterioration of the fried fish cracker. Thus, this result indicated that the developed device was suitable for evaluating MDA in fried food samples used.

Table 6. The concentration of MDA in fried food samples using a UV-Vis spectrophotometer and a smartphone-based device.

Sample	Description	The concentration of MDA from UV-Vis spectrophotometer ($\mu\text{mol/L}$)	Concentration of MDA from developed device ($\mu\text{mol/L}$)	Precision	% Accuracy	% Error
S1= fried fish cracker crisps	Fried wheat flour mixed with fish meat and seasoning (Thin piece) 	55.842 \pm 2.22	63.216 \pm 8.30	0.96	88.334	11.666
S2= fried fish cracker sticks	Fried wheat flour mixed with fish meat and seasoning (Thick piece) 	53.214 \pm 4.82	41.118 \pm 36.12	0.86	78.181	21.819
S3=French fries	Fried potato chips 	58.899 \pm 3.23	142.843 \pm 22.32	0.93	56.760	43.240

Data are expressed as mean \pm SD from triplicate samples

4. Conclusions

The smartphone-based spectrophotometer was constructed and applied to determine MDA concentration in fried food samples compared to the standard UV-Vis spectrophotometric method. The developed method was simpler, lens-free, portable, cost-effective, and yielded high sample throughput. No power supply is needed for the in-field analysis. This device can be handmade, constructed in minutes, and used to determine MDA in fried food samples ranging from 6.25 to 100 $\mu\text{mol/L}$ precisely and accurately. Compared to a commercial instrument, the readout of this device revealed similar analytical features; nevertheless, the limitations are its lower sensitivity and higher LOD. This research would accommodate TBARS evaluation in other food matrices for quality control in the food industries or regular food inspection systems in the future.

5. Acknowledgements

This research was funded by the Department of Science, Faculty of Science and Technology, Prince of Songkla University, Pattani Campus. High appreciation is also rendered to the staff in the chemistry division, PSU, Pattani.

Author Contributions: For research articles with several authors, a short paragraph specifying their individual contributions must be provided. The following statements should be used “Conceptualization, Weeraya Treewanjutha and Tanyarath Utaipan; methodology, Weeraya Treewanjutha and Trin khawsung; software, Tanyarath Utaipan; validation, Weeraya Treewanjutha and Tanyarath Utaipan; formal analysis, Tanyarath Utaipan; investigation, Weeraya Treewanjutha and Tanyarath Utaipan; resources, Weeraya Treewanjutha, Tanyarath Utaipan and Trin khawsung; data curation, Tanyarath Utaipan; writing—original draft preparation, Weeraya Treewanjutha and Tanyarath Utaipan; writing—review and editing, Weeraya Treewanjutha and Tanyarath Utaipan; visualization, Weeraya Treewanjutha; supervision, Weeraya Treewanjutha; project administration, Faculty of Science and Technology, PSU; funding acquisition, Faculty of Science and Technology, PSU. All authors have read and agreed to the published version of the manuscript.” Please turn to the CRediT taxonomy for the term explanation. Authorship must be limited to those who have contributed substantially to the work reported.

Funding: This research was funded by funded by the Department of Science, Faculty of Science and Technology, Prince of Songkla University, Pattani Campus.

Conflicts of Interest: The authors declare no conflict of interest. The funders had no role in the design of the study; in the collection, analyses, or interpretation of data; in the writing of the manuscript, or in the decision to publish the results.

References

- [1] Bordin, K.; Kunitake, M. T.; Aracava, K. K.; Trindade, C. S. Changes in food caused by deep fat frying – A review. *Archivos Latinoamericanos de Nutrición*. **2013**, *63*(1), 5-13. ISSN 0004-0622.
- [2] Wang, D.; Xiao, H.; Lyu, X.; Chen, H.; Wei, F. Lipid oxidation in food science and nutritional health: A comprehensive review. *Oil Crop Science*. **2023**, *8*(1), 35-44. <https://doi.org/10.1016/j.ocsci.2023.02.002>.
- [3] Ahmed, M.; Pickova, J.; Ahmad, T.; Liaquat, M.; Farid, A.; Jahangir, M. Oxidation of lipids in foods. *Sarhad Journal of Agriculture*. **2016**, *32*(3), 230-238. <http://dx.doi.org/10.17582/journal.sja/2016.32.3.230.238>.
- [4] Ma, L.; He, Q.; Qiu, Y.; Liu, H.; Wu, J.; Liu, G.; Brennan, C.; Brennan, M. A.; Zhu, L. Food matrixes play a key role in the distribution of contaminants of lipid origin: A case study of malondialdehyde formation in vegetable oils during deep-frying. *Food Chemistry*. **2021**, *347*, 129080. <https://doi.org/10.1016/j.foodchem.2021.129080>.
- [5] Velasco, J.; Dobarganes, C.; Márquez-Ruiz, G. Oxidative rancidity in foods and food quality. *Chemical Deterioration and Physical Instability of Food and Beverages*. **2010**, *5*, 3-32. <https://doi.org/10.1533/9781845699260.1.3>.
- [6] Papastergiadis, A.; Mubiru, E.; Van Langenhove, H.; De Meulenaer, B. Malondialdehyde measurement in oxidized foods: evaluation of the spectrophotometric thiobarbituric acid reactive substances (TBARS) test in various foods. *Journal of agricultural and food chemistry*. **2012**, *60*(38), 9589–9594. <https://doi.org/10.1021/jf302451c>.
- [7] Całyniuk, B.; Grochowska-Niedworok, E.; Walkiewicz, K. W.; Kawecka, S.; Popiołek, E.; Fatyga, E. Malondialdehyde (MDA) – product of lipid peroxidation as marker of homeostasis disorders and aging. *Annales Academiae Medicae Silesiensis*. **2016**, *70*, 224-8. <https://doi.org/10.18794/aams/65697>
- [8] Ghani, Md. A.; Barril, C.; Bedgood, D. R.; Prenzler, P. D. Measurement of antioxidant activity with the thiobarbituric acid reactive substances assay. *Food Chemistry*. **2017**, *230*, 195-207. <https://doi.org/10.1016/j.foodchem.2017.02.127>.
- [9] Aguilar Diaz De Leon, J.; Borges, C. R. Evaluation of oxidative stress in biological samples using the thiobarbituric acid reactive substances assay. *Journal of visualized experiments*. **2020**, *159*, e61122. <https://doi.org/10.3791/61122>.
- [10] Zeb, A.; Ullah, F. A simple spectrophotometric method for the determination of TBARS in fried fast foods. *Journal of Analytical Methods in Chemistry*, 2016; *4*, 9412767. <https://doi.org/10.1155/2016/9412767>.
- [11] Fashi, A.; Cheraghi, M.; Badiee, H.; Zamani, A. An analytical strategy based on the combination of ultrasound assisted flat membrane liquid phase microextraction and a smartphone reader for trace determination of malondialdehyde. *Talanta*. **2020**, *209*, 120618. <https://doi.org/10.1016/j.talanta.2019.120618>.

4. Conclusions

There is a contamination of *E. coli* O45 in meats at high levels. Even though O45 strains in this study are not in the EHEC/STEC group, some contain virulence factors and belong to phylogenetic group D, indicating the potential to cause illnesses. Moreover, they are resistant to numerous antimicrobial agents, and almost half of them show a multi-drug resistant phenotype and the possibility of gaining a *stx2*-phage that makes them more dangerous in the future. These data are important from a public health standpoint.

5. Acknowledgements

We thank the Department of Microbiology, Division of Biological Science, Faculty of Science, Prince of Songkla University for providing the essential facilities.

Author Contributions: Conceptualization, P.S.; methodology, P.S.; software, P.R.; validation, P.S., P.R. and A.S.; formal analysis, P.S. and A.S.; investigation, A.S.; writing—original draft preparation, A.S.; writing—review and editing, P.S. and P.R.; supervision, P.S.; project administration, P.S.; funding acquisition, P.S. All authors have read and agreed to the published version of the manuscript.

Funding: This work was supported in part by Prince of Songkla University (grant no. SCI600588S).

Conflicts of Interest: The authors declare no conflict of interest.

References

- [1] Centers for Disease Control and Prevention. Global diarrhea burden. Available: (Accessed 8 November 2023)
- [2] Kaper, J.B.; Nataro, J.P.; Mobley, H.L.T. Pathogenic *Escherichia coli*. *Nature Reviews Microbiology*. **2004**, *2*, 123-140.
- [3] Michino, H.; Araki, K.; Minami, S.; Takaya, S.; Sakai, N.; Miyazaki, M.; Ono, A.; Yanagawa, H. Massive outbreak of *Escherichia coli* O157: H7 infection in schoolchildren in Sakai City, Japan, associated with consumption of white radish sprouts. *American Journal of Epidemiology*. **1999**, *150*(8), 787-796.
- [4] Dundas, S.; Todd, W.A.; Stewart, A.I.; Murdoch, P.S.; Chaudhuri, A.; Hutchinson, S.J. The central Scotland *Escherichia coli* O157: H7 outbreak: risk factors for the hemolytic uremic syndrome and death among hospitalized patients. *Clinical Infectious Diseases*. **2001**, *33*(7), 923-931.
- [5] Rangel, J. M.; Sparling, P. H.; Crowe, C.; Griffin, P. M.; Swerdlow, D. L. Epidemiology of *Escherichia coli* O157: H7 outbreaks, United States, 1982–2002. *Emerging Infectious Diseases*. **2005**, *11*(4), 603-609.
- [6] Nataro, J.P.; Kaper, J.B. Diarrheagenic *Escherichia coli*. *Clinical Microbiology Reviews*. **1998**, *11*(1), 142-201.
- [7] Karmali, M.; Petric, M.; Steele, B.; Lim, C. Sporadic cases of a haemolytic-uraemic syndrome associated with fecal cytotoxin and cytotoxin-producing *Escherichia coli* in stools. *The Lancet*. **1983**, *321*(8325), 619-620.
- [8] Paton, A.W.; Paton, J.C. *Enterobacter cloacae* producing a Shiga-like toxin II-related cytotoxin associated with a case of hemolytic-uremic syndrome. *Journal of Clinical Microbiology*. **1996**, *34*(2), 463-465.
- [9] Arthur, T.M.; Barkocy-Gallagher, G.A.; Rivera-Betancourt, M.; Koohmaraie, M. Prevalence and characterization of non-O157 Shiga toxin-producing *Escherichia coli* on carcasses in commercial beef cattle processing plants. *Applied and Environmental Microbiology*. **2002**, *68*(10), 4847-4852.
- [10] Barkocy-Gallagher, G.A.; Arthur, T.M.; Rivera-Betancourt, M.; Nou, X.; Shackelford, S.D.; Wheeler, T.L.; Koohmaraie, M. Seasonal prevalence of Shigatoxin-producing *Escherichia coli*, including O157: H7 and non-O157 serotypes, and *Salmonella* in commercial beef processing plants. *Journal of Food Protection*. **2003**, *66*(11), 1978-1986.
- [11] Sukhumungoon, P.; Nakaguchi, Y.; Ingviya, N.; Pradutkanchana, J.; Iwade, Y.; Seto, K.; Son, R.; Nishibuchi, M.; Vuddhakul, V. Investigation of *stx2+* *eae+* *Escherichia coli* O157: H7 in beef imported from Malaysia to Thailand. *International Food Research Journal*. **2011**, *18*(1), 381-386.
- [12] Pannuch, M.; Sirikaew, S.; Nakaguchi, Y.; Nishibuchi, M.; Sukhumungoon, P. Quantification of enteropathogenic *Escherichia coli* from retailed meats. *International Food Research Journal*. **2014**, *21*(2), 547-551.



Gid Crypto: Application for End-to-End Encrypt and Decrypt E-mail and Data

Alain Jean¹, and Tossaporn Alherbe^{2*}

¹ Department of Mathematics Statistics and Computer, Faculty of Science, Ubon Ratchathani University, Ubon Ratchathani, 34190, Thailand; alain.j@ubu.ac.th

² Department of Mathematics Statistics and Computer, Faculty of Science, Ubon Ratchathani University, Ubon Ratchathani, 34190, Thailand; tossaporn.c@ubu.ac.th

* Correspondence: tossaporn.c@ubu.ac.th

Citation:

Jean, A.; Alherbe T.; Gid Crypto: Application for End-to-End Encrypt and Decrypt E-mail and Data. *ASEAN J. Sci. Tech. Report.* **2024**, *27*(2), 90-102. <https://doi.org/10.55164./ajstr.v27i2.251127>.

Article history:

Received: October 2, 2023

Revised: February 27, 2024

Accepted: February 28, 2024

Available online: March 1, 2024

Publisher's Note:

This article is published and distributed under the terms of Thaksin University.

Abstract: Privacy and security in our digital environment have become essential today. Some data stored on hard disks, in flash memory, or exchanged through our communication channels is sensitive and should be kept confidential. Additionally, documents containing confidential information, such as business algorithms or new application coding, require adequate measures to ensure privacy and security. Therefore, data encryption is crucial in protecting information from being intercepted, misused, or stolen. While encryption tools are available for business e-mails, using these tools often requires subscribing as a member and paying extra fees. Effective tools are not limited to e-mail alone. Still, they can also be applied to any text data that requires a high level of security and complexity to ensure the protection of the data for a duration longer than it needs to be safeguarded. Our research aims to develop a stand-alone application that encrypts data to ensure its confidentiality without additional subscriptions or fees. The application is designed to be user-friendly, with fast encryption and decryption capabilities. It can be used not only for encrypting and decrypting e-mail messages but also for programming languages and Excel data. The application development utilizes techniques such as Diffie-Hellman, Mersenne Twister, and AES, arranged in layers to generate complex ciphertext that is difficult to decrypt without the developed application. LabVIEW was used for testing encryption speed. The attempt to attack encrypted data was subjected, but the result yielded no successful key retrieval.

Keywords: Encryption and decryption; Diffie-Hellman; Mersenne Twister; Advanced Encryption Standard; LabVIEW

1. Introduction

Since E-mail was developed in 1971 [1], it has become one of the primary communication channels and is widely used on the internet. According to data research from Raicati Group [2], in 2022, the number of worldwide e-mails, including both business and consumer users, was 4.26 billion, with the daily volume of sent/received e-mails per day being 333 billion. Along with the rise in the number of e-mail users, it is predicted to reach 4.6 billion users in 2025.

Currently, e-mail has mainly been used in any kind of online activity for personal and group communication. It is used not only for instant messaging but also for signing up for online commerce, sending updated news notifications,



and authorizing other forms when one is present on the internet. While users use e-mail for communication, they may be imprudent to send the most sensitive kind of secret data such as credential numbers, application passwords, birth dates, important business data, personal contact names, numbers, or medical health data. Unfortunately, they are unsecured since regular e-mail and data sending are not encrypted. It allows for phishing and other service providers unauthorized access.

There are 2 protocols commonly utilized for e-mail encryption: Encrypting an e-mail while it is in transit (Transport Layer Security: TLS) and end-to-end e-mail encryption. TLS is a cryptographic protocol that provides security for data sent between mail server to mail server. It uses public critical infrastructure (PKI) to encrypt messages while they are in transit from sender to recipient. TLS stops e-mails from being read after the sending but before the messages are delivered to the end system. It can avoid eavesdropping or altering e-mail contents while delivering data over the internet. The advantage of using TLS is that it is easy for users to send e-mails without extra work beyond clicking the send button, as it is provided by e-mail providers such as Google (Ghali et al. [3]) and Apple [4]. However, if a cybercriminal can attack an e-mail account through phishing, they can still read e-mail. Since TLS does not encrypt e-mail messages and cannot hide the messages from the e-mail servers themselves, e-mail providers can still access the contents of our messages.

End-to-end encryption is also known as public key encryption. It is a method where e-mail messages are encrypted by the stand-alone on the sender's system, and only the intended recipient can decrypt and read them on their device. End-to-end encryption provides the highest level of confidentiality as it prevents any third party or cybercriminal from reading or accessing messages at any delivery state. The encrypted messages also cannot be read by the e-mail server. Moreover, the attackers cannot access data on e-mail servers since they are encrypted on users' endpoints. If an attacker tries to retrieve data from the servers, they will get gibberish. End-to-end encryption makes communication safe. One may want to ensure sending financial and private communication using end-to-end encryption since it is difficult for cybercriminals to retrieve sensitive information.

Our work presents the Gid Crypto application, a stand-alone text data encryption and decryption; it is easy to use with any e-mail text body. This tool ensures the generation of secure e-mails and encrypted text data. We utilize various techniques, such as Diffie-Hellman [5] for key exchange, Mersenne Twister [6] for issuing genuinely random numbers, and Advanced Encryption Standard (AES) [7] for creating cipher texts, to ensure the utmost security of the information content.

The rest of the paper is organized as follows: Section 2 describes the material and methods used to develop the tool. The results and discussion of our work are presented in Section 3, and the conclusion is provided in Section 4.

2. Materials and Methods

2.1 Encryption and Decryption Principles

Encryption is turning plain text content, like text messages or e-mails, into cipher text/scrambled text to protect it from being read by unintended parties. When the intended recipient receives the message, only the person with the appropriate private key that matches the public key used to encrypt the message can read it, which is called decryption.

Our goal is to make an application that is easy to use and maintains the highest security and cryptographic standards. We follow 3 principles when developing this application. The first is implementing Diffie-Hellman as a key exchange protocol; the second is issuing a new and unique encryption key with each contact so we do not establish a similar pattern; we use Mersenne Twister. Finally, we use the Advanced Encryption Standard (AES) to generate cipher and decrypted texts.

2.2 Diffie-Hellman Principles

Diffie-Hellman (DH) [5], or exponential key exchange, was one of the first public-key protocols conceptualized initially by Ralph Merkle and named after Whitfield Diffie and Martin Hellman. It is a method for securely exchanging cryptographic keys over an insecure public channel. For example, if two people, Alice and Bob, wish to communicate over the internet, they need a way to exchange information that will be known only to them. To do that, Alice and Bob first generate their private and public keys and then send them to the

other side. After both parties obtain copies of each other's public keys, they compute shared keys. The shared keys will be used for symmetric cipher communication.

These steps can be understood with the diagram depicted in Figure 1. Our work uses the DH method of securely exchanging cryptographic keys on a secure channel and even over an insecure channel.

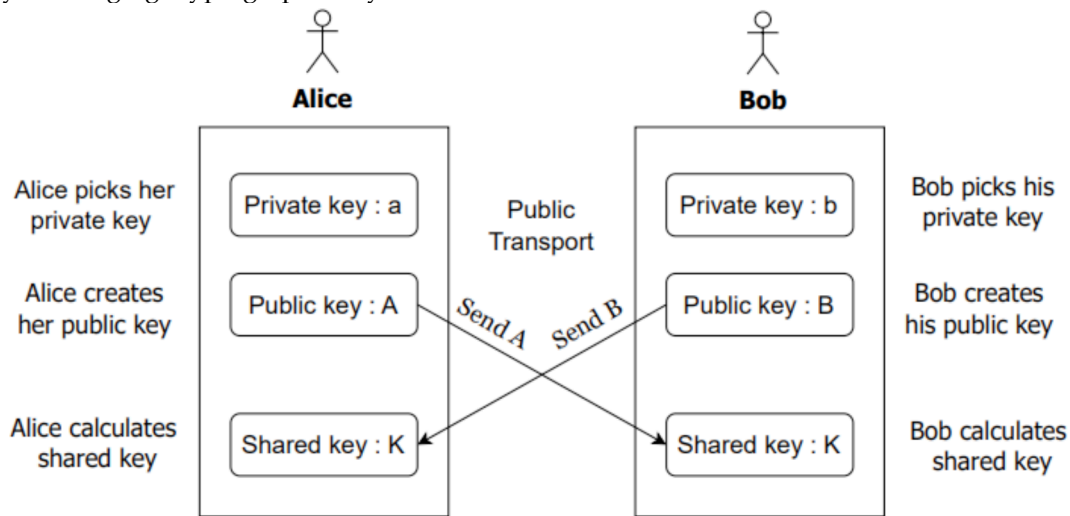


Figure 1. Diffie-Hellman Key Exchange

There are some methods for the key exchange, such as Elliptic Curve Diffie-Hellman (ECDH), RSA, Lattice-based Cryptography (LBC), and Post-Quantum Cryptography (PQC). We selected DH for its simplicity, high effectiveness, and widely standardized. Moreover, even ECDH [8] offers more efficiencies but would not offer more secure computation, while RSA [8] is used for key exchanges that lack forward secrecy. LBC [9] holds some good promises for the future, but like RSA, it is more of a classical Public Key systems certificate. On the other hand, PQC [9] is mainly to thwart attacks from a quantum computer, which is not yet widely accessible, regardless of whether it is not a key exchange mechanism, and AES-256 has so far demonstrated robustness against quantum threats. Our development work aims to make it usable on general-purpose computers. With the Gid Crypto, we would like to create a stand-alone encryption system with no certificates.

2.3 Mersenne Twister (MT)

Mersenne Twister is the most widely used pseudo-random solid numbers generator (PRNG). A version of Mersenne Twister, MT19957, can generate an extremely long sequence with a period of $2^{1,9937} - 1$ numbers before the identical series of numbers repeats [6]. If we compare MR19957 to the native Excel random number generator function, (RND), it can only generate up to 2^{24} sequences of numbers [10]. To ensure a higher level of security, it is important to consider the length of sequences. The shorter the periods of sequence, the easier the sequence can be detected and potentially reused by attackers. Therefore, we used MT as it provides a more extended period and enhances the generation of truly random numbers.

While the MT is considered the default random number generator (RNG) in Python, it does have some drawbacks, as outlined below [11] :

- If one can retrieve its previous bits, it is possible to predict the subsequent bits.
- Despite its massive size, MT may fail to meet specific statistical tests.
- It is not flexible; it follows a specific mechanism.

After conducting numerous thorough tests, studying other advancements, and using our experience to prevent the retrieval of bits by utilizing an MT random number generator, we iterate the process of generating a random number using the MT output as an input 10 times. This ensures enhanced randomness and makes it exceedingly difficult to reconstruct the original bits.

2.4 Advanced Encryption Standard (AES)

The AES is a standardized symmetric block cipher developed by the U.S. National Institute of Standards and Technology (NIST) [7]. It operates with a fixed data block size of 16 bytes, with each block being converted by using key sizes of 128, 192, or 256 bits long. After these blocks are encrypted, they are combined to form a ciphertext. Other features of AES are also concerning:

- Stronger and faster than Triple-DES
- It comes with detailed specifications and design.
- It is highly resistant to brute-force attacks, as it would take 36 quadrillion years to crack a 128-bit key [12]. Even with substantial computing power, cracking a 256-bit key would require more time.

AES encryption is widely recognized as the standard for symmetric encryption due to its fast and secure nature. It requires a 32-byte key, a 16-byte IV, and a ciphertext as input to generate the corresponding plaintext output. The encryption levels can vary from 64 to 256 bits. In our work, we employ a 256-bit key length.

2.5 Database Technology

To make it practical for users, we added a database so the different keys (private, public, and shared) could be saved, and the key exchange only had to be done once or at the users' discretion, making recurrent e-mail easier or the saving of multiple documents.

We use MongoDB as a local light and flexible database server. Moreover, PyMongo, the standard MongoDB driver library for Python, is easy to use; it offers an intuitive API and interface, as shown in Figure 2, for accessing databases, collections, and documents. It also lets administrators encrypt data in transit and data in permanent storage. Objects retrieved from MongoDB through PyMongo are compatible with dictionaries and lists, so one can easily manipulate, iterate, and print them.

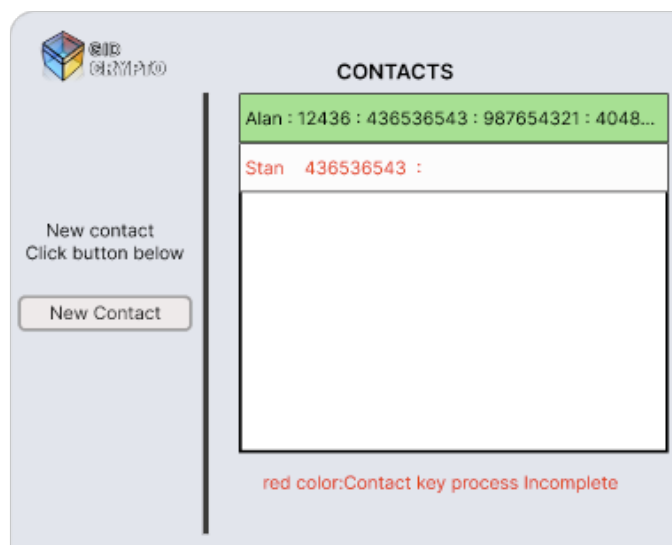


Figure 2. Contact list in MongoDB

2.6 Interface

We aimed to create an interface that is both intuitive and simple. To achieve this, we applied UX/UI technology, starting with creating a persona and an interaction design focused on simplicity of use. The Gid Crypto encrypted and decrypted program has multiple interface screens: Contacts, Role Setting, Contact Name, Keys generation, and encrypted and decrypted screens.

2.6.1 Contacts

The initial page is the Contact page, shown in Figure 2, where users can create new contacts to initiate communication. For those who have interacted previously, a window displays a list of contacts and their corresponding encrypted keys on the right-hand side.

2.6.2 Role Setting and Contact Name

If a user selects to create a new contact, the user has to determine if he is a sender or receiver. Thus, the ROLE SETTING page is utilized. Once the user selects their role, they must input the contact name for communication records, as seen in Figure 3.

Figure 3. Role Setting and Contact Name pages

2.6.3 Keys Generation

The Keys Generation page is used when creating a new contact. This page is designed to work based on the Diffie-Hellman key exchange algorithm. In this process (Figure 4), the sender, responsible for initiating the communication, selects any desired private key and clicks the 'Save' button to save it to the database. Next, the sender can generate a public key automatically by clicking the 'Get Public key' button. The next step involves the sender sending their public key to the recipient on the other side. The recipient will then follow a similar process by selecting a private key and generating their public key. The recipient will send their public key back to the sender.

To generate the shared key on the sender's side, the private key of the sender, the public key of the sender, and the public key of the recipient are used.

Figure 4. Keys Generation page

Figure 4 illustrates generating a Secret key at the bottom of the screen. To make it practically impossible to crack, we designed to have another key, the Secret key. The Secret key is generated by adding a 2-layer extension of the Diffie-Hellman key exchange. The first layer, the MT algorithm, generates random numbers, which are inputs for generating another random number for many rounds. This procedure makes it

difficult for malicious individuals to calculate back to the initial MT numbers. The second layer is used with the SHA-256 algorithm once a random number is obtained to generate the final Secret key. Hence, our developed application utilizes a variety of algorithms to achieve highly efficient message encryption. As a user, all they have to do is click the 'Create Secret Key' button, and Gid Crypto will automatically generate the Secret key based on the previously described processes. In this paper, implementation details and code samples will not be shown to keep the application secure for anyone using it.

2.6.4 Encrypted and Decrypted Interface

The encrypted and decrypted interface is designed to provide ease of use for users. To access this interface, there are two options: selecting a contact list in Figure 2 or following the steps in Figure 4 to create a new contact. Using this window is straightforward, as shown in Figure 5. Users can easily encrypt a message by typing the desired text in the left-hand text box and clicking the 'Encrypt' button. The message will be encrypted and displayed in the right-hand text box. Similarly, to decrypt a message, users can paste the encrypted text in the left-hand box and click the 'Decrypt' button, and the original message will be displayed in the right-hand box. Examples of encrypted and decrypted interfaces for text e-mail, a CSV file, and coding are displayed in Figure 5.

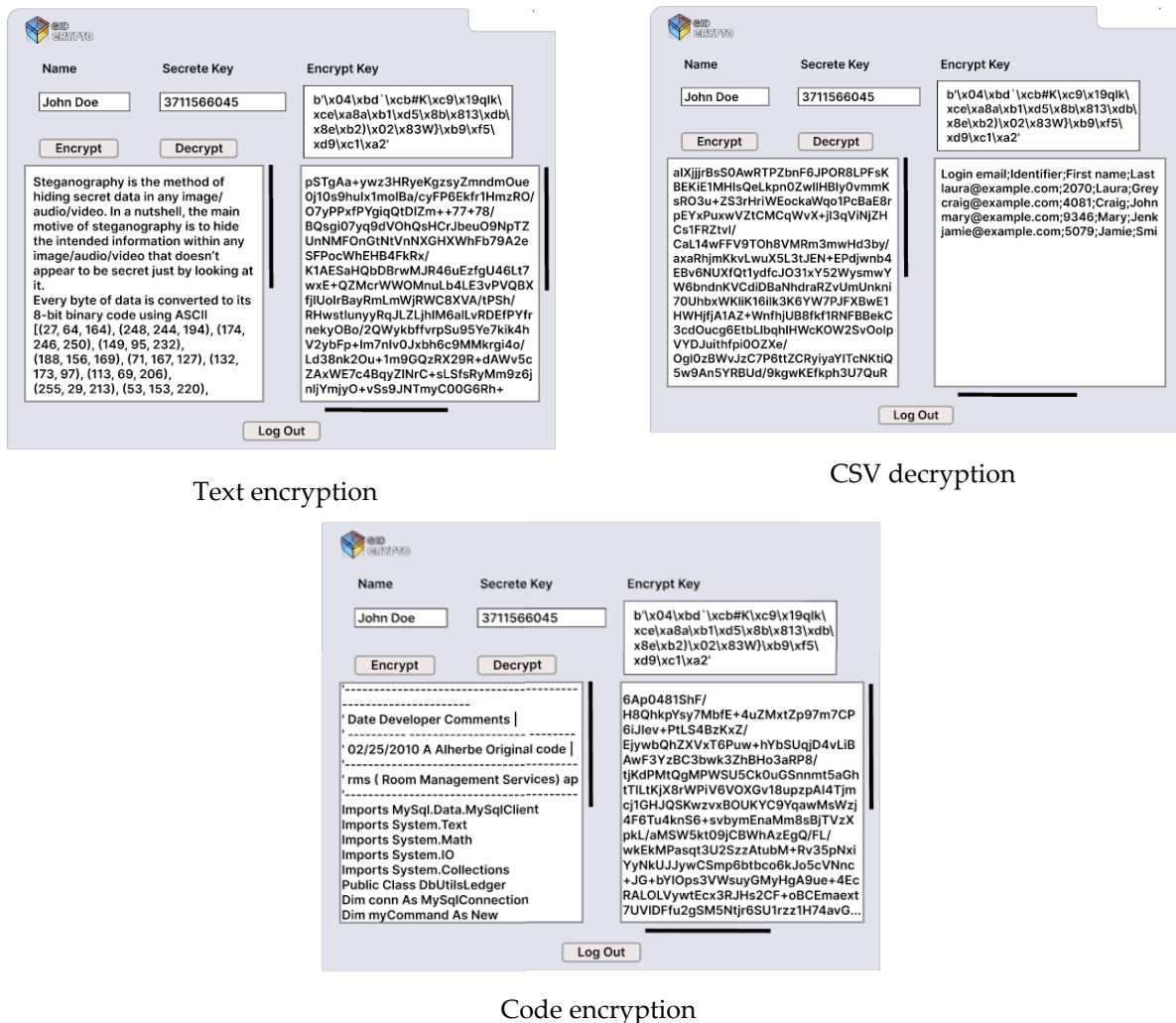


Figure 5. Encrypted and decrypted Interfaces

To use the application, if one wants to keep his e-mail message secure, he will type his message into Gid Crypto for encryption. Then, he can paste the encrypted message into his e-mail body and send it to the recipient, who can decrypt it using his version of Gid Crypto.

3. Results and Discussion

3.1 Testing: AES Block Ciphers

We need to understand that AES relies on the substitution-permutation network principle to test our encryption strength. This means it performs linked operations involving replacing and shuffling input data. To evaluate the encryption capabilities of a stream cipher, it relies on 3 main components :

- Generating greater uniqueness and sensible cryptography
- AES Information Blocks testing
- To test the encryption speed

The details of each test are as follows.

3.1.1 *Generating greater uniqueness and sensible cryptography*

To create the maximum entropy for our secret key, we employ a coding process consisting of four consecutive steps; however, the details of these steps are not provided here. This approach is essential because a possible attacker could compromise the public and shared keys. In the event of an attack, the adversary's best strategy involves attempting to guess the key via brute force, Padding attack (PA), Chosen plaintext attack (CPA), or Chosen ciphertext attack (CCA) [13-15]. For the chance of being right, it needs to compute the stream cipher, then check to see whether it produces the observed outputs, and if so, guess the next bit it produces. So, it is a lengthy and highly complex process and seems unlikely to succeed.

We apply the Mersenne Twister on the resulting secreted key for E-mail, Coding-data, and database-data as follows :

1. Text E-mail: The application was tested for descending regular text e-mails. We first exchanged our Public key, then made our Shared key, exchanged that key also, then encrypted regular text and sent it. The party receiving the e-mail on a different computer had no problem decrypting the text.

2. Coding-data: In a second test, we took code in C# and Python and did the same. We sent our encrypted code through e-mail and saved it in a directory to keep the code private.

3. Database-data: In our third test, we export data from the database/excel table and save it in "comma-separated" format, encrypted and like with code before, e-mailing it to a third party or saving it in a local directory for safekeeping.

According to our attempt to test it in a brute force attack covering 4 days, the testing yielded no success in obtaining even the first 16 bits of the key. While it remains a theoretical possibility, achieving such a feat would require an exceptionally powerful computer and extensive time and resources that were not at our disposal during the testing process.

Our application uses a 256-bit key length to encrypt and decrypt a block of messages. The process involves 14 rounds of 256-bit keys, each including processing steps that entail substitution, transposition, and mixing plaintext to transform it into ciphertext. By selecting $k = 256$, we aim to provide robust protection against potential adversaries. While standard cryptography typically opts for a key length of $k \geq 128$ for security purposes, our implementation surpasses this standard by choosing $k \geq 256$. This decision helps mitigate multi-target attacks and potential future quantum cryptanalysis, ensuring high security.

3.1.2 *AES Information Blocks*

It is important to note that our primary objective is not to safeguard a network against penetration but rather to protect the privacy of a text message. Therefore, our focus is on establishing a robust encryption key. Even if decryption were possible, the considerable time and specialized hardware required to achieve it would render the effort futile, ensuring the preservation of the message's confidentiality.

For this, we use Symmetric Encryption AES-256 to provide quick encoding or decoding operations for those who want to make an easy first choice for local or e-mail data encryption. As we mentioned above, AES is an algorithm for block encryption that is in widespread use. There are six modes of operation of the AES algorithm that were standardized and are the most well-known: ECB (Electronic Code Book), CBC (Cipher

Block Chaining), CFB (Cipher Feedback), OFB (Output Feedback), CTR (Counter), and GCM (Galois-Counter-Mode).

We evaluated those 6 encryption modes to determine the most suitable option based on the level of security provided. Each mode offers a different level of security, so we examined the data from each mode to make our decision. CTR and GCM stood out among the modes considered since AES-GCM is a well-known and documented process. The GCM utilizes symmetric block encryption with CTR as the underlying cipher mode. It also integrates authentication to protect the cipher, eliminating the need for separate integrity measures and significantly enhancing encryption efficiency and security. While the time difference between the two modes was minimal, we ultimately chose GCM due to its stronger security capabilities. Using GCM, we could measure the time it takes to encrypt and decrypt data in LabVIEW [16].

3.1.3 Encryption speed

We used LabVIEW [16], an application for measurement, control, and testing systems, to test our encryption speed (as depicted in Figure 6). This testing aims to confirm that encryption of lengthy text can be completed in a reasonable amount of time. Table 1 shows our testing speed, as demonstrated by various examples. Those examples have been chosen to illustrate various approaches for testing text e-mail, CSV, and source code files.

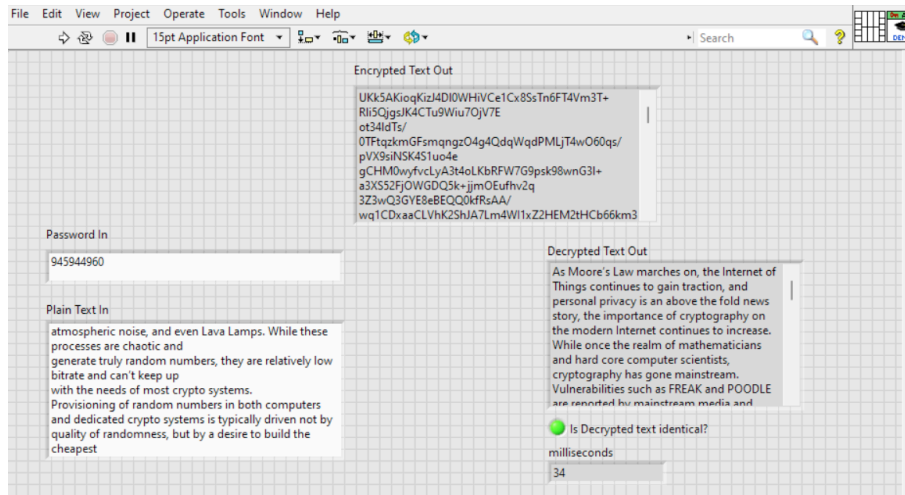


Figure 6. LabVIEW module for test speed: Mode-GCM/e-mail: text of 1945 characters with the encrypt and decrypt speed of 34 milliseconds

Table 1. Testing speed

Clear Text	Length (char)	Encrypted text	Length (char)	Encryption/Decryption Time (ms.)	Mode
A stream cipher—a deterministic mathematical function—is considered secure if an adversary who does not know the k-bit key is chosen uniformly at random and can only ...	425	pRvh7gqfHbrQTl1Qz/sVk7Og7PZ7 RKN//jBw2zIPUP2H1Q8DES2qhio Lg+e/mfpdfD6hvhtCz3YqIN4/TMz Bk9kbMhl0kQS/RjY9wF502iH3xI3 YZ/zDan2YHh2k3MAK3IEVpOYu bR4x1ZZQAFAPhLe7zkf4aZwZ8Nj k7Z3mFQUtqjhTXNgSzaGDY4JFG zYyWdTu...	1088	3 ms. 5 ms.	GCM/e-mail: text

Clear Text	Length (char)	Encrypted text	Length (char)	Encryption/Decryption Time (ms.)	Mode
As Moore's Law marches on, the Internet of Things continues to gain traction, and personal privacy is an above-the-fold news story, the importance of cryptography...	1946	E51Lv/WFLiFOi3KpBzdLXp5q+h0vG578z3asuLAW9jgYcBYzbHICQZrKgoems7ssgo/zf0z9+VnOaD2f9N4G/4WKxjLyhzce1j7Ao9V5Fbuau9fjcfQUjgBJr0KwL87hFULo0jhohqR1FuDv9xrEmdmUhW1eynz2BldJsXl6KF ...	4748	15 ms. 21 ms.	GCM/ mail: text
spinoza-francis.net,2020-08-26,http://www.escobar.org/2,10dAcafEBbA5FcA,Kristina,Ferrell,"Horn, Shepard and Watson",Aaronville,Andorra,932-062-1802,(209)172-7124x3651,xreese@hall-donovan.com,2020-04-27,https://tyler-pugh.info/3,67DAB15Ebe4BE4a,Briana,Andersen,Irwin-Oneal,East Jordan,Nepal,8352752061,(567)135-1918,haleybraun@blevins-sexton.com,2022-03-...	169994 7	wXNMWiGpjIdI2c0ah5hm3ClO6ZHioo7dt2v3GCycqez49tEldm8X6MazuDoh0kjoRfUMLpfuXu2aPS/2cqDBkzf69p+TiaOXMKt1WWK15LQYtyjTmsV8dx5jTeLcCbG9YWCVM6x3L19IzUd0EqeUVr2S61gnXItemJadnlEubmRETD58sJRADLPY2ZvkVuEqEnNdmYE4Gd3ay+cU//1WJJGR21sNBKGxD/12WmgIRVDsXSWQmSispMuLz6igw7rQ0+myxNhpOaf5QcCYmeWgUO3nDILL4CqgLkqAHB7OnUI8J/HBPP97rFYrU8OfXAmTQ/4gA+E+tItY02vXpwagcCmflotAzbn5HH5RVsD3zzI24rCGBF7bc+PqNntjfE46Y+XVLLpswjoJgyvHfiD+ ...	405327 2	117 ms. 161 ms.	GCM/ CSV: text
'----- ' Date Developer Comments '----- ----- ' 02/25/2010 A Alherbe Original code '----- ----- ' rms (Room Management Services) application/web service '----- Imports MySQL.Data.MySqlClient Imports System.Text Imports System.Math Imports System.IO Imports System.Collections Public Class DbUtilsLedger Dim conn As MySQLConnection ...	7334	6Ap0481ShF/H8QhkpYsy7MbfE+4uZMxtZp97m7CP6ijIev+PtLS4BzKxZ/EjywbQhZXVxT6Puw+hYbSUqjD4vLiBAwF3YzBC3bwk3ZhBHo3aRP8/tjKdPMtQgMPWSU5Ck0uGSn nmt5aGhtTILtKjX8rWpIv6VOXGv18upzpAI4Tjmcj1GHJQSKwzvxBOKYCY9YqawMsWzj4F6Tu4knS6+svbymEnaMm8sBjTVzXpkl/aMSW5kt09jCBWhAzEgQ/FL/wkEkMPasqt3U2SzzAtubM+Rv35pNxiYyNkUJJywCSmp6btbco6kJo5cVNnc+JG+bYIOps3VWsuYGMMyHgA9ue+EcRALOLVywtEc3RJHs2CF+oBC Emaext7UVIDFfu2gSM5Ntjr6SU1rzz1H74avGP96Grd61H7v24umKCZBs/SqKjFy5WlijsyEmXg+WlmnVuXpkj7xvQgcRjyz3hFDsGYUNYu dY0HPiUrPp6e+DBFejg06l2UOkHxlyceplSyCH6yW7T1x7HOJ9cCNPcalsjZx0nji5QkpD3CJsXgeZ1s/7DVEf0MLPvX1UidjWOzDuCFNVTTUu7cUPVJyzv6q53/OlcoQu+htp9GC+Ne08Pv7BDUS ...	18108	53 ms. 73 ms.	GCM/ code: text

AES-256 GCM was tested versus CTR, as we expected GCM to require slightly more processing times (0.059896 milliseconds) than Mode CTR because of its key-chaining nature.

We test 2 factors: the first is the issuing of the shared key and the second is the text encryption. Testing was done with the keys' bit length with a system running 16 GB RAM and Intel core I5. A private (secret) different key length from 4 to 10 digits, with a public key length from 8 to 16 digits. The bigger the private and public keys, the longer the Shared key calculation time.

For the best results, see Figure 7. Testing has shown that a 6-digit private key and 16-digit public key offered the best security versus functionality and speed (less than 1 second to create a 16-bit share key). The best results were obtained with a 4-digit to 6-digit private key and 2 full 64-bit public keys.

My private Key	Primary (The sender Public Key)	My Share Key	
1234567	45582810984602531		Make Share Key
	Secondary (The receiver Public Key)	Secondary(receiver) Share Key	
Get Public Key	40560104219817839	26205624126592645	Make Secret Key

Figure 7. 64-Bits Shared key

3.2 Related work

Our work proposed Gid Crypto, a stand-alone encryption end decrypt application that runs independently of network connectivity. The systems that operate similarly to Gid Crypto are rarely found. Most available systems utilize certificates, a feature that Gid Crypto does not employ. Other applications that work on cloud platforms or utilize key servers are as follows.

Microsoft Outlook [17] and Yahoo [18] are examples of services that use encryption in transit, which means they protect the message only while in transit and cannot guarantee that it stays encrypted after the messages reach the recipients. However, Microsoft 365 [19] provides options that use OME, IRM, and S/MIME technology for users to set up e-mail encryption communication.

There are commercial tools that provide end-to-end encryption, such as Posteo [20], Tutanota [21], and Lavabit [22]. Those e-mail providers generate closed platforms where the services handle key management on their servers. Only users using the same platform can encrypt the messages to each other. To use their services, one needs to register on their domains. Posteo has a trial account and later enforces an extra monthly charge if users prefer additional storage space. Tutanota provides a free account for 1GB storage with basic private communication. If users prefer multi-user support options, they must pay for a business account, while Lavabit does not have a free trial account.

Trustifi [23] is cloud-based end-to-end security; it uses 256-bit AES encryption as our work. The same as Posteo and Tutanota, it requires users to register on the system to use the service on their platform; both senders and recipients must be members of Trustifi to communicate with each other; otherwise, the sender must issue an advanced method on how to secure the sending message, for example, setting up a password or phone number; yet merely 10 countries are covered. Trustifi service charges vary depending on the number of users and the size of the organization.

Privilege [24] is an encrypted file-sharing and e-mail application. For e-mail, after Preveil is installed, it creates a set of mailboxes for encrypted messages stored on PrevVeil's server. It can be used with Gmail and Outlook e-mails. If a PreVeil user sends an e-mail to another PreVile member, the message will be automatically encrypted; if the recipient is not a PreVail user, the message will be sent as regular mail or selected to be sent encrypted, then the recipient will be invited to join PreViel. It is free for basic features usage. For a business/professional level, a monthly payment is required. Using PreVeil, one needs to have an e-mail account while our work is free from applying for an account.

Signal [25] is a free encrypted application for private messaging on Android and iOS mobile and Desktop. However, to use Signal on a desktop, one must first install it on his mobile phone. Signal supports secure conversation, shared photos, and video calls.

Work by (Livingston et al. [26]) also has a class of encryption that provides a client-side encrypt-on-receipt mechanism. Still, as we learn from Snowden [27], most of the work now is done at the server level or by infiltration or official request, as it was done with "Silent Mail" whereby the data is checked as soon as it reaches the Imap server, and before encryption whatever you are sending or receiving mail. In the case of receiving, the user receives the ciphertext, the key decrypts it, and the spy software reads it. Whether working for the government or not, a good hacker can infiltrate a mail server. This type of encryption will protect your data during transport but will not offer the complete security of someone with sensitive data.

4. Conclusions

As our world becomes increasingly digital, the importance of privacy and security has grown significantly. Communication has been one very important facet of coping with the challenges induced by societal digitization. We need a multidisciplinary approach to develop the necessary tools for communication. It is crucial to balance usability and security, so Gid Crypto was designed with these considerations in mind. We aimed to make the application as secure as possible while being user-friendly and easy to navigate. Thus, Gid Crypto was designed to encrypt e-mail messages, text files in .doc or .docx, and CSV file formats. We also must remember that we live in a world of constant evolution where progress is advancing rapidly. So, Gid Crypto was created with a flexible architecture that allows updates and upgrades.

Gid Crypto is a compact yet potent application explicitly designed for users seeking absolute control over their data encryption process. It stands apart from other e-mail encryption systems, which sometimes have potential backdoors compromising security. Gid Crypto guarantees no such vulnerabilities exist, offering users peace of mind. It is an ideal choice for ensuring the seamless operation and enhanced security of a Silent Mail system. With its advanced encryption algorithms and robust functionality, Gid Crypto is exceptionally well-suited for safeguarding the privacy and security of sensitive data. It provides a reliable solution to complete a Silent Mail system and ensure the secure exchange of information.

We understand that our current work has limitations, particularly in terms of the accessibility of data that needs to be encrypted and the evolving field of cryptanalysis. To overcome these limitations, our goal is to enhance our work by introducing a function that enables the direct importation of file formats such as .docx, .pdf, and excel into the application. Additionally, the current version of our work does not negotiate any communication channel, but we are considering implementing this in future performance.

Currently, our main focus is creating a new method for enhancing security by using the distinct randomness present in images. By utilizing parallel processing and an efficient randomness extractor, images can exhibit a high level of randomness. Our ultimate aim is to create a complete and extremely secure cryptographic system that can be used to protect data.

5. Acknowledgements

Author Contributions: Conceptualization T.A.; methodology T.A.; software A.J. and T.A.; validation A.J. and T.A.; formal analysis T.A.; writing-original draft preparation A.J. and T.A.; writing-review and editing A.J. and T.A.; visualization T.A.

Funding: This research received no external funding.

Conflicts of Interest: The authors declare no conflict of interest.

References

- [1] cloudHQ. (2021, April 6). 50 Years of E-mail. *CISION*. <https://www.prnewswire.com/news-releases/50-years-of-email-301262676.html>

- [2] Radicaati Team (2021, February 22). E-mail Statistics Report, 2021-2025. *Statista Radicati*, <https://www.radicati.com/?p=17209>
- [3] Ghali, C.; Stubblefield, A.; Knapp, E.; Li, J.; Schmidt, B.; Boeuf, J. (2017, December 27), Application Layer Transport Security, *Google Cloud whitepaper*. <https://cloud.google.com/docs/security/encryption-in-transit/application-layer-transport-security>
- [4] Nohe, P. (2018, October 15), Apple, Microsoft, Google Announce Plans to Disable TLS 1.0, TLS 1.1. *hashedout*. <https://www.thesslstore.com/blog/apple-microsoft-google-disable-tls-1-0-tls-1-1/>
- [5] Just, M. Diffie-Hellman Key Agreement. In Van Tilborg H.C.A. (Eds.), *Encyclopedia of Cryptography and Security* (pp. 154-163). Springer. 2005. https://www.academia.edu/63723313/Springer_Encyclopedia_of_Cryptography_and_Security
- [6] Jagannatham, A. (2008), *Mersenne Twister – A Pseudo Random Number Generator and its Variants*. [Technical report, Department of Electrical Computer Engineering, George Mason University].
- [7] Kak, A. *Lecture 8: AES: The Advanced Encryption Standard*, Lecture Notes on Computer and Network Security, Purdue University. 2020. <https://engineering.purdue.edu/kak/compsec/NewLectures/Lecture8.pdf>
- [8] O S. N.; Vankamanidi S. N. Comparative Analysis of MOD-ECDH Algorithm and Various Algorithms. *Journal of Industrial Engineering & Production Research*. 2020, 31(2), 302-308. <https://doi.org/10.22068/ijiepr.31.2.301>
- [9] Hamid N.; Nikil D.; Sandip R.; Francesco R.; Indranil B.; Rosario C. Post-quantum Lattice-based Cryptography Implementations: A Survey. *ACM Computing Surveys*. 2019, 51(6), 1-41. <https://doi.org/10.1145/3292548>
- [10] Tain, X.; Benkrid, K. (2009, July 29 – August 1). *Mersenne Twister random number generation on FPGA, CPU and GPU NASA/ESA* [Conference session]. 2009 Conference on Adaptive Hardware and System, San Francisco, CA, United States. <https://ieeexplore.ieee.org/document/5325420>
- [11] Vigna, S. (2019, November 14). Is it high time we let go of the Mersenne Twister. *Arxiv*. <https://arxiv.org/pdf/1910.06437.pdf>
- [12] Rimkienė, R. (2022, August 29), What is AES encryption and how does it work?. *Cybernews*, <https://cybernews.com/resources/what-is-aes-encryption/>
- [13] Schwenk, J. *Guide to Internet Cryptography: Security Protocols and Real-World Attack Implications*. Springer. 2022. <https://link.springer.com/book/10.1007/978-3-031-19439-9>
- [14] Kiltz, E., O'Neill A.; Smith, A. Instantiability of RSA_OAEP Under Chosen-Plaintext Attacj. *Journal of Cryptology*. 2017, 30(1), 889-919. <https://doi.org/10.1007/s00145-016-9238-4>
- [15] Huang, Z.; Liu, S.; Qin, B. Sender Equivocal Encryption Schemes Secure against Chosen-Ciphertext Attacks Revisited. *Journal of Applied Mathematics and Computer Science*. 2015. 25(2), 369-389. https://doi.org/10.1007/978-3-642-36362-7_23
- [16] Latif, I. H. (2021, August 14). *Time Evaluation Of Different Cryptography Algorithms Using Labview* [Conference session]. The 4th Postgraduate Engineering Conference in Materials Science and Engineering, Baghdad, Iraq. <https://iopscience.iop.org/article/10.1088/1757-899X/745/1/012039>
- [17] Microsoft (2023, July 31). Preparing for TLS 1.2 in Office 365 and Office 365 GCC. *Microsoft*, <https://docs.microsoft.com/en-us/microsoft-365/compliance/prepare-tls-1.2-in-office-365?view=o365-worldwide>
- [18] Egress (2021, January 17). How to encrypt Outlook e-mails in transit. *egress*. <https://www.egress.com/blog/email-encryption/encrypt-outlook-emails-in-transit>
- [19] Microsoft 365 (2023, August 8), E-mail encryption. *Microsoft*, <https://docs.microsoft.com/en-us/microsoft-365/compliance/email-encryption?view=o365-worldwide>
- [20] Posteo (2021, December 12). POSTEO: E-mail, calendar, address, book, notes. *POSTEO*. <https://posteo.de/en>
- [21] Tutanota (2022, March 25). Tutanota Secure e-mail for everybody. *Tutanota*. <https://tutanota.com/>
- [22] Lalabit (2022, June 10). Secure e-mail for the world. *Lavabit*. 2022. <https://lavabit.com/>
- [23] Trustifi, (2022, October 7). Trustifi E-mail Security that is Easy to Deploy, Manage, and Use. *Trustifi*. <https://trustifi.com/>
- [24] Preveil, (2022, August 19). Preveil Simple Secure Compliment. *Preveil*. <https://www.preveil.com/>

- [25] Signal, (2022, February 26). Speak Freely. *Signal*. <https://signal.org/en/>
- [26] Livingston, J. D.; Kirubakarn, E.; Johnraja, J. I (2021, August 4). *Implementing Client-Side Encryption for Enforcing Data Privacy on the Web Using Symmetric Cryptography: A Research Paper* [Conference session]. Third International Conference on Information Management and Machine Intelligence, Singapore. https://link.springer.com/chapter/10.1007/978-981-19-2065-3_2
- [27] Moon, M. E.; Colonel, M. E. How America Lost its Secrets: Edward Snowden, The Man and The Thief By Edward Jay Epstein New York, N.Y.; Alfred A. Knopf. *Journal of Strategic Security*. 2017, 10(1), 143-147. <https://www.jstor.org/stable/26466898>



Effect of Chlorine Dioxide on Micropropagation of *Gymnocalycium mihanovichii* LB2178 Agua Dulce (Cactaceae)

Phakarat Rotduang¹, Supawadee Ramasoot^{2*} and Tassanee Khawniam³

¹ Department of Creative Innovation in Science and Technology, Faculty of Science and Technology, Nakhon Si Thammarat Rajabhat University, Nakhon Si Thammarat, 80280, Thailand; phakarat_rot@nstru.ac.th

² Department of Biology, Faculty of Science and Technology, Nakhon Si Thammarat Rajabhat University, Nakhon Si Thammarat, 80280, Thailand; supawadee_ram@nstru.ac.th

³ Department of Agricultural Innovation and Management Division, Faculty of Natural Resources, Prince of Songkla University, Songkhla, 90110, Thailand; tassanee.kh@psu.ac.th

* Correspondence: supawadee_ram@nstru.ac.th

Citation:

Rotduang, P.; Ramasoot, S.; Khawniam, T. Effect of Chlorine Dioxide on Micropropagation of *Gymnocalycium mihanovichii* LB2178 Agua Dulce (Cactaceae). *ASEAN J. Sci. Tech. Report.* **2024**, 27(2), 103-111. <https://doi.org/10.55164/ajstr.v27i2.252123>.

Article history:

Received: December 19, 2023

Revised: February 27, 2024

Accepted: March 1, 2024

Available online: March 6, 2024

Publisher's Note:

This article is published and distributed under the terms of the Thaksin University.

Abstract: *Gymnocalycium mihanovichii* LB2178 Agua Dulce is a succulent species popular in many areas. It has been cultivated for a long time. It is considered one of the easiest cacti to grow in Thailand. Therefore, the objective of this study was 1) to study the effect of Chlorine dioxide (ClO₂) on culture medium sterilization on micropropagation of *G. mihanovichii* LB2178 Agua Dulce. and 2) to study the effect of Chlorine dioxide on shoot and root induction of *G. mihanovichii* LB2178 Agua Dulce. The *G. mihanovichii* LB2178 Agua Dulce seeds were used as plant material. After 2 months of culture, the results showed that MS medium supplemented with 50 ppm ClO₂ gave the highest survival rate at 54.17%. After 3 months of culture, the results showed that shoot and root induction can be achieved in *G. mihanovichii* LB2178 Agua Dulce seeds were cultured on MS medium supplemented with 50 ppm ClO₂ gave the highest number of roots at 9.00 roots/explant, length of root 3.45 cm, length of shoot 0.54 cm and diameter of shoot 0.44 cm.

Keywords: *Gymnocalycium mihanovichii* LB2178 Agua Dulce; Chlorine dioxide; *in vitro*

1. Introduction

Cactus is a plant in the family Cactaceae (*Mila* sp.) and is a native plant that originates in the desert. It is a plant with a strange stem shape and is different from other plants in that the stems of almost all varieties are leafless. The trunk has a wax coating to reduce dehydration on the trunk surface. The stem has green chlorophyll, which performs photosynthesis instead of leaves [1]. A study report from The Global Succulent & Cactus Plants Market Report 2021 revealed that the cactus and succulent plant market will have an average overall growth of 16.8% per year for over 6 years until 2027. Many species of cactus grow only in certain areas. It tends to grow slowly, making it popular among people who love cacti and collectors especially interested in rare plant species [2].

In Thailand, *Gymnocalycium* cacti are popularly called "Gymno". There are many species, but *G. mihanovichii* LB2178 Agua Dulce is a popular species to



grow. It is the cactus species *G. mihanovichii* LB2178 Agua Dulce. The code LB2178 is the code that a Dutch botanist, an expert in this genus named Mr. C.A. Ludwig Bercht, found and collected samples from its origins in the Agua Dulce area, Alto Province, Paraguay, since 2000. It has a round stem. The number of lobes in LB2178 usually ranges from 9 up to 13 lobes. The ridges are thin. The next distinctive feature is the surface. You will see a green pattern alternating with dark green or black. It will look slightly raised. This pattern is called the "chevron" or bone pattern. The more frequent the chevrons, the more beautiful they look, and the price will be higher. Because it is easy to grow and beautiful, *G. mihanovichii* LB2178 Agua Dulce is a popular cactus. It has been cultivated for a long time. It is considered one of the cacti that are easy to grow in Thailand, and it is also a type that is popular worldwide. Furthermore, some types are popular and have a higher price than normal [3].

This genus of cacti has been cultivated and bred for a long time, resulting in hybrids that are different from the original, such as the spotted gymnosperm or some with longer and larger thorns resistant to hot weather. In addition, the cactus species *G. mihanovichii* LB2178 Agua Dulce is also in demand in the market because it is a beautiful ornamental plant. It can be propagated by separating shoots, or if you want a large number, you must use seeds. This takes approximately 1-3 months, causing delayed propagation and easy diseases such as fungal diseases. This is usually found during the rainy season due to the humid air of cacti that have been cultivated and bred for a long time, resulting in hybrids that are different from the original, such as the spotted gymnosperm, or some with longer and larger thorns that are resistant to hot weather [4]. This results in the death of the cacti, and there is not enough for commercial production. Plant tissue culture techniques have been introduced to help increase the number of plants to a large quantity in a short period. It can also be applied in plant breeding to propagate plants commercially. Studies have shown that plant cell culture is a process of growing cells under sterile conditions, reducing the time needed to produce new plants and creating new characteristics in the plant cells we want to culture through induced mutations [5]. Tissue culture can quickly increase the number of plants in large quantities. Techniques for sterilizing culture media are an important step that affects the success of plant tissue culture. An autoclave is a standard method for sterilizing media preparation before plant parts are placed in the culture. This requires expensive equipment and electricity for sterilization. Chemical methods, such as adding silver nanoparticles, can synthesize options for making media sterile. This may involve using toxic chemicals in the synthetic process and be expensive [6]. And the addition of Chlorine dioxide (ClO_2), a synthetic chemical that can eliminate bacteria, fungi, and viruses. It is effective in a wide pH-alkaline range from 3.0 to 9.0, resulting in a high sterility percentage. Does not react with organic substances. Able to remove contaminants well, even with low concentrations. Moreover, it saves time. The preparation method is not difficult and provides better efficiency in developing new plants than sterilization with a steam autoclave [7]. There are reports of using ClO_2 for plant tissue culture, such as Krajoed culture, by adding ClO_2 at a concentration of 25 mg/l in the culture medium to create sterile conditions for cultivating krajoed in a bioreactor, immersion, and aeration system [8]. To test the chemical sterilization of culture medium using ClO_2 for *in vitro* gerbera cultivation. ClO_2 could replace autoclaving with the production of a sterilized culture medium without phytotoxic problems to Gerbera *in vitro* cultivation [9]. In addition, it has been reported that ClO_2 is used to sterilize the medium for potato tissue culture. To identify alternative methods of sterilizing culture conditions, the disinfection effects of ClO_2 at 88.0, 29.3, 17.6, 12.6, and 8.8 μM were evaluated in potato medium and vessels. The potato seedlings had similar morphological features as those grown on autoclaved medium, with some exceptions. [10]

Currently, there are studies on the tissue culture of cactus seeds of various species, resulting in large quantities of plants quickly. Healthy seedlings with healthy shoots and roots will increase their survival rate after being removed from sterile conditions. Using tissue culture technology increases the potential for development in breeding, resulting in a new species of cactus reducing the removal of plants from their natural state. Currently, there are no reports of using ClO_2 in cacti tissue culture in sterile conditions. Therefore, this research studied the effect of ClO_2 on the sterilization of culture media and the effect of ClO_2 on the induction of shoots and roots of the cactus strain *G. mihanovichii* LB2178 under sterile conditions. As an alternative to solving the problem of microbial contamination in tissue culture, it helps increase work speed by reducing steps in preparing synthetic food instead of using an autoclave.

2. Materials and Methods

2.1 Plant materials

After pollination, a planted parent plant, *G. mihanovichii* LB2178 Agua Dulce seed pieces, was extracted from the pods and immersed in distilled water to select and discard floating seeds. The seeds were wrapped in nylon cloth and tied tightly with sewing thread. After that, they were soaked in 70% alcohol for 30 seconds and then dipped in a 20% sodium hypochlorite (Chlorox) solution for 20 minutes. I added 2 drops of Tween 20 and rinsed it with distilled water sterile. Three times in an aseptic environment with a laminar flow cabinet.

2.2 Effect of Chlorine dioxide (ClO₂) on *G. mihanovichii* LB2178 Agua Dulce micropropagation through culture medium sterilization

The seeds of *G. mihanovichii* LB 2178 Agua Dulce were cultured on autoclaved Murashige and Skoog (1962) [11] (MS) free medium at 1.05 kg/cm², 121°C for 15 min and MS medium supplemented with 0, 10, 25, 50, 75 and 100 ppm ClO₂. All culture mediums were supplemented with 30 g/l of sucrose and 8 g/l of agar. The pH was adjusted to 5.7. The culture was kept in 3000 lux light-intensity for 14 hours per day at 25±2 °C and subcultured every 4 weeks on the same medium component for 3 months. The percentage of contamination of the culture medium, percentage of contamination over a four week, and percentage of survival rate were recorded. The germination was evaluated daily for 20 days after the first seed germinated, considering the emission of radicle as evidence of germination. The variables used in the analysis were germination (%G), mean germination time (MGT), and germination speed index (GSI) [12]. The experiment design was completely randomized design (CRD), and the mean differences were compared using Duncan's multiple range test (DMRT).

mean germination time (MGT)

$$MGT = (\sum n_i t_i) / \sum n_i \quad (1)$$

Where n_i = number of seeds that germinated in a day "i," and t_i = day "i" in evaluated time

germination speed index (GSI)

$$GSI = \sum (n_i / t_i) \quad (2)$$

where n_i = number of seeds that germinated in day "i" t_i = day "i" in evaluated time

2.3 Effect of Chlorine dioxide on proliferation and induction of shoot and root of *G. mihanovichii* LB2178 Agua Dulce

The shoots of *G. mihanovichii* LB 2178 Agua Dulce derived from previous experiments were tested. They were cultured on autoclaved MS-free medium at 1.05 kg/cm², 121 °C for 15 min and MS medium supplemented with 0, 10, 25, 50, 75 and 100 ppm ClO₂. All culture media were supplemented with 30 g/l of sucrose and 8 g/l of agar. The pH was adjusted to 5.7. The culture was placed in 3,000 lux light-intensity for 14 hours per day at 25±2 °C and subcultured every 4 weeks on the same medium component for 3 months. The number of roots, root length, shoot length, and shoot diameter were recorded. The experiment design was planned using a completely randomized design (CRD), and the mean differences were compared using Duncan's multiple range test (DMRT).

2.4 Statistical analysis

A completely randomized design with 3 replicates (each with 10 explants) was performed for experimental design and statistical analysis. Data was analyzed using ANOVA.

3. Results and Discussion

3.1. Effect of Chlorine dioxide on *G. mihanovichii* LB2178 Agua Dulce micropropagation through culture medium sterilization

The seeds were cultured on autoclaved MS-free medium and MS medium supplemented with various concentrations of ClO₂. The result found that MS medium supplemented with 0 and 10 ppm ClO₂ gave the highest percentage of contamination, 100 %, followed by MS medium supplemented with 25, 50, and 75 ppm ClO₂, 70.17%, 55.83%, and 45.83%, respectively. Autoclaved MS medium and MS medium supplemented with 100 ppm ClO₂ gave the same percentage of contamination, 0.00 %, significant difference at $p \leq 0.05$. For the percentage of survival rate, the result found that seeds of *G. mihanovichii* LB 2178 Agua Dulce were cultured on MS medium supplemented with 50 ppm ClO₂ gave the best survival rate at 54.17 %, followed by MS medium supplemented with 75 ppm ClO₂ and autoclaved MS medium, 32.50% and 21.26% respectively, significant difference at $p \leq 0.05$. (Table 1 and Figure 1)

This study found that high concentrations of ClO₂ were effective in killing a germ both in seeds of *G. mihanovichii* LB 2178 Agua Dulce and culture media. Still, low concentrations of ClO₂ were not able to control contamination. According to reports, using an Oreactor system and 100 parts per million ClO₂ effectively eliminated fungal contamination in Phulae pineapple cultivation. However, high levels of ClO₂ cause the growth of Phulae pineapple to stop in the early stages and improve growth. After culturing for 2 months, ClO₂ has been reported to be used in the culture of other plants [13], such as using ClO₂ to sterilize the medium for potato tissue culture. To substitute techniques for disinfecting culture conditions, the disinfection effects of ClO₂ at 88.0, 29.3, 17.6, 12.6, and 8.8 μM were evaluated in potato medium and vessels. During a 30-minute fumigation process, the $\geq 12.6 \mu\text{M}$ gaseous ClO₂ efficiently disinfected the vessel, and its aqueous solution similarly effectively disinfected the potato medium. In the presence of 12.6 μM ClO₂ in the medium, with a few exceptions, the potato seedlings' morphological characteristics were comparable to those of those grown on autoclaved medium [14]. Comparing media sterilized by autoclave to media sterilized with ClO₂ for Gerbera tissue culture is consistent with this finding. It was found that Gerbera grew better in the killed media sterilized with ClO₂. It also grows better than those grown on media sterilized media using an autoclave. ClO₂ is effective in killing bacteria, fungi, and viruses. It is stable in solutions with a pH of 3.0-9.0. Moreover, sterilizing media with ClO₂ is not easy. Fortunately, there is no need to use the autoclave method, which necessitates costly instruments and electrical power [15]. Additionally, it states that ClO₂ is a gas that dissolves in water and does not react with it. Effective in killing microorganisms even when used in small amounts. and does not create chloramine, which is toxic to animals. This research found that there was no statistically significant difference in the fresh weight of seedlings grown on autoclaved media and media supplemented with ClO₂. It demonstrates that, in sterile conditions, Black Miracle Nepenthes seedlings are not toxically affected by low concentrations of ClO₂. Additionally, it was discovered that there was no difference in the growth outcomes of seedlings grown on autoclaved media and media supplemented with 5 ppm ClO₂. Although the mode of action of Chlorine in microorganisms is not fully elucidated, the ClO₂ acts by destroying cell membranes and oxidizing intracellular components of microorganisms [16]. Tested ClO₂ and liquid Chlorine in water and demonstrated that ClO₂ killed several types of bacteria more effectively than liquid Chlorine and is superior to Chlorine against spore-forming bacteria; thus, they concluded that ClO₂ was a safe and effective alternative disinfectant for the treatment of water. ClO₂ acts by transferring electrons; it penetrates the cell wall easily, dehydrating and destroying the cell membrane and finally oxidizing the intracellular components of both Gram-positive and Gram-negative microorganisms [17]. The polar nature of ClO₂ contributes to its sanitizing and sporicidal action due to its higher solubility in complex organic molecules such as the components of most viruses and bacteria [18].

Table 1. The percentage of contamination and survival rate of *G. mihanovichii* LB2178 Agua Dulce was cultured on an autoclaved culture medium and sterilized with different concentrations of Chlorine dioxide

Chlorine dioxide (ppm)	Contamination (%)		Contamination (%)				Survival rate (%)
	With explants	Without explants	1 week	2 weeks	3 weeks	4 weeks	
sterilized	0.00 ^d	0.00	0.00 ^b	40.00 ^b	0.00 ^d	0.00 ^b	21.26 ^b
0	100.00 ^a	0.00	100.00 ^a	100.00 ^a	100.00 ^a	100.00 ^a	0.00 ^c
10	100.00 ^a	0.00	100.00 ^a	100.00 ^a	100.00 ^a	100.00 ^a	0.00 ^c
25	70.17 ^b	0.00	0.00 ^b	14.17 ^c	0.00 ^d	0.00 ^b	0.00 ^c
50	55.83 ^c	0.00	0.00 ^b	0.00 ^d	25.00 ^b	0.00 ^b	54.17 ^a
75	45.83 ^c	0.00	0.00 ^b	0.00 ^d	15.83 ^{bc}	0.00 ^b	32.50 ^b
100	0.00 ^d	0.00	0.00 ^b	0.00 ^d	11.67 ^c	0.00 ^b	0.00 ^c
F-test	*	-	*	*	*	*	*
C.V.(%)	0.45	-	0.63	0.57	0.59	0.63	1.53

* = significant difference at $p \leq 0.05$

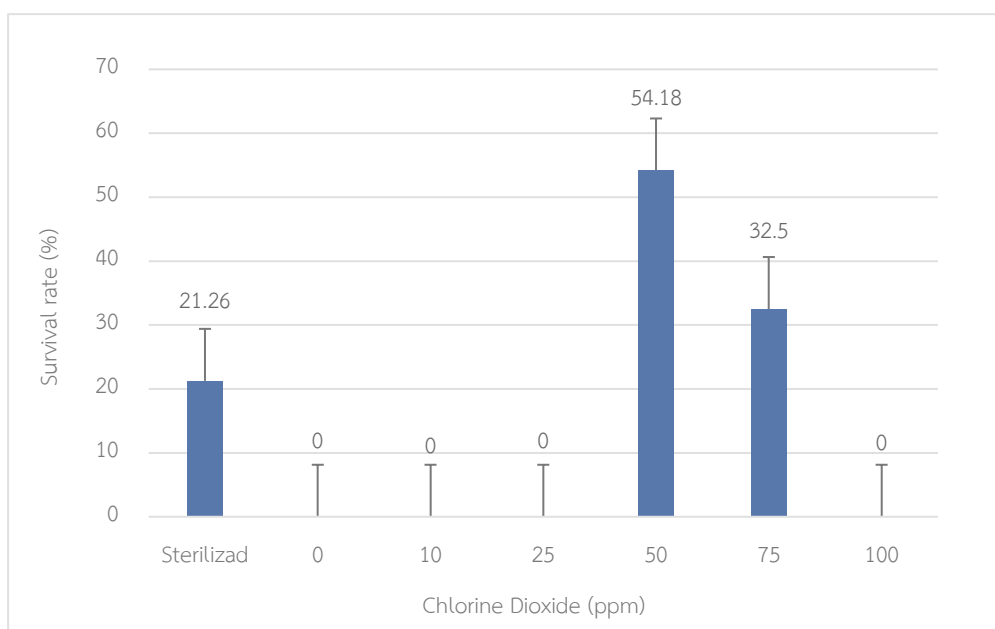


Figure 1. Survival rate formation of *G. mihanovichii* LB2178 Agua Dulce was cultured autoclaved or sterilized with different concentrations of Chlorine dioxide

The initial germination of *G. mihanovichii* LB 2178 Agua Dulce was observed 20 days following the experiment. The different concentrations of ClO₂ interfered in germination for each variable under study, and there was interaction between mediums in the evaluated variables. It was found that *G. mihanovichii* LB 2178 Agua Dulce seeds germination on MS medium supplemented with 50 ppm ClO₂ gave the highest germination at 61.67 %. Regarding *G. mihanovichii* LB 2178 Agua Dulce's germination time, the result found that *G. mihanovichii* LB 2178 Agua Dulce seeds germination on MS medium supplemented with 50 ppm ClO₂ gave the highest germination time at 15.50 days, followed by MS medium supplemented with 75 ppm ClO₂ (10.23 days) and autoclaved MS free medium (7.77 days), respectively. While MS medium supplemented with 0, 10, 25, and 100 ppm, ClO₂ gave germination time at 0.00 day, significant difference at $p \leq 0.05$. Germination speed index studies, the result found that seeds of *G. mihanovichii* LB 2178 Agua Dulce were cultured on MS medium supplemented with 50 ppm ClO₂ gave the highest germination speed index at 0.11, followed by MS medium supplemented with 75 ppm ClO₂ (0.06) and autoclaved MS free medium (0.04). While MS medium

supplemented with 0, 10, 25, and 100 ppm, ClO₂ gave a germination speed index of 0.00, a significant difference at $p \leq 0.05$. (Table 2). MS medium supplemented with 50 ppm ClO₂ gave the highest germination than other mediums because it is a concentration that does not damage seeds and helps reduce their dormancy period. As a result, seeds grown on MS medium with 50 ppm ClO₂ germinate at the fastest pace possible. Furthermore, ClO₂ effectively destroys viruses, fungi, and bacteria in the culture medium. This helps reduce the percentage of contamination in the culture medium. Corresponding with the report, the nutrient media recommended for *in vitro* germination of *Micranthocereus flaviflorus* is 1/2MS since it is the most economical option and has nutrients to allow healthy initial development of seedlings. Similar results were found for other plants. [19] Similar results were found for other plants, such as the effect of culture medium on seed germination and seedling performance, which was studied with a significantly higher number of seeds germinated per day on 1/4 and 1/2 MS media strengths than on full and 1/4 strengths of MS media. The highest GRI (7.74 seeds/day) was obtained for the gelrite culture, which differed significantly from the GRI for all strengths of MS media except the 1/4 strength. However, these seed cultures proved unsustainable for seedling establishment, which was best supported on a full-strength MS medium. *In vitro* seed propagation of *Hibiscus coddii* subsp. *barnardii* could be beneficial for faster commercial production of seedlings. [20]

Table 2. Effect of Chlorine dioxide on germination (%G), mean germination time (MGT), and germination speed index (GSI) of *G. mihanovichii* LB2178 Agua Dulce seeds were cultured on autoclaved culture medium and sterilized with different concentrations of Chlorine dioxide

Chlorine dioxide (ppm)	Germination (%)	Mean Germination Time (days)	Germination speed index
sterilized	31.67 ^b	7.77 ^b	0.04 ^b
0	0.00 ^c	0.00 ^c	0.00 ^c
10	0.00 ^c	0.00 ^c	0.00 ^c
25	0.00 ^c	0.00 ^c	0.00 ^c
50	61.67 ^a	15.50 ^a	0.11 ^a
75	39.17 ^b	10.23 ^b	0.06 ^b
100	0.00 ^c	0.00 ^c	0.00 ^c
F-test	*	*	*
C.V.(%)	1.18	1.42	1.54

* = significant difference at $p \leq 0.05$

3.2. Effect of Chlorine dioxide on proliferation and induction of shoot and root of *G. mihanovichii* LB2178 Agua Dulce

The shoots of *G. mihanovichii* LB 2178 Agua Dulce were cultured on autoclaved MS-free medium and MS medium supplemented with 0, 10, 25, 50, 75, and 100 ppm ClO₂. The result found that shoots of *G. mihanovichii* LB 2178 Agua Dulce were cultured on MS medium supplemented with 50 ppm ClO₂ and gave the highest number of roots at 9.00 roots/explant, root length at 3.45 cm, shoot length at 0.54 cm and shoot diameter at 0.44 cm., significantly different ($p \leq 0.05$) (Table 3). Shoots generated from *G. mihanovichii* LB 2178 Agua Dulce seeds germinated in a medium supplemented with 50 ppm ClO₂ were round and dark green. The characteristics of the roots are fibrous roots, long and slender, and light brown (Figure 2).

The study found that the concentration of ClO₂ affects the induction of shoots and roots of *G. mihanovichii* LB 2178 Agua Dulce seedlings. Because ClO₂ prevents cell expansion, high concentrations cause the plant to grow slowly, reducing growth in an autoclaved medium. This is because heat exposure during autoclaving might lead to the decomposition of some nutrients. As reported, Gerberas grown on medium supplemented with ClO₂ grew as well or better than gerberas grown on autoclaved medium. This may be because sterilization causes some nutrients to be lost from the use of high heat [21]. While reported on a study that contrasted the amounts of ClO₂ (1-25 mg/l) to the *in vitro* culture of fragrant rice parts to increase the number of shoots, it was found that bacterial and fungal contamination happened after the culture was kept

for three days. While the number of shoots could be increased up to 12 when the sterile parts were grown in a medium with 25 mg/l ClO₂, when compared to those grown in a medium sterilized by autoclave, it was found that the plates could be increased. The number of shoots can be doubled. This is because steam sterilization with an autoclave is a sterilization method for tissue culture medium that changes the chemical composition of the medium, such as some nutrients being lost from using heat, to make it sterile [22]. Additionally, sterilizing media with ClO₂ can prolong the sterilizing effect. However, it is also a strong oxidizing agent that can cause stress to potato seedlings. Thus, the effect of ClO₂ on the growth of potato seedlings requires further systematic evaluation. In this study, the morphological indices, including plant height, root length, branches, and biomass, decreased with increasing ClO₂ concentrations. Although some differences were observed among the three cultivars when cultured on Chlorine dioxide -sterilized media, seedlings cultured on 12.6 µM Chlorine dioxide -sterilized media were morphologically like those cultured on autoclaved media. In addition, microtubers induced on 17.6 µM ClO₂ sterilized media maintained an aseptic niche for two months, like autoclaved media [23]. The similar morphological features and rates of microtuber induction between autoclaved and ClO₂ sterilized media align with previous studies, including [24]. Recently, [25] reported that the elimination of epidermal wax from explants increased the *in vitro* growth of lily, suggesting that the status of explants is a probable factor that affects plant tissue culture. When disinfecting plant explants for tissue culture, a balance should be maintained between antimicrobial effects and plant cell viability [26]

Table 3. Effect of Chlorine dioxide on shoot and root induction of *G. mihanovichii* LB2178 Agua Dulce were cultured on an autoclaved culture medium and sterilized with different concentrations of Chlorine dioxide

Chlorine dioxide (ppm)	Number of roots (roots/explant)	Length of root (cm)	Length of shoot (cm)	Diameter of shoot (cm)
sterilized	2.53 ^c	0.53 ^c	0.23 ^c	0.18 ^c
0	0.00 ^d	0.00 ^d	0.00 ^d	0.00 ^d
10	0.00 ^d	0.00 ^d	0.00 ^d	0.00 ^d
25	0.00 ^d	0.00 ^d	0.00 ^d	0.00 ^d
50	9.00 ^a	3.45 ^a	0.54 ^a	0.44 ^a
75	4.07 ^b	1.38 ^b	0.34 ^b	0.29 ^b
100	0.00 ^d	0.00 ^d	0.00 ^d	0.00 ^d
F-test	*	*	*	*
C.V. (%)	0.71	1.02	0.79	0.69

* = significant difference at $p \leq 0.05$

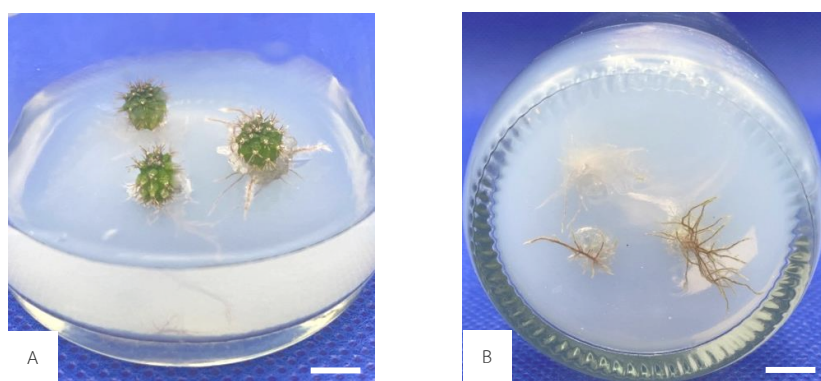


Figure 2. Characteristics of shoot and root formation of *G. mihanovichii* LB2178 Agua Dulce were cultured on MS medium supplemented with 50 ppm of Chlorine dioxide after culturing for 3 months (bar = 1 cm) (A) shoot formation (B) root formation

4. Conclusions

The results showed that *G. mihanovichii* LB2178 Agua Dulce can be propagated using *in vitro* techniques. After 2 months of culture, the results showed that MS medium supplemented with 50 ppm ClO₂ gave the highest survival rate at 54.17%. The initial germination of *G. mihanovichii* LB 2178 Agua Dulce was observed 20 days following the experiment. It was found that *G. mihanovichii* LB 2178 Agua Dulce seeds germination on MS medium supplemented with 50 ppm ClO₂ gave the highest germination at 61.67 %, the highest germination time at 15.50 days, and the highest germination speed index at 0.11. After 3 months of culture, the results showed that shoot and root induction can be achieved in *G. mihanovichii* LB2178 Agua Dulce seeds were cultured on MS medium supplemented with 50 ppm ClO₂ gave the highest number of roots at 9.00 roots/explant, length of root 3.45 cm, length of shoot 0.54 cm and diameter of shoot 0.44 cm. Sterilization by ClO₂ may help increase efficiency and an alternative to solving the problem of microbial contamination in tissue culture. It also helps increase work speed by reducing steps in preparing synthetic food instead of using an autoclave.

5. Acknowledgements

We thank Miss Wariya Nuannut for supervising and controlling the tissue culture room at the science center. And thank the science center in the Faculty of Science and Technology, Nakhon Si Thammarat Rajabhat University.

Author Contributions: A short paragraph specifying their individual contributions must be provided for research articles with several authors. The following statements should be used “Conceptualization, P.R. and S.R.; methodology, P.R.; software, S.R.; validation, P.R., S.R. and T.K.; formal analysis, P.R.; investigation, P.R.; resources, P.R. and T.K.; data curation, P.R.; writing—original draft preparation, P.R.; writing—review and editing, S.R.; visualization, T.K.; supervision, S.R.; project administration, P.R. and S.R. All authors have read and agreed to the published version of the manuscript.” Please turn to the CRediT taxonomy for the term explanation. Authorship must be limited to those who have contributed substantially to the work reported.

Funding: This research received no external funding

Conflicts of Interest: The authors declare no conflict of interest.

References

- [1] Supanantanon, P. *Cactus*. Bangkok: Amarin printing and publishing. **2019**, 3-6.
- [2] Verified Market Research. *Global Succulent Plant Market Size By Types, By Application, By Geographic Scope And Forecast*. Available online: <https://www.verifiedmarketresearch.com/product/succulent-plant-market/>. (access on 7 October 2023).
- [3] Supanantanon, P. *Cactus*. Bangkok: Amarin printing and publishing. **2019**, 7-10.
- [4] Kanchanakul, S. *Roiphan Phrueksa Cactus*. Bangkok: Amarin printing and publishing, 2014; 105-108.
- [5] Ramasoot, S. *Textbook on plant tissue culture*. Nakhon Si Thammarat: Nakhon Si Thammarat Rajabhat University. **2016**, 106-108.
- [6] Balashanmugam, P.; Balakumaran, M.D.; Murugan, R.; Dhanapal, K.; Kalaiichelvan, P.T. Phytogetic synthesis of silver nanoparticles, optimization and evaluation of *in vitro* antifungal activity against human and plant pathogens. *Microbiological Research*. **2016**, 192, 52-64. <http://dx.doi.org/10.1016/j.micres.2016.06.004>
- [7] Cardoso, J. C.; da Silva, J. A. T. Micropropagation of Gerbera using chlorine dioxide (ClO₂) to sterilize the culture medium. *In Vitro Cellular & Developmental Biology-Plant*. **2012**, 48(3), 362-368.
- [8] Te-chato, S.; Yuso, A.; Domyoas, P. Proliferation of *Lepironia articulate* from Culturing Shoots by Air Bubble Bioreactor. *Princess of Naradhiwas University Journal*. **2017**, 9(2), 83-88.
- [9] Cardoso, J. C. & Imthurn, A. C. P. Easy and efficient chemical sterilization of the culture medium for *in vitro* growth of Gerbera using chlorine dioxide (ClO₂). *Ornamental Horticulture*. **2018**, 24(3), 218-224. <http://dx.doi.org/10.14295/oh.v24i3.1222>

- [10] Duan, Y.; Zhang, H.; Sun, M.; Zhao, F.; Xue, T.; Xue, J. Use of chlorine dioxide to sterilize medium for tissue culture of potato. *Scientific Reports*. **2019**, *9*, 1-9. <https://doi.org/10.1038/s41598-019-46795-4>
- [11] Murashige, T.; Skoog, F. (1962). A revised medium for rapid growth and bioassays with tobacco tissue cultures. *Physiol Plant*. **1962**, *15*, 473–497. <https://doi.org/10.1111/j.1399-3054.1962.tb08052.x>
- [12] Brasil. *Rules for seed analysis*. Ministry of Agriculture, Livestock and Food Supply. Secretariat of Agricultural and Livestock Defense. Brasília: MAPA/ACS. **2009**, 148-224.
- [13] Srichuay, W.; Te-chato, S. Effect of chlorine dioxide (ClO₂) on sterilization in micropropagation of pineapple cv. Phulae by bioreactor system. *KHON KAEN AGRICULTURE Journal*. **2014**, *42*(3), 75-80.
- [14] Duan, Y.; Zhang, H.; Sun, M.; Zhao, F.; Xue, T.; Xue, J. Use of chlorine dioxide to sterilize medium for tissue culture of potato. *Scientific Reports*. **2019**, *9*, 1-9. <https://doi.org/10.1038/s41598-019-46795-4>
- [15] Cardoso, J. C.; da Silva, J. A. T. Micropropagation of Gerbera using chlorine dioxide (ClO₂) to sterilize the culture medium. *In Vitro Cellular & Developmental Biology-Plant*. **2012**, *48*(3), 362-368.
- [16] Lennotech. *Disinfectants: Chlorine dioxide*. Available online: <http://www.lennotech.com/processes/disinfection/chemical/disinfectants-chlorine-dioxide.htm>. (access on 10 October 2023).
- [17] Huang, J.; Wang, L.; Ren, N.; Ma, F.; Ma, J. Disinfection effect of chlorine dioxide on bacteria in water. *Water Res*. **1997**, *31*, 607–613. [https://doi.org/10.1016/S0043-1354\(96\)00275-8](https://doi.org/10.1016/S0043-1354(96)00275-8)
- [18] Srebernich, S.M. Using chlorine dioxide and peracetic acid as substitutes for sodium hypochloride in the sanitization of minimally processed green seasoning. *Ciência e Tecnologia de Alimentos*. **2007**, *27*(4), 744-750.
- [19] Civatti, L.M.; Marchi, M.N.G.; Bellintani, M.C. Micropropagation of two species of *Micranthocereus* (Cactaceae) with ornamental potential native to Bahia, Brazil. *African Journal of Biotechnology*. **2017**, *16*(14), 749-762. <https://doi.org/10.5897/AJB2016.15901>
- [20] Plessis, H.J.d.; Nikolova, R.V.; Kleynhans, R.; Egan, B.A. *In vitro* seed germination and seedling performance of *Hibiscus coddii* subsp. *Barnardii*. *Ornamental Horticulture*. **2020**, *26*(4), 598-606. <https://doi.org/10.1590/2447-536X.v26i4.2191>
- [21] Cardoso, J. C.; da Silva, J. A. T. Micropropagation of Gerbera using chlorine dioxide (ClO₂) to sterilize the culture medium. *In Vitro Cellular & Developmental Biology-Plant*. **2012**, *48*(3), 362-368.
- [22] Yusoh, A.; Te-chato, S. Propagation of hom Kra-Dang-Nga rice through tissue culture technic and its conservation *in vitro*. *Songklanakarin Journal of Plant Science*. **2015**, *2*(3), 12-16.
- [23] Duan, Y.; Zhang, H.; Sun, M.; Zhao, F.; Xue, T.; Xue, J. Use of chlorine dioxide to sterilize medium for tissue culture of potato. *Scientific Reports*. **2019**, *9*, 1-9. <https://doi.org/10.1038/s41598-019-46795-4>
- [24] Pais, A. K. *et al.* Sodium hypochlorite sterilization of culture medium in micropropagation of *Gerbera hybrida* cv. *Essandre*. *African Journal of Biotechnology*. **2016**, *15*, 1995–1998. <https://doi.org/10.5897/AJB2016.15405>
- [25] Askari, N.; De Klerk, G.J. Elimination of epidermal wax from explants increases growth in tissue culture of lily. *Scientia Horticulturae-Amsterdam*. **2020**, *274*, 109637. <https://doi.org/10.1016/j.scienta.2020.109637>
- [26] Duan, Y.; Zhao, F.; Li, H.; Zhou, Y.; Zhu, X.; Li, F.; Chen, W.; Xue, J. Evaluation of aqueous chlorine dioxide for disinfecting plant explants. *In Vitro Cellular and Developmental Biology*. **2016**, *52*, 38–44. <https://doi.org/10.1007/s11627-015-9736-3>



ASEAN

Journal of Scientific and Technological Reports

Online ISSN:2773-8752



Type of the Paper (Article, Review, Communication, etc.) *about 8,000 words maximum*

Title (Palatino Linotype 18 pt, bold)

Firstname Lastname¹, Firstname Lastname² and Firstname Lastname^{2*}

¹ Affiliation 1; e-mail@e-mail.com

² Affiliation 2; e-mail@e-mail.com

* Correspondence: e-mail@e-mail.com; (one corresponding authors, add author initials)

Citation:

Lastname, F.; Lastname, F.;
Lastname, F. Title. *ASEAN J.
Sci. Tech. Report.* 2023, 26(X),
xx-xx. <https://doi.org/10.55164/ajstr.vxxix.xxxxxx>

Article history:

Received: date

Revised: date

Accepted: date

Available online: date

Publisher's Note:

This article is published and distributed under the terms of the Thaksin University.

Abstract: A single paragraph of about 400 words maximum. Self-contained and concisely describe the reason for the work, methodology, results, and conclusions. Uncommon abbreviations should be spelled out at first use. We strongly encourage authors to use the following style of structured abstracts, but without headings: (1) Background: Place the question addressed in a broad context and highlight the purpose of the study; (2) Methods: briefly describe the main methods or treatments applied; (3) Results: summarize the article's main findings; (4) Conclusions: indicate the main conclusions or interpretations.

Keywords: keyword 1; keyword 2; keyword 3 (List three to ten pertinent keywords specific to the article yet reasonably common within the subject discipline.)

1. Introduction

The introduction should briefly place the study in a broad context and highlight why it is crucial. It should define the purpose of the work and its significance. The current state of the research field should be carefully reviewed and critical publications cited. Please highlight controversial and diverging hypotheses when necessary. Finally, briefly mention the main aim of the work. References should be numbered in order of appearance and indicated by a numeral or numerals in square brackets—e.g., [1] or [2, 3], or [4-6]. See the end of the document for further details on references.

2. Materials and Methods

The materials and methods should be described with sufficient details to allow others to replicate and build on the published results. Please note that your manuscript's publication implicates that you must make all materials, data, computer code, and protocols associated with the publication available to readers. Please disclose at the submission stage any restrictions on the availability of materials or information. New methods and protocols should be described in detail, while well-established methods can be briefly described and appropriately cited.

Interventional studies involving animals or humans, and other studies that require ethical approval, must list the authority that provided approval and the corresponding ethical approval code.

2.1 Subsection

2.1.1 Subsubsection

3. Results and Discussion

This section may be divided by subheadings. It should provide a concise and precise description of the experimental results, their interpretation, as well as the experimental conclusions that can be drawn. Authors should discuss the results and how they can be interpreted from previous studies and the working hypotheses. The findings and their implications should be discussed in the broadest context possible. Future research directions may also be highlighted.

3.1 Subsection

3.1.1 Subsubsection

3.2. Figures, Tables, and Schemes

All figures and tables should be cited in the main text as Figure 1, Table 1, etc.



Figure 1. This is a figure. Schemes follow the same formatting.

Table 1. This is a table. Tables should be placed in the main text near the first time they are cited.

Title 1	Title 2	Title 3
entry 1	data	data
entry 2	data	data ¹

¹ Table may have a footer.

3.3. Formatting of Mathematical Components

This is example 1 of an equation:

$$a = 1, \tag{1}$$

The text following an equation need not be a new paragraph. Please punctuate equations as regular text. This is example 2 of an equation:

$$a = b + c + d + e + f + g + h + i + j + k + l + m + n + o + p + q + r + s + t + u \tag{2}$$

The text following an equation need not be a new paragraph. Please punctuate equations as regular text. The text continues here.

4. Conclusions

Concisely restate the hypothesis and most important findings. Summarize the significant findings, contributions to existing knowledge, and limitations. What are the future directions? Conclusions MUST be well stated, linked to original research question & limited to supporting results.

5. Acknowledgements

Should not be used to acknowledge funders - funding will be entered as a separate. As a matter of courtesy, we suggest you inform anyone whom you acknowledge.

Author Contributions: For research articles with several authors, a short paragraph specifying their individual contributions must be provided. The following statements should be used “Conceptualization, X.X. and Y.Y.; methodology, X.X.; software, X.X.; validation, X.X., Y.Y. and Z.Z.; formal analysis, X.X.; investigation, X.X.; resources, X.X.; data curation, X.X.; writing—original draft preparation, X.X.; writing—review and editing, X.X.; visualization, X.X.; supervision, X.X.; project administration, X.X.; funding acquisition, Y.Y. All authors have read and agreed to the published version of the manuscript.” Please turn to the CRediT taxonomy for the term explanation. Authorship must be limited to those who have contributed substantially to the work reported.

Funding: Please add: “This research received no external funding” or “This research was funded by NAME OF FUNDER, grant number XXX” and “The APC was funded by XXX”. Check carefully that the details given are accurate and use the standard spelling of funding agency names at <https://search.crossref.org/funding>. Any errors may affect your future funding.

Conflicts of Interest: Declare conflicts of interest or state “The authors declare no conflict of interest.” Authors must identify and declare any personal circumstances or interest that may be perceived as inappropriately influencing the representation or interpretation of reported research results. Any role of the funders in the design of the study; in the collection, analyses or interpretation of data; in the writing of the manuscript, or in the decision to publish the results must be declared in this section. If there is no role, please state “The funders had no role in the design of the study; in the collection, analyses, or interpretation of data; in the writing of the manuscript, or in the decision to publish the results”.

References

References must be numbered in order of appearance in the text (including citations in tables and legends) and listed individually at the end of the manuscript. We recommend preparing the references with a bibliography software package, such as EndNote, ReferenceManager to avoid typing mistakes and duplicated references. Include the digital object identifier (DOI) for all references where available.

Citations and references in the Supplementary Materials are permitted provided that they also appear in the reference list here.

In the text, reference numbers should be placed in square brackets [] and placed before the punctuation; for example [1], [1-3] or [1, 3]. For embedded citations in the text with pagination, use both parentheses and brackets to indicate the reference number and page numbers; for example [5] (p. 100), or [6] (pp. 101-105).

Using the American Chemical Society (ACS) referencing style

- [1] Author 1, A.B.; Author 2, C.D. Title of the article. *Abbreviated Journal Name* Year, Volume, page range.
- [2] Author 1, A.; Author 2, B. Title of the chapter. In *Book Title*, 2nd ed.; Editor 1, A., Editor 2, B., Eds.; Publisher: Publisher Location, Country. 2007, Volume 3, pp. 154-196.

- [3] Author 1, A.; Author 2, B. *Book Title*, 3rd ed.; Publisher: Publisher Location, Country, 2008, pp. 154-196.
- [4] Author 1, A.B.; Author 2, C. Title of Unpublished Work. *Abbreviated Journal Name* stage of publication (under review; accepted; in press).
- [5] Author 1, A.B. (University, City, State, Country); Author 2, C. (Institute, City, State, Country). Personal communication, 2012.
- [6] Author 1, A.B.; Author 2, C.D.; Author 3, E.F. Title of Presentation. In Title of the Collected Work (if available), Proceedings of the Name of the Conference, Location of Conference, Country, Date of Conference; Editor 1, Editor 2, Eds. (if available); Publisher: City, Country, Year (if available); Abstract Number (optional), Pagination (optional).
- [7] Author 1, A.B. Title of Thesis. Level of Thesis, Degree-Granting University, Location of University, Date of Completion.
- [8] Title of Site. Available online: URL (accessed on Day Month Year).

Reviewers suggestion

1. Name, Address, [e-mail](#)
2. Name, Address, [e-mail](#)
3. Name, Address, [e-mail](#)
4. Name, Address, [e-mail](#)

URL link:

Notes for Authors >>

<https://drive.google.com/file/d/1r0zegnlVeQqe4iLOyT1xDEInNggINPD/view?usp=sharing>
<https://drive.google.com/file/d/1r0zegnlVeQqe4iLOyT1xDEInNggINPD/view?usp=sharing>

Online Submissions >> <https://ph02.tci-thaijo.org/index.php/tsujournal/user/register>

Current Issue >> <https://ph02.tci-thaijo.org/index.php/tsujournal/issue/view/16516>

AJSTR Publication Ethics and Malpractice >> <https://ph02.tci-thaijo.org/index.php/tsujournal/ethics>

Journal Title Abbreviations >> <http://library.caltech.edu/reference/abbreviations>



ASEAN

Journal of Scientific and Technological Reports

Online ISSN:2773-8752



ASEAN
Journal of Scientific and Technological Reports
Online ISSN:2773-8752

